Structural Performance of Mass Timber Panel-Concrete Composite Floors with Notched Connections

by

Lei Zhang

A thesis submitted in partial fulfillment of the requirements for the degree of

Doctor of Philosophy

in

Structural Engineering

Department of Civil and Environmental Engineering
University of Alberta

Abstract

This thesis focuses on the structural performance of mass timber panel-concrete composite floors with notches. Mass timber panels (MTPs) such as cross-laminated timber, glue-laminated timber, and nail-laminated timber, are emerging construction materials in the building industry due to their high strength, great dimensional stability, and prefabrication. The combination of MTPs and concrete in the floor system offers many structural, economic, and ecological benefits. The structural performance of MTP-concrete composite floors is governed by the shear connection system between timber and concrete. The notched connections made by cutting grooves on timber and filling them with concrete are considered as a structurally efficient and cost-saving connecting solution for resisting shear forces and restricting relative slips between timber and concrete. However, the notched connection design in the composite floors is not standardized and the existing design guidelines are inadequate for MTP-concrete composite floors.

To study the structural performance of notched connections and notch-connected composite floors, this thesis presented experimental, numerical, and analytical investigations. Push-out tests were conducted on the notched connections first, and then bending tests and vibration tests were conducted on full-scale composite floors. Finite element models were built for the notched connections to derive the connection shear stiffness. Finally, analytical solutions were developed to predict the internal actions of the composite floors under external loads.

This study shows that the structural performance of notched connections is affected by the geometry of the connections and material properties of timber and concrete. The notch-connected MTP-concrete composite floors showed high bending stiffness but were not fully composite. The floors with shallow notches tended to fail in a ductile manner but had lower bending stiffness than

floors with deep notches. The composite floors with deep notches, however, often fail abruptly in the concrete notches. By reinforcing the notched connections with steel fasteners, the composite floor can achieve high bending stiffness, high load-carrying capacity, and controlled failure pattern. The proper number and locations of notched connections in the composite floors can be determined from the proposed composite beam model.

This thesis presented promising results in terms of the static and dynamic structural performance of notch-connected MTP-concrete composite floors. The test investigations added additional data to the current research body and prompted further evolvement of timber-concrete composite floors. The proposed empirical equations for estimating the connection stiffness and strength and composite beam model for predicting the serviceability and ultimate structural performance of composite floors provide useful tools to analyze the notch-connected MTP-concrete composite floors. The design recommendations for MTP-concrete composite floors with notches are provided in the thesis.

Preface

This thesis is an original work by Lei Zhang. Chapter 3, Chapter 4, and Chapter 5 of this thesis are restructured from the published peer-reviewed journal papers or submitted manuscripts by the author and collaborators.

Section 3.3 of Chapter 3 has been published as L. Zhang, Y. H. Chui, and D. Tomlinson, "Experimental investigation on the shear properties of notched connections in mass timber panel-concrete composite floors," *Construction and Building Materials*, 2020, vol. 234, 117375.

Section 3.4 of Chapter 3 and Sections 5.4 and 5.5 of Chapter 5 are restructured from a manuscript titled "Bending Stiffness Prediction to Mass Timber Panel-Concrete Composite Floors with Notched Connections" that is under review by *Engineering Structures*. The manuscript was submitted by Lei Zhang as the first author.

Section 4.2 of Chapter 4 has been published as L. Zhang, J. Zhou, Y. H. Chui, and D. Tomlinson, "Experimental investigation on the structural performance of mass timber panel-concrete composite floors with notched connections," *ASCE Journal of Structural Engineering*, 2022, vol. 148, issue 2, 04021249.

Section 4.3 of Chapter 4 is restructured from a manuscript titled "Development of High-Performance Timber-Concrete Composite Floors with Reinforced Notched Connections" that is under review by *Structures*. The manuscript was submitted by Lei Zhang as the first author.

Section 4.4 of Chapter 4 is restructured from a manuscript titled "Vibration Performance and Stiffness Properties of Mass Timber Panel-Concrete Composite Floors with Notched Connections" which is under review by *ASCE Journal of Structural Engineering*. The manuscript was submitted by Lei Zhang as the first author.

Sections 5.2 and 5.3 of Chapter 5 have been published as L. Zhang, S. Zhang, and Y. H. Chui, "Analytical evaluation to the timber-concrete composite beam connected with notched connections," *Engineering Structures*, 2021, vol. 227, 111466.

Acknowledgments

Throughout my Ph.D. study, I have received enormous help and support from different people. Firstly, I would like to express my sincere gratitude to my supervisor Prof. Ying Hei Chui for his continuous support of my Ph.D. study. His patience, insightful feedback, and immense knowledge in timber engineering pushed me to sharpen my thinking and brought my work to a higher level. Besides my supervisor, I would like to thank the rest of my advisory committee, Dr. Douglas Tomlinson and Dr. Yuxiang Chen, for their constructive comments, encouragement, and guidance throughout my research. Without their precious support, it would not be possible to conduct this research.

My sincere gratitude also goes to Dr. Jianhui Zhou and Dr. Thomas Tannert at the University of Northern British Columbia for providing me the opportunity to conduct my experimental research at Wood Innovation Research Laboratory. Dr. Sigong Zhang provided constructive feedback on my analytical modeling. Dr. Jan Niederwestberg offered valuable advice for designing my experiments. I am grateful for my time working with Dr. Zhou, Dr. Zhang, and Dr. Niederwestberg at the University of Alberta.

Finally, I would like to acknowledge the financial support from the Natural Sciences and Engineering Research Council of Canada (NSERC) through the Industrial Research Chair program that was granted to Dr. Ying Hei Chui. I am also grateful to Western Archrib and Rothoblaas for providing the materials used in my research.

Last but not least, I would like to thank my parents, my grandparents, and my sister for their unconditional love and support throughout my Ph.D. study.

Table of Contents

List of Tables

List of Figures

List of Symbols

Roman letters

A_c	Cross-section area of concrete
A_t	Cross-section area of timber
A_{ti}	Cross-section area of timber in segment ***i*** of the composite floor
a_1	Distance from the centroid of concrete to the neutral axis of timber in the gamma method
a_2	Distance from the centroid of timber to the neutral axis of timber in the gamma method
b	Width of the beam or floor
b_c	Width of concrete
b_t	Width of timber
D	Slip vector
d_i	Slip between timber and concrete at two sides of the restored segment ***i***
d_{nc}	Notch depth
d_v	Effective shear depth of concrete
E_c	Young's modulus of concrete
E_t	Young's modulus of timber in the longitudinal direction
E_{TT}	Young's modulus of timber in the transverse direction
EI	Bending stiffness of floors in the serviceability state
$(EI)_{bt}$	Bending stiffness of bare timber floor
$(EI)_{ca}$	Bending stiffness of cantilevers in the framework model
$(EI)_d$	Dynamic flexural stiffness of composite floors
$(EI)_{dt}$	Dynamic flexural stiffness of bare timber panels
$(EI)_{eff}$	Effective bending stiffness of the composite beams or floors
$(EI)_{eqv}$	Equivalent bending stiffness of the composite floor
$(EI)_{ful}$	Bending stiffness of the full composite floor
$(EI)_{no}$	Bending stiffness of the non-composite floor
$(EI)_{ult}$	Ultimate bending stiffness of composite floors

e_1	Distance from the centroid of concrete to the interface of the composite floor in the framework model
e_2	Distance from the centroid of timber to the interface of the composite floor in the framework model
e_{ci}	Eccentricity of axial forces to the centre of concrete in the restored segment ***i***
e_{ti}	Eccentricity of axial forces to the centre of timber in the restored segment ***i***
F_{max}	Peak load of notched connections under shear
f_1	Fundamental natural frequency
f_{20}	First flexural frequency
f_{30}	Second flexural frequency
f_{21}	First torsional frequency
f_{40}	Third flexural frequency
f_c'	Compressive strength of concrete
f_{ct}	Tensile strength of concrete
f_{tb}	Bending strength of timber
f_{tc}	Compressive strength of timber in the longitudinal direction
f_{ts}	Shear strength of timber in the longitudinal direction
f_{tt}	Tensile strength of timber in the longitudinal direction
f_{TTc}	Compressive strength of timber in the transverse direction
G_{LT}	Shear stiffness of timber in the longitudinal-transverse plane
G_{TR}	Shear stiffness of timber in the transverse plane
h_c	Thicknesses of concrete
h_{ct}	Cracked height of concrete
h_{cy}	Yield height of concrete
h_{gi}	Gap between timber and concrete in segment ***i***
h_t	Thicknesses of timber
h_{ti}	Thicknesses of timber in segment ***i***
$\boldsymbol{I}$	Identity matrix
I_c	Second moment of area of concrete cross-section
I_t	Second moment of area of timber cross-section

I_{ti}	Second moment of area of timber cross-section in segment ***i***
$\boldsymbol{K}$	Stiffness matrix of shear connections in the composite floor
K_{ser}	Shear stiffness of notched connections at the serviceability state
K_{ult}	Shear stiffness of notched connections at the ultimate state
k	Stiffness of shear connectors
k_i	Stiffness of shear connection ***i***
L	Beam span or floor span
l_i	Length of segment ***i*** in the composite floor
l_{nw}	Length of the notch
l_{ts}	Timber shear length in front of the notch
M	External bending moment
$\hat{M}$	Bending moment caused by a unit force
$\bar{M}_i$	Averaged external bending moment in segment ***i*** of the composite floor
M_c	Bending moment in concrete
M_t	Bending moment in timber
M_{tn}	Updated bending moment in timber after concrete yields under compression
M_{tr}	Bending moment resistance of timber
M^{tot}	Summation of bending moments in concrete and timber
$\widetilde{M}_c$	Bending moment in concrete in the released segment
$\widetilde{M}_t$	Bending moment in timber in the released segment
$\widehat{M}_c^i$	Bending moment in concrete in the restored segment ***i***
$\widehat{M}_t^i$	Bending moments in timber in the restored segment ***i***
M_{ult}	Ultimate moment-carrying capacity of composite floors
N	Axial force in timber and concrete
N_{cb}	Imaginary axial force acting on the concrete tension zone
N_{ct}	Imaginary axial force acting on the concrete compression zone
N_{de}	Reduced axial force in timber and concrete after concrete cracking
N_i	Axial force in timber or concrete in segment ***i***
N_{in}	Additional tensile force in timber after concrete cracking
N_{tn}	Updated axial force in timber after concrete cracking and yielding

P	Concentrated force
P_{cc}	Notched connection strength due to concrete compressive failure
P_{cs}	Notched connection strength due to concrete shear failure
P_{max}	Peak load of composite floors under bending
P_{tc}	Notched connection strength due to timber compressive failure
P_{ts}	Notched connection strength due to timber shear failure
q	Uniformly distributed load
R	Ratio between the shear modulus of timber in the longitudinal-transverse plane to the Young's modulus of timber in the longitudinal direction
r	Rotation of the cross-section
S_1	Slip vector
S_2	Slip vector
S_t	Section modulus of timber
s	Spacing of shear connections in the composite floor
s_{i1}	Slip between timber and concrete at the left side of the released segment ***i***
s_{i2}	Slip between timber and concrete at the right side of the released segment ***i***
T_i	Shear force transmitted by connection ***i*** in the composite floor
T_{tr}	Tensile load resistance of timber
V	Shear force in the composite floor
V_c	Shear force in concrete
V_{cr}	Shear force resistance of concrete
V_t	Shear force in timber
V_{tr}	Shear force resistance of timber
v_c	Poisson's ratio of concrete
v_{LT}	Poisson's ratio of timber in the longitudinal direction
$\boldsymbol{W}_1$	Coefficient matrix
$\boldsymbol{W}_2$	Coefficient matrix
w	Maximum live load floors can sustain while satisfying the deflection limit
x	Distance between the left support to a certain point in the composite floor
x_i	Distance between the left support to the left-hand side of segment ***i*** in the floor

Greek letters

α	Average change in the mechanical properties of timber due to one percent change in moisture content
β	Factor accounting for shear resistance of cracked concrete
γ	Factor accounting for the effectiveness of the composite action in the Gamma method
Δ	Relative slip between timber and concrete at the interface
Δ_0	Relative slip between timber and concrete at the left support of the floor
$\bar{\Delta}$	The difference of length change between the bottom of concrete and top of timber
$\tilde{\Delta}_c^{btm}$	Length change at bottom of concrete in the released segment
$\tilde{\Delta}_t^{top}$	Length change at top of timber in the released segment
$\hat{\Delta}_c^{btm}$	Length change at bottom of concrete in the restored segment
$\hat{\Delta}_t^{top}$	Length change at top of timber in the restored segment
δ	Deflection of the composite beam or floor
δ_{ful}	Deflection of the full composite floor
δ_{no}	Deflection of the non-composite floor
ε_{co}	Concrete yield strain
ε_{cto}	Ultimate tensile strain of concrete
ε_{cu}	Ultimate compressive strain of concrete
ε_{tco}	Timber compressive yield strain parallel to grain
ε_{tto}	Ultimate tensile strain of timber parallel to grain
ε_c^{btm}	Strain at the bottom of concrete
ε_t^{top}	Strain at the top of timber
$\tilde{\varepsilon}_c^{btm}$	Strain at the bottom of concrete in the released segment
$\tilde{\varepsilon}_t^{top}$	Strain at the top of timber in the released segment
$\hat{\varepsilon}_c^{btm}$	Strain at the bottom of concrete in the restored segment
$\hat{\varepsilon}_t^{top}$	Strain at top of timber in the restored segment
$\boldsymbol{\Theta}$	Coefficient matrix
θ_i	Parameter in the discrete bond composite beam model

κ	Curvature of the composite floor
κ_1	Curvature of the released segment
κ_2^i	Curvature of restored segment ***i***
Λ	Coefficient vector
λ	Modification factor for concrete density
λ_1	Composite efficiency by stiffness
λ_2	Composite efficiency by deflection
λ_i	Difference of length change between the bottom of concrete and top of timber in the released segment ***i***
ρ_c	Concrete density
ρ_t	Timber density
σ_{cb}	Stresses at the bottom of concrete
σ_{cm}	Updated stress at the bottom of concrete compression zone after concrete cracking
σ_{ct}	Stresses at the top of concrete
σ_{ctn}	Updated stress at the top of concrete after concrete cracking
σ_{tb}	Stresses at the bottom of timber
σ_{tt}	Stresses at the top of timber
$\tilde{\sigma}_c^{top}$	Stresses at the top of concrete in the released segment
$\tilde{\sigma}_c^{btm}$	Stresses at the bottom of concrete in the released segment
$\tilde{\sigma}_t^{top}$	Stresses at the top of timber in the released segment
$\tilde{\sigma}_t^{btm}$	Stresses at the bottom of timber in the released segment
$\hat{\sigma}_c^{top}$	Stresses at the top of concrete in the restored segment
$\hat{\sigma}_c^{btm}$	Stresses at the bottom of concrete in the restored segment
$\hat{\sigma}_t^{top}$	Stresses at the top of timber in the restored segment
$\hat{\sigma}_t^{btm}$	Stresses at the bottom of timber in the restored segment
φ_{cs}	Correction factor for the concrete shear strength in the notched connection strength prediction
φ_{kc}	Ratio of the ultimate connection stiffness to the initial connection stiffness

φ_{tc}	Correction factor for the timber compressive strength in the notched connection strength prediction
φ_{ts}	Correction factor for the timber shear strength in the notched connection strength prediction

Chapter 1

Introduction

1.1 Motivation

Mass timber constructions have been experiencing an upward trend over the past twenty years in the move towards sustainable construction (Harte 2017). The significant advances in technology-enhanced engineered wood products and high-performance connection systems allow timber to be used in larger and more complex structures. Mass timber panels, such as cross-laminated timber, glued laminated timber, and mechanically laminated timber (dowel or nail laminated timber), are large-dimension engineered wood products that have become popular in the floor, wall, and roof applications due to their ease of prefabrication and fast erection (Gong 2019). The implementation of mass timber panels in mid- and high-rise construction markets leads to buildings with lower carbon footprint and lighter weight but also brings numerous design challenges. For instance, floor systems transfer vertical loads to beams, columns, or walls, and lateral loads to shear walls, braced frames, or moment-resisting frames. However, it is known that floors constructed with bare mass timber panels are prone to producing excessive deflection and vibration as well as unfavorable sound transmission issues (Martins et al. 2015; Harte 2017; Gong 2019). These issues reduce the competitiveness of mass timber floors compared with reinforced concrete or steel-concrete composite floors.

Mass timber panel-concrete composite floors provide a compelling alternative solution for floors with long spans and heavy loads (Clouston and Schreyer 2008; Higgins et al. 2017). By combining mass timber panels with a concrete layer through connections, the timber panels replace the tension zone in traditional reinforced concrete floors and act as both stay-in-place formwork for concrete and structural component to carry tension. Compared to bare timber floors, the concrete layer in mass timber panel-concrete composite floors improves both flexural stiffness and strength of the floor, thereby allowing larger spans to be achieved (Higgins et al. 2017). The acoustical properties, fire-resistance rating, as well as thermal mass of the floor are also enhanced with the addition of concrete (Ceccotti 2002; Martins et al. 2015; Shephard et al. 2021).

The shear connection system between concrete and timber has a major influence on both the bending stiffness and load-carrying capacity of composite floors. The past few decades have seen numerous research efforts put into developing various connection systems for timber-concrete composite floors. The dominant connection systems are mechanical steel fasteners such as self-tapping screws (Higgins et al. 2017; Mai et al. 2018; Mirdad and Chui 2019; Shephard et al. 2021) and steel mesh plates (HBV connectors) (Clouston and Schreyer 2008; Higgins et al. 2017). Continuous connection systems that rely on friction or adhesive have also gained some attention (Doehrer et al. 2006; Negrão et al. 2010a; Negrão et al. 2010b; Tannert et al. 2020). Interlocking notch shear keys are another commonly used connection system made by cutting grooves on timber and filling them with concrete (Gutkowski et al. 2004; Boccadoro and Frangi 2014; Zhang et al. 2020).

The choice of connections in the composite floors depends on the mechanical performance, cost, and constructability of the connections. Dowel-type fasteners are usually flexible under shear forces generated between the timber and concrete while steel mesh plates, adhesives, and notches are relatively stiff (Dias and Jorge 2011; Yeoh et al. 2011a). In terms of cost, steel fasteners are often expensive and labor-intensive to install during floor construction. Notched connections, however, can be pre-cut in the fabrication shop before the shipment of panels to the site. Overall, notched connections show excellent structural performance and rapid construction, thus a great potential in expanding the market for timber-concrete composite floors (Yeoh et al. 2011a; Dias et al. 2018). Despite this, the notched connections are less prevalent than dowel-type fasteners, especially in North American constructions. The most important reason is that the highly variable notch geometries and strengthening techniques hinder the standardization and development of design guidelines for the notched connections.

The mechanical properties of notched connections are affected by the notch geometry, reinforcing techniques in the notch, and material properties of timber and concrete. Unlike the continuous connections such as adhesive or closely spaced mechanical fasteners such as self-tapping screws, notched connections are usually widely spaced in the floors, thus timber and concrete are only connected at discrete locations. The structural performance of discretely connected mass timber panel-concrete composite floors is not only affected by the connection stiffness, but also by the number and layout of connections. Previous experimental investigations found that mass timber

panel-concrete composite floors with different notched connection designs had different efficiencies of composite action between timber and concrete (Gutkowski et al. 2008; LeBorgne and Gutkowski 2010; Boccadoro and Frangi 2014; Boccadoro et al. 2017; Jiang and Crocetti 2019).

Low composite action and large relative slip between timber and concrete result in low flexural stiffness and load-carrying capacity, leading to large deflection and early failure of floors. To date, guidelines for proper notched connection design in timber-concrete composite floors to achieve high composite action are scant. The COST Action FP 1402/WG 4 report (Dias et al. 2018) provides recommendations in terms of the minimal dimension and spacing of notches in the floor as well as minimal requirements on the materials. However, the notched connection design in mass timber panel-concrete composite floors is far from standardized. There has been limited research into addressing factors that play important roles in the structural performance of mass timber panel-concrete composite floors, such as the optimal number and locations of notches in the floor, the optimal concrete layer thickness, the maximum span floors can reach while still satisfying design limit states, the minimal number of steel reinforcements needed in the connection to prevent concrete shear failure, and the floor performance under negative bending moment in multi-span continuous floors. The vibration performance of the timber-concrete composite floors is also largely uncertain since the concrete layer increases both the weight and the bending stiffness of the composite floors. Research on notch-connected mass timber panel-concrete composite floors is required to investigate effective measures to minimize the relative slip between two layers and enhance the composite efficiency and load-carrying capacity in the floor, and thus, increase the competitiveness and industry presence of mass timber panel-concrete composite floors.

1.2 Objectives and Tasks

The overall purpose of this thesis is to understand the structural performance of mass timber panel-concrete composite floors connected with notches and develop appropriate design provisions for designers and engineers to use. To achieve these objectives, the following tasks are pursued in this thesis:

(1) Conduct push-out tests on the notched connections to understand the mechanisms of notched connections in resisting the shear forces and investigate effective measures to

restrict the relative slip and prevent gap opening between timber and concrete in the notched connections. Develop design equations to estimate the connection stiffness, load-carrying capacity, and failure pattern.

(2) Conduct bending tests on the mass timber panel-concrete composite floors to understand the mechanisms of the composite floors under static bending. Evaluate the structural performance of composite floors affected by different geometry and connection design factors. Study effective measures to improve the composite efficiency in mass timber panel-concrete composite floors.

(3) Investigate the dynamic properties and dynamic performance of mass timber panel-concrete composite floors. Evaluate effects of the concrete layer and connection design on the dynamic properties of mass timber panel-concrete composite floors. Evaluate the validity of existing design criteria in designing the dynamic performance of mass timber panel-concrete composite floors.

(4) Develop a closed-form analytical solution for mass timber panel-concrete composite floors with notches to determine the internal actions and deflection at the serviceability limit state and load-carrying capacity and failure pattern at the ultimate limit state. Conduct parametric studies to optimize the geometries of the composite floors. Propose design guidelines for notched connections and notch-connected mass timber panel-concrete composite floors.

1.3 Limitations

The limitations of this thesis are stated as below:

(1) This thesis focuses on the structural performance of mass timber panel-concrete composite floors in simple support conditions under the positive bending moment. The structural behaviours of the composite floors under negative bending moments are not investigated adequately.

(2) Only the one-way behaviour of the composite floors is investigated and the tested composite floors could be simplified as beams due to the narrow width.

(3) Although the proposed reinforcing technique in the notched connections is effective in preventing the shear failure of concrete, the reinforcing technique is not yet practical to be widely used.
(4) Due to the narrow width of the tested composite floor specimens, the dynamic performance of the specimens cannot completely reflect the dynamic performance of composite floors in reality.
(5) In the proposed composite beam model, the gap opening and shear deformation in timber and concrete are not considered.
(6) The long-term performance, fire resistance, and acoustic performance of the composite floors are not discussed in the thesis.

1.4 Overview of the Thesis

The structure of the thesis is shown in Fig. 1.1. Following the introduction of Chapter 1, Chapter 2 summarizes the background of the subject in the thesis including the current research on engineered wood products and the limitations of bare timber floors, the existing research on timber-concrete composite floors and the connection systems, the characteristics of notched connections and the current research gap, and finally the existing composite beam models to describe the structural behaviour of timber-concrete composite floors and their restrictions.

Chapter 3 discusses the experimental investigations on the notched connection segments. The connections were fabricated in different configurations and tested under shear in the laboratory. The test results were compared with the push-out tests conducted by other researchers. Finite elements models were built to model the notched connections under shear. Based on the test results and finite element modeling, an empirical formula was proposed to estimate the notched connection stiffness. Finally, empirical equations were proposed to estimate the notched connection strength and were verified by the test results.

Chapter 4 discusses the bending tests and vibration tests on the full-scale timber-concrete composite floors. Phase 1 bending tests included nine floor specimens with different connection designs. Phase 2 bending tests included three floor specimens with reinforced notched connections. From the bending tests, the composite efficiency, load-carrying capacity, and failure pattern of the

floor specimens were investigated. The vibration tests were conducted on the floor specimens before the destructive bending tests to measure the dynamic properties of the floors including natural frequencies, damping ratios, and mode shapes, and evaluate the dynamic performance of the composite floors.

Chapter 5 presents a composite beam model that considered the discrete and semi-rigid features of notched connections. The composite beam model is verified by the existing analytical composite beam models and numerical composite beam models. Parametric studies were carried out to investigate the effects of geometric features of notched connections on the composite floor bending stiffness. Finally, the composite beam model is extended beyond the elastic stage to predict the ultimate strength and failure pattern of the timber-concrete composite floors, and the predictions were verified by the test results.

Chapters 6 and 7 present the main conclusions and an outlook for further research on the subject.

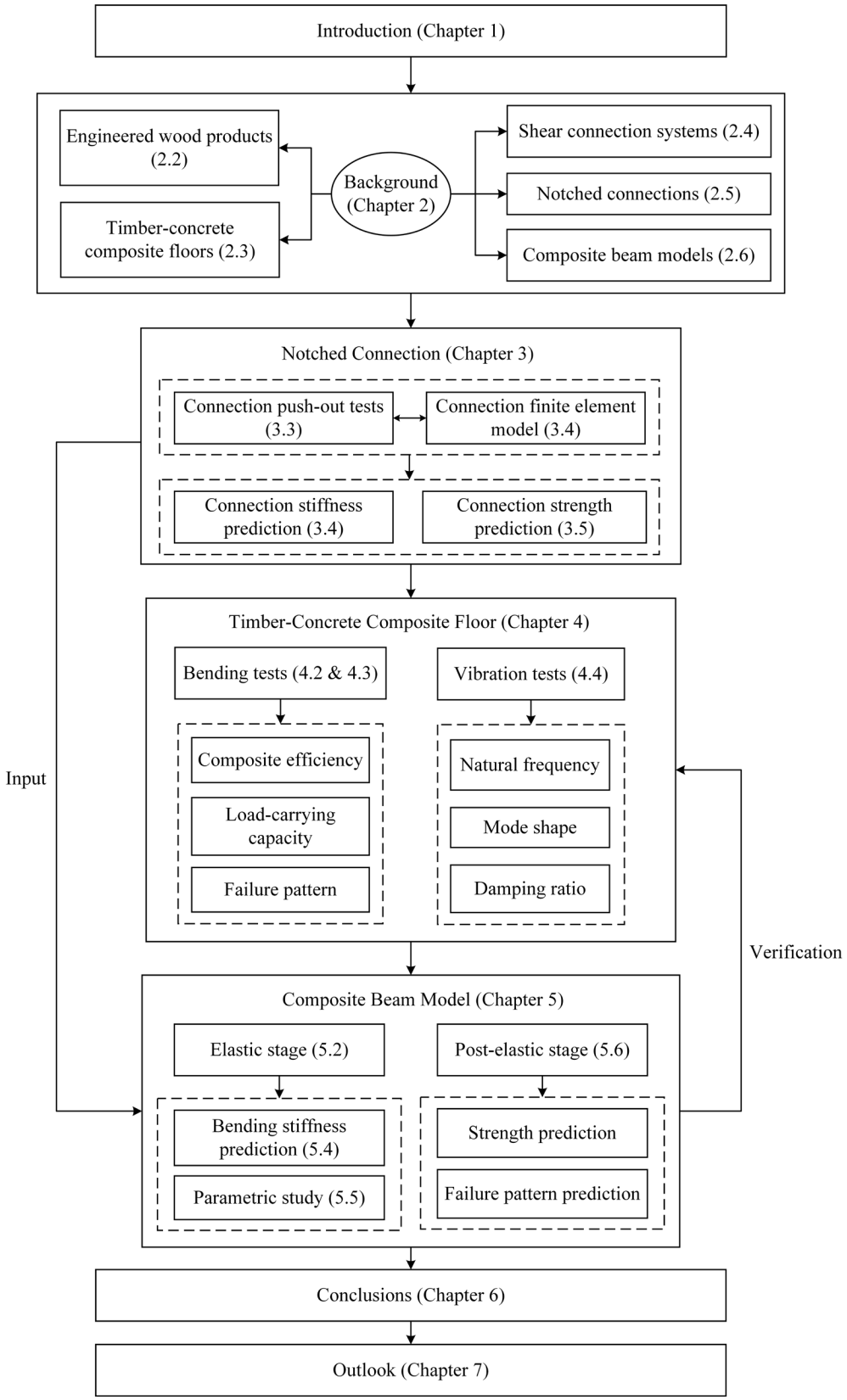

Fig. 1.1 Overview of the thesis

Chapter 2

Background

2.1 Introduction

This chapter introduces the background of the research on timber-concrete composite floors. The engineered wood products including their applicability and limitations are introduced first. And then, timber-concrete composite floor systems are introduced followed by the connection system in timber-concrete composite floors. A detailed discussion on the connections focuses on notched connections. Finally, the existing composite beam models for timber-concrete composite floor design are discussed.

2.2 Engineered Wood Products

Wood is one of the oldest building materials in human history. In North America, wood has been a primary building material before the availability of rolled steel and reinforced concrete. In recent years, wood has been experiencing a renaissance as a building material in the move towards a sustainable built environment. However, the dimensions of traditional wood products are restricted by small-diameter logs and the strength is impacted by the fast-growing plantation species. As a result, engineered wood products (EWP) are created to provide better and more predictable physical and mechanical properties than traditional wood products (Gong 2019).

In recent years, much attention has been paid to mass timber products due to the increased demands in using wood in mid- and high-rise buildings. Mass timber products are a family of engineered wood products that have large section sizes and great dimensional stability, offering the construction industry a viable alternative to steel and reinforced concrete (Harte 2017). Mass timber products can be lumber-based products such as glue-laminated timber (GLT or glulam), nail-laminated timber (NLT), dowel-laminated timber (DLT), and cross-laminated timber (CLT). Mass timber products can also be structural composite lumber (SCL) which is panel-like products manufactured with wood veneers or strands bonded together with adhesive, such as laminated

veneer lumber (LVL), laminated strand lumber (LSL), orientation strand lumber (OSL), and parallel strand lumber (PSL).

Mass timber products have a high strength-to-weight ratio, and the use of mass timber products results in reduced carbon emissions (Liang et al. 2020) and fast erections due to prefabrication. During a fire incident, the cross-sections of the mass timber products reduce at a predictable rate. Due to the large section size of mass timber products and the formation of a charring layer, the mass timber products have an inherent fire resistance (Harte 2017). Multistory buildings using mass timber products for primary structural elements are being planned and constructed globally. The product that has received the most attention in the past two decades is the cross-laminated timber, which consists of several layers of boards stacked crosswise (typically at 90 degrees) and glued together on the wide faces and, sometimes, on the narrow faces as well (CLT handbook 2019). Alternating layers of boards in CLT give the product a high level of in-plane stability and high strength in both directions, thus CLT is well-suited for walls, roofs, and floors. The adhesively or mechanically laminated linear elements with the grain of all laminations running parallel with the lengths of the member, such as glulam, GLT, NLT, and DLT, are also widely used in mass timber construction as floors, roofs, beams, and columns.

It is widely accepted that the use of engineered wood products leads to buildings with lighter weight, reduced carbon footprint, less embodied energy, and operating energy. However, the reduced weight can have a negative impact on the mass timber floor vibration behaviour (Higgins et al. 2017). Besides, bare mass timber floors are seldom used largely due to inadequate acoustic performance. To improve the floor acoustical performance, additional mass, noise barrier, or decoupler are needed in the floor assembly (McLain 2018). Concrete is often poured as the additional mass on top of timber floors to address the vibration and acoustic issues of mass timber floors. A compelling alternative is to use structurally composite timber-concrete floors which have shear connections between timber and concrete to create a composite action. The use of timber-concrete composites in long-span floors with heavy loads is attracting increasing attention from builders and designers (Clouston and Schreyer 2008). Research shows that the use of engineered wood products in construction has been increased due to the popularity of timber-concrete composite systems (Dias et al. 2016).

2.3 Timber-Concrete Composite Floors

A timber-concrete composite floor, or TCC floor, is a floor system that combines bottom timber elements and a top concrete layer through shear connections. TCC floors were initially developed to replace steel reinforcements in concrete with timber due to the shortage of steel in construction during the two world wars. Another incentive for the development of TCC floors was to use concrete to strengthen existing timber floors in some historical buildings (Dias et al. 2018a). Recently, TCC floors are gaining increasing interest in mass timber constructions due to the advances in engineered wood products and high-performance shear connections. The TCC floor system utilizes the best material properties of timber and concrete by letting concrete at the top mainly subjected to compression and timber at the bottom primarily subjected to tension.

Compared to the traditional reinforced concrete floors, TCC floors have reduced self-weight since the timber members in TCC floors replace the ineffective cracked zone in traditional reinforced concrete floors. The use of timber reduces carbon footprint in the floor construction and the reduced self-weight of TCC floors is beneficial in terms of lower seismic forces, smaller foundation requirements, and soil improvement measures. Compared to bare timber floors, the concrete layer in TCC floors improves both flexural stiffness and strength of the floor, thereby allowing a larger span to be achieved (Higgins et al. 2017). The addition of the concrete layer increases the thermal mass of the floor which can mitigate the temperature swings in the indoor environment. The sound transmission issue of the floor especially the airborne sound transmission is alleviated with the addition of concrete (Martins et al. 2015; Wymelenberg et al. 2019). The fire resistance rating of the floor is also enhanced as the concrete layer acts as a natural barrier against fire propagation. (Shephard et al. 2021). Moreover, due to the increased mass of TCC floors compared with bare timber floors, the floor is less susceptible to vibrations under serviceability conditions.

In the TCC floor systems, the concrete layer can be placed on top of the spaced timber beams such as glulam beams, LVL beams, or solid timber beams to form a ribbed ceiling system (T-beam type TCC system), as shown in Fig. 2.1(a). The concrete layer in TCC floors can also be placed on top of mass timber panels (MTPs) such as CLT, GLT, NLT, or DLT, to form a flat slab system, as shown in Fig. 2.1(b). The choice between the two floor systems is largely based on architectural needs. However, the T-beam type TCC floors are generally used in bridge construction, such as

the Vihantasalmi Bridge in Finland (Rantakokko and Salokangas 2000). Compared to the T-beam type TCC system, the MTP-concrete composite floor system can reach a larger span-to-total depth ratio thus is more suitable in floor construction where a clear height in each story needs to be maximized. In the T-beam type TCC floors, a plywood layer is often used between timber and concrete to act as the formwork of concrete. The mass timber panels in MTP-concrete composite floors can act as stay-in-place formwork for concrete and be exposed in the ceiling as the biophilic design. This thesis mainly focuses on the structural performance of MTP-concrete composite floors.

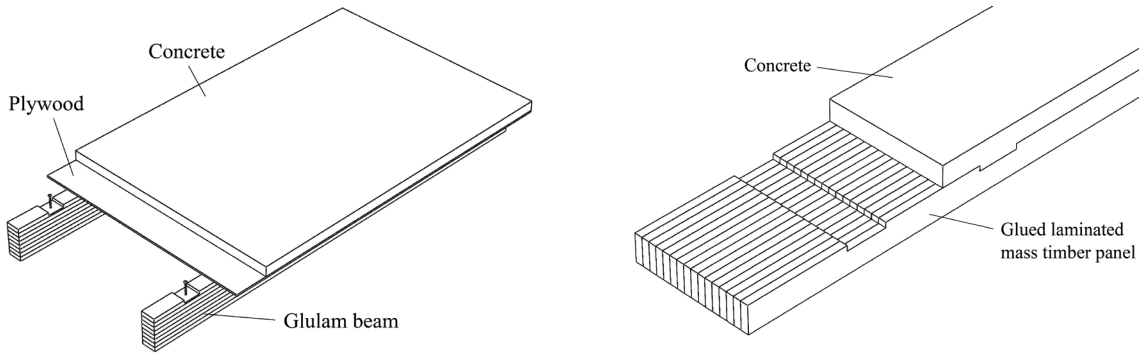

(a) T-beam type TCC floor system (b) MTP-concrete composite floor system

Fig. 2.1 Two types of timber-concrete composite floor systems

The shear connection system between timber and concrete has a major impact on both the bending stiffness and load-carrying capacity of composite floors. If timber and concrete are not connected, the relative slip between two layers is not restricted and timber and concrete act independently from each other. If shear connections are added between timber and concrete, the connections resist relative slip between timber and concrete and the composite action is thus generated. In the most ideal case, the interlayer slip is completely constrained by the connections and a plane section before bending remains plane after bending. Fig. 2.2 shows the strain profiles in TCC floors with different composite efficiencies. The non-composite floor has no interaction between two layers in the longitudinal direction and timber and concrete are only subjected to bending. The full composite floor is rigidly connected between timber and concrete which creates a system with the

highest structural efficiency and no relative slip between the two components. However, connections in reality are always flexible to some extent, thus only partial composite action can be achieved and the strain profile is not continuous at the interface. The timber and concrete in the full composite and partial composite floors are subjected to bending moments and axial forces.

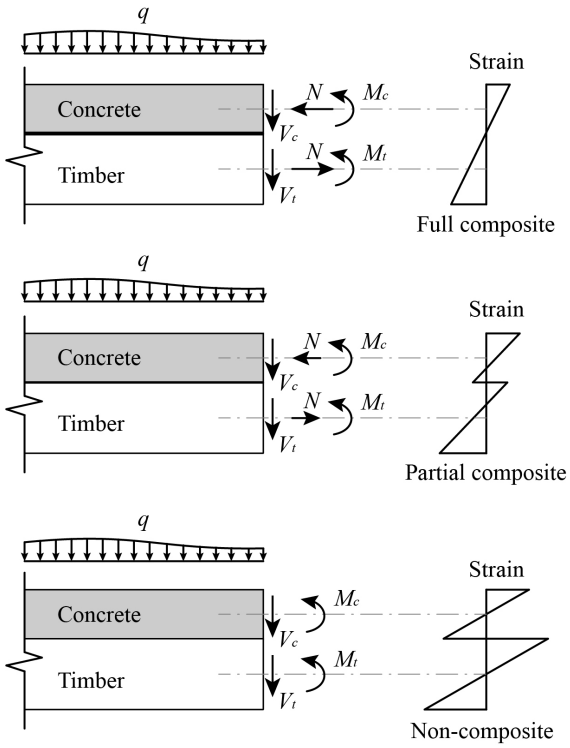

Fig. 2.2 Strain profiles in the cross-sections of timber-concrete composite floors with different composite efficiencies

In the past two decades, several TCC floors have been built in North America, such as the Earth Sciences Building at UBC and John W. Olver Design Building at UMASS Amherst, and several projects with TCC floors are under planning. In practice, however, the concrete layer is often added as a topping on the timber floors without shear connections. While the concrete topping can reduce the vibration and acoustic performance and increase the thermal mass of the floors, the benefits of the composite action are not fully exploited. Up to now, TCC floors are not widely used in North America. The main reason being the difficulty of joining timber and concrete together as well as the long-term performance of the composite floors. Since the mechanical properties of timber and

concrete are very different, it appears very difficult to obtain a harmonious marriage between the two materials. The hygro-thermal behaviours of the two materials are also very different which cause concerns about the long-term behaviour of the composite system (Ceccotti 2002). Other drawbacks of TCC floors being the difficulty of achieving complete prefabrication (Lukaszewska 2008), and the potential of increasing the cost in the floor construction due to the added construction time and cost to prepare and install the shear connectors. More research on TCC floors is required to improve the TCC floor performance and increase the competitiveness of TCC floors compared with traditional reinforced concrete and steel-concrete composite floors.

2.4 Shear Connection Systems

The structural efficiency of a TCC floor highly depends on the stiffness of the interlayer connections. The frictional bond between concrete and timber is often too weak to prevent the relative slip, thus shear connectors are needed to provide a composite action. The choice of the connection system is crucial to make the composite system both structurally efficient and economically competitive. Irrespective of which type of connection is to be used, the connection system must be strong and stiff enough to transfer the interlayer shear forces and provide effective composite action. A connection system that results in high composite action allows a significant reduction in the floor deflection and floor thickness (Yeoh et al. 2011b). However, almost all shear connections are semi-rigid to some extent and the relative slip between timber and concrete cannot be completely eliminated (Dias and Jorge 2011).

The behaviours of connections in the TCC floors vary from very stiff with low ductility to very flexible and ductile. The past few decades have seen numerous research efforts put into developing various connection systems for TCC floors. The dominant connection systems are mechanical fasteners such as self-tapping screws (Higgins et al. 2017; Mai et al. 2018; Mirdad and Chui 2019; Shephard et al. 2021), steel dowels (Dias et al. 2010), and steel mesh plates (HBV connectors) (Clouston and Schreyer 2008; Higgins et al. 2017). Continuous connection systems that rely on friction or adhesive have also gained some attention (Doehrer et al. 2006; Brunner et al. 2007; Negrão et al. 2010a; Negrão et al. 2010b; Tannert et al. 2020). Another type of commonly used connection is the discrete notch made by cutting grooves on timber and then filling them with concrete.

Direct gluing can provide near rigid composite action between timber and concrete. The shear forces generated in the interlayer are transmitted uniformly over the entire surface without local stress peaks (Negrão et al. 2010a, 2010b). The composite floor using this type of connection can be designed using the transformed section method. However, the drawbacks of adhesives are the brittle failure pattern under the shear load, the displacement of adhesive during concrete casting (Brunner et al. 2007), and the long-term performance of the adhesive. To address these issues, the adhesive can be combined with mechanical fasteners such as screws which act as the backup system for the potential failure of the adhesive (Tannert et al. 2020). So far, the adhesive connectors have been mainly tested in the laboratory but rarely used in practice.

A vast majority of the studies have been focused on dowel-type fasteners (Dias et al. 2010). Dowel-type fasteners such as screws, dowels, and rebar are characterized by a load transmission mechanism predominantly in bending and shear of steel dowels. The screws such as the self-tapping screws (Higgins et al. 2017; Mai et al. 2018; Mirdad and Chui 2019; Shephard et al. 2021) or coach screws (Tao et al. 2021) are the most used fasteners due to their high axial load-bearing capacity. The self-tapping screws can be made deconstructable (Derikvand and Fink 2021) to reuse the concrete and timber members after the floor disassembly. Most of the dowel-type fasteners have a flexible behaviour under the shear load, thus a large number of connectors are needed to achieve the required composite action in the floor. The mechanical properties of the screw fasteners can be improved by inclining the screws to 45° to subject them primarily to axial force instead of shear (Steinberg et al. 2003).

It is possible to use solely natural bond between timber and concrete to create a composite floor system without additional connectors. The connection systems relying on friction are achieved by making the timber panels teethed or cutting small notches on the timber panels to increase the contact area between timber and concrete. The shear forces are transferred by natural wood-to-concrete bond and friction on the rough surface between timber and concrete (Döhrer 2006). There are also a large number of proprietary connection systems developed for TCC floors. One type of widely used proprietary connection system is the HBV shear connector (TiComTec 2014). The HBV shear connectors consist of thin metal mesh that is half glued in timber and half embedded into the concrete. The HBV connectors can be installed continuously along the span and can accommodate a rigid insulation layer between timber and concrete. The composite action provided

by the HBV shear connectors is near rigid. Other types of shear connections in TCC floors can be found in Deam et al. (2008), Lukaszewska et al. (2008), and Marchi and Pozza (2021).

The choice of the connection system in MTP-concrete composite floors depends on the mechanical performance, cost, and constructability of the connections. Dowel-type fasteners are usually flexible under shear forces while steel meshes, adhesives, and notches are relatively stiff (Dias and Jorge 2011; Yeoh et al. 2011b). In terms of cost, proprietary connections are often expensive and labor-intensive to install during floor construction. Notched connections, on the other hand, can be cost-effective by pre-cutting notches before the shipment of panels to the site. The notched connections are introduced in detail in the next section.

2.5 Notched Connections

The notched connections are made by cutting or drilling grooves on timber and then filling them with concrete. Similar connection configurations can be found in timber structures such as halved and tabled timber scarf joints (Aira et al. 2015a, 2015b), or reinforced concrete structures such as the shear keys in precast segmental bridges (Shamass et al. 2015). Since the connection stiffness and strength of notched connections are much higher than traditional dowel-type fasteners, the notched connections are often classified as one of the most structurally efficient and cost-saving connecting solutions in MTP-concrete composite floors. The high stiffness of notched connections arises from the compressive contact of timber and concrete at the load-bearing surface. The high stiffness of notched connections provides high composite action between timber and concrete in the composite floors. Although the notches are often reinforced with steel fasteners such as self-tapping screws or coach screws (Yeoh et al. 2011a) to prevent the uplifting of concrete, the total number of steel fasteners used is far less than the floors connected with steel fasteners only. Moreover, the notches are often pre-cut in the manufacturing facility of panel suppliers, often with a high-precision computer numerical control (CNC) machine, before the panels are sent to the site. This allows for a faster erection of floors and a reduced cost on the connections compared with steel fasteners such as self-tapping screws or steel mesh plates.

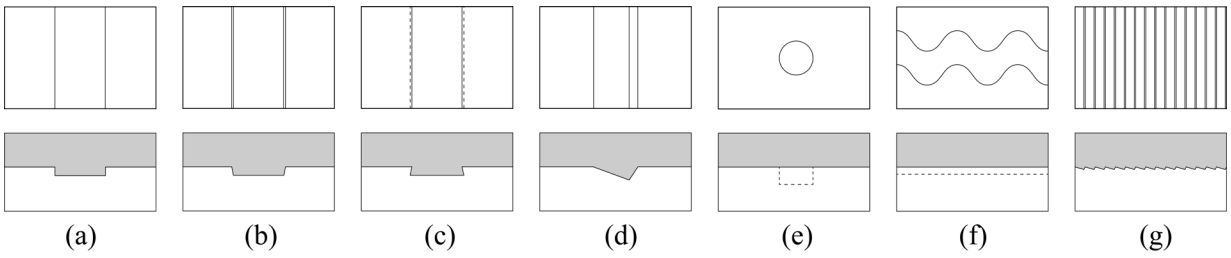

Fig. 2.3 Different shapes of notches cut on the timber (a) rectangular notch; (b) trapezoidal notch; (c) inverse trapezoidal notch; (d) triangular notch; (e) round notch; (f) notch curve; and (g) micro notches.

The structural behaviour and failure modes of the composite systems are strongly affected by the geometry of notched connections and material properties of timber and concrete. Depending on the design of notches in the composite floor system, the floor can be almost fully rigid (Müller and Frangi 2018) or partially composite (Gutkowski et al. 2008). In notched connections, grooves cut on the timber can be isolated rectangular (Jiang and Crocetti 2019; Zhang et al. 2020), trapezoidal (Gutkowski et al. 2008), inverse trapezoidal (Ouch et al. 2021), triangular (Yeoh et al. 2011a, 2011c), and round shapes (Auclair et al. 2016). The notches can also be made continuous such as notch waves (Boccadoro and Frangi 2014) and jagged micro-notches (Müller and Frangi 2018), as shown in Fig. 2.3. To date, the prevalent notch shapes are rectangular and trapezoidal, while other notch shapes are less common. The trapezoidal notches can alleviate the stress concentration effect around the notched corners. However, the connection stiffness of trapezoidal notches is often lower than the rectangular notches. The connection stiffness of trapezoidal notches measured by Gutkowski et al. (2004) was less than 300 kN/mm (per metre width) which was lower than the connection stiffness of rectangular notches. The inverse trapezoidal notch can resist the uplifting of concrete. However, due to the stress concentration and low tensile strength of concrete, the concrete notch has to be reinforced with additional reinforcements to prevent concrete shear failure (Ouch et al. 2021). The triangular notches are less stiff than rectangular notches but have the advantage of easier and faster construction (Yeoh et al. 2011a). Auclair et al. (2016) tested round notches made of ultra-high performance fiber-reinforced concrete (UHPFRC) with steel cylindrical core in T-beam type TCC floors. The connections exhibited ductile behaviour due to the steel core. Boccadoro and Frangi (2014) tested the continuous notch curves and found that the

notch curves were less efficient than the discrete rectangular notches. Müller and Frangi (2018) tested timber-concrete composite slabs with micro-notches and found that the composite action in the composite floors with micro notches was comparable to a full composite floor.

As discussed previously, the notched connections resist shear forces in the tangential direction through the interlocking effect. In addition, steel fasteners are often used in the notched connections as additional reinforcement to prevent the uplifting of concrete under shear forces and gap opening due to the shrinkage of concrete and drying of wood. Fig. 2.4 demonstrates several reinforcing techniques in the notched connections that have been investigated by researchers. The most common reinforcing technique is to use vertical screws, either self-tapping screws or coach screws, inside the notch (Yeoh et al. 2011a; Yeoh et al. 2011c; Zhang et al. 2020) or in timber in front of the notch (Kudla et al. 2016), as shown in Fig. 2.4(a) and (b). Fig. 2.4(c) shows the concrete part in the notched connection is reinforced with the double head steel dowels (Schnell et al. 2016; Boccadoro et al. 2017a). The bottom of the steel dowel is fastened to timber using screws while the top of the steelhead act as an anchor in the concrete. Another way to reinforce the notched connections is to use post-tensioned steel dowels (Gutkowski et al. 2008; LeBorgne and Gutkowski 2010), as shown in Fig. 2.4(d). The dowels are embedded into wood with adhesive. A plastic sleeve around the shank of the dowel is embedded within concrete to prevent the attachment of concrete to the dowel. After the concrete is hardened, torque can be applied to the dowels to eliminate the gap formed between timber and concrete. Fig. 2.4(e) shows a similar concept to tighten timber and concrete using end-to-end steel rods which are installed by drilling holes in wood and the hardened concrete (Boccadoro et al. 2017a). The concrete protrusion in the notched connections can also be strengthened by steel rebar as shown in Fig. 2.4(f) where the longitudinal steel rebar in the concrete layer is bent in the notched regions (Schnell et al. 2016). Other reinforcing techniques in the notches can be found in Khelil et al. (2019) and Ouch et al. (2021).

Depending on the number and size of steel fasteners used in the notched connections, the above-mentioned steel fasteners can contribute to the shear stiffness, strength, and ductility of notched connections or have little effect on the connection shear capacity and only physically connect timber and concrete in the vertical direction. The self-tapping screws can prevent the separation of timber and concrete but are less effective in preventing gap opening and crack development in

concrete. In terms of the double head steel dowels and bent steel rebar, the gap opening between timber and concrete is not addressed. The bent steel rebar also has an anchorage issue as the development length is hardly enough in the often-shallow notches. While the end-to-end rods are efficient in restricting the gap opening between timber and concrete, it is not yet suitable to be employed in practice. Similarly, the post-tensioned dowels are complicated to install, and the dowels are not always available. To date, there is no standard technique to reinforce the notches that can prevent concrete uplifting and crack enlargement at the same time. A structurally efficient yet economic reinforcing solution is needed to restrict the gap opening and crack enlargement in concrete.

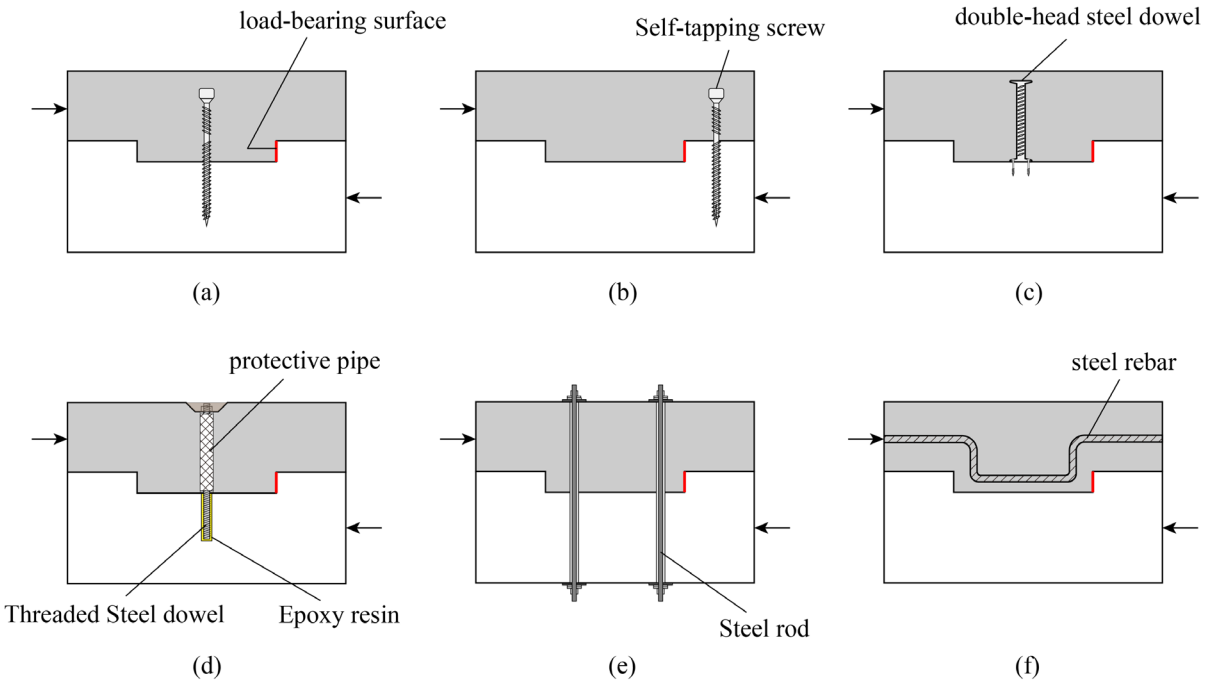

Fig. 2.4 Reinforcing techniques in notched connections

Although the notched connections have been successfully used as shear connectors in MTP-concrete composite floors, such as timber-concrete composite floors in HoHo Wien and Legero United Campus in Austria, the design of notched connections is not standardized and the use of notched connections in MTP-concrete composite floors is hindered by the lack of design guidelines. The COST Action FP 1402/WG 4 report (Dias et al. 2018a) recommended that the depth of notches

should be no less than 20 mm in building applications, the length of notches should be no less than 150 mm, and the timber shear length in front of the notch should be no less than 8 times of the notch depth. The requirements for the material properties of timber, concrete, and axial fasteners are also included in the COST Action report (Dias et al. 2018a). Similar recommendations can be found in Schönborn et al. (2011). The COST Action FP 1402/WG 4 report (Dias et al. 2018a) further recommended using 1000 kN/mm (per metre width) as the connection stiffness for notches with a depth between 20 and 30 mm, and 1500 kN/mm (per metre width) for notches deeper than 30 mm. The suggested connection stiffness can generally be achieved in the push-out tests on the notched connections. However, research shows that the stiffness of the notched connections in MTP-concrete composite floors can be much lower than the measured stiffness from the connection push-out tests (Kudla 2017). In addition to the existing guidelines about the geometry of notches and minimal connection spacing, other considerations such as the minimal number of notched connections required in the floor, optimal connection spacing to achieve the maximum composite efficiency, and maximum notch depth that does not reduce the timber bending capacity should also be considered in the notched connection design. Moreover, there are no well-accepted design equations to predict the stiffness and ultimate strength of notched connections under shear. More research on notch-connected MTP-concrete composite floors is required to investigate effective measures that can minimize the relative slip between two components and enhance the composite efficiency and load-carrying capacity of MTP-concrete composite floors.

2.6 Composite Beam Theories

The shear forces in the interlayer between timber and concrete in the TCC floors transmit in different ways when different connections are used. For the floor systems connected with adhesive or continuous steel mesh plates, the shear forces are transmitted uniformly along the floor without any breaks. When the connections are discrete but closely spaced such as dowel-type fasteners, the bond between timber and concrete is often treated as continuous by smearing the connection stiffness along the floor axis. The approximation using smeared stiffness is often sufficiently accurate in construction practice and has an essential importance in the application. Most of the composite beam models proposed to date dealt with the continuous bond between two layers. The well-known Newmark's model (1951) was developed for beams consisting of two interacting

elements with a continuous incomplete connection. A general-purpose differential equation was derived in the model by employing Euler-Bernoulli's beam theory. Since then, exact analytical solutions for the continuously bonded beams with partial interaction in different boundary and loading conditions have been derived by several authors (Oven et al. 1997; Girhammar and Pan 2007; Schnabl et al. 2007; Focacci et al. 2015). In many instances, the continuous bond models involve solving several governing differential equations to determine deflection and internal actions, which may become tedious if complex loading or boundary conditions need to be considered.

For TCC floors, the only design method that has been included in design standards is the method given in Eurocode 5 (CEN 2014), which is based on what is commonly known as the gamma method (γ-method). The gamma method was developed from the model originally proposed by Möhler (1956) for timber-timber composite beams with semi-rigid connections. Later, Linden (1999) developed the same solution with gamma (γ) expressed in a different form. The gamma method assumes a simply supported beam subjected to a sinusoidal distributed load with a deflection also in a sinusoidal shape. By assuming a uniform interaction between timber and concrete, an effective bending stiffness of the beam can be introduced to account for the semi-rigidity of the shear connections, as shown in Eq. 2.1 (CEN 2014).

$$(EI)_{eff} = E_c I_c + E_t I_t + \gamma E_c A_c a_1^2 + E_t A_t a_2^2 \tag{2.1}$$

In Eq. 2.1, E, I, and A represent Young's modulus, second moment of area, and cross-section area, respectively; and subscripts c and t represent concrete and timber, respectively; gamma (γ) is a parameter indicating the effectiveness of the composite action. Gamma (γ) is determined from Eq. 2.2 which is confined between zero for no composite action to 1 for fully composite action (CEN 2014).

$$\gamma = \frac{1}{1+\frac{\pi^2 E_C A_C s}{kL^2}} \tag{2.2}$$

In Eq. 2.2, s is the connection spacing, k is the connection stiffness, and L is the floor span. The inner lever arms a_1 and a_2 in Eq. 2.1 are the distances from the centroids of concrete and timber to the neutral axis of timber, respectively, as shown in Fig. 2.5 (CEN 2014).

$$a_2 = \frac{\gamma E_c A_c (h_c + h_t)}{2(\gamma E_c A_c + E_t A_t)} \tag{2.3}$$

$$a_1 = \frac{h_c + h_t}{2} - a_2 \tag{2.4}$$

In equations 2.3 and 2.4, h_c and h_t are the heights of concrete and timber, respectively.

The simplified method (γ-method) is widely used for TCC floor design and is particularly accurate for predicting the structural performance of the composite floor when all materials remain linear-elastic (Yeoh et al. 2011b). This simplified method, however, has some limitations in its application:

(1) The connection stiffness between timber and concrete is assumed to be continuous and uniform, which is valid for connectors such as adhesives and continuous steel mesh plates, or equally and closely spaced steel fasteners. But for discrete connections that are widely spaced, this assumption can lead to unacceptable errors.

(2) The method assumes a simply supported beam subjected to a sinusoidal distributed load with a deflection also in the sinusoidal shape. For other supporting conditions and loading forms, the method can provide non-conservative predictions.

(3) This method is based on the theory of linear elasticity, cracking of concrete and plasticity of connections are thus not taken into account.

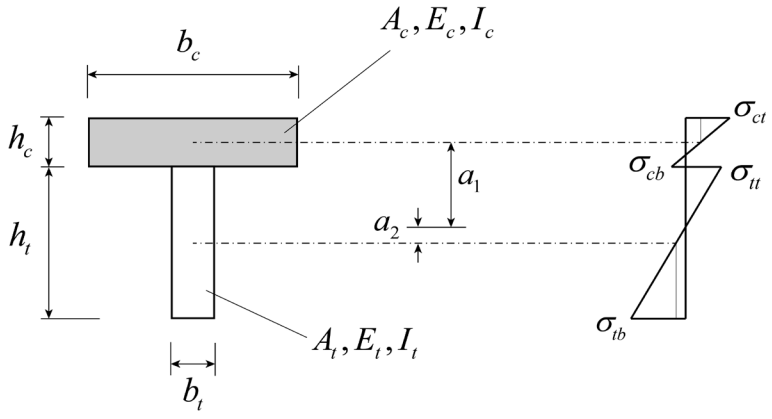

Fig. 2.5 Cross-section of the TCC floor (left) and distribution of bending stresses (right)

Parallel to the Gamma method, Girhammar (2009) developed a simplified analysis method for composite beams with interlayer slip in several common boundary conditions, such as cantilever, simply supported, propped, and built-in. Similarly, in this approximate method, the deflection and internal actions of the beam are predicted by the effective bending stiffness, but the actual beam span is replaced by the effective beam span which is dependent on the boundary conditions.

Despite the wide acceptance of continuous bond models, when the notched connections are used in the TCC system to connect two layers, the shear forces are only transmitted at discrete locations and the spacing of notches is usually too large to assume the connections as continuous. Grosse et al. (2003a, 2003b) suggested that the distance of discrete connectors should not exceed 3% of the beam span if a continuous bond is assumed. The continuous bond models also presume a constant slip modulus between two components, but in practice, the connections are not necessarily spaced uniformly. Although Eurocode 5 (2014) provides a modified equation when the connections are spaced according to the shear force, the equation has been found to be inaccurate in some cases (Auclair 2020).

To date, only limited composite beam models have been proposed to consider the effect of discrete connections. Byfield (2002) adopted a novel release-and-restore method to solve the steel-concrete composite beam with breaks in the shear connection at the interface. However, the model assumes a rigid behaviour of connections that does not permit relative slip at connecting locations. A similar assumption was found in the laminated beam model proposed by Clark (1953). The common types of shear connections for TCC floors, including notches, undergo deformation under the shear load. Thus, the models of Byfield (2002) and Clark (1953) can only be regarded as the upper bound for the composite behaviour. Zhang and Gauvreau (2015) proposed an elasto-plastic model for predicting the load-deflection relation for TCC beams connected with discrete ductile connections based on the work of Tommola and Jutila (2001). In their model, the connections yield progressively under the shear load which causes the nonlinear behaviour of the composite system. This method, however, was developed only for simply supported beams with identical connections that are symmetrically arranged about the mid-span. Fernandez-Cabo et al. (2013) extended the method to consider composite timber beams with arbitrary connection stiffness and locations. However, as the flexibility matrix is obtained for the whole beam, that method cannot easily be adapted to complex boundary conditions. Frangi and Fontana (2003) proposed an elasto-plastic

model for TCC floors with ductile connections to predict the ultimate strengths of the composite floors. However, in their model, the connections are assumed to be rigid-perfectly plastic which can lead to overestimations of the floor bending stiffness under serviceability limit states.

In addition to the closed-form analytical solutions, numerical or hybrid models have also been developed for TCC floors with discrete connections. Grosse et al. (2003a, 2003b) proposed a framework model for timber-concrete composite beams connected with notches. The timber and concrete components are modeled with beam elements located at the centroids of each layer. The beam elements are coupled with hinged compression struts that have infinite axial stiffness so timber and concrete can have the same displacement vertically. The discrete connections between timber and concrete are modeled by cantilevers hinged together at the location of the interlayer, as shown in Fig. 2.6. The bending stiffness of the cantilevers can be adjusted to attain the same rigidity as the actual shear connections according to

$$(EI)_{ca} = \frac{k}{3}(e_1^3 + e_2^3) \tag{2.5}$$

where k is the shear stiffness of the original connection, and e_1 and e_2 are the distances between the centroids of concrete and timber to the interface, respectively. The framework model is relatively easy to implement in software and is capable of modeling TCC floors under any loading cases in any supporting conditions. The locally transferred shear forces can be simulated accurately in the model, and the internal forces and deflection could readily be determined. This model is often used as an alternative to the Gamma method when the connectors are widely spaced. However, the framework model is not an analytical model but has to rely on structural analysis software.

Nguyen et al. (2010, 2011a, 2011b) proposed hybrid numerical-analytical models for the composite beams in different scenarios, such as discrete or continuous shear connections, shear deformable or non-deformable components, and short- or long-term deflections. Their hybrid models employed exact finite elements for the composite beams which are built from rigorous analytical solutions. From the analytical expressions for the displacement and force fields, the space-exact stiffness matrix for a generic two-layer beam element can be deduced, which can be incorporated in any displacement-based finite element code for the linear static analysis of two-layer beams with interlayer slip and arbitrary loading and supporting conditions. The model can

further incorporate the time-discretized solution to consider the time effects such as creep and shrinkage of the concrete slab.

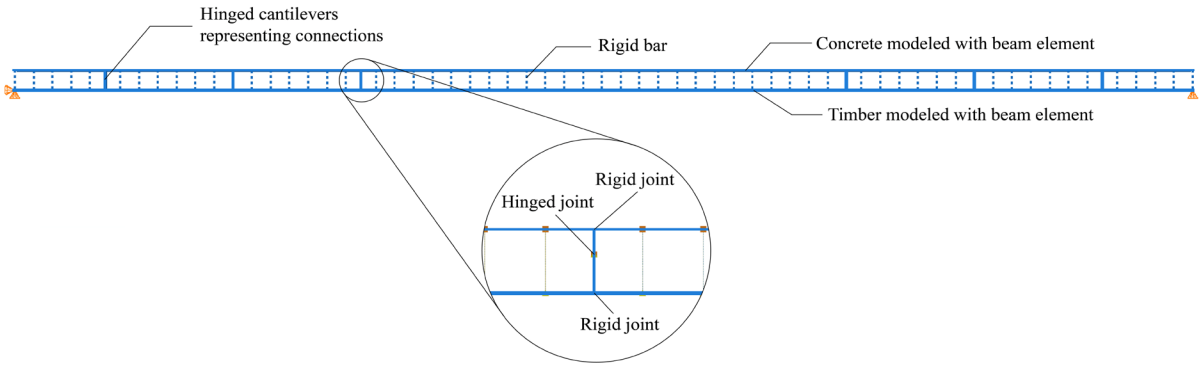

(a) Framework model

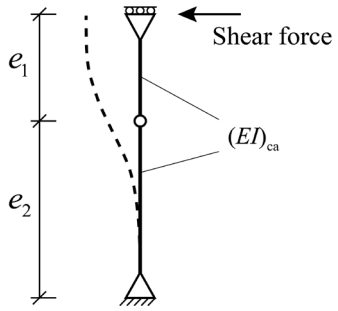

(b) Hinged cantilevers mimicking shear connections

Fig. 2.6 Framework model to model timber-concrete composite floors with notches

The above-mentioned composite beam models are either restricted in application due to the boundary conditions, loading conditions, and connection locations, or can only be implemented in a structural analysis software or finite element software. Furthermore, most of the composite beam models are restricted in the linear elastic stage without considering the damage or nonlinearity of material behaviours and the plasticity of connections at the ultimate limit states. The design of TCC floors can be governed by the ultimate strength limits of timber, concrete, or connections, or the deflection and vibration criteria at the serviceability limit states. For TCC floors with notched connections, a theoretically correct and practically sound analytical model is desired to accurately predict the deflection and internal forces in the floors.

2.7 Summary

The need for green and sustainable architecture motivated the increasing use of mass timber products as a “green” alternative to steel and concrete in mid- and high-rise buildings. The combination of timber and concrete through connections presents a promising solution to address the inadequate serviceability performance of bare timber floors such as vibration and acoustic problems. Notched connections in timber-concrete composite floors have the potential to reduce the total cost, accelerate the construction, and enhance the structural performance of composite floors compared with commonly used dowel-type fasteners. To increase the competitiveness of notch-connected timber-concrete composite floors, more research is needed to standardize the notched connection design and provide design guidelines for engineers and designers. The structural performance of timber-concrete composite floors with notches under the serviceability limit states and ultimate limit states need to be thoroughly evaluated. Additionally, an analytical composite beam model that takes into account the discrete and flexible features of notched connections in timber-concrete composite floors is desired to accurately determine the internal actions in the composite floors thus reliably predict the floor bending stiffness and ultimate strength. This thesis aims at addressing the above-mentioned research gaps.

Chapter 3

Notched Connections under Shear

3.1 Introduction

The structural performance of MTP-concrete composite floors is affected by the supporting conditions, floor span, material properties of timber and concrete, and most importantly, the shear connection system. The mechanical performance of notched connections in MTP-concrete composite floors affects the composite floor bending stiffness, ultimate load-carrying capacity, and floor failure pattern under bending. As the first stage of the research work on notch-connected MTP-concrete composite floor systems, the structural performance of notched connections under shear is investigated first. In this chapter, the general behaviour of notched connections under shear is introduced first followed by the description of push-out tests on notched connections. The push-out tests were conducted on ten different notched connection configurations. Based on the connection shear test results and finite element modeling, an empirical formula is proposed to estimate the notched connection shear stiffness. In the end, empirical equations are proposed to estimate the ultimate strengths of notched connections under shear, and the predicted results are validated by the test results.

3.2 Performance of Notched Connections under Shear

Among different connection systems in MTP-concrete composite floors, notches are considered as one of the most structurally efficient connecting solutions due to their high stiffness, high strength, and ease of fabrication (Yeoh et al. 2011b). The notched connections are often made by cutting grooves on timber and then filling them with concrete, although the notches can also be made by gluing timber blocks on the timer members (Monteiro et al. 2013). The notches can be made in different shapes, but previous research has shown that rectangular notches are the simplest and most efficient notch shape (Boccadoro and Frangi 2014). As shown in Fig. 3.1, the geometry of a rectangular notch is defined by the notch length l_{nw}, notch depth d_{nc}, and timber shear length

l_{ts} in front of the notch. Rounded corners can be made in the notches to alleviate the stress concentration effect (Dias et al. 2016).

The high stiffness of the notched connections under the shear load arises from the compression contact of timber and concrete at the bearing surface. While the connections can provide high slip resistance in the tangential direction along the floor span, the resistance of notches in the normal direction is low and can cause gap opening or uplifting of concrete under the shear force. Thus the notches often have additional steel fasteners installed such as self-tapping screws to prevent the uplifting of concrete. The total number of steel fasteners used to reinforce the notched connections is far less than the floors connected with steel fasteners only.

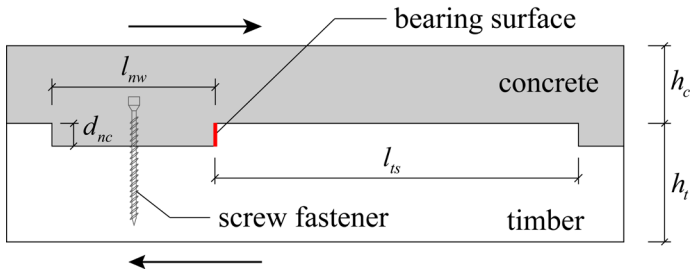

Fig. 3.1 Notched connection geometry (l_{nw}: notch length; d_{nc}: notch depth; l_{ts}: timber shear length; h_c: concrete thickness; and h_t: timber thickness)

Under the shear load, the possible failure modes of the notched connections are shown in Fig. 3.2. The shear forces resisted by the notched connections cause local stress peaks in concrete and timber around the notched corners. As a result, the failure pattern of the connection under shear is often brittle. Due to the low tensile strength of concrete, the concrete crack around the notched corner is usually developed under the serviceability load level. With the further increase of the shear force, the possible failure modes of the notched connections can be the concrete shear failure due to crack propagation, local concrete crushing at the load-bearing area, local timber crushing at the load-bearing area, and timber shear failure in front of the notch (Schönborn et al. 2011). The most desirable failure pattern of the connections is the timber crushing failure which is ductile due to the local buckling of wood fibers. The rest of the failure modes are brittle and should be prevented. The compressive crushing of concrete can be prevented by choosing a concrete strength

class that is higher than timber. The timber shear failure can be prevented by leaving enough space between notches. According to COST Action FP1402 / WG 4 (Dias et al. 2018b), the timber shear length between adjacent notches should be at least eight times of the notch depth. The shear failure of concrete due to shear crack propagation can be difficult to prevent especially in deep notches where the ductile failure of timber is difficult to trigger. COST Action FP1402 / WG 4 (Dias et al. 2018) recommended the notch length should be no less than 150 mm. In addition, steel fasteners can be installed in the notches to restrict the shear crack propagation in concrete.

It is desirable to maintain enough connection stiffness and load-carrying capacity while achieving the ductile failure pattern in the notches. The notched connection serviceability performance, ultimate strength, and failure pattern are affected by the connection geometry, material properties of timber and concrete, and additional steel reinforcements. These factors are investigated through the connection push-out tests which are discussed in the following Section 3.3 and composite floor bending tests which will be discussed in Chapter 4.

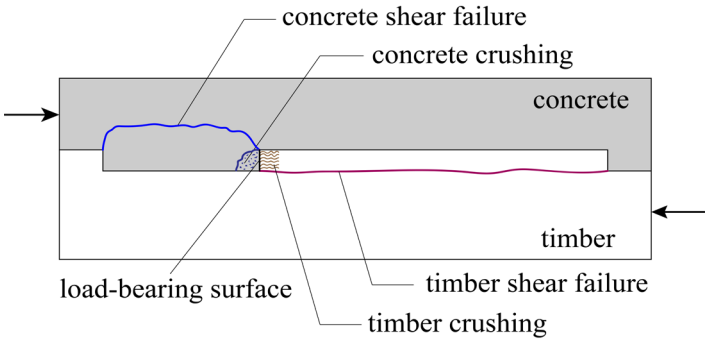

Fig. 3.2 Four possible failure modes of notched connections under shear

3.3 Push-out Tests on Notched Connections

3.3.1 Introduction

This section introduces the experimental investigation on notched connections in MTP-concrete composite floors. The notched connections were constructed with GLT, normal strength concrete, and self-tapping screws. Push-out tests were conducted on ten types and a total of 60 specimens of notched connections to compare their slip stiffness, load-carrying capacity, and failure modes.

The main purpose of the push-out tests is to investigate some important factors that affect the structural performance of notched connections under shear, including the geometry of connections, presence of steel fasteners in the notch, and timber orientation. Results from the connection shear tests serve as an important reference for the next step of the research work on MTP-concrete composite floor systems.

3.3.2 Specimen Design

As discussed previously, rectangular notches are the most common and efficient notched connections. Thus, only rectangular notches were constructed and tested in the push-out tests. A total of ten configurations of notched connections were fabricated and each configuration had six repetitions, as shown in Table 3.1. Among different configurations, seven were made with the connection axis aligned with the timber longitudinal direction (referred to as "L") and three were made with the connection axis aligned with the timber transverse direction (referred to as "T"), as shown in Fig. 3.3. The width of the specimens was 200 mm but the bottom of the timber had additional wings for the purpose of clamping the timber down during the test. The heights of timber and concrete were 130 mm and 100 mm, respectively. Except for the timber orientation, the variations between specimens were the notch depth, timber shear length, and the existence and locations of self-tapping screws in the connections. The geometry properties of specimens are summarized in Table 3.1 where the specimens were labeled with the direction of timber, notch depth, timber length in front of the notch, and position of self-tapping screws. For example, L-25-250 represents the specimen in the longitudinal direction with a notch depth of 25 mm and a timber shear length of 250 mm.

For the longitudinal specimens, the length of notches was 150 mm, which is the minimum notch length suggested by Dias et al. (2018a). The depth of notches varied between 10 mm to 40 mm, while the length of timber in front of the notch varied between 150 mm to 350 mm. The ratio of timber shear length to the notch depth varied between 6 to 25, with the smallest ratio residing in specimen L-25-150 and the largest ratio residing in specimen L-10-250. Specimen L-25-250 was designed as the reference case.

Compared to the longitudinal specimens, the transverse specimens had shorter notch length (110 mm) and timber shear length (180 mm) due to the restrictions of the timber size. The depth of notches in the transverse specimens was 25 mm. The transverse specimens had the same dimensions, the only difference being the existence and positions of screws.

Table 3.1 Notched connection specimen design

Specimen	Timber orientation	Notched depth (mm)	Notch length (mm)	Timber shear length (mm)	Screws
T-25-180	Transverse	25	110	180	None
T-25-180-N	Transverse	25	110	180	in the notch
T-25-180-T	Transverse	25	110	180	in the timber
L-25-250	Longitudinal	25	150	250	None
L-10-250	Longitudinal	10	150	250	None
L-40-250	Longitudinal	40	150	250	None
L-25-150	Longitudinal	25	150	150	None
L-25-350	Longitudinal	25	150	350	None
L-25-250-N	Longitudinal	25	150	250	in the notch
L-25-250-T	Longitudinal	25	150	250	in the timber

Among ten types of notched connections, four types had self-tapping screws installed in the connections to strengthen the connections under the shear load. In these connections, two screws at a spacing of 100 mm were installed into the timber. The specimens with “N” in the label had screws inserted into notch at a location of 30 mm away from the load-bearing surface. The screws installed in the notch were to restrict the crack enlargement of concrete under the shear load. The specimens with “T” at the end of the label had screws inserted into timber in front of the notch to prevent the shear failure of timber. The positions and embedment depth of screws into timber are shown in Fig. 3.3(c) and (d).

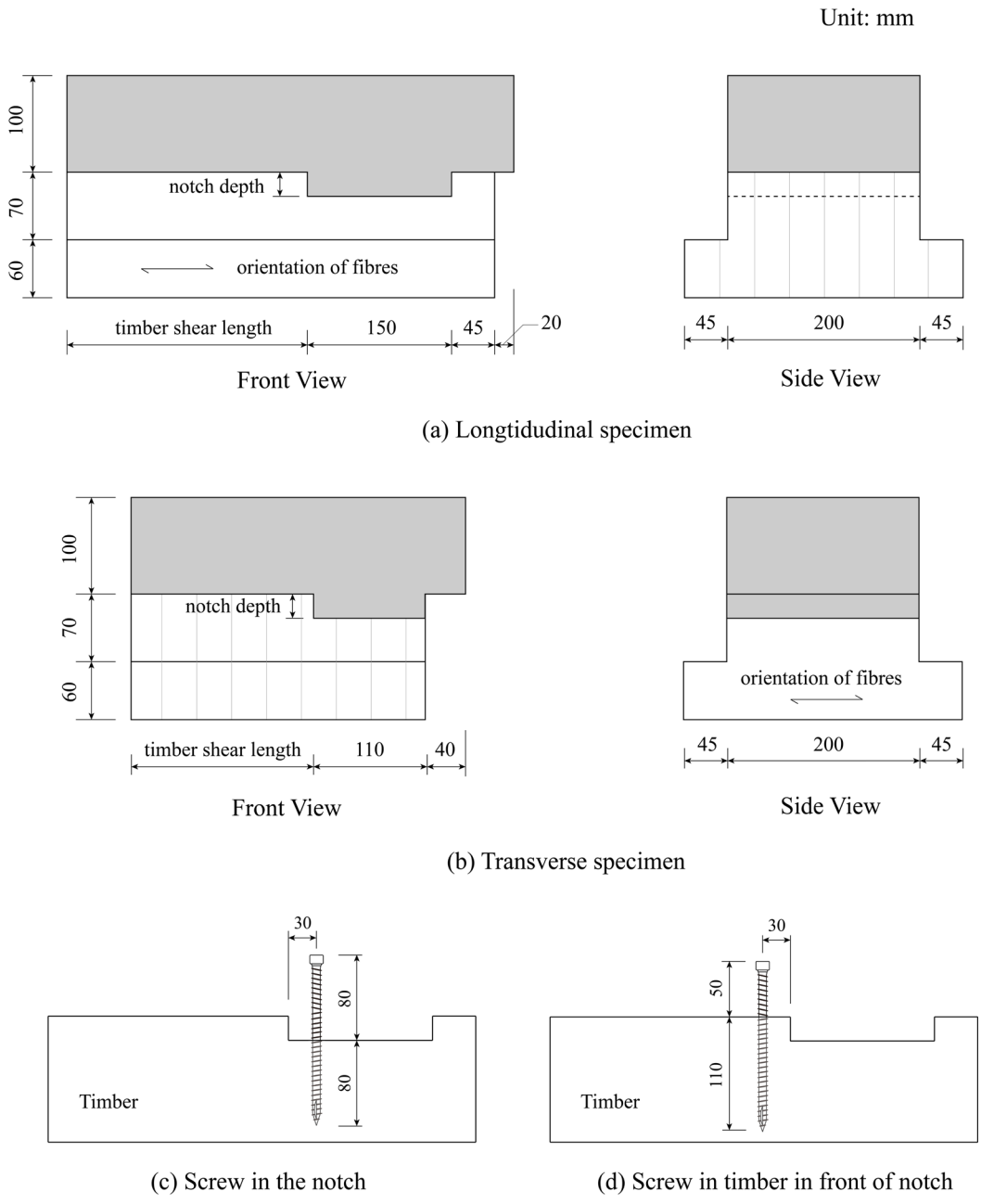

Fig. 3.3 Configurations of notched connection specimens in the longitudinal and transverse directions and locations of self-tapping screws in the notch

3.3.3 Materials

Glued laminated timber (GLT) manufactured with No. 2 or better grade spruce-pine-fir (SPF) lumber from western Canada was used in the fabrication of the specimens. The thickness of one

layer of lamination in GLT was 38 mm and the glue used to make GLT was melamine formaldehyde. The notches on timber were cut using a circular saw blade in the laboratory. The moisture content of timber measured immediately after the test was 8.5%. To measure the material properties of timber, small samples were cut from the untested timber in the same batch and tested for compression and shear according to ASTM D143-14 (ASTM 2014). The numbers of small clear samples for the compression tests in the longitudinal direction (parallel to grain direction) and transverse direction (perpendicular to grain direction), and shear tests in the longitudinal direction were 22, 21, and 49, respectively. The details of the material tests on timber can be found in Appendix II. The measured Young's moduli and compressive strengths of timber in the longitudinal and transverse directions, the Poisson's ratio in the longitudinal direction, and the shear strength in the longitudinal direction are listed in Table 3.2. Since the transverse direction contains different annual ring angles, the modulus of elasticity E_{TT} had a low average value and a large coefficient of variation.

Table 3.2 Material properties of timber in the connection specimens measured from compression and shear tests

E_t (GPa)	E_{TT} (GPa)	f_{tc} (MPa)	f_{TTc} (MPa)	υ_{LT}	f_{ts} (MPa)
12.0 (18.7%)	0.2 (41%)	49.5 (11.4%)	3.6 (19.8%)	0.52 (21.0%)	7.2 (16.7%)

Note: E_t and E_{TT} are the moduli of elasticity of timber in the longitudinal and transverse directions, respectively. f_{tc} and f_{TTc} are the compressive strengths of timber in the longitudinal and transverse directions, respectively. υ_{LT} is the Poisson's ratio of timber in the longitudinal direction. f_{ts} is the shear strength of timber in the longitudinal direction. Numbers in the brackets are the coefficients of variation.

After the grooves were cut on timber, the formwork was made with plywood on four sides of timber, and concrete was mixed and cast on top of timber into the formwork, as shown in Fig. 3.4. Concrete was mixed in five batches and consolidated using a manually operated vibrator. After casting, concrete was covered with plastic membranes for one week before the removal of formwork. The nominal diameter of the coarse aggregate in concrete was 10 mm to avoid the formation of voids in the corners of notches. Steel welded wire mesh with a diameter of 5 mm and

a grid size of 100 mm × 100 mm was placed at the mid-depth of concrete to prevent potential cracking due to shrinkage and temperature strain. To measure Young's modulus and compressive strength of concrete, 15 cylinders (three per batch) were cast and tested at 60 days according to ASTM C39/C39M-18 (2018) and ASTM C469/C469M-14 (2014). The Young's modulus and Poisson's ratio of concrete were measured using a compressometer mounted on the concrete cylinders. Results from cylindrical concrete specimen tests are summarized in Table 3.3.

(a) (b) (c)

Fig. 3.4 Notched connection specimen preparation (a) Timber after notch cutting and screw drilling (b) Formworks and steel mesh (c) Specimens after concrete casting.

Table 3.3 Results obtained from cylindrical concrete specimen tests

f_c' (MPa)	E_c (GPa)	v_c	D (mm) × H (mm)	Number	Time (day)
52.0 (3.9%)	29.5 (4.2%)	0.18 (5.1%)	100 × 200	15	60

Note: f_c' is the concrete compressive strength; E_c is the Young's modulus of concrete; v_c is the Poisson's ratio of concrete; D is the diameter of concrete cylinders; H is the height of concrete cylinders; Numbers in the brackets are the coefficients of variation.

Self-tapping screws were installed in four types of specimens as additional steel fasteners to the notch. The screws used in the specimens were the CLC8160 wood-concrete connectors made by HOLZ Technic. The nominal diameter of the screws was 8 mm and the total length was 160 mm which contained 110 mm thread length and 50 mm upper thread length. The provided characteristic tensile strength and characteristic withdrawal resistance of screws by the manufacturer were 21

kN and 11 N/mm^2, respectively. The screws were vertically installed into wood, as shown in Fig. 3.3(c) and (d).

3.3.4 Test Setup and Loading Procedure

The testing frame for the notched connection specimens is shown in Fig. 3.5(a). In this test setup, shear force was applied horizontally by a hydraulic actuator at a loading rate of 1mm/min. The shear force was applied according to EN 26891 (1991) which contained a pre-load cycle at 40% of the estimated peak load. The timber wings were clamped to the testing frame to prevent the rotation of specimens. Two layers of plastic foams were placed between the specimen and the load cell to reduce the bending of the load cell caused by friction. The relative displacement between concrete protrusion and timber in front of the notch was measured using linear variable differential transformers (LVDTs) mounted on both sides of the specimen, as shown in Fig. 3.5(b).

For specimens L-25-150, L-25-250, and L-25-350, two samples from each type were measured with the digital image correlation (DIC) method (Pan et al. 2009) on one side of the specimen to capture the entire displacement field around the notched region. A two-dimensional DIC system with one camera was used to capture the deformed images every 6 seconds. At this time interval, the critical failure pattern of notched connections under shear can be captured without causing a large file size. A facet size of 19 pixels and a point distance of 16 pixels were used to analyze the deformed images which contain 6000 pixels and 3376 pixels in horizontal and vertical directions, respectively, and 350 dpi resolution in each direction. The relative slip of these specimens on the other side was measured using LVDT. The pre-load cycle was not applied to the specimens measured with DIC.

The specimens were supported by a wooden brace with a height of 80 mm, which allows the shear-off failure of timber under the shear load. This was close to reality and is the common practice for most shear tests from the literature. If timber was braced on its full height (Jiang and Crocetti 2019), the timber shear failure would be prevented, and the connections would yield higher and unrealistic strength and stiffness values.

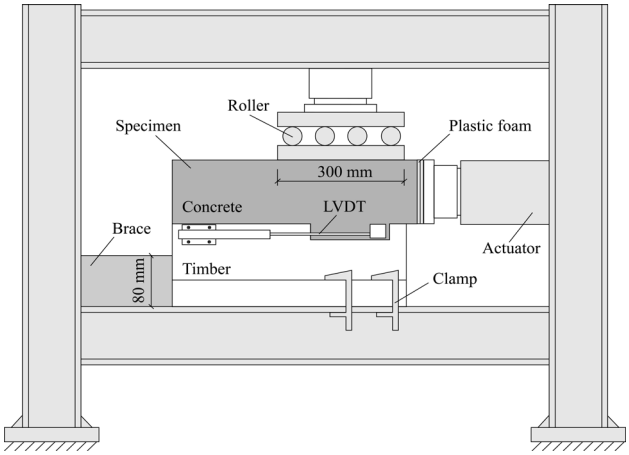

(a) Schematic of the testing frame (in mm)

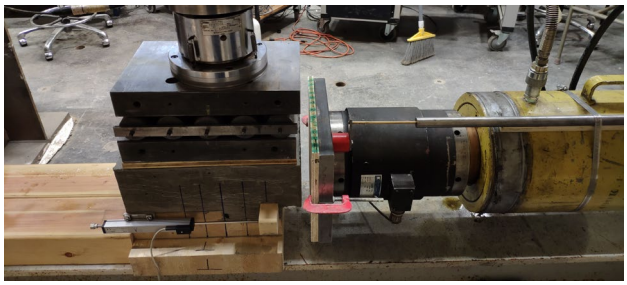

(b) Test setup in the laboratory

Fig. 3.5 Notched connection push-out test setup

Under the shear load, there was a tendency for concrete to uplift due to the eccentricity of the applied horizontal load with respect to the reaction force provided by the load-bearing surface between timber and concrete. Trial tests showed that, without any vertical restriction, the concrete uplifting can cause an early timber tensile failure perpendicular to the grain. However, this effect is much less in real-world large-dimension MTP-concrete composite floors subjected to bending. To restrict the uplifting of concrete, an additional restraint with a load cell was mounted on top of the specimens. A roller was placed between the load cell and the specimen to allow horizontal movement of concrete. The restraint carries a small load to the specimen initially and stayed at this position afterward. The vertical reaction force caused by the uplifting of concrete during the test was recorded. In previous experimental research on notched connections, both single shear tests (asymmetric specimens) (Gutkowski et al. 2004) and double shear tests (symmetric specimens with the arrangement of timber-concrete-timber or concrete-timber-concrete) (Jiang and Crocetti

2019) have been conducted. However, irrespective of the test set-up, the restriction perpendicular to the shear force has to be applied to the specimens due to the eccentricity of the shear force. The impact of this transverse restriction on the shear properties of notched connections will be discussed in later sections.

3.3.5 Test Results

For each type of specimen, the load-slip curves measured from six repetitions were averaged and the results are shown in Fig. 3.6. The preloading cycle was not considered in the averaged load-slip curves. The original load-slip curves for the specimens can be found in Appendix I. The peak load obtained before failure is taken as the shear capacity F_{max} for each specimen. The average shear capacities F_{max} for all test groups are listed in Table 3.4. Also listed in Table 3.4 are the shear stiffness values and failure patterns of the notched connections. Two shear stiffness properties were derived from the test data, namely the serviceability shear stiffness K_{ser} and the ultimate shear stiffness K_{ult}. The serviceability shear stiffness K_{ser} was calculated from the linear regression to the load-slip curve within 10% to 40% of the peak load. The ultimate shear stiffness K_{ult} was determined from

$$K_{ult} = \frac{0.8F_{max}}{\Delta_{0.8}} \tag{3.1}$$

where $\Delta_{0.8}$ is the measured relative slip when 80% of the peak load F_{max} was reached.

From Fig. 3.6 and Table 3.4, it can be seen that the specimens with timber loaded in the transverse direction showed a much lower shear stiffness and strength than the longitudinal specimens. The notch depth and timber shear length also had major impacts on the connection stiffness and ultimate strength, while the presence of self-tapping screws only had minor impacts on the connection performance.

The stiffness and strength of the notched connections presented in Table 3.4 are for specimens with 200 mm width. However, the stiffness and strength of notched connections are often normalized to one-metre width to make comparisons with the other researchers' test results. According to Table 3.4, the normalized serviceability stiffness K_{ser} for the notched connections is in the range of 125 – 231 kN/mm for transverse specimens and 667 – 1275 kN/mm for longitudinal

specimens. The normalized strength for the notched connections is in the range of 270 – 372 kN for transverse specimens and 417 – 977 kN for longitudinal specimens. The shear stiffness of 1000 kN/mm per metre width has been suggested by some researchers for notched connections with depths in the range of 20 to 30 mm (Dias et al. 2018a). The measured serviceability stiffness K_{ser} for the specimens in the longitudinal direction with a notch depth of 25 mm was slightly above the suggested value. However, the specimen with a notch depth of 40 mm only had a serviceability stiffness of 1167 kN/mm (per metre width), which was lower than the suggested value of 1500 kN/mm for notches deeper than 30 mm (Dias et al. 2018a).

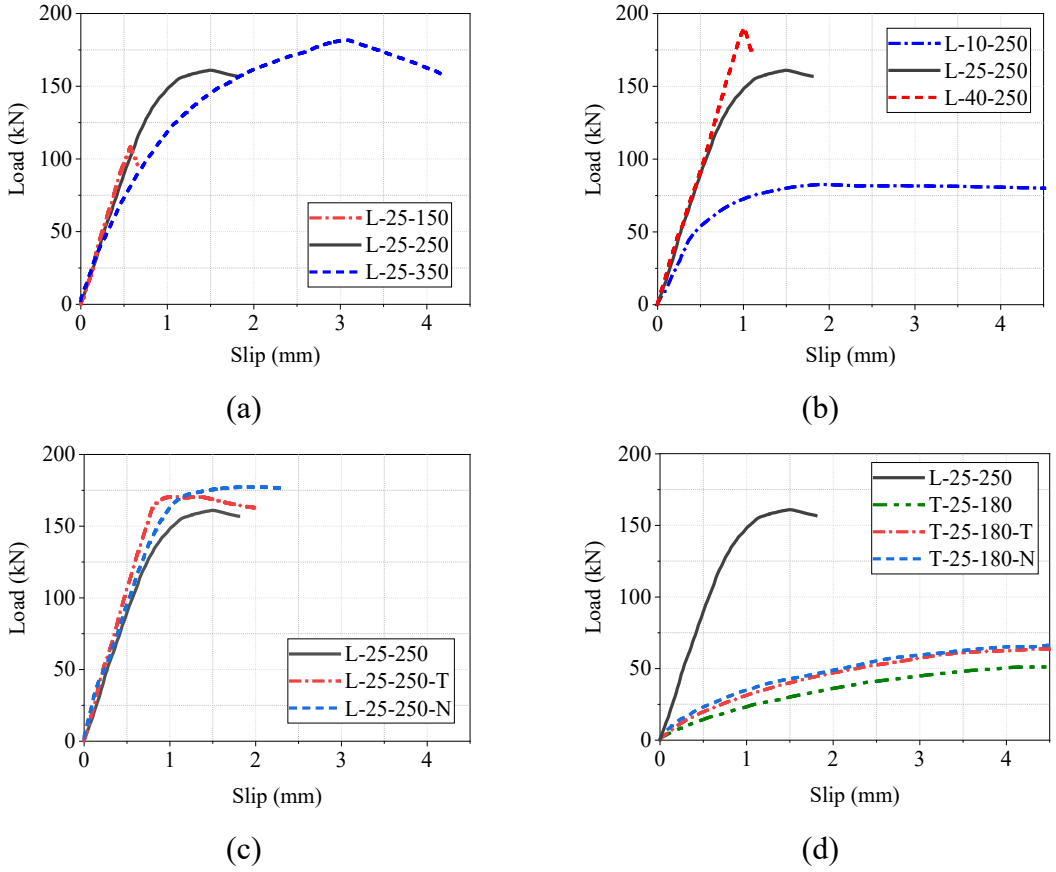

Fig. 3.6 Averaged load-slip curves of notched connections under the shear load affected by different factors (a) Timber shear length in front of the notch (b) Notch depth (c) Presence and locations of self-tapping screws (d) Timber orientation and the presence of self-tapping screws

Table 3.4 Results from the notched connection push-out tests

Specimen	F_{max} (kN)	K_{ser} (kN/mm)	K_{ult} (kN/mm)	Failure pattern
T-25-180	54.1 (14.7%)	25.1 (20.4%)	16.3 (19.0%)	Combined TR, TC and TT
T-25-180-N	74.3 (14.7%)	46.1 (20.3%)	23.4 (15.7%)	Combined TR and TT
T-25-180-T	67.8 (5.0%)	40.2 (22.7%)	20.5 (17.4%)	Combined TR and TT
L-25-250	164.9 (2.5%)	227.6 (22.4%)	191.1 (16.2%)	CC followed by TS
L-10-250	83.4 (9.0%)	133.4 (18.5%)	99.6 (12.3%)	CC followed by TC
L-40-250	195.3 (11.6%)	233.4 (5.9%)	214.2 (4.4%)	CC followed by TS
L-25-150	117.5 (24.8%)	231.3 (18.3%)	217.1 (13.8%)	CC followed by TS
L-25-350	182.5 (6.2%)	217.4 (21.1%)	145.9 (10.8%)	CC followed by TS
L-25-250-N	178.8 (4.3%)	229.2 (13.0%)	193.2 (20.9%)	CC followed by TS
L-25-250-T	173.0 (6.5%)	254.9 (10.9%)	225.3 (10.2%)	CC followed by TS

Note: F_{max} is the peak load; K_{ser} is the serviceability slip stiffness; K_{ult} is the ultimate slip stiffness. Numbers in the brackets are the coefficients of variation.

The damages and failures of the notched connections under shear observed from the shear tests are defined as follows:

- CC: Concrete cracking from the notched corner.
- TS: Timber in front of notch parallel to grain shear-off failure.
- TR: Timber in front of notch rolling shear failure.
- TT: Timber tensile failure perpendicular to the grain.
- TC: Timber in front of notch compression failure (parallel or perpendicular to the grain).

The concrete shear failure and crushing failure were not observed in the test probably due to the high compressive strength of concrete in the specimens and the relatively short timber shear length. In general, a combination of failure modes was observed in each type of specimen. Overall, four typical failure patterns can be summarized as shown in Table 3.4 and Fig. 3.7.

As shown in Fig. 3.7(a), for specimens in the transverse direction without screws T-25-180, the failure was a combination of timber rolling shear, tension, and compression perpendicular to grain.

The specimens with screws inserted into notch T-25-180-N showed no obvious compression failure of timber but an additional tensile crack in timber appeared at an early stage at the location of screws, as shown in Fig. 3.7(b). The specimens with screws inserted into timber in front of notch T-25-180-T failed mainly due to tension perpendicular to grain along the load-bearing surface of timber, as shown in Fig. 3.7(c). For all the specimens in the transverse direction, the concrete portion was almost intact without any obvious signs of damage.

The specimens with timber in the longitudinal direction were less ductile than the transverse specimens with the exception of specimen L-10-250. Different from the transverse specimens, the concrete in the longitudinal specimens cracked shortly at the notched corner after being loaded, usually before 40% of the peak load was reached. The concrete crack can cause disturbance in the load-slip curves for some specimens; however, this was averaged out in the load-slip curves in Fig. 3.6. The crack in concrete could propagate towards the top of the specimen, but there was no complete fracture because of the steel mesh in the concrete. With the increase of loading, two different failure modes could be observed for specimens in the longitudinal direction: while most of the specimens failed exclusively due to timber shear-off in front of the notch, specimen L-10-250 (Fig. 3.7(e)) failed due to timber crushing in front of the notch.

The specimen L-10-250 had the most ductile failure pattern among all the longitudinal specimens due to the crushing of wood fibers. In contrast, specimens L-25-150 and L-40-250 were the most brittle types which could tell from their almost linear to failure load-slip curves in Fig. 3.6. The reductions of the ultimate stiffness K_{ult} from the serviceability stiffness K_{ser} for specimens L-25-150 and L-40-250 were less than 10%.

The specimens with the longest length of timber in front of notch L-25-350 had moderate ductility as the load increased in a nonlinear manner after an initial linear stage and a relatively large slip was reached before the specimen failed. The nonlinearity of the load-slip response came from the compression of timber in front of the notch. However, unlike specimen L-10-250, the crushing of wood fibers in specimen L-25-350 was not triggered before the timber shear strength was reached.

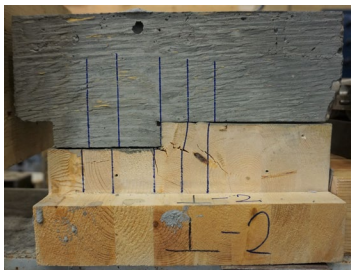

(a) T-25-180

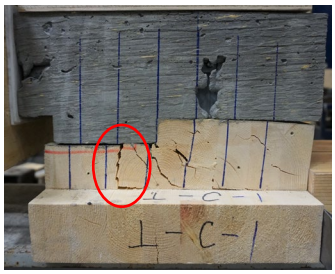

(b) T-25-180-N

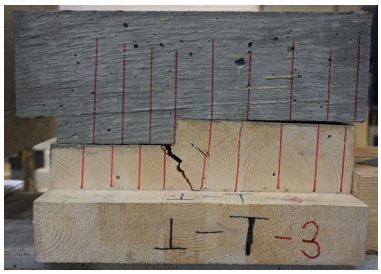

(c) T-25-180-T

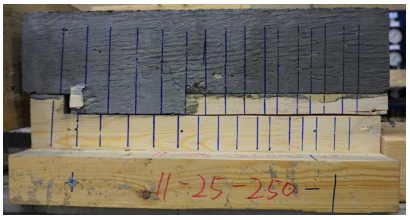

(d) L-25-250

(e) L-10-250

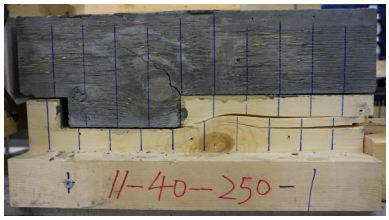

(f) L-40-250

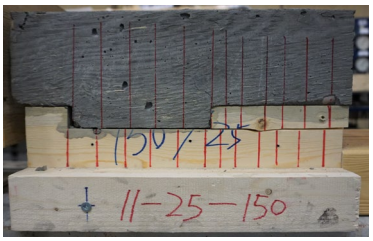

(g) L-25-150

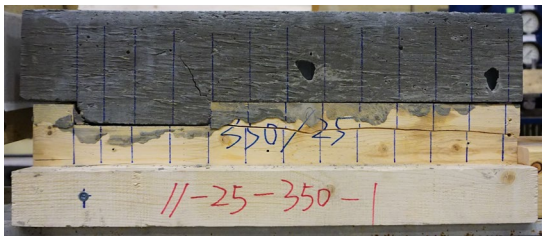

(h) L-25-350

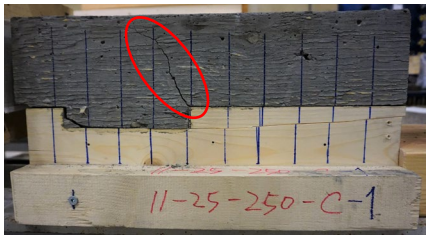

(i) L-25-250-N

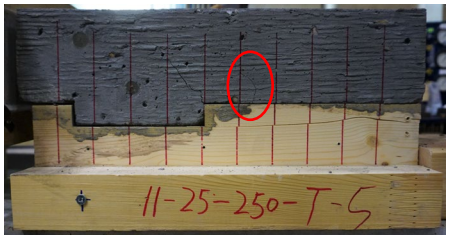

(j) L-25-250-T

Fig. 3.7 Typical failure patterns for different types of notched connection specimens

The specimens L-25-250, L-25-250-T, and L-25-250-N showed limited ductility before the timber failure. The screws in the connections did not improve the ductility. The screws inserted into the notch failed to prevent the crack propagation of concrete. Instead, the concrete tended to develop cracks at a larger angle, as can be seen from Fig. 3.7(i). Screws inserted into the timber in front of the notch did not prevent the shear failure of timber and a minor crack in concrete was developed

at the position of screws in addition to the main crack developed at the notched corner, as can be seen from Fig. 3.7(j).

After the specimens with screws were tested, the timber was removed using a chisel and a hammer to see the screw deformation. As shown in Fig. 3.8, the screws were bent under the shear load at varying angles. In general, the screws in the transverse specimens bent more than the screws in the longitudinal specimens simply because the longitudinal specimens failed early in timber before the screws were able to deform further.

(a) T-25-180-N (b) T-25-180-T (c) L-25-250-N (d) L-25-250-T

Fig. 3.8 Deformation of screws after the notched connection specimens were tested

The displacement field in the notched regions under the shear load was captured using Digital Image Correlation (DIC) method in a few tests. Fig. 3.9 shows the horizontal displacement field of one L-25-250 specimen at different load levels. In the initial elastic stage before concrete cracking, Fig. 3.9(a), there was practically no deformation in the timber part. The displacement field in concrete was continuous but not uniform, which was caused by the slight rotation of concrete due to the eccentricity of the applied load. After the concrete was cracked, Fig. 3.9(b), the displacement field of concrete split into two. The front part of concrete had larger displacement since it moved with the loading head while the rear part of concrete was restricted by timber from moving. At this stage, the gap opening in the notch due to the rotation of concrete was obvious. With the further increase of load, the crack in concrete propagated to the top. At the same time, the shear crack in timber in front of the notch was initiated and propagated towards the end of timber till the timber was completely sheared off, as can be seen from Fig. 3.9(c) and (d). The contribution of the notch in resisting the relative slip was obvious from DIC images as the displacement field around the bearing surface was always continuous at different stages.

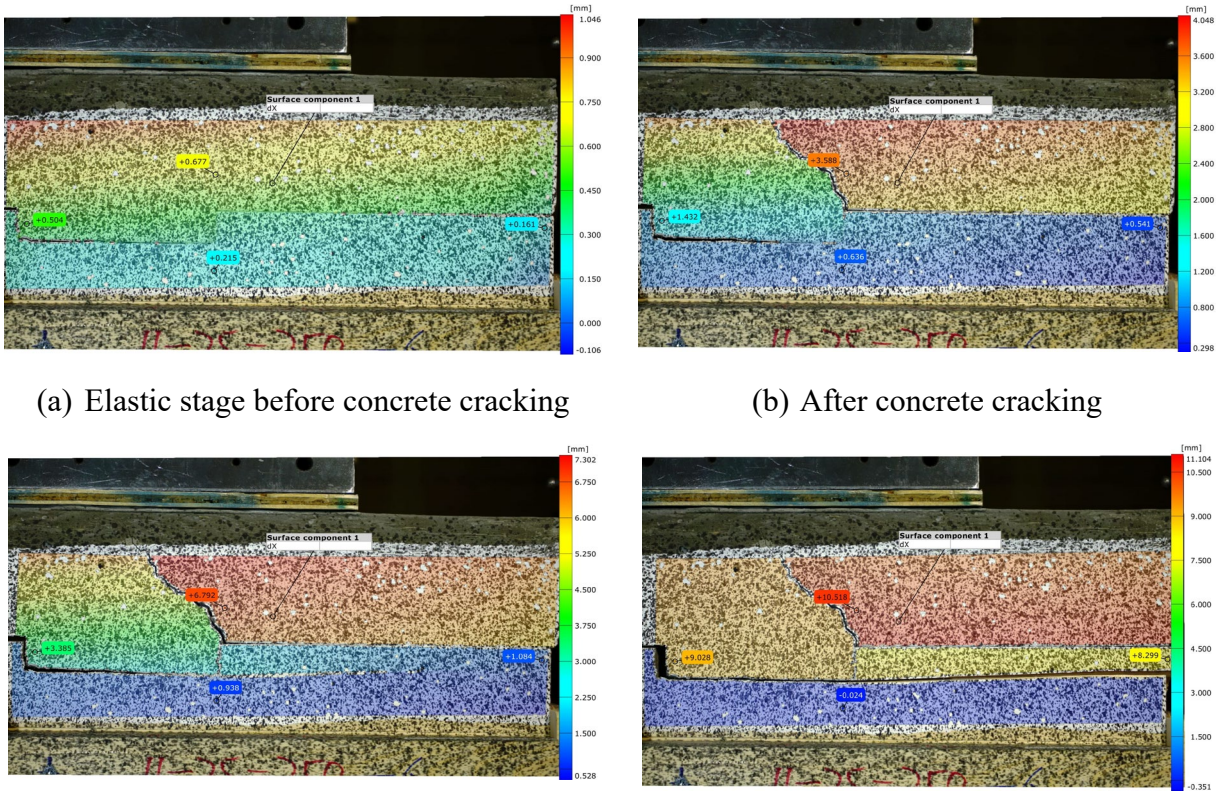

(a) Elastic stage before concrete cracking

(b) After concrete cracking

(c) Before timber shear failure

(d) After timber shear failure

Fig. 3.9 Typical horizontal displacement field of the notched connection under shear captured using digital image correlation (DIC) method

After the specimens were tested, the moisture content of timber was measured. As described in Section 3.3.3, concrete was cast directly on top of timber without any films or waterproofing paint. After concrete pouring, timber can absorb water from concrete and its moisture content would rise. The moisture content change in timber due to concrete bleeding has been investigated by Fragiacomo et al. (2007). They measured the moisture content change of wood after concrete pouring using a moisture meter and found that the moisture content of wood at the interface with concrete rose significantly in the first 5 days. However, a gradual reduction to the initial moisture content was observed during the next 10 days. The change in moisture content of wood with time was not monitored in this test. Instead, the moisture content of wood for specimens L-40-250 was measured through the oven-dry method right after the shear tests (which was about 50 days after concrete casting). As shown in Fig. 3.10(a), small timber samples with approximate dimensions of 40 mm × 40 mm × 40 mm were cut from the specimens below the interface with concrete and

at the bottom of timber. Twelve moisture samples were cut from each specimen: six samples were cut near the upper surface and six were cut near the bottom of timber. The measured moisture contents of the samples are shown in Fig. 3.10(b). As can be seen, for specimens 1, 2, and 3, the moisture content values at the top and bottom of timber were very close. For specimens 4, 5, and 6, the moisture content below the interface was slightly higher than the moisture content at the bottom. This result indicates that it may take a long time for timber to completely recover to a uniform moisture content after concrete casting. Nevertheless, the discrepancy of the moisture contents at the top and bottom was not significant (less than 2.5%).

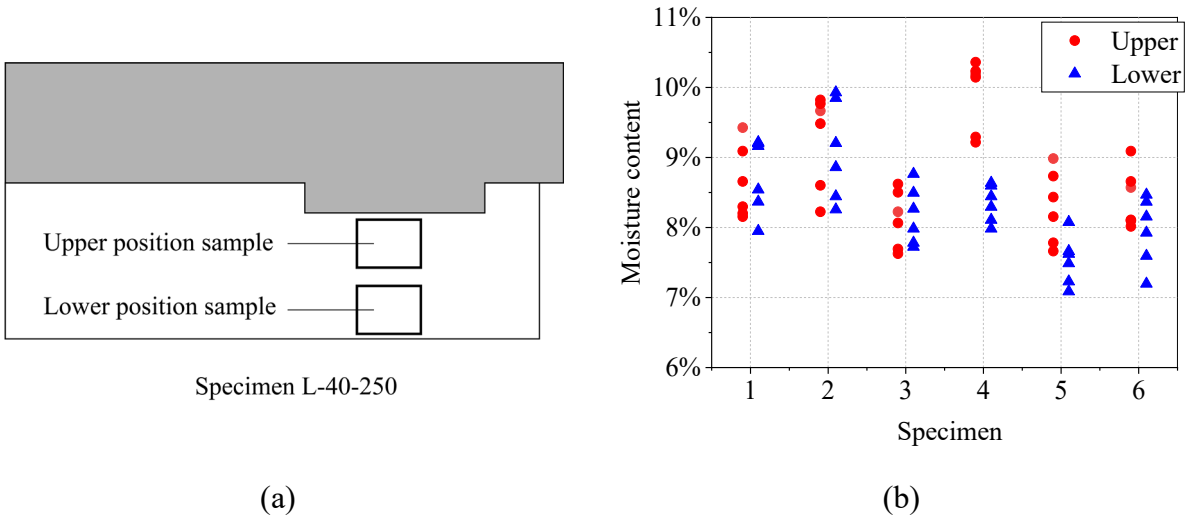

Fig. 3.10 Moisture content of GLT measured after the push-out tests (a) Moisture content samples cut from specimen L-40-250 (b) Moisture content at upper and lower positions of six L-40-250 specimens

3.3.6 Discussion

Based on the push-out test results, some important factors that affect the structural performance of notched connections under shear, including timber orientation, connection geometry, presence of additional steel fasteners, as well as the testing method, are discussed below.

Timber orientation

In MTP-concrete composite floors, connections should be installed between timber and concrete so that the relative slip between concrete and timber in any direction is restricted under the gravity and lateral loads. For notched connections, due to the anisotropic nature of wood, the connections in the transverse direction can only reach a fraction of the shear stiffness and load-carrying capacity of connections in the longitudinal direction. Without any self-tapping screws, the connections in the longitudinal direction had about 9 times of the serviceability stiffness K_{ser} and 3 times of the load-carrying capacity F_{max} of the connections in the transverse direction with the same notch depth. This could be explained by the material properties of timber shown in Table 3.2 which shows that the modulus of elasticity and compressive strength of timber in the longitudinal direction were 60 times and 14 times, respectively, of the corresponding properties in the transverse direction. The huge disparity of the connection performance in two orthogonal directions would lead to challenges in using the notched connections in two-way slabs. For GLT-concrete composite floors, this is not a major issue since GLT is mainly designed and used as one-way slabs in the main direction. However, for cross-laminated timber (CLT) slabs which are capable of bearing load biaxially (i.e. used as two-way slabs), the notches in the secondary direction will have to go deeper to reach the second layer in order to gain more shear resistance (Loebus et al. 2017).

Timber shear length

Comparing the strengths of specimens L-25-150, L-25-250, and L-25-350, it can be concluded that, with the increase of timber shear length in front of the notch, the strength of the connection also increases. The strengths of connections L-25-150 and L-25-350 were 71% and 111%, respectively, of the strength of the reference case L-25-250. However, the serviceability stiffness K_{ser} for three types of specimens were fairly close, with differences of less than 5% between the reference case and the other two. The minor decreasing trend of K_{ser} with the increased timber shear length could be attributed to the slightly different serviceability range (10 – 40% of the peak load) of different specimens due to their different ultimate strengths. The ultimate stiffness K_{ult} of three types of specimens differs more than their serviceability stiffness K_{ser}. The reason is that

longer specimens had both increased load-carrying capacity and ductility than shorter specimens. With the increased timber shear length, the specimens exhibited more nonlinear behaviour and significantly larger relative slip when 80% of the peak load was approached.

According to German National Annex for EN 1995-1-1 (2013), a minimum timber shear length in front of the notch should be no less than eight times of the notch depth to reduce the risk of timber shear failure. Schönborn et al. (2011) suggested the timber shear length should be at least 12.5 times of the notch depth. These requirements are likely not enough to prevent timber shear failure, since specimens L-25-250 and L-25-350 had timber shear lengths that were 10 and 14 times of the notch depth, respectively, but their final failure mode was still timber shear-off. The tension tests on the halved and tabled tenoned timber scarf joints conducted by Aira et al. (2015) showed that timber shear failure could even occur when the length of timber was 22 times of the notched depth.

Since the specimens had different dimensions, the connection properties such as stiffness and strength that smeared along the specimen axis are more comparable than the measured absolute values (Linden 1999). The normalized stiffness and strength could be calculated by dividing the measured values by the total connection length. The total length (notch length plus timber shear length which is also the spacing of connectors in the composite floors) of specimens L-25-150, L-25-250, and L-25-350 were 300 mm, 400 mm, and 500 mm, respectively. The calculated normalized stiffness (for both serviceability and ultimate) is in the order of L-25-150 > L-25-250 > L-25-350 while the normalized strength is in the order of L-25-250 > L-25-150 > L-25-350. In terms of ductility, longer specimens were more ductile than shorter specimens. This result indicates that the optimal stiffness, strength, and ductility may not be achievable in the same connection configuration and longer specimens are not necessarily more efficient than shorter specimens in terms of strength and stiffness.

Notch depth

Comparing the test results on specimens L-10-250, L-25-250, and L-40-250, it could be concluded that the connection stiffness and strength both increase with the notch depth but the failure mode becomes more brittle. Due to the different failure mechanisms, a significant rise of the serviceability stiffness (71%) and strength (98%) could be observed from 10 mm notch depth to

25 mm notch depth. Although the failure mode for L-25-250 and L-40-250 was both timber shear failure and the timber shear length was the same in two types of specimens, the deeper notch in specimen L-40-250 had a larger eccentricity thus requiring a higher load (18% more) to break the timber.

Although the depth of notched connections has been suggested to be no less than 20 mm for building applications (Dias et al. 2018a), the 10 mm notch depth was tested as a lower-bound value for research purposes. Test results showed that a shallow notch can fail in a ductile way but had low stiffness and strength, while a deep notch had improved stiffness and load-carrying capacity but can fail in a brittle way. A deep notch can also seriously reduce the cross-section of timber. The bending tests conducted by Gutkowski et al. (2008) on composite beams connected with notches showed that timber flexural failure often occurs from the base of the notch. An optimal notch depth should be able to provide sufficient shear resistance without undermining the bending capacity of the timber member too much. The effect of the notch depth will be discussed again in the composite floor systems in Chapter 4 and Chapter 5.

Self-tapping screws

The effect of lag screws or self-tapping screws as additional reinforcement in the notched connections has been investigated by researchers. Yeoh et al. (2011c) found that lag screws inserted into the beam type notched connections improved the slip modulus and enabled a more ductile failure mode. However, Kudla et al. (2016) found that for the slab-type notched connections, only the closely spaced self-tapping screws had an observable effect on the strength and stiffness of the notched connections.

In this study, two self-tapping screws at a spacing of 100 mm were installed in four types of specimens. By comparing the specimens with and without screws, some observations could be drawn. As discussed before, without any steel fasteners, the connections in the transverse direction were significantly less effective than the connections in the longitudinal direction. Thus it could be expected that the same amount of self-tapping screws installed into the connections would have different effects on specimens in different directions. For specimens in the transverse direction, the screws increased the serviceability stiffness by about 70% and the shear capacity by about 30%

on average. The screws have also changed the failure mode of the connection from combined compression, tension, and rolling shear failure to mainly tension failure. However, even with self-tapping screws, the specimens in the transverse direction were still too flexible compared to the longitudinal specimens, as can be seen from Fig. 3.6(d).

For specimens in the longitudinal direction, the screws did not affect the failure mode of the connections and resulted in only minor increases in stiffness, strength, and ductility of the connections. Considering that two screws at a spacing of 100 mm were used in each specimen, the effect of a single screw on the shear performance of the connection in the longitudinal direction will be even harder to detect. This also implied that the notched connections in the longitudinal direction have stiffness remarkably higher than self-tapping screws. To effectively prevent the crack enlargement in concrete around the notched corner, horizontal reinforcement should be used in addition to the vertical screws. The combination of horizontal and vertical reinforcements in the notched connections is discussed in Chapter 5.

Due to concrete shrinkage and timber drying, small gaps between timber and concrete could be observed in specimens after the concrete has cured. The self-tapping screws inserted into the connections did not completely prevent this gap opening. To reduce the gap opening, post-tensioning dowels (Gutkowski et al. 2004; 2008) or low shrinkage concrete (2011a) could be used. Besides the steel fasteners installed in the notches, the application of self-tapping screws at mid-span of MTP-concrete composite floors is suggested by researchers (Jiang and Crocetti 2019) for the purpose of maintaining the same curvature of timber and concrete under bending.

Effect of the vertical restriction

In the push-out tests, the asymmetric shear specimens were designed and the load was applied horizontally to the specimens to simulate the notched connections in real MTP-concrete composite floors under bending. When the horizontal load is applied to the specimens, the concrete had a tendency to rotate because of the eccentricity of the applied load. This rotation was prevented by the load cell on top of the specimens and a reaction force has resulted. This top reaction force increased with the applied horizontal load and was approximately in the range of 22% – 33% of the horizontal load with higher reaction forces found in shorter specimens or specimens with a

deeper notch and lower reaction forces found in longer specimens or specimens with a shallower notch.

The confining pressure applied to the connections that held the notched components together could have a positive effect on the shear performance of the connections (Linden 1999). An example is that in concrete segmental bridges connected with keyed dry joints, not only does the ultimate shear strength and stiffness of the joints increase with the confining stress, the ductility and crack pattern of the joints will also alter (Shamass et al. 2015).

Although the confining pressure does not necessarily exist in real MTP-concrete composite floors, it is extremely challenging to create the real boundary conditions for the notched connections in the composite floors by taking out a segment and testing it in a shear test. Thus the confining pressure will always exist in the commonly used shear test set-ups (double shear and asymmetric shear) no matter it is applied through external load or reaction force from constraint or friction. Monteiro et al. (2013) conducted a numerical parametric study on the notched connections and concluded that different test set-ups would not significantly affect the obtained results. The vertical load acting on the specimens was not acting proactively but only existed as a reaction force. The concrete was allowed to move freely in the horizontal direction without any significant increase of friction between concrete and timber. Compared with the proactively applied top load that existed from the beginning of the test, the effect of the top load is minimized in the shear tests, thus the strength and slip modulus of the connections obtained from the push-out tests could be seemed as close to the true characteristics of the connections in MTP-concrete composite floors.

3.3.7 Conclusions from Shear Tests

The following conclusions can be drawn from the push-out tests on the notched connections:

1. Due to the anisotropic nature of timber, connections with timber in the longitudinal direction had significantly higher strength and stiffness than connections with timber in the transverse direction. While the addition of self-tapping screws can help improve the shear performance of connections in the transverse direction to some extent, it is still a challenge to use notches in two-way mass timber panel-concrete composite floors.

2. The shear length of timber in front of the notch is an important factor in determining the spacing of the notched connections. With the increase of timber shear length, the strength of the connection will increase until an upper limit is reached. At the same time, the failure mode of the connection will change from brittle timber shear failure to ductile timber compression failure. The obtained normalized stiffness and strength show that longer notched connections are not necessarily more efficient than shorter notched connections.
3. The depth of the notch is another important factor that impacts the connection performance. With the increase of the notch depth, the stiffness and strength of the connections both increase. The connection stiffness is impacted more by the notch depth than by the timber shear length. However, a deeper notch can reduce the cross-section of the timber member thus potentially causing an early failure of timber under bending. A reasonable notch depth should have enough shear resistance without compromising the bending strength of the timber member.
4. Self-tapping screws inserted into the notched connections can improve the strength and stiffness of specimens in the transverse direction. For specimens in the longitudinal direction, the contribution from a limited number of self-tapping screws to the stiffness, strength, and failure mode is negligible.

3.4 Stiffness Prediction of Notched Connections

An ultimate goal for the studies on the shear connections is to determine the connection stiffness that can be used for the composite floor design. The connection stiffness is essential for the composite efficiency in MTP-concrete composite floors but can be difficult to determine without conducting the experimental tests. This section discusses the prediction of the notched connection stiffness based on test results and finite element modeling. In addition to the test results discussed in Section 3.3, the shear test results on notched connections conducted by other researchers are also summarized. A finite element model was built to investigate the notched connection stiffness affected by various geometry and material properties. Based on the test results and numerical modeling, an empirical formula is proposed for estimating the notched connection stiffness.

3.4.1 Previous Test Investigations

The stiffness of notched connections has been investigated by researchers through connection push-out tests. Some of the test results are summarized in Table 3.5. While the notched connections can be made in various shapes, only the most common rectangular notches are summarized here. In Table 3.5, the depth of notches varies from 20 mm to 50 mm; the notch length varies from 120 mm to 300 mm; while the timber shear length varies from 150 mm to 400 mm. The concrete and timber were of different strength grades. The timber members were GLT, glulam, and CLT. If the timber member was CLT, then the notch was only cut within the first layer. Only the test results from connections with minimal steel fasteners (such as self-tapping screws or coach screws) in the notch or without additional steel fasteners are summarized in Table 3.5, as previous research shows that additional steel fasteners in the notched connections have no distinct effect on the connection stiffness unless a large number of fasteners are used (Kudla et al. 2016).

From Table 3.5, the effects of various factors, such as the notch depth, notch length, timber shear length, concrete strength, and the presence of steel fasteners, on the connection stiffness can be observed. The test results of Kudla et al. (2016) and Minh et al. (2020) show that the notch length has no remarkable effect on the notched connection stiffness. From the test results of Jiang et al. (2020) and Minh et al. (2020), it can be concluded that the timber shear length also has no significant effect on the notched connection stiffness, although the test data from Michelfelder (2006) and Mönch and Kuhlmann (2018) indicate a potential positive effect of the timber shear length. In terms of the notch depth, the test results from Michelfelder (2006) showed a clear increasing trend of the notched connection stiffness with the notch depth while this was not obvious from the test results of Minh et al. (2020). The effect of a limited number of steel fasteners can be safely disregarded according to the test data of Michelfelder (2006), Kudla et al. (2016), and Jiang et al. (2020). In terms of the effect of concrete strength class on the notched connection stiffness, no clear trend can be found according to the test results summarized in Table 3.5.

Results from test investigations provide inconclusive or even contradictory results in terms of the notched connection stiffness affected by different factors. The notched connection stiffness measured by researchers also showed a large variation within and between different tests. One possible reason could be the relatively small slip between timber and concrete due to the large stiffness of the connections, thus even a small absolute error in the slip measurement can lead to a

large variation of the measured connection stiffness. Accordingly, the measured connection stiffness from tests is not only affected by the connection properties (geometry and material properties) but also sensitive to the quality of the slip measurement setup. The connection stiffness measured by Michelfelder (2006) was significantly lower than the rest of the tests shown in Table 3.5, which was most likely because the sensors in the test setup of Michelfelder (2006) were not installed next to the load-bearing surface of notches which resulted in a larger relative slip measurement. As Mönch and Kuhlmann (2018) have discussed, the connection stiffness obtained from different slip measurement methods within one specimen can potentially differ by more than 100%. Overall, the connection stiffness summarized in Table 3.5 varies between 271 to 1970 kN/mm, based on which it is not possible to derive a design value for the notched connection stiffness. Instead, finite element models were built to derive the notched connection stiffness.

Table 3.5 Notched connection stiffness measured from previous push-out tests

Researcher	Testing method	Notch dimensions			Timber shear length (mm)	Concrete compressive strength	Timber material	Additional steel fastener	Replicate	Connection stiffness [j] (kN/mm)
		Width (mm)	Depth (mm)	Length (mm)						
Michelfelder (2006)	Double shear [a]	500	20	200	250	C20/25 [c]	Stacked board S7 (C16) [d] E_t = 8.9 ~ 9.8 GPa	2 Screws [f]	16	376 (78)
			20		150	C20/25 [c]		2 Screws [f]	2	279 (4)
			40		250	C20/25 [c]		2 Screws [f]	2	594 (120)
			20		250	C20/25 [c]		None	3	410 (78)
			20		250	C12/15 [c]		2 Screws [f]	3	271 (60)
Kuhlmann and Aldi (2010)	Double shear [a]	220	40	200	400	C30/37 [c]	Glulam GL 32h [d]	None	3	1757 (378)
Kudla et al. (2016)	Double shear [b]	200	20	160	300	C 30/37 [c]	GLT GL 24h [d]	1 screw [g]	7	1371 (274)
				120				1 screw [g]	3	1567 (190)
				200				1 screw [g]	3	1970 (322)
				160				None	4	1628 (374)
Mönch and Kuhlmann (2018)	Double shear [b]	200	20	160	300	C 30/37 [c]	GLT GL 24h [d]	1 screw [g]	6	1230 (169)
					160				6	878 (193)
Jiang et al. (2020)	Double shear [a]	150	50	150	350	29.2 MPa	Glulam E_t = 10.7 GPa	None	3	1531 (71)
					350	28.7 MPa		None	3	1563 (114)
					150	28.7 MPa		1 screw [h]	3	1546 (129)
					200	28.7 MPa		1 screw [h]	3	1649 (83)
					275	28.7 MPa		1 screw [h]	3	1594 (87)
					350	28.7 MPa		1 screw [h]	3	1663 (23)

Table 3.5 (Continued) Notched connection stiffness measured from previous push-out tests

Researcher	Testing method	Notch dimensions			Timber shear length (mm)	Concrete compressive strength	Timber material	Additional steel fastener	Replicate	Connection stiffness [j] (kN/mm)
		Width (mm)	Depth (mm)	Length (mm)						
Minh et al. (2020)	Single shear	200	20	300	300	36.8 MPa	5-ply CLT E_t = 11.7 GPa [e]	2 screws [i]	10	1005 (100)
			20	250	350				3	1010 (10)
			20	200	400				10	1095 (170)
			25	300	300				3	1040 (10)
			25	250	350				5	1060 (125)
			25	200	400				6	1210 (155)
			35	300	300				10	1010 (140)
			35	250	350				3	1025 (70)
			35	200	400				10	1215 (120)

a. Timber sandwiched by concrete.

b. Concrete sandwiched by timber.

c. According to Eurocode EN 1992-1-1 (2004).

d. According to Eurocode EN 14080 (2013).

e. Young's modulus for the longitudinal layers of CLT. The notch depths were not exceeding the maximum thickness of the first CLT layer.

f. Screw type (coach screw and self-drilling screw) and screw diameter (12-16 mm) in the original specimens are not distinguished here due to the insignificant effects on the connection stiffness.

g. Self-drilling washer head screw SPAX® 8×160 according to National Technical Approval Z-9.1-449 (2012).

h. Lag screw diameter was 16 mm and lag screw length was 200 mm.

i. ASSY VG countersunk head screw with a diameter of 8 mm and a length of 160 or 220 mm.

j. Mean value with standard deviation in parentheses. Connection stiffness is normalized to one-metre width.

3.4.2 Finite Element Analysis

Two-dimensional finite element models are built for the notched connections in the general-purpose finite element software ABAQUS (Dassault Systèmes® 2017). The connections are simulated with four-node bilinear plane stress quadrilateral elements (CPS4), as shown in Fig. 3.11(a). The element size in the finite element models is set as 10 mm, except for the concrete protrusion area in the notch and timber in front of the notch, where a denser mesh of 5 mm is used. The thickness of the model is set as 600 mm and the connection stiffness is linearly transformed to 1 m width. The contact between timber and concrete in the tangential direction is set as frictionless while a hard contact is defined in the normal direction. In the load-bearing surface, the stiffness scale factor in the normal direction is set as 5 to reduce the element penetration effect and mesh sensitivity issue. The boundary conditions of the finite element model are demonstrated in Fig. 3.11(b), where the bottom of timber and top of concrete are restricted from moving vertically and the right side of timber was restricted from moving horizontally. A distributed force is acting on the left end of concrete to push the concrete into the timber. The heights for timber h_t and concrete h_c are set as 130 mm and 90 mm, respectively.

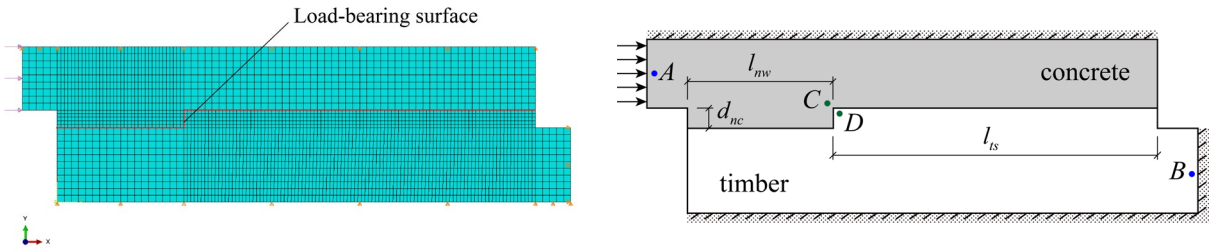

(a) Notched connection finite element model (b) Boundary conditions of the model

Fig. 3.11 Finite element modeling of notched connection under shear

As shown in Fig. 3.11(b), the geometry of a rectangular notched connection is defined by the notch length l_{nw}, notch depth d_{nc}, and timber shear length in front of the notch l_{ts}. In the reference notched connection model, the notch depth is set as 25 mm, the notch length is 180 mm, and the timber shear length is 500 mm. The material properties of timber and concrete used in the reference finite element model are listed in Table 3.6. The concrete Young's modulus E_c and Poisson's ratio

v_c are assumed to be 29 GPa and 0.2, respectively. The Young's modulus of timber in the longitudinal direction is assumed to be 10 GPa. The Young's modulus of timber in the transverse direction E_{TT} is set as 6.05% of the Young's modulus in the longitudinal direction E_t; the shear moduli of timber in the longitudinal-transverse plane G_{LT} and transverse plane G_{TR} are taken as 6.25% and 0.3% of the longitudinal Young's modulus E_t, respectively. These ratios are determined according to the properties of Spruce (Sitka) (Wood Handbook 2010). The Poisson's ratio of timber in the longitudinal-transverse direction is taken as 0.3.

Table 3.6 Material properties of timber and concrete in the reference finite element model

E_c (GPa)	v_c	E_t (GPa)	E_{TT} (MPa)	G_{LT} (MPa)	G_{TR} (MPa)	v_{LT}
29	0.2	10	605	625	30	0.3

Note: E_c is the Young's modulus of concrete. v_c is the Poisson's ratio of concrete. E_t is the Young's modulus of timber in the longitudinal direction. E_{TT} is the Young's modulus of timber in the transverse direction. G_{LT} is the shear modulus of timber in the longitudinal-transverse plane. G_{TR} is the shear modulus of timber in the transverse plane. v_{LT} is the Poisson's ratio of timber in the longitudinal-transverse plane.

The variables in the connection finite element models are the dimensions including the notch depth d_{nc}, notch length l_{nw}, and timber shear length l_{ts}, as shown in Fig. 3.11(b), and material properties including Young's moduli of concrete E_c and timber E_t (and correspondingly E_{TT}, G_{LT}, and G_{TR} of timber). The slip stiffness of notched connections is determined by dividing the applied force by the relative slip between timber and concrete. Depending on the slip measurement method, the obtained connection stiffness could be apparent stiffness or discrete stiffness. As shown in Fig. 3.11(b), if the relative slip is measured between A and B, then the connection stiffness is the apparent stiffness that contains deformation from the main bodies of timber and concrete. If the relative slip is measured between C and D, then the measured slip stiffness is the discrete stiffness of the connection, in which case the notched connection is treated as a discrete connection that only provides shear resistance at the load-bearing surface.

From the finite element analysis, the connection stiffness varying with different factors is illustrated in Fig. 3.12. As can be seen, the notched connection stiffness is most sensitive to the notch depth d_{nc} and timber Young's modulus E_t, while other factors (notch length l_{nw}, timber

shear length l_{ts}, and concrete Young's modulus E_c) have no remarkable effect on the connection stiffness within the investigated range. The apparent stiffness of notched connections is significantly lower than the discrete stiffness as expected. Since the deformation of timber and concrete components will be considered in the composite floor analysis, only the discrete connection stiffness will be discussed henceforth so that the deformation from the main bodies of timber and concrete will not be considered both in the connections and in the composite floor system.

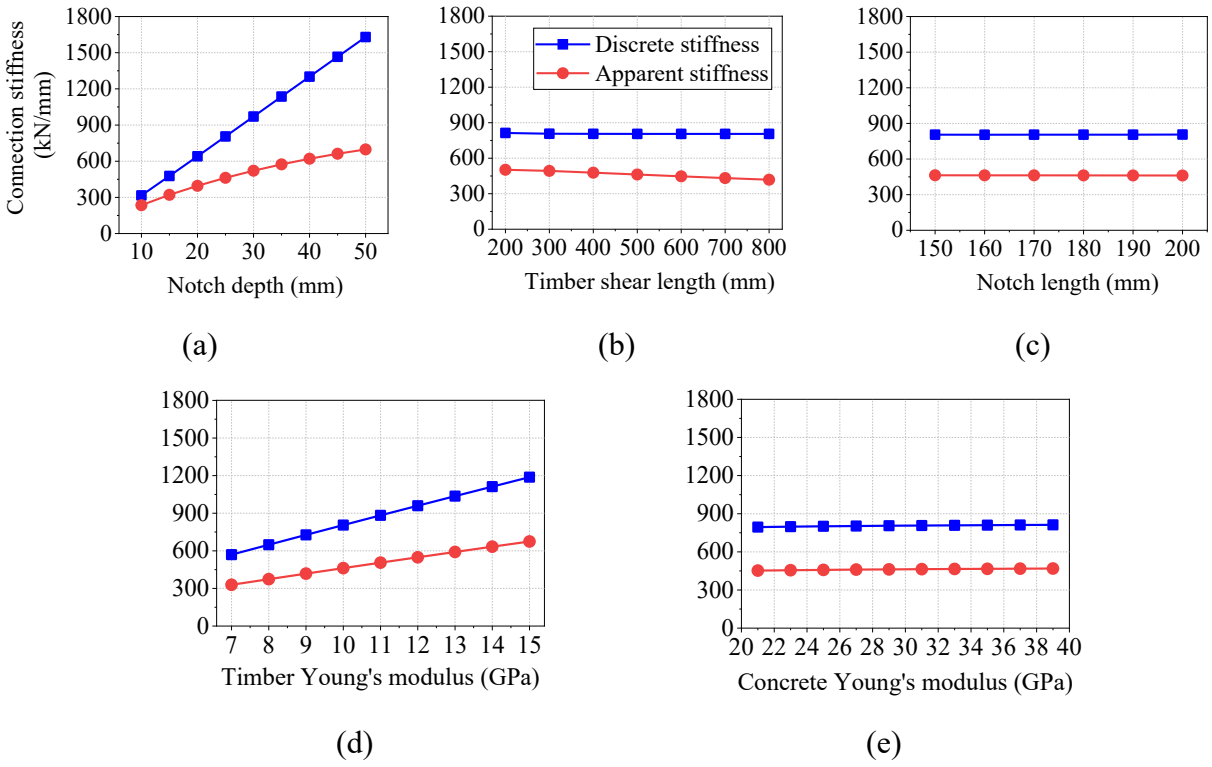

Fig. 3.12 Parametric studies on the notched connection stiffness (1 m width) (a) Notch depth; (b) Timber shear length; (c) Notch length; (d) Young's Modulus of Timber; and (e) Young's Modulus of Concrete

Fig. 3.12 shows a linear increasing trend of the notched connection stiffness with the notch depth d_{nc} and timber Young's modulus E_t. A further investigation found that the connection stiffness is not solely affected by the Young's modulus of timber E_t, but also depends on the ratio of timber

shear modulus G_{LT} to the Young's modulus E_t, while the effects of the transverse Young's modulus E_{TT}, Poisson's ratio v_{LT}, and transverse shear modulus G_{TR} can be neglected. Fig. 3.13(a) shows the effect of timber Young's modulus E_t on the notched connection stiffness when the ratio of G_{LT} to E_t is between 0.05-0.08. The higher the ratio of G_{LT} to E_t is, the higher the connection stiffness will be. An examination to the finite element results in Fig. 3.13(a) shows that the connection stiffness almost linearly varies with the ratio of G_{LT} to E_t.

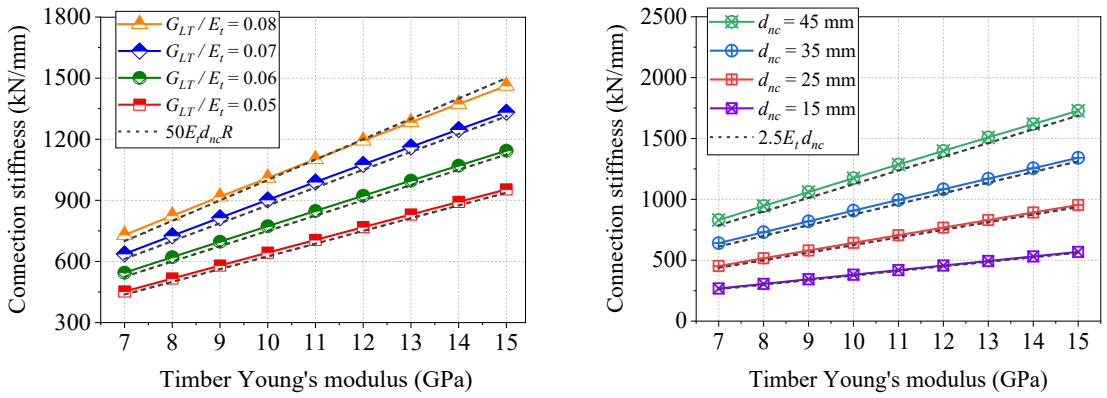

(a) Different ratios of G_{LT} to E_t (notch depth is 25 mm)

(b) Different notch depth (ratio of G_{LT} to E_t is 0.05)

Fig. 3.13 Notched connection stiffness (1 m width) versus timber Young's modulus

3.4.3 Empirical Formula of Connection Stiffness

The finite element analysis demonstrates that, in a certain range, the notched connection stiffness linearly varies with the notch depth d_{nc}, timber Young's modulus E_t, and the ratio of timber shear modulus G_{LT} to Young's modulus E_t. Based on the finite element results, an empirical formula of notched connection stiffness can be proposed as shown in Eq. 3.2.

$$k = 50E_t d_{nc} R \tag{3.2}$$

In Eq. 3.2, k is the notched connection stiffness per metre width (in kN/mm), E_t is the timber Young's modulus (in GPa), d_{nc} is the notch depth (in mm), and R is the ratio of G_{LT} to E_t. The comparison of the proposed connection stiffness with the finite element modeling results is shown in Fig. 3.13(a).

The shear modulus G_{LT} of mass timber panels is usually not measured and the exact ratio of G_{LT} to E_t is often unknown. For one-directional mass timber panels (GLT, DLT, and NLT), the shear modulus can be approximated by the shear modulus of lumber in the panels. However, the ratio of G_{LT} to E_t for common softwood species varies in a wide range of 0.032-0.21 (Wood Handbook 2010). For conservative purposes, the ratio of G_{LT} to E_t can be assumed to be 0.05 since most wood species can meet this threshold. Eq. 3.2 can then be simplified as

$$k = 2.5E_t d_{nc} \tag{3.3}$$

A higher ratio of G_{LT} to E_t can be used in Eq. 3.2 if a higher shear modulus G_{LT} is measured from tests. Fig. 3.13(b) compares the simplified connection stiffness formula with the finite element modeling results when the timber Young's modulus E_t and notch depth d_{nc} are in different values.

In equations 3.2 and 3.3, Young's modulus of concrete is not considered in the connection stiffness estimation since the contribution from the increase of concrete Young's modulus is negligible and concrete acts as a rigid body relative to the timber in the connection. However, the concrete properties will be considered in the composite system analysis. The timber shear length and notch length are not considered in the connection stiffness estimation. Similarly, these geometry factors will be considered in the composite system as the location and spacing of connections. The conditions to use empirical equations 3.2 and 3.3 are stated as below:

(1) The timber element can either be solid timber or laminated timber products with uniform laminate properties, such as GLT, DLT, and NLT, so that the notched connection stiffness linearly increases with the notch depth. For CLT, equations 3.2 and 3.3 can be used if the notch is cut within the first layer. The Young's modulus of timber is not less than 7000 MPa. For Eq. 3.3, the shear modulus of timber in the longitudinal-transverse plane G_{LT} is not less than 5% of the Young's modulus in the longitudinal direction E_L.

(2) The concrete Young's modulus is not less than 21 GPa. The maximum coarse aggregate size in concrete is small enough to fill the notch without leaving voids.

(3) The shape of the notch is rectangular with vertical bearing surfaces. The depth of the notch is no less than 10 mm and no deeper than 50 mm. The notch length is between 150 mm and 200 mm. The timber shear length is not less than 200 mm.

It should be noted that these requirements are proposed for the validation of equations 3.2 and 3.3. The requirements on notched connections in the composite floors should also take into account of the overall structural performance of the composite system, thus more stringent requirements are expected. Fig. 3.14 compares the proposed empirical formula with the measured connection stiffness in Section 3.3 and Table 3.5. The recommended notched connections stiffness in the COST Action report (Dias et al. 2018b) is also shown in Fig. 3.14. Compared to the connection stiffness recommended by the COST Action report (Dias et al. 2018b) which only considered the effect of the notch depth d_{nc}, the proposed formula allows the consideration of the material properties of timber in the connection stiffness estimation. The accuracy of the proposed notched connection stiffness will be examined in the MTP-concrete composite floor systems in Chapter 5.

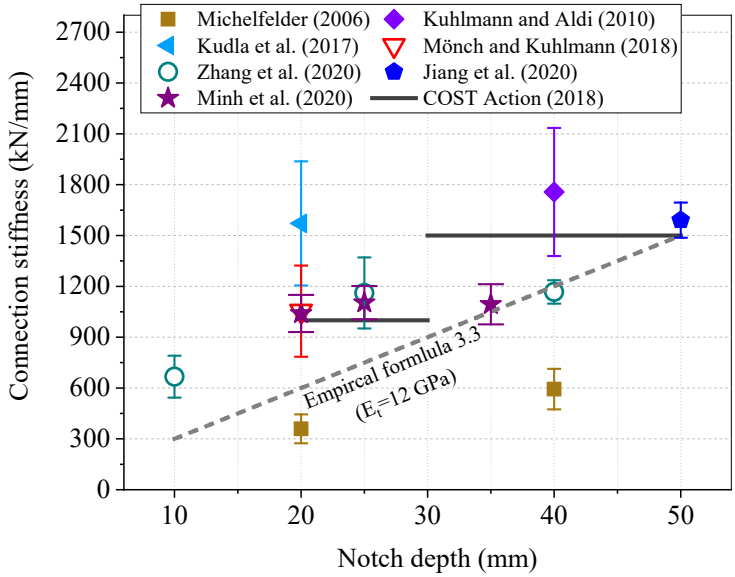

Fig. 3.14 Comparison between the measured notched connection stiffness (per metre width) and the proposed empirical formula

3.5 Strength Prediction of Notched Connections

This section discusses the ultimate strength prediction to the notched connections. The failure of the notched connections under shear could be in timber or concrete. Since the shear force between timber and concrete is only transferred at the load-bearing surface, local stress peaks appear around the notched regions and the normal stresses and shear stresses in timber and concrete are not

uniformly distributed. As an example, Fig. 3.15 shows the compressive stresses and shear stresses in concrete and timber around the notched connection obtained from finite element analysis. Specifically, the distribution of compressive stresses along path A and path B and shear stresses along path C and path D are derived from finite element analysis. The theoretical mean stresses which are calculated from the applied load divided by the cross-section areas of paths A, B, C, and D are also shown in Fig. 3.15 and compared with the actual stress distributions.

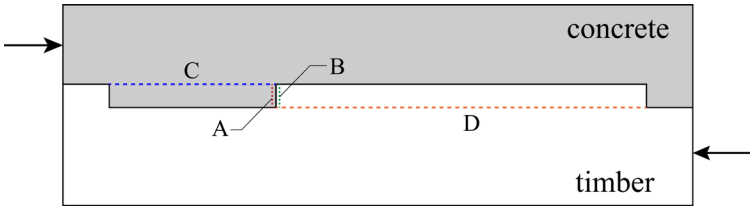

(a) Four paths in timber and concrete around the notched connection

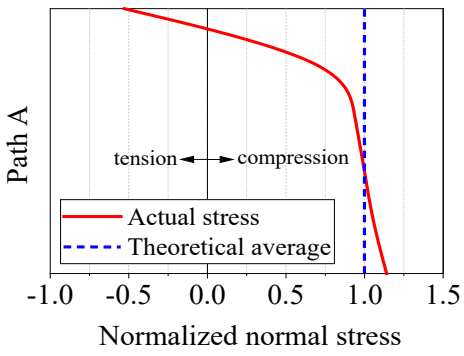

(b) Normal stresses in concrete

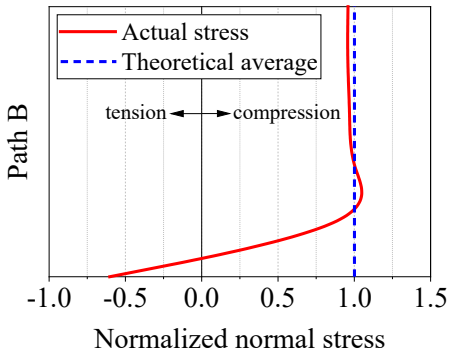

(c) Normal stresses in timber

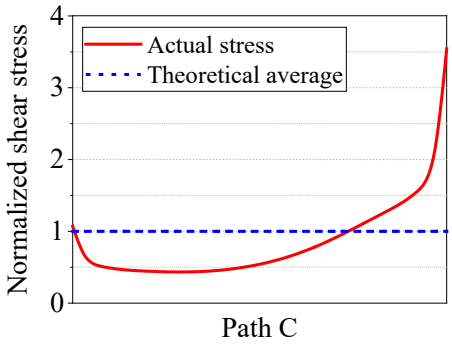

(d) Shear stresses in concrete

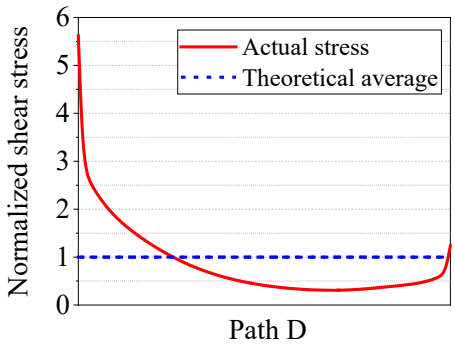

(e) Shear stresses in timber

Fig. 3.15 Stress distributions in timber and concrete around the notched region

As can be seen from Fig. 3.15(b) and (c), timber and concrete in the load-bearing surfaces are mainly subjected to compressive stresses, except for concrete at the top and timber at the bottom where the materials are under tension due to the sharp corners. The compressive stresses in concrete and timber are close to their theoretical average compressive stresses. The ultimate load for the notched connection when the connection fails due to concrete compression or timber compression can be approximated by equations 3.4 and 3.5, respectively.

$$P_{cc} = f_c' b d_{nc} \tag{3.4}$$

$$P_{tc} = \varphi_{tc} f_{tc} b d_{nc} \tag{3.5}$$

In equations 3.4 and 3.5, b is the width of the notch; d_{nc} is the notch depth; f_c' and f_{tc} are the compressive strengths of concrete and timber, respectively; and φ_{tc} is the correction factor for the compressive strength of timber due to the non-uniform stress distribution. Due to the low tensile strength of concrete, the cracking of concrete usually happens before the compressive failure of concrete. After the concrete cracking, the concrete at the load-bearing surface is expected to have more uniform compressive stresses. However, the compressive failure of concrete can happen early when the notches are cast in pour quality and the notches contain voids around the load-bearing area. In the properly cast notched connections, the compressive failure of concrete rarely governs. Among the tested longitudinal specimens in Section 3.3, only specimen L-10-250 failed due to compressive failure in timber. According to the measured connection strength and the compressive strength of timber f_{tc} shown in Table 3.2, the correction factor for timber compressive strength φ_{tc} can be estimated as 0.84.

The shear stresses in concrete and timber along path C and path D are not uniformly distributed especially at the regions close to the load-bearing surface, as shown in Fig. 3.15(d) and (e). To estimate the connection strength due to timber shear failure, the effective shear length of timber is often assumed to be eight times of the notch depth. However, this assumption can lead to overestimation of the connection strength if the timber shear length is shorter than eight times of the notch length, or underestimation of the connection strength if the timber shear length is much longer than eight times of the notch depth. In order to address this problem, the actual timber shear length is considered to predict the connection strength due to timber shear failure as shown in Eq. 3.6.

$$P_{ts} = \varphi_{ts} f_{ts} b l_{ts} \tag{3.6}$$

In Eq. 3.6, f_{ts} is the timber shear strength in the longitudinal direction; l_{ts} is the timber shear length; and φ_{ts} is the correction factor due to the non-uniform distribution of shear stresses along the failure plane. In the connection shear tests, connections L-25-250, L-40-250, L-25-150, and L-25-350 failed due to timber shear. According to the test results, the correction factor φ_{ts} is estimated to be 0.4. Fig. 3.16 compares the measured connection strengths with the predicted results using Eq. 3.6. The prediction that uses eight times of the notch depth as the effective timber shear length is also shown in Fig. 3.16 as the dashed line which overestimates the connection strength. It can be expected that after the timber shear length increased to a certain point, the actual connection strength due to timber shear will be higher than the dashed line.

Finally, the connection strength due to concrete shear failure P_{cs} can be empirically estimated as

$$P_{cs} = \varphi_{cs} \sqrt{f_c'} b l_{nw} \tag{3.7}$$

In Eq. 3.7, P_{cs} is the connection strength (in N), b and l_{nw} are the notch width (mm) and notch length (mm), respectively; f_c' is the concrete compressive strength (MPa), and φ_{cs} is the correction factor for concrete shear strength. The value of φ_{cs} can be difficult to determine as the concrete shear failure in the notches is a process of crack propagation and the concrete shear failure was not observed in the push-out tests. However, since the concrete shear strength was higher than the measured connection strength, the correction factor φ_{cs} should be greater than 0.85 according to the measured connection strengths and the concrete compressive strength f_c' in Table 3.3. According to the notched connection shear tests conducted by Jiang et al. (2020), the value of φ_{cs} can be estimated as 1.32. Without considering the contribution from normal compressive stresses vertical to the shear plan of concrete, the American Association of State Highway and Transportation Officials standard (2003) suggests the use of 0.99 for φ_{cs} to calculate the shear strength of concrete shear keys in segmental concrete bridges. The value of φ_{cs} will be examined in Chapter 5 to estimate the ultimate strength of the composite floors due to concrete shear failure in the notches.

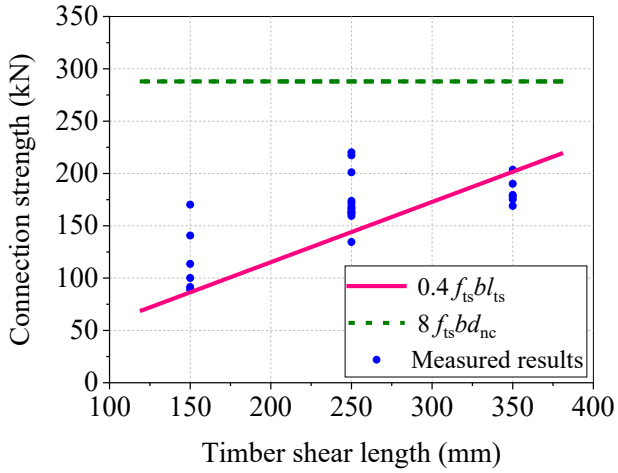

Fig. 3.16 Prediction of the notched connection strength due to timber shear failure

3.6 Conclusions

This chapter discussed the structural performance of notched connections under the shear force. The connection push-out tests were conducted first on different configurations of notched connections. Then the push-out tests on the rectangular notched connections conducted by other researchers were summarized. To estimate the notched connection stiffness, an empirical formula was proposed based on finite element modeling results. Finally, empirical equations were proposed to estimate the notched connection ultimate strengths. Based on the experimental and numerical investigations on the notched connections, the following conclusions can be drawn:

1. The stiffness, ultimate load-carrying capacity, and failure pattern of the notched connections are affected by the connection geometry and material properties of timber and concrete. The orientation of timber is the most important factor that impacts the connection structural performance. A limited number of self-tapping screws in the notch had a negligible effect on the connection performance.
2. The timber shear length in front of the notch affects the load-carrying capacity and failure pattern of the notched connections under shear. The strength of the connection increases with the timber shear length and the connection failure pattern becomes more ductile when the timber shear length increases.
3. The notch depth affects the connection stiffness, load-carrying capacity, and failure pattern of the connections under shear. Deeper notches have higher stiffness and strength but brittle

failure pattern, while shallower notches have lower stiffness and strength but ductile failure pattern.

4. The notched connection stiffness exhibited a large variation among the connection shear tests conducted by different researchers. Except for the differences in the geometry and material properties of the connection specimens, the variation of the measured results could come from different relative slip measurement methods.
5. The finite element modeling on notched connections indicates that the timber Young's modulus, timber shear modulus, and notch depth are three critical factors affecting the notched connection stiffness. The serviceability connection stiffness of notched connections can be estimated from Young's modulus of timber and the notch depth when the connection sizes and material properties satisfy certain requirements.
6. Empirical equations are proposed to estimate the ultimate strengths of notched connections in different failure modes. While being practical in estimating the connection strengths, further research is required to accurately determine the correction factors in the empirical equations.

Based on the experimental and numerical analysis on notched connections, full-scale MTP-concrete composite floor specimens were designed and tested under bending. The bending tests on MTP-concrete composite floors are described in Chapter 4. The proposed empirical equations to estimate the stiffness and ultimate strength of notched connections are verified in the discrete bond composite beam model in Chapter 5.

Chapter 4

Bending and Vibration Tests on the Composite Floor Systems

4.1 Introduction

This chapter discusses the bending tests and vibration tests on the full-scale mass timber panel-concrete composite floors with notched connections. The bending tests on the floors were conducted in two phases. In each phase, vibration tests were conducted on the floors before the destructive bending tests. Totally twelve composite floors specimens were fabricated and tested and each floor had its unique features. The tests focused on both the overall structural performance of the composite system and the local damages of the notched connections. The floor performance at both the serviceability state, such as dynamic and static bending stiffness, and the ultimate state, such as load-carrying capacity and failure pattern, were investigated and discussed. The outcome of this research is the recommended design approach for mass timber panel-concrete composite floors with notched connections.

4.2 First Phase Bending Tests

4.2.1 Introduction

In the first phase bending tests, nine composite floor specimens were constructed and tested under four-point bending. The bending tests were aimed at investigating several factors that affect the static structural performance of notch-connected MTP-concrete composite floors through experimental testing on full-scale floor strips. The variations between the nine specimens were the floor span, number of notched connections, notch geometry, concrete layer thickness, presence of screws in the notch, and loading direction. By comparing the stiffness, strength, and ductility of different specimens, the specimen with the most efficient connection design was identified. The overall objective of the bending tests was to gain insights into the structural performance of MTP-concrete composite floors with notched connections and provide additional data to the current state

of the art. Test results and findings from the bending tests serve as an important reference for the continued evolvement of MTP-concrete composite floors with notches.

4.2.2 Floor Specimen Design

In the first phase bending tests, nine composite floor specimens were fabricated as shown in Fig. 4.1. The width of the specimens was 600 mm and the length was 6.3 m, except for specimen SPU-2 which had a length of 7.4 m. The thickness of the timber panel in the specimens was 130 mm while the concrete thickness varied between 60 mm and 85 mm. The detailed dimensions of specimens can be found in Fig. 4.1 and Table 4.1 while the specimen preparation process is demonstrated in Fig. 4.2.

The reference specimen (specimen SPU-1) had a concrete thickness of 85 mm and a length of 6.3 m (6m span) corresponding to a typical span in a residential or office building. Six notched connections were symmetrically spaced about the mid-span. The notches were cut into a rectangular shape which has been proven to be the stiffest shape for notch geometries (Yeoh et al. 2011c; Boccadora and Frangi 2014). The width and depth of these notches were 180 mm and 25 mm, respectively, as suggested by Dias et al. (2018a), while the length of timber between notches was 500 mm. Two self-tapping screws at a spacing of 300 mm were installed at mid-span vertically and in each notch at an angle of 45°.

Specimen SPU-2 had a longer span (7.4 m length and 7.1 m span) and the same number and sizes of notches in a slightly wider spacing (600 mm timber shear length between notches). The number of connections in specimen SPU-3 was reduced to four to study the structural performance of the composite floor affected by the number of connections. Specimens SPU-4 and SPU-5 were designed to study the effect of the notch depth on the composite behaviour of the floors. The notch depth in Specimen SPU-4 (13 mm) was reduced to about half of the notch depth in the reference specimen SPU-1 (25 mm), while specimen SPU-5 had varying notch depths along the span. Considering that the internal notches resist lower shear forces than the external notches, the depth of notches in specimen SPU-5 was increasing from mid-span to the supports from 15 mm to 25 mm. Specimen SPU-6 had the same geometry as the reference specimen but with no screws installed in the notches to investigate the contributions from screws to the stiffness and strength of

the floor. Specimens SPU-7 and SPU-8 had a thinner concrete layer (60 mm). The geometry and locations of notches in specimen SPU-7 were the same as the reference specimen while specimen SPU-8 did not contain any form of mechanical connection except two vertical screws at mid-span to hold timber and concrete together. Specimen SPU-9 had swapped positions of timber and concrete to mimic the situation when the composite floor is subjected to a negative bending moment (i.e. timber resists compression and concrete resists tension). The notches in specimen SPU-9 were shifted closer to the supports so that the load-bearing surfaces were in the same locations as the reference specimen SPU-1.

Table 4.1 Dimensions of the composite floor specimens

Specimen	Length /Span (m)	Concrete thickness (mm)	Number of notches	Notch depth (mm)	Timber shear length (mm)	Screws in the notch
SPU-1	6.3/6	85	6	25	500	2
SPU-2	7.4/7.1	85	6	25	600	2
SPU-3	6.3/6	85	4	25	750	2
SPU-4	6.3/6	85	6	13	500	2
SPU-5	6.3/6	85	6	15-25	500	2
SPU-6	6.3/6	85	6	25	500	0
SPU-7	6.3/6	60	6	25	500	2
SPU-8	6.3/6	60	0	NA	NA	NA
SPU-9	6.3/6	85	6	25	500	2

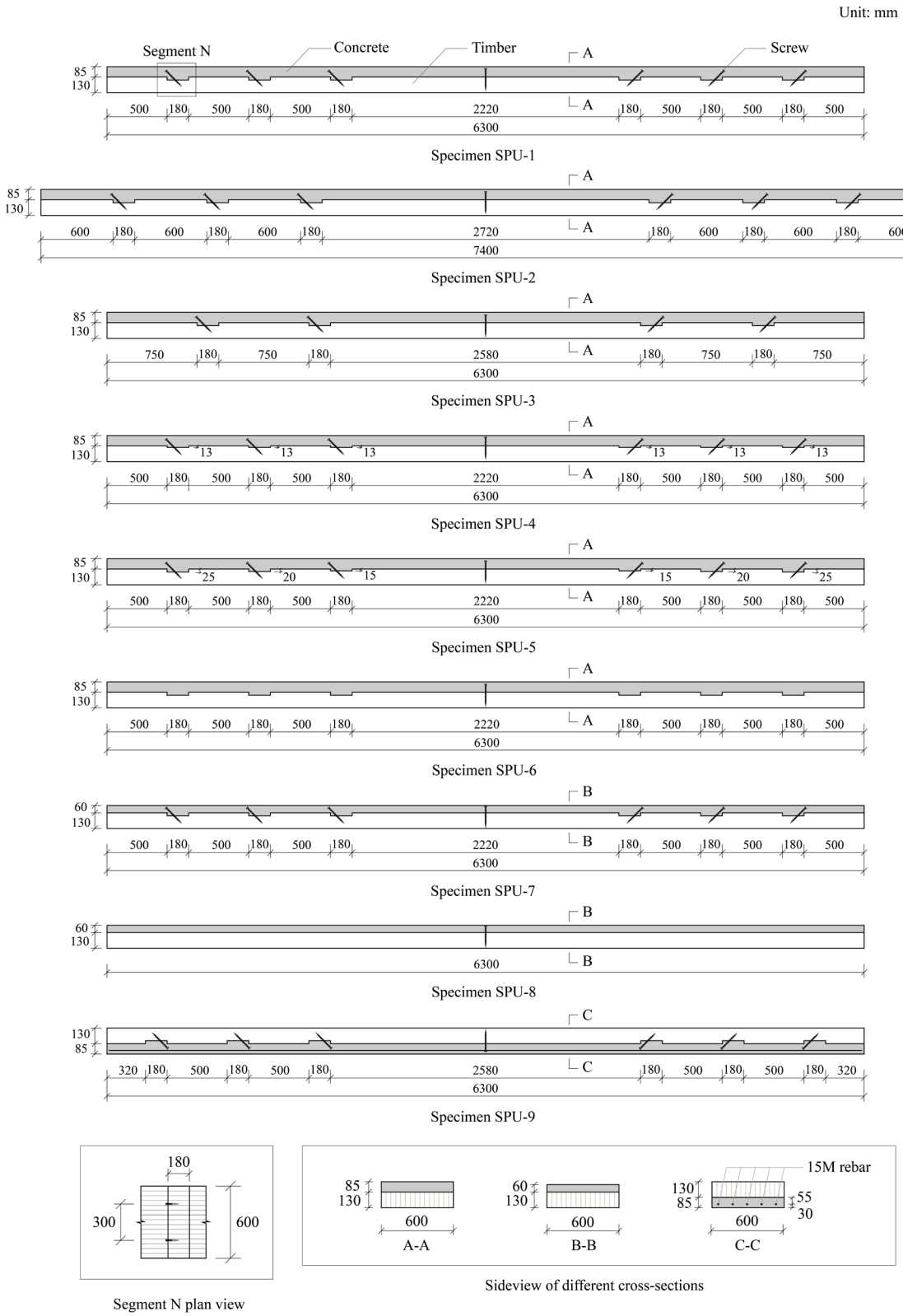

Fig. 4.1 Mass timber panel-concrete composite floor specimen configurations (the unmarked depth of notches is 25 mm)

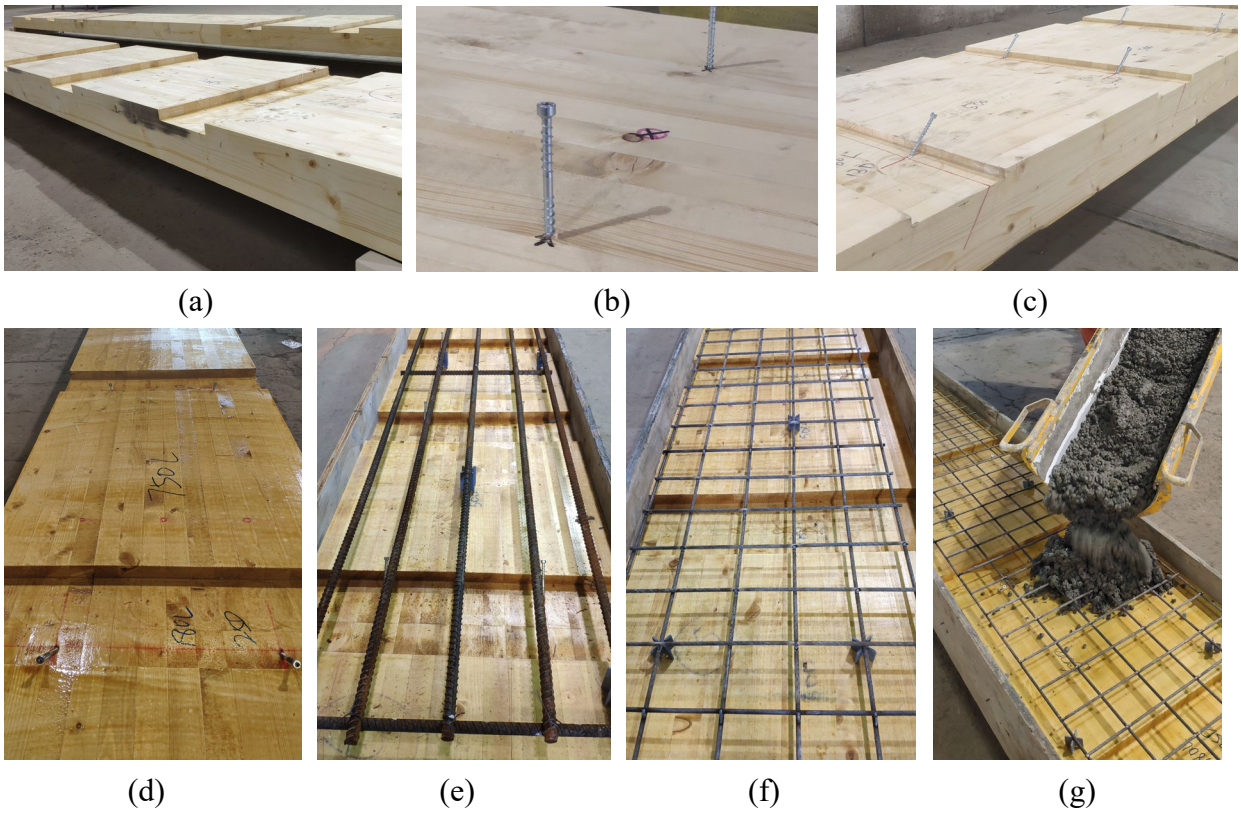

Fig. 4.2 Composite floor specimen preparation (a) Notches cut on the GLT panels; (b) Screws installed at mid-span of floors; (c) Screws installed in the notches; (d) Timber treated with waterproof sealer; (e) Steel rebar in specimen SPU-9; (f) Wire mesh in rest of the specimens; and (g) Concrete casting

4.2.3 Materials

Commercial Glued-Laminated Timber (GLT) panels were used to fabricate the specimens. The GLT panels were manufactured with No. 2 or better grade spruce/pine dimension lumbers and a structural adhesive (melamine formaldehyde). The density of GLT panels was 423 kg/m^3 and the moisture content measured right before the bending test was 15.8%. The notches on the panels were cut with a computer numerical control (CNC) machine (Fig. 4.2(a)). Before concrete casting, the surface of timber was treated with the waterproof sealer (Olympic® Waterguard®) to prevent the absorption of water from concrete by the wood (Fig. 4.2(d)). To determine the modulus of elasticity (MOE) and modulus of rupture (MOR) of timber, three-point bending tests were conducted on nine timber beams (span: 1.9 m; height: 100 mm; width: 190 mm; loading rate: 2

mm/min) cut from one GLT panel produced from the same batch. The measured modulus of elasticity (MOE) and modulus of rupture (MOR) of timber were 9061 MPa and 45.9 MPa, with coefficients of variation of 5.3% and 6.7%, respectively. The full test results on the timber beams can be found in Appendix III.

Self-tapping screws were used as additional steel fasteners in the specimens to connect timber and concrete and prevent gap opening, as shown in Fig. 4.1. The screws (CTC7160 manufactured by Rothoblaas) were the timber-to-concrete fastener with specific CE certification according to European Technical Assessment ETA 19/0244 (2019). The screws were made of carbon steel with bright zinc plated. The diameter of the screws was 7 mm and the length was 160 mm. According to ETA-19/0244 (ETA 2019), the characteristic yield moment of the screws is 20 Nm, the characteristic withdrawal-resistance parameter is 11.3 N/mm^2, and the characteristic tensile strength is 20 kN. The actual tensile strength measured on 13 screws was 23.4 kN with a coefficient of variation of 8.9%. The tensile test results on the screws can be found in Appendix V.

Two screws were used at mid-span in each specimen to connect two layers in the vertical direction. In specimens SPU-1, SPU-2, SPU-3, SPU-4, SPU-5, and SPU-7, screws were installed in the notched connections in a diagonal direction of 45º towards the nearest support. This way the screws were under tension when the floors were subjected to bending (Marchi et al. 2017). The diagonal screws may also restrict the crack opening in concrete developed from the notched corner. In specimen SPU-9, screws in the notches were installed at 45º towards the support at the far end due to the reversed bending moment. The distance of screws to the edge of the notch is shown in Fig. 4.3. The embedment length of screws into timber was 80 mm (105 mm for the vertical screws in specimens SPU-7 and SPU-8 due to the thinner concrete layer).

After screw drilling, the formwork was constructed around the timber panels and steel reinforcement was placed into the formwork. Concrete was then cast directly on top of the timber panels. Concrete in all specimens was cast in the same batch. The nominal maximum coarse aggregate size was 10 mm to avoid the formation of voids around the corners of notches. The measured slump for concrete was 70 mm with an air content of 2.5%. Four cylinders with a nominal diameter of 100 mm and a height of 200 mm were cast at the same time and tested at 8 days (1 cylinder) and 28 days (3 cylinders) according to ASTM C39/C39M-20. The concrete cylinder tested at 8 days had a compressive strength of 31.7 MPa. The average compressive

strength of concrete cylinders at 28 days was 40.2 MPa with a 0.9% coefficient of variation. The density of concrete cylinders was 2330 kg/m^3. Based on the density (ρ_c) and 28-day compressive strength (f_c') of concrete, Young's modulus of concrete was estimated to be 28369 MPa according to Eq. 4.1 (CSA A23.3-19).

$$E_c = (3300\sqrt{f_c'} + 6900)\left(\frac{\rho_c}{2300}\right)^{1.5} \tag{4.1}$$

Except for specimen SPU-9, the concrete in the rest of the specimens was reinforced with welded steel mesh (Fig. 4.2(f)) with a diameter of 6 mm, a grid size of 100 mm ×100 mm, and a clear cover of 25 mm from the top surface of GLT. The steel mesh was used to reduce the shrinkage of concrete and cracking due to temperature strain. Specimen SPU-9 was reinforced with five 15M bars (Grade 400R) in the longitudinal direction to resist tensile forces in concrete. The rebar in specimen SPU-9 was spaced at 120 mm and the distance from the rebar centre to the bottom of GLT was 55 mm (Fig. 4.1). The rebar in specimen SPU-9 was designed in such a way that it would yield before the failure of the timber member. The concrete in all specimens was painted white before the bending test to facilitate crack observation.

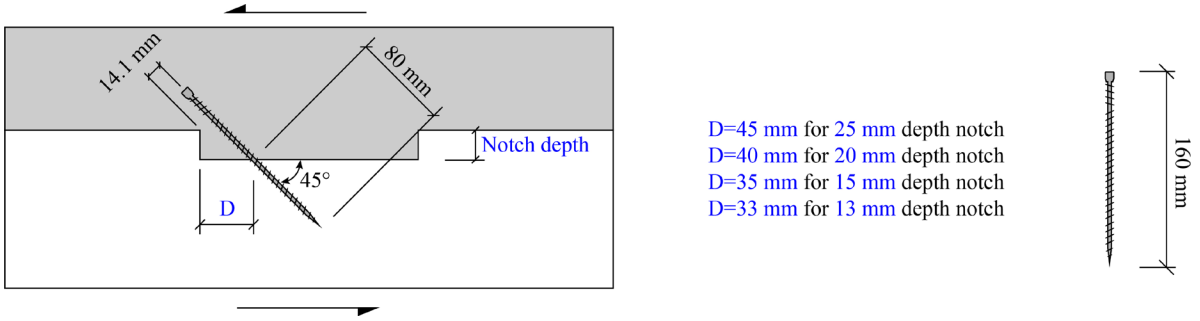

Fig. 4.3 Inclined self-tapping screws in the notches of composite floor specimens

4.2.4 Testing Methods

Four-point bending tests were conducted on the composite floor specimens, as shown in Fig. 4.4. The notched connections in the specimens were in the constant shear zones between the supports and the loading points. The specimens were supported on a roller at one end and a pin at the other. The width of the supports was 200 mm to minimize indentation of timber at supports. The middle

of the supports was 150 mm away from the edge of the floor so the effective floor span was 300 mm shorter than the length of the specimens. The load was applied from an actuator (250 kN capacity and 500 mm stroke) and transferred to the composite floors at two third-points through a spreader steel beam. The steel beam loaded the specimens through steel dowels, each of which was sitting on a C-channel and a plywood layer. The plywood was used to distribute the load transferred to the specimens. In some specimens, the plywood layer was replaced by a CLT block to increase the travel of the actuator. Douglas fir blocks were also used in the supports to raise the specimens.

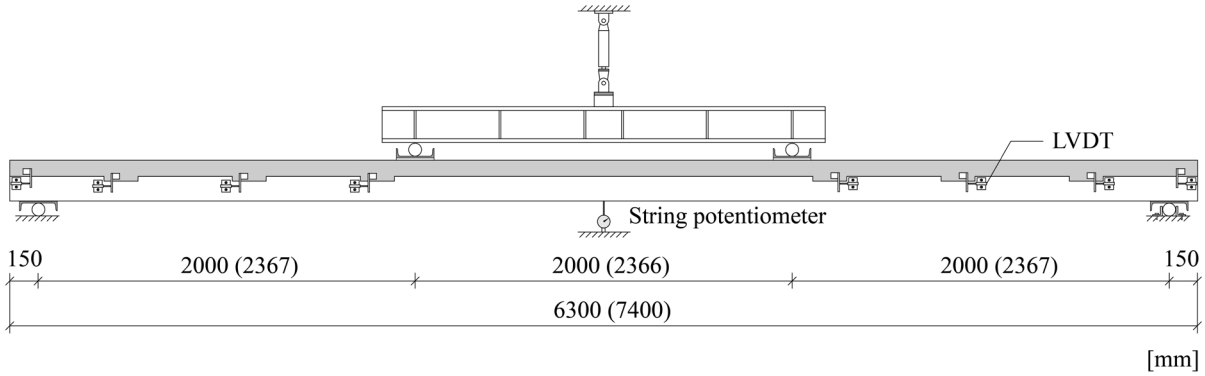

(a)

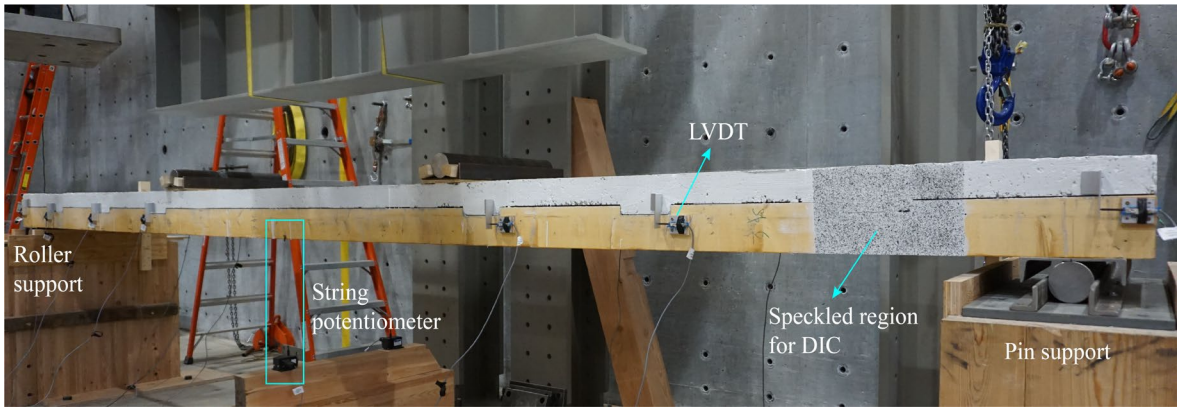

(b)

Fig. 4.4 Four-point bending test setup (a) Schematic of the test setup (numbers in the brackets are the dimensions of specimen SPU-2); and (b) Test setup in the laboratory

The load was applied using displacement control until the failure of the specimens. Displacement from the actuator was applied monotonically with a loading rate of 3-4 mm/min to ensure that specimens would fail in about 30 mins to prevent any short-term creep. As shown in Fig. 4.4, displacement at the mid-span of each specimen was measured by two string potentiometers mounted at each side. Linear variable differential transformers (LVDTs) were mounted at each notch and at the floor ends to measure the relative slip between concrete and timber. For specimen SPU-8 which had no notched connection, LVDTs were mounted at the floor ends and the third points.

In addition to the use of LVDTs, the digital image correlation (DIC) technique was applied in one speckled notched region in each specimen (except for specimen SPU-8) to capture the displacement field and failure mode of the notched connections. A two-dimensional DIC system (GOM Correlate) with a single camera was used to capture the images every 10 seconds over the course of the test. A facet size of 19 pixels and a point distance of 16 pixels were used to analyze the deformed images (dimensions 6000 by 3376 pixels and resolution 350 by 350 dpi).

4.2.5 Test Results

Failure modes of floor specimens

Different connection designs in the specimens resulted in different failure modes between tests. The notched connections resisted shear forces when the floor was under bending. Due to the stress concentration around the notched corners, diagonal concrete cracking at the notched corners (shear cracks) could be observed in almost all specimens with notches, as shown in Fig. 4.5(a). Other major damages and failures in the specimens observed during the bending tests are summarized as follows and illustrated in Fig. 4.5.

- NSC: notch shear failure in concrete (due to shear crack propagation), Fig. 4.5(b) and (e).
- NCT: notch crushing in timber, Fig. 4.5(c).
- NCC: notch crushing in concrete, Fig. 4.5(d).
- TB: timber bending failure at the bottom (rupture of wood fibers in tension), Fig. 4.5(i).

- TTB: timber combined tension and bending failure at the bottom (rupture of wood fibers in tension), Fig. 4.5(g) and (h).
- TCB: timber combined compression and bending failure at the top (crushing of wood fibers), Fig. 4.5(k).
- CB: concrete buckling under compression (due to uplifting), Fig. 4.5(e).
- CS: concrete shear failure in the cross-section (due to uplifting), Fig. 4.5(f).
- CC: concrete flexural crack at the bottom, Fig. 4.5(k).
- SY: steel rebar yielding, Fig. 4.5(k).

For the specimens subjected to positive bending moments, the failure patterns can be categorized into two types: failure in concrete and failure in timber. Specimen SPU-1 which was designed as the reference case failed in the concrete portion. Under the shear load between timber and concrete, shear cracks of concrete initiated from notches around the load-transfer areas. These cracks started in a diagonal or close to vertical direction from the notched corners then propagated more or less to the horizontal direction. Except for the shear cracks, the crushing of concrete can also be observed around the load-bearing surfaces in some notches (Fig. 4.5(d)). With the increased load, the rotation of the notch protrusion can be observed and a gap was formed between timber and concrete. The notched connections eventually sheared off under the shear load, started from one external notch (notch near the support), and followed by the notch next to the external one. The failure of notches caused an abrupt gap opening between timber and concrete. As a result, the concrete layer which was under compression failed due to buckling. The sudden uplifting of concrete outside the loading points also caused the shear failure of the concrete layer at the location near one loading point. The failure of the specimen was abrupt and brittle. No obvious damage could be observed in the timber portion and flexural crack was not found at the bottom of concrete at mid-span. The same general failure modes were observed in specimens SPU-2, SPU-3, SPU-6, and SPU-7, as demonstrated in Fig. 4.5(a), (b), (e), (f), and (j).

Specimens SPU-4, SPU-5, and SPU-8 failed in the timber portion. Due to the shallow notches, SPU-4 exhibited a large deflection under bending but ductile failure pattern. The ductility of specimen SPU-4 came from the crushing of timber fibers in the notched connections under the

shear load (NCT), as shown in Fig. 4.5(c). Minor cracks were observed in concrete around the notched corners but these cracks propagated slowly. The final failure of SPU-4 was in the timber component with a splintering tension failure under the notch near a loading point (Fig. 4.5(g)). The failure mode of specimen SPU-5 (Fig. 4.5(h)) was similar to SPU-4 except that SPU-5 was more rigid under bending and exhibited higher load-carrying capacity. The ductility of SPU-5 mainly came from the shallower notches close to the mid-span and the high strength and rigidity could be attributed to the deeper notches near the supports. Specimen SPU-8 had no connection between timber and concrete except two screws at mid-span. No composite action existed between two layers except friction. Specimen SPU-8 experienced large deflection and large gap opening between timber and concrete during the test. The final failure of specimen SPU-8 was the timber member bending failure (TB) underneath one loading point (Fig. 4.5(i)).

Specimen SPU-9 had the reversed positions of timber and concrete simulating negative bending, and concrete was reinforced with steel rebar to resist tensile forces. Specimen SPU-9 was the only specimen where concrete developed visible flexural cracks due to tensile stresses (Fig. 4.5(k)). Cracks at the bottom of concrete were observed shortly after the test started (around 13 kN vertical load). After that, the tensile forces in the concrete layer were mainly resisted by the rebar. Since a large portion of concrete had cracked, the deflection of specimen SPU-9 was much higher than the reference specimen SPU-1. However, the rebar in tension and timber under compression provided excellent ductility to the floor. The relative slip between two layers was notably small indicating that the large deflection of specimen SPU-9 was attributed to concrete cracking rather than low connection stiffness. Tensile stresses at the bottom of timber were significantly reduced because of the composite action, but the crushing of wood fibers could be observed at the top of timber (TCB), as shown in Fig. 4.5(k). After unloading, it was observed the specimen had permanent curvature indicating that the steel rebar had yielded (SY).

(a) Concrete shear crack (SPU-6)

(b) Notch shear failure in concrete (SPU-2)

(c) Notch crushing in timber (SPU-4)

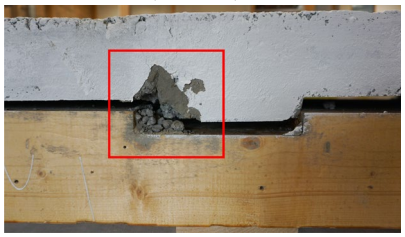

(d) Notch crushing in concrete (SPU-1)

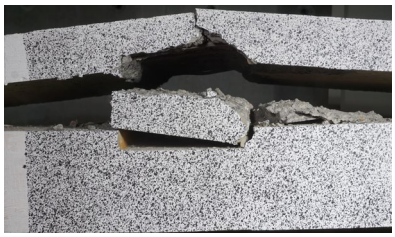

(e) Notch shear failure and concrete buckling (SPU-7)

(f) Concrete layer shear failure (SPU-3)

(g) Timber combined tension and bending failure (SPU-4)

(h) Timber combined tension and bending failure (SPU-5)

(i) Timber bending failure (SPU-8)

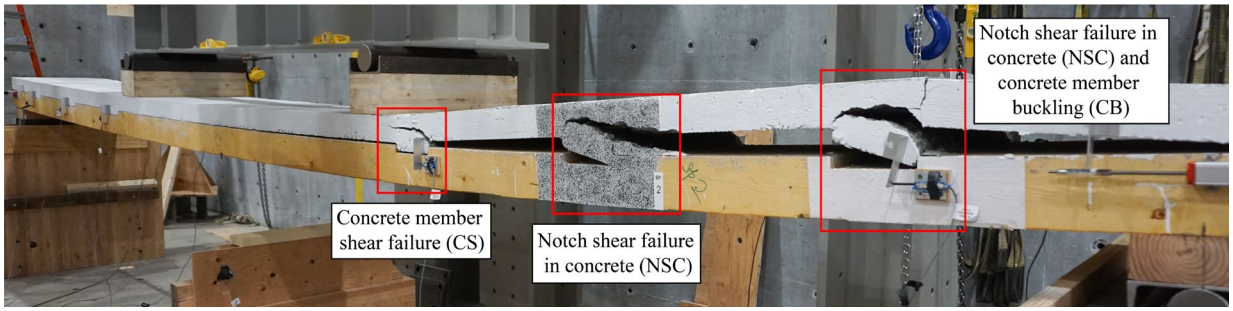

(j) Failure of specimen SPU-2

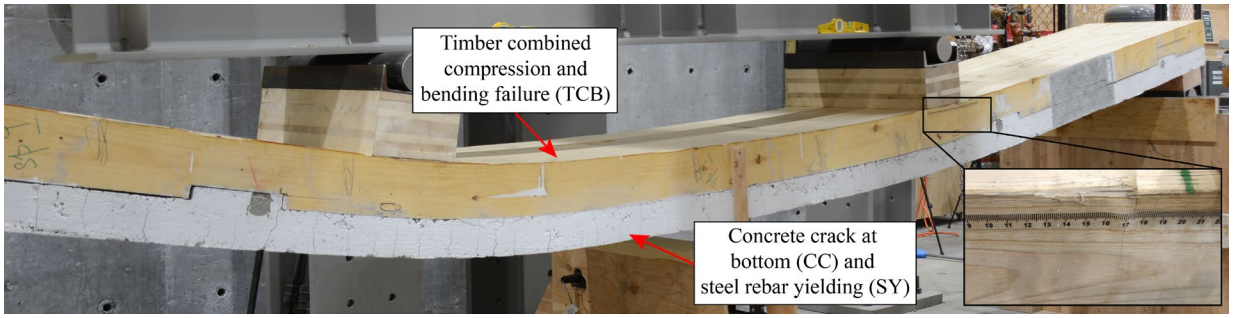

(k) Failure of specimen SPU-9

Fig. 4.5 Typical failure modes of composite floors observed from the bending tests

Failure modes of notched connections

Different failure modes of the floor specimens under bending were largely the results of different notched connection behaviours under shear. The localized failure and damage of the notched connections in the floor specimens were captured by the DIC images. Fig. 4.6 shows the horizontal strain fields for the notches in specimens SPU-3, SPU-5, and SPU-9 under the shear load, which represent three typical failure modes. The general response of connections under shear was categorized into three phases. Phase 1 represents the initial elastic stage where notches started to resist slip. Phase 2 represents the stage where damage started to grow in timber and concrete. Phase 3 corresponds to the stage just before the failure of the specimen.

A typical shear failure in concrete (NSC) can be observed in the internal notch (notch close to the mid-span) in specimen SPU-3 (Fig. 4.6(a)). In the elastic stage, compression between timber and concrete at the load-bearing area was seen. With the increase of load, the crushing and cracking of concrete were initiated. The concrete cracking was the result of stress concentration at the notched corner and the low tensile strength of concrete. The crack initially grew in a close to vertical direction then propagated progressively to the horizontal direction until the connection failed. The failure of the connection was mainly in concrete while the timber part was almost intact.

The middle notch in specimen SPU-5 showed a different failure pattern under the shear load due to a slightly shallower notch (20 mm). As shown in Fig. 4.6(b), at the elastic stage, the connection behaviour was similar to the connection in specimen SPU-3. Then the crushing of concrete and timber can be observed at the compression area (NCT and NCC). Before the failure of the specimen (outside of the DIC field of view), a severe crushing of both concrete and timber along with a gap between two components was noticeable. Since the timber crushing was initiated, no large crack was developed in concrete.

The notched connection in specimen SPU-9 had opposite positions of timber and concrete (Fig. 4.6(c)). Under the shear load, the concrete crack developed from the notched corner and propagated from top to bottom. At the same time, cracks also developed from the bottom of concrete due to tensile stresses (CC) under bending. The gap opening between two layers at failure was small compared to specimens SPU-3 and SPU-5.

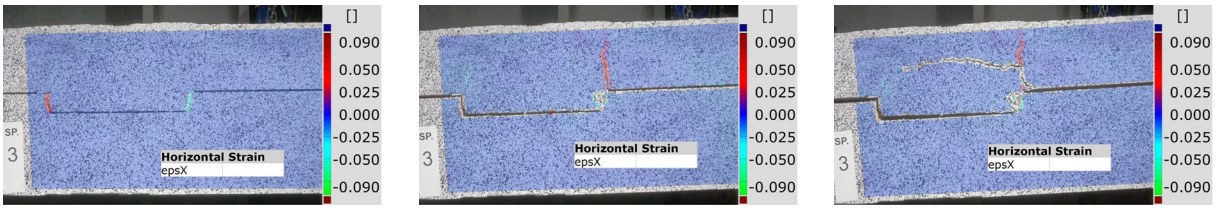

Phase 1 Phase 2 Phase 3

(a) Internal notch in specimen SPU-3

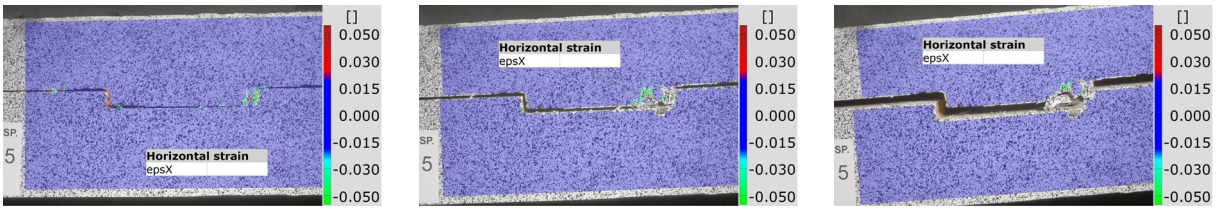

Phase 1 Phase 2 Phase 3

(b) Middle notch in specimen SPU-5

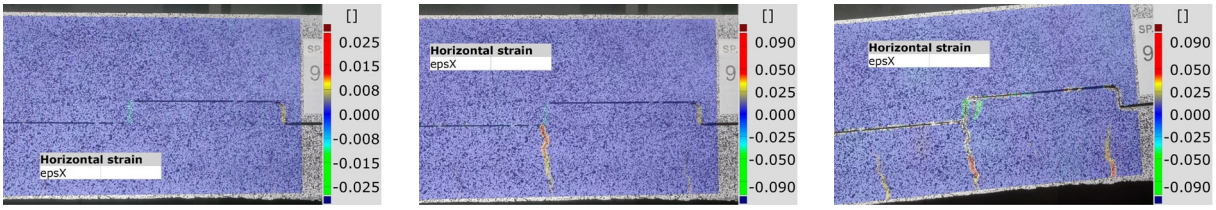

Phase 1 Phase 2 Phase 3

(c) Middle notch in specimen SPU-9

Fig. 4.6 Horizontal strain fields of the notched regions captured by the digital image correlation technique showing three types of notched connection failure pattern

Load-deflection behaviours

The obtained load-deflection curves for the floor specimens are shown in Fig. 4.7 where the mid-span deflection was taken as the average of deflections measured at two sides of each specimen. For comparison purposes, the theoretical linear elastic load-deflection responses for the non-composite floor, full composite floor, and bare GLT floor (130 mm thickness) are also plotted in Fig. 4.7. The bending stiffness for the non-composite floor is determined according to Eq. 4.2

$$(EI)_{no} = E_c I_c + E_t I_t \tag{4.2}$$

where E_c and E_t are the moduli of elasticity for concrete and timber, and I_c and I_t are the second moment of areas of concrete and timber, respectively. Eq. 4.2 was derived by assuming no interaction between timber and concrete thus the effective bending stiffness of the floor is simply the summation of the bending stiffness of timber and concrete. The bending stiffness for the full composite floor is determined according to Eq. 4.3

$$(EI)_{ful} = E_c I_c + E_t I_t + \frac{(\frac{h_c+h_t}{2})^2}{\frac{1}{E_c A_c}+\frac{1}{E_t A_t}} \tag{4.3}$$

where A_c and A_t are the cross-section areas of concrete and timber, and h_c and h_t are the depths of concrete and timber, respectively. Eq. 4.3 was derived by assuming the equal curvature of timber and concrete and the same strain at the bottom of concrete and top of timber.

The load-deflection curves in Fig. 4.7 demonstrate different responses of specimens under bending. Table 4.2 summarizes the strength, stiffness, and failure modes for all the specimens. The strength P_{max} of the specimens is taken as the peak load the floor sustained during the test. As shown in Table 4.2, specimen SPU-8 with no connection had the lowest strength. Except for specimens SPU-2 (longest span among the tested specimens) and SPU-4 (shallowest notches among the tested specimens), the specimens with notches had strengths of no less than 100 kN. The ultimate bending moment M_{ult} in each specimen corresponding to the peak load P_{max} was calculated and normalized to one-metre width as shown in Table 4.2. A typical factored design load level in an office building is about 10.3 kPa (2.5 kPa specified dead load and 4.8 kPa specified live load with load factors of 1.25 and 1.5, respectively, according to the National Building Code of Canada 2015) which generates bending moments of 46.4 kNm and 64.9 kNm for the 6 m span floor and 7.1 m span floor, respectively. As shown in Table 4.2, the actual load-carrying capacities of the tested floors were well above the design load level even for specimen SPU-8.

Under the four-point bending scheme, the serviceability bending stiffness (referred to as "bending stiffness or EI" henceforth) of the floors was determined from Eq. 4.4 (ASTM D198-15)

$$EI = \frac{23L^3}{1296}\frac{P}{\delta(L/2)} \tag{4.4}$$

where L is the floor span and $P/\delta(L/2)$ is the slope of the load-deflection curve between 10% - 40% of the peak load, which is considered to be the load level at serviceability limit states (EN 26891:1991).

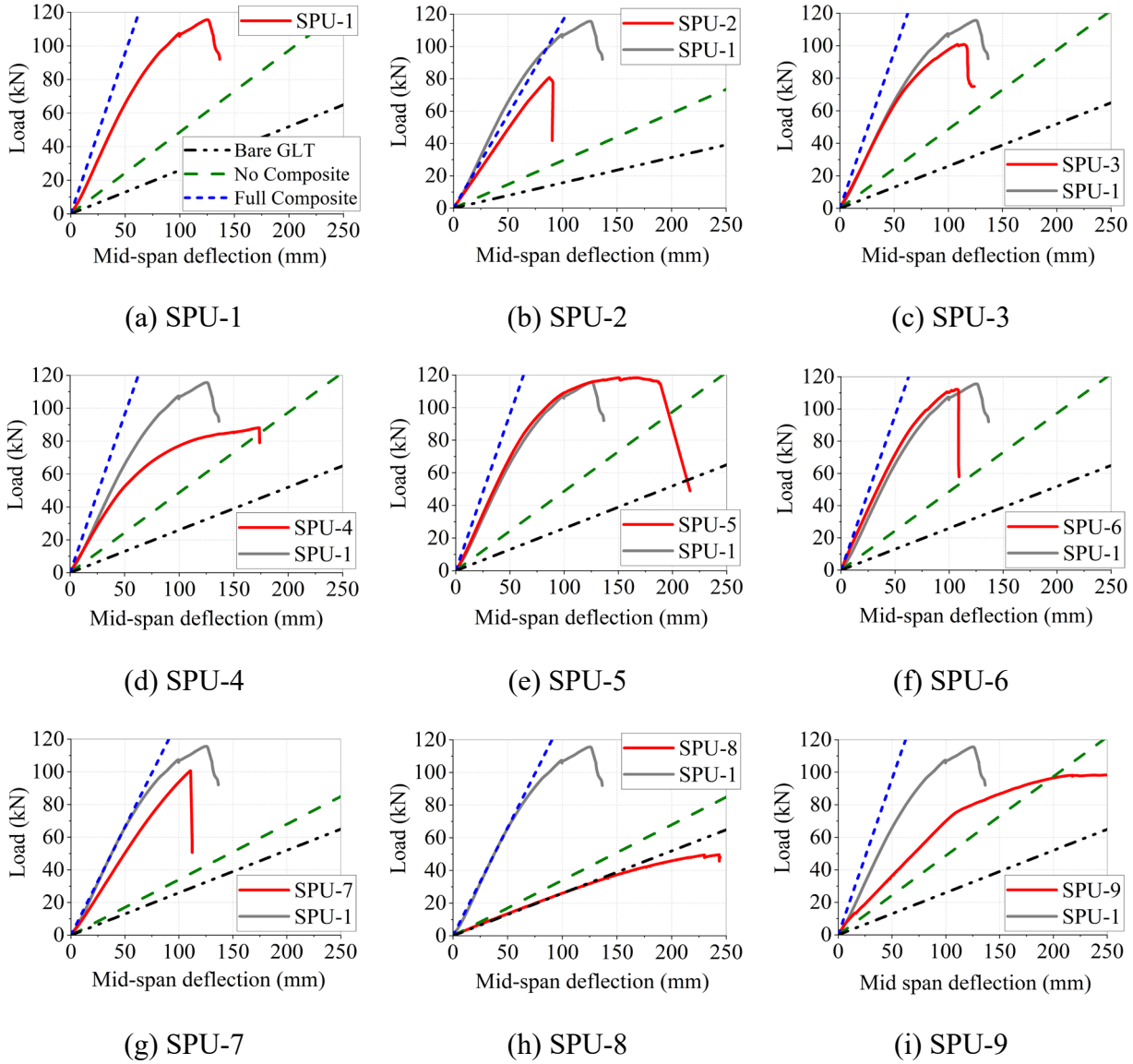

(a) SPU-1 (b) SPU-2 (c) SPU-3

(d) SPU-4 (e) SPU-5 (f) SPU-6

(g) SPU-7 (h) SPU-8 (i) SPU-9

Fig. 4.7 Load-deflection relationships of the composite floor specimens

As shown in Fig. 4.7, most specimens had bending stiffness EI that was considerably higher than that of the bare GLT panels and close to the theoretical full-composite floor, except for specimens

SPU-8 and SPU-9. The bending stiffness of specimen SPU-9 was less than half of the reference specimen SPU-1 due to concrete cracking under a negative bending moment. The bending stiffness of SPU-8 was closer to that of the bare timber panel rather than to the non-composite floor, indicating that the concrete layer did not contribute to the bending stiffness of the floor.

Table 4.2 Summary of bending test results on mass timber panel-concrete composite floors

Specimen	P_{max} (kN)	M_{ult} (kNm)	EI (kNm^2)	λ_1	λ_2	w (kPa)	$(EI)_{ult}$ (kNm^2)	Decrease of EI	End slip at peak load (mm)
SPU-1	115.6	192.7	5473	65.7%	88.3%	9.0	4680	14.5%	4.6
SPU-2	80.8	159.4	6223	79.4%	93.8%	6.2	6146	1.2%	1.0
SPU-3	100.9	168.1	5152	59.9%	85.5%	8.5	4436	13.9%	4.7
SPU-4	88.1	146.8	4356	45.4%	76.6%	7.2	3201	26.5%	9.2
SPU-5	118.4	197.3	5686	69.6%	90.0%	9.4	4814	15.3%	6.0
SPU-6	112.2	187.1	5642	68.8%	89.7%	9.3	5055	10.4%	3.7
SPU-7	100.6	167.7	3975	70.9%	90.5%	6.5	3767	5.2%	1.4
SPU-8	49.7	82.8	986	0	0	1.6	917	7.0%	13.8
SPU-9	102.3	170.4	2583	13.1%	37.2%	4.3	2286	11.5%	1.2

P_{max}: peak load; M_{ult}: ultimate moment-carrying capacity, normalized to 1 m width; EI: Serviceability bending stiffness; λ_1: composite efficiency by stiffness; λ_2: composite efficiency by deflection; w: maximum live load to satisfy the deflection limit of span/360; $(EI)_{ult}$: ultimate bending stiffness.

The efficiency by stiffness of composite floors (Mai et al. 2018) is determined according to Eq. 4.5

$$\lambda_1 = \frac{EI-(EI)_{no}}{(EI)_{ful}-(EI)_{no}} \tag{4.5}$$

which falls between 0 (non-composite) and 1 (fully composite). As shown in Table 4.2, the efficiency of specimen SPU-9 was the lowest among specimens with shear connections. The specimens that resist positive bending moment displayed higher composite efficiency. However, a remarkable difference of the composite efficiency can be observed between the tested floors and the theoretical full composite floor, which means that there is room for further improvement in the bending stiffness of the composite floors. However, it is possible that the estimated Young's modulus of concrete according to Eq. 4.1 was higher than the actual value which led to an underestimation of the composite actions in the specimens.

Another definition of composite efficiency is based on deflection (Gutkowski et al. 2008) as shown in Eq. 4.6.

$$\lambda_2 = \frac{\delta_{no} - \delta}{\delta_{no} - \delta_{ful}} = \frac{\frac{1}{(EI)_{no}} - \frac{1}{EI}}{\frac{1}{(EI)_{no}} - \frac{1}{(EI)_{ful}}} \tag{4.6}$$

In Eq. 4.6, δ_{no}, δ_{ful}, and δ represent deflections for the non-composite floor, full composite floor, and the tested floor under the same load (10% - 40% of peak load). As presented in Table 4.2, the efficiencies of the specimens calculated according to deflection were closer to the full-composite action, showing that the deflection is less sensitive to the bending stiffness once the bending stiffness reached a certain level.

If the deflection limit for the floor is set as $L/360$ under the live load, then the maximum allowable live load can be determined from the measured bending stiffness according to Eq. 4.7 (ASTM D198-15)

$$w = \frac{48EI}{225L^3 b} \tag{4.7}$$

where b is the width of the floors (600 mm). As demonstrated in Table 4.2, except for specimens SPU-8 and SPU-9, the remaining floors can resist more than 6 kPa specified live load which is above the design load for common office (4.8 kPa) and residential buildings (1.9 kPa) without reaching the deflection limit.

The ultimate bending stiffness of the floors was determined from Eq. 4.8 (ASTM D198-15)

$$(EI)_{ult} = \frac{23L^3}{1296} \frac{0.8P_{max} - 0.1P_{max}}{\delta_{0.8} - \delta_{0.1}} \tag{4.8}$$

where $\delta_{0.8}$ and $\delta_{0.1}$ are the mid-span deflections when 80% and 10% of the peak load were reached, respectively (EN 26891:1991). The decline of stiffness from the serviceability state to the ultimate state is listed in Table 4.2 for each specimen. Specimen SPU-4 showed the largest drop of stiffness, although specimens SPU-5 and SPU-9 also demonstrated an extensive plastic behaviour before final failure.

Relative slips

The relative slip between timber and concrete in the composite floor is a direct indicator of the shear connection effectiveness. The relative slip between timber and concrete at the end of each floor at the peak load P_{max} is listed in Table 4.2, where the relative slip was taken as the average of four measured slips by LVDTs mounted at the floor ends. The load-slip relationships of specimens measured at front-right, front-left, back-right, and back-left are plotted in Appendix IV. Most specimens had similar relative slips at two sides of the floors while other specimens had large differences between the relative slips measured at two sides. On average, Specimens SPU-2, SPU-7, and SPU-9 had the lowest relative slips, while specimen SPU-8 had the highest relative slip even though its peak load P_{max} was considerably lower than other specimens.

Relative slips between timber and concrete in specimens SPU-1, SPU-4, and SPU-8 measured at front-left half-span (roller support) are shown in Fig. 4.8. Relative slip increased from the mid-span to the floor ends in each specimen. The theoretical relative slip at the end of the non-composite floor is also plotted in Fig. 4.8 to show the effectiveness of shear connections in resisting the slide between timber and concrete. The relative slip in the non-composite floor was determined by integrating strains at the bottom of concrete and top of timber without considering the gap opening or material damage. Specimens SPU-1, SPU-4, and SPU-8 showed three levels of connection stiffness—high stiffness, low stiffness, and effectively zero stiffness. By comparing the floor slip with the slip of the non-composite floor, Fig. 4.8 displayed a clear trend that relative slip between timber and concrete increases when the connection stiffness decreases. Specimen SPU-8 had a larger slip than the theoretical non-composite floor at the floor end, which is a result of the large gap opening and concrete cracking during the test.

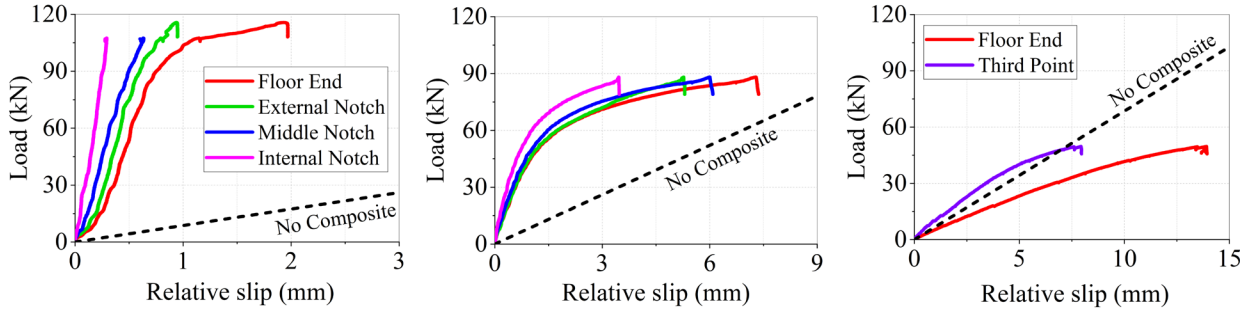

(a) SPU-1 (b) SPU-4 (c) SPU-8

Fig. 4.8 Load-slip relationships of three composite floor specimens

Moisture content change in timber

The moisture content of GLT at about 10 mm below the interface of two materials was monitored with a moisture metre before and after the concrete casting as well as right before the bending test. Fig. 4.9 shows the moisture content change of GLT during the specimen preparation process (mean value with standard deviation). It can be seen that, although the timber surface was treated with a waterproof sealer, the moisture content of timber still increased after the concrete casting, implying that timber had absorbed water from concrete. The loss of water from concrete can cause heterogeneity, permeability, and reduction of strength in concrete while timber expands after water absorption. The quality of notched connections may also deteriorate due to water loss from concrete. The local crushing of concrete in the notched regions (Fig. 4.5(d)) is likely caused by the water loss of concrete. The moisture content of timber gradually decreased to the original level after the formwork was removed, indicating that the water loss from concrete to timber may have a greater impact on concrete rather than on timber. A more effective water barrier between timber and concrete should be investigated in the future.

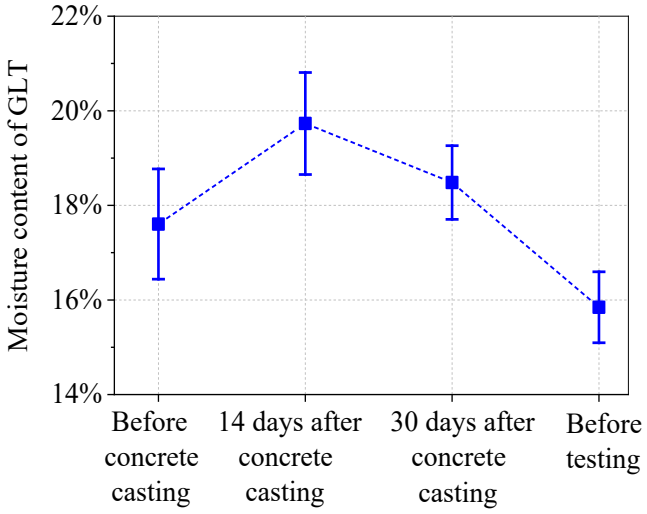

Fig. 4.9 Moisture content of timber before and after concrete casting in the composite floor specimens

4.2.6 Discussion

This section discusses how the structural performance of MTP-concrete composite floors is affected by factors such as connection number, notch depth, the existence of self-tapping screws, concrete thickness, floor span, and negative bending moment. Based on the test results, some recommendations of the notched connection and composite floor design are provided. Since the design of MTP-concrete composite floors is usually governed by the serviceability limit states, this section mainly focuses on the discussion of the bending stiffness of MTP-concrete composite floors.

Number of connections

In MTP-concrete composite floors, fully composite action is hard to achieve as shear connections are always flexible to some extent (Dias and Jorge 2011). When designed properly, notched connections can be fairly stiff relative to other types of connections such as self-tapping screws and steel dowels. However, the efficiency of notch-connected composite floors also depends on the number and positions of notches since timber and concrete are only discretely connected. In a simply supported floor, the notches made around the mid-span will not be as effective as notches

made closer to the supports. Using a large number of notches in the floor unnecessarily reduces the bending strength of the timber member, while a small number of connections cause low composite action as well as large deflection and early failure of the floor. It is thus important to determine the proper number of connections to achieve a certain level of composite efficiency in the floor.

Specimen SPU-8 is an extreme case where no connection was used to connect two layers and the efficiency of the floor was effectively zero. When four notches were used in specimen SPU-3, the efficiency of the floor increased dramatically to around 60%. Specimens SPU-1, SPU-6, and SPU-7 used six notched connections and their composite efficiencies were similar. On average, efficiency had increased less than 10% from four connections to six connections. More notched connections may further improve the efficiency of the floor but, predictably, the increase will not be significant if the stiffness of each connection has not been improved. For MTP-concrete composite floors at around the tested span (6 – 7 m), at least six notched connections should be used to achieve no less than 65% of the composite efficiency (by stiffness).

Depth of notches

The notch geometry (length, width, depth, and shape) affects the stiffness and failure mode of the connection under shear. The push-out tests on notched connections showed that high stiffness and good ductility are difficult to achieve at the same time in a single connection. Deeper notches typically have higher stiffness but poor ductility while shallower notches have lower stiffness but better ductility. The stiffness and ductility of connections can in turn affect the bending stiffness and failure mode of the composite floor.

The notched connections in specimens SPU-1, SPU-4, and SPU-5 were designed at the same locations but with different depths. Specimen SPU-1 failed due to notched connection shear failure in concrete (NSC). Shear failure of the notch in concrete, however, should be prevented as it is brittle and has high variability in load-carrying capacity. When the notch depth was reduced from 25 mm to 13 mm in specimen SPU-4, the failure mode of connections was the ductile timber compression failure (NCT), and the final failure mode of the floor was the timber member combined bending and tension failure at the bottom (TTB). Compared to the reference specimen,

the bending stiffness and strength of specimen SPU-4 decreased 20.4% and 23.8%, respectively, due to the reduced composite efficiency. It is noteworthy that the timber member failed in the specimen with shallower notches (SPU-4) instead of deeper notches (SPU-1). This again was because the specimen with deeper notches had higher composite action thus lower tensile stresses at the bottom of timber, and the ultimate strength of notched connections was reached before the ultimate strength of the timber component was reached.

Specimen SPU-5 contained variable notch depths (15-25 mm). Deeper notches were placed near supports to resist higher shear forces than shallower notches placed close to the mid-span. Test results showed that specimen SPU-5 had stiffness and strength at the same level as specimen SPU-1 but superior ductility before the final failure of the timber member. The compression failure of timber (NCT) was triggered in both the shallower notches and deeper notches. This demonstrates that high stiffness, high strength, and good ductility of MTP-concrete composite floors can be accomplished by the proper arrangement of notches with different geometries. Deeper notches can be used at areas with high shear forces and low bending moments while shallower notches should be used towards high bending moment zones where a larger timber cross-section should be preserved. A similar concept has been adopted by Boccadoro et al. (2017a) for LVL-concrete composite floors with notches made with different widths.

Self-tapping screws

In a composite floor that relies on notches to provide shear resistance, using too many steel fasteners can significantly increase the total cost and labor intensity during floor construction. However, a minimal number of steel fasteners should be used to prevent the uplifting of the concrete layer. In this study, self-tapping screws were used at the mid-span of all the specimens to connect timber and concrete in the vertical direction. Screws were also used in each notch at a 45° angle to restrict the gap opening between two components, except for specimens SPU-6 and SPU-8.

Specimen SPU-8 had a bending stiffness lower than the theoretical non-composite floor which indicates the concrete layer cannot act together with timber without any connections. In terms of the stiffness and strength of the notched connections, however, screws often have limited

contribution unless the diameter of screws is large relative to the size of the notch or a significant number of screws are used (Yeoh et al. 2011a; Kudla et al. 2016; Zhang et al. 2020). Among the tested specimens, Specimens SPU-1 and SPU-6 had the same geometry, the only difference being the existence of screws in the notches. Comparing the test results of two specimens, it can be concluded that screws in the notches had almost no effect on the bending stiffness, load-carrying capacity, and failure pattern of the specimens. The screws also cannot eliminate gap opening between timber and concrete. This is because the number and sizes of screws used in the specimens were relatively small compared to the size of the notch. It is also possible that the development length of screws in concrete (Fig. 4.3) was not enough to prevent the cracking of concrete.

Concrete thickness

The thickness of concrete in MTP-concrete composite floors may be controlled by either structural requirements such as load-carrying capacity and deflection limit, or non-structural requirements such as acoustic performance. It is advantageous to keep the self-weight of the floor low while maintaining the required level of stiffness and strength. Fig. 4.10 shows the normalized bending stiffness for all the specimens (except for SPU-9) along with the theoretical stiffness for the fully composite and non-composite MTP-concrete composite floors with varying concrete thickness. The normalized bending stiffness in Fig. 4.10 is the ratio of the tested or predicted bending stiffness to the bending stiffness of the 130 mm thick timber floor (when the concrete thickness is zero in the floor). As shown in Fig. 4.10, the bending stiffness of the composite floors increases with the concrete thickness. The stiffness of specimen SPU-7 (60 mm concrete thickness) was lower than all the tested floors with 85 mm concrete thickness, even for the floor with fewer connections (SPU-3) and the floor with flexible connections (SPU-4). In terms of the composite efficiency, however, specimen SPU-7 had the highest efficiency among all the 6 m span specimens (Table 4.2).

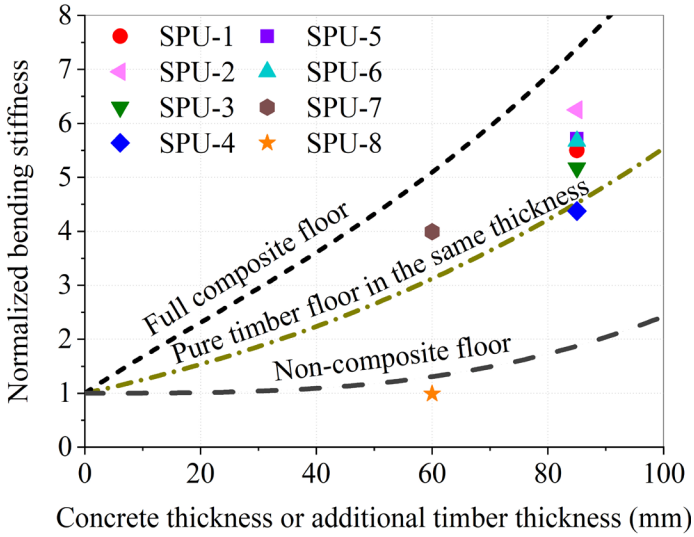

Fig. 4.10 Normalized bending stiffness of composite floors (according to 130 mm thick bare timber panel) versus concrete thickness or additional timber thickness

In Fig. 4.10, the bending stiffness of the pure timber floor with the same thickness as MTP-concrete composite floors was also plotted. The stiffness of the MTP-concrete composite floors should be at least higher than the pure timber floor of the same thickness to show advantages. The concrete layer cannot contribute to the bending stiffness of the floor without being connected to the timber in specimen SPU-8. Due to the flexible connections, specimen SPU-4 had stiffness lower than the bare timber floor with the same thickness. Considering concrete significantly increases the floor weight, the competitiveness of MTP-concrete composite floors in these cases is seriously undermined.

When the notched connections are designed effectively, it is recommended to use at least 60 mm concrete (45% of the timber thickness) and 85 mm concrete (65% of the timber thickness) in the composite floor to achieve 4 and 5 times of the bare timber panel (130 mm thickness) bending stiffness, respectively. The determination of the concrete thickness in MTP-concrete composite floors should also consider the vibration performance, thermal performance, sound isolation, and fire-resistance rating of the floor. Some of these aspects will be discussed in later sections and chapters.

Floor span

With the additional concrete layer and high-efficient connection system, MTP-concrete composite floors can reach larger spans than bare timber panels alone. The longest span among the tested floor specimens was 7.1 m in specimen SPU-2, which satisfies the requirements of both deflection and load-carrying capacity. Compared with the reference case SPU-1 which had a 6 m span, specimen SPU-2 was 13.7% higher in bending stiffness. The higher bending stiffness of specimen SPU-2 is probably because the specimen experienced less gap opening during the test. The moment resisting capacity of specimen SPU-2 was reduced by 17% compared to the reference case. Besides, the ultimate bending stiffness EI_{ult} of specimen SPU-2 was almost the same as its serviceability stiffness EI, indicating that specimen SPU-2 was essentially linear elastic before failure. The main reason that specimen SPU-2 failed early in the notched connections was that notches in specimen SPU-2 attracted higher shear forces due to their larger spacing. The maximum allowable span of MTP-concrete composite floors is also restricted by the floor vibration performance which will be discussed in section 4.4.

Negative bending moment

Most MTP-concrete composite floors are designed to allow concrete to resist compression and timber to resist tension. However, in practice, continuous floors are more common than simply-supported floors. The continuous floors resist positive bending moments with each span and negative bending moments near supports. To date, scant research has been conducted to study the behaviour of timber-concrete composite floors when concrete resists tension and timber resists compression (Hehl et al. 2014; Sebastian 2019).

Since concrete has low tensile strength, steel rebar was used in specimen SPU-9 to resist tension after concrete cracking. Comparing test results of SPU-9 and SPU-1, it can be seen that the bending stiffness of the composite floor was reduced by more than 50% under the negative bending moment as a result of concrete cracking. This indicates that, for continuous MTP-concrete composite floors, the stiffness of the floor in the positive bending moment zone and negative bending moment zone needs to be considered separately. However, the bending stiffness of SPU-9 was significantly higher than the bare GLT stiffness, indicating that high composite action existed between timber,

cracked concrete, and the steel rebar. The strength of the composite floor under negative bending moment only slightly decreased (11.5%) and the specimen showed good ductility owing to the rebar under tension and timber under compression. It is thus recommended to reinforce the negative bending moment zone in MTP-concrete composite floors with proportioned reinforcement to maintain the load-carrying capacity and achieve a ductile failure pattern. With the proportioned reinforcement, the reinforcement can take tensile forces after concrete cracking and yield before timber crushes at the top. The level of reinforcement can be adjusted to achieve the desired floor bending stiffness and load-carrying capacity.

The gap opening in SPU-9 was notably lower than the rest of the specimens during the test. This phenomenon can be attributed to the material difference between timber and concrete. Since concrete has a much larger modulus of elasticity than timber, the curvature of concrete under bending tends to be smaller than that of timber. This inconsistency resulted in the gap opening between two members when the more flexible timber is at the bottom and the stiffer concrete is at the top. However, when concrete is at the bottom and timber is at the top, this inconsistency could be accommodated by the crack opening at the bottom of concrete which reduces the bending stiffness of the concrete layer.

4.2.7 Conclusions from Phase-1 Bending Tests

The first stage bending tests experimentally investigated the static performance of nine mass timber panel-concrete composite floors with different notched connection designs. From the test results, the following conclusions can be drawn:

1. The bending stiffness and strength of MTP-concrete composite floors increase with the notch depth and the number of notched connections. The notch depth also affects the ductility and failure mode of the composite floor. By putting deeper notches closer to the supports and shallower notches closer to the mid-span, the composite floor can achieve high bending stiffness, high strength, and good ductility.
2. When notched connections are designed efficiently, a thicker concrete layer enhances the bending stiffness and load-carrying capacity of MTP-concrete composite floors.

3. Steel fasteners are required to prevent the uplifting of the concrete layer in MTP-concrete composite floors. However, a small number of self-tapping screws installed in notches have almost no effect on the bending stiffness and load-carrying capacity of MTP-concrete composite floors.

4. Compared to the MTP-concrete composite floors under positive bending moments, the floors resisting negative bending moments have substantially lower stiffness and slightly reduced strength, but excellent ductility when concrete is reinforced with proportioned reinforcement to resist tension.

5. The notched connections made in the composite floors were semi-rigid, thus only partial composite action in the floors was achieved. The quality control for the notched connections during concrete casting is a crucial factor affecting the performance of the composite system. Nevertheless, the bending stiffness and strength for most of the tested specimens were large enough to satisfy design needs.

Except for the factors investigated in the first phase bending tests, other factors that could contribute to the variation of the bending performance of MTP-concrete composite floors, such as spacing and locations of connections as well as shape and size of notches should be investigated in future studies.

4.3 Second Phase Bending Tests

4.3.1 Introduction

From the first phase bending tests on nine MTP-concrete composite floors, it was found that the cracking of concrete was concentrated around the load-bearing zones in the notched connections. The cracking of concrete caused a gap opening between timber and concrete and the brittle shear failure of concrete in the notch. The failure load of concrete shear in the notch is hard to predict and the brittle failure of a single notch can lead to the failure of the entire floor system. Due to the stiffness degradation and failure of the connections, the bending strength of timber in the floor system was not fully utilized. To address these issues, three MTP-concrete composite floors were constructed and tested in the second phase bending tests. In the newly constructed specimens, the

notched connections were reinforced with orthogonal steel ties around the load-bearing areas to take tensile forces after concrete cracking. The tensile ties were designed to restrict the enlargement of concrete cracks and maintain the connection stiffness until the final failure of the floor. The orthogonal steel ties designed in the specimens are expected to be more efficient than traditional self-tapping screws or coach screws installed at the middle of the notches.

4.3.2 Floor Specimen Design

Three mass timber panel-concrete composite floors were built in the second phase bending tests, as shown in Fig. 4.11. The specimens had identical dimensions and material properties but different levels of reinforcements in the notched connections. The total length of the floors was 6.3 m, the width of the floors was 590 mm, and the thicknesses of concrete and timber were 85 mm and 127 mm, respectively. Each floor had six notched connections symmetrically spaced about the mid-span. The length of notches was 180 mm and the depth was 25 mm. The timber shear length in front of notches was 500 mm.

The notches in the specimens were reinforced with vertical self-tapping screws and horizontal steel hooked rods around the load-transfer areas where the concrete crack could develop. The diameter of the screws and steel rods were 7 mm and 6 mm, respectively; while their lengths were 160 mm and 300 mm, respectively, as shown in Fig. 4.12. The distance between the centres of screws to the bearing surface of notches was 15 mm, as well as the distance between the centres of steel rods to the upper surface of the timber panels. The vertical screws serve a dual purpose: physically connect timber and concrete in the vertical direction and act as the reinforcement of concrete in the notch. The anchorage of screws into timber was 55 mm, which left a 5 mm concrete cover between the screw head and the top surface of the concrete. The steel rods intersected the screws in the middle which resulted in a 150 mm development length on each side. Since this development length cannot meet the requirements of the development length for straight bars, standard hooks with a diameter of 25 mm and an extension of 60 mm were made at two free ends of the steel rods (CSA A23.3 2019), as shown in Fig. 4.12. The steel rods were fastened to the self-tapping screws through steel wires.

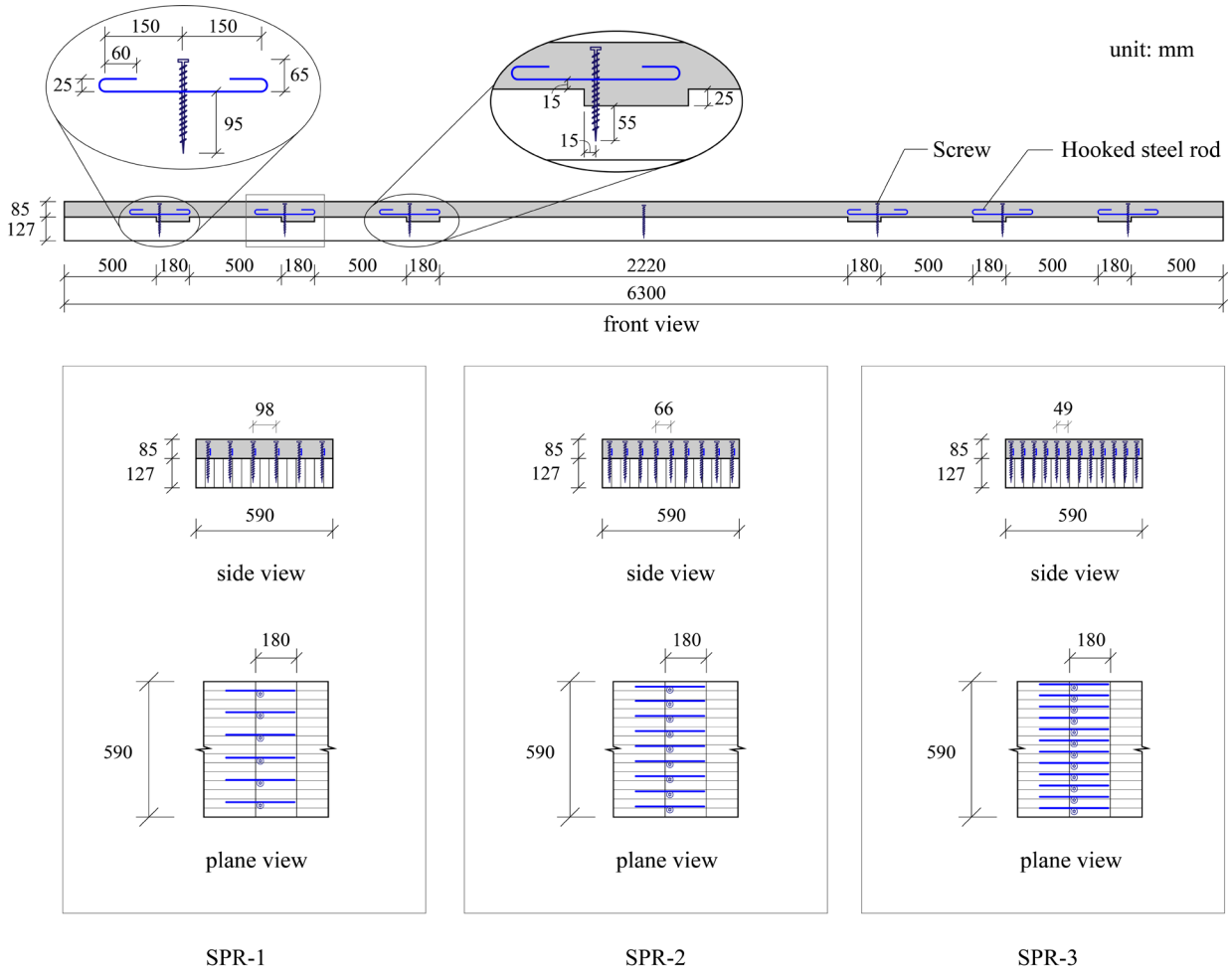

Fig. 4.11 Mass timber panel-concrete composite floors with reinforced notched connections

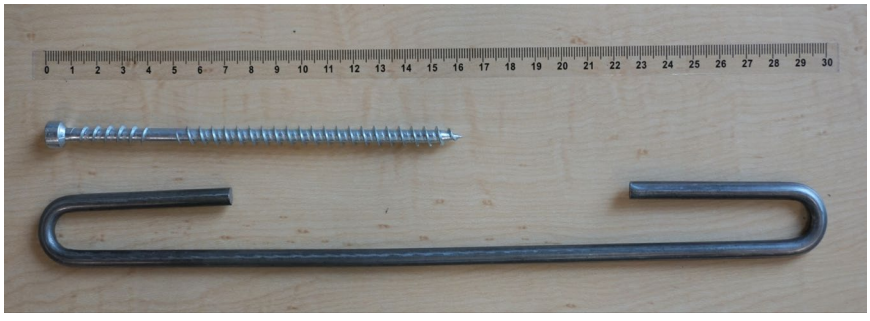

Fig. 4.12 Dimensions of self-tapping screws and hooked steel rods in composite floors (in cm)

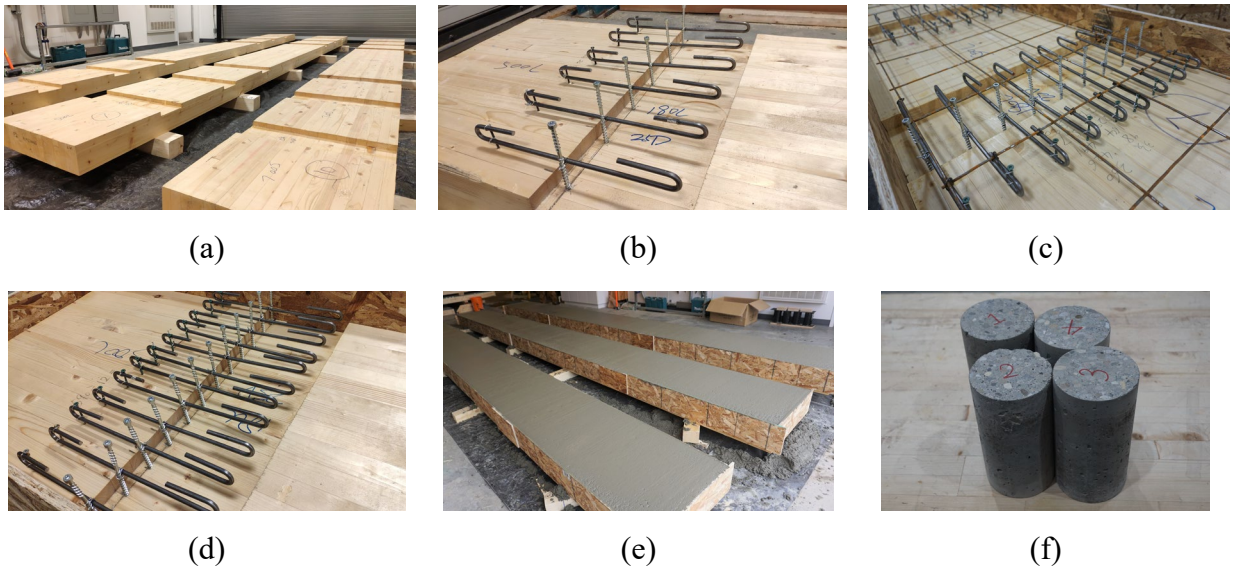

Fig. 4.13 Reinforced composite floor specimen preparation (a) GLT panels with notches (b) Six rows of reinforcement in the notch (c) Nine rows of reinforcement in the notch and steel mesh (d) Twelve rows of reinforcement in the notch (e) Concrete casting and (f) Concrete cylinders

The specimen preparation process is shown in Fig. 4.13. In specimens SPR-1, SPR-2, and SPR-3, six, nine, and twelve rows of reinforcement were used in each notch, respectively. The reinforcements were equally spaced in the floor width direction with a spacing of 98 mm, 66 mm, and 49 mm for specimens SPR-1, SPR-2, and SPR-3, respectively, as shown in Fig. 4.13(b)-(d). In each floor, two self-tapping screws were used in the floor mid-span to prevent the separation of timber and concrete. A layer of steel mesh (3 mm diameter and 150 mm × 150 mm grid size) was placed in the middle of the concrete layer. After the reinforcements were installed, concrete was cast directly on top of timber into the formwork and the floor specimens were conditioned in the laboratory environment for 44-48 days before testing.

4.3.3 Materials

The mass timber panels in the floor specimens came from the same batch as the timber panels used in the first phase bending tests. However, after about one year, the moisture content of timber reduced from 15.8% to 12.9%. As a result, the width of the panels shrunk from 600 mm to 590

mm, and the thickness shrunk from 130 mm to about 127 mm. The shrinkage along the longitudinal direction of the panels was negligible. The modulus of elasticity (MOE) and modulus of rupture (MOR) of timber panels measured at the moisture content of 15.8% were 9061 MPa and 45.9 MPa, respectively. According to Smith et al. (2003), MOE and MOR of timber at the moisture content of 12.9% can be estimated as

$$(E_t)_{12.9} = (E_t)_{15.8} + (E_t)_{15.8}(15.8 - 12.9)\alpha \tag{4.9}$$

$$(f_{tb})_{12.9} = (f_{tb})_{15.8} + (f_{tb})_{15.8}(15.8 - 12.9)\alpha \tag{4.10}$$

where α is the average change in the mechanical properties of timber due to one percent change in moisture content and can be taken as 2% for MOE and 4% for MOR. The MOE and MOR of timber at the moisture content of 12.9% are estimated to be 9602 MPa and 51.2 MPa, respectively.

Normal strength concrete with a nominal coarse aggregate size of 10 mm was used in the specimens. Four concrete cylinders with 100 mm diameter and 200 mm height (Fig. 4.13(f)) were cast at the same time as floor specimens and tested according to ASTM C39/C39M (2020) at 51 days after concrete casting. The average compressive strength f_c' of concrete cylinders was 51 MPa with a 2.1% coefficient of variation. The average density ρ_c of concrete cylinders was 2261 kg/m^3. The modulus of elasticity of concrete can thus be estimated according to Eq. 4.1. The estimated concrete modulus of elasticity was 29704 MPa.

The reinforcements installed in the notches consisted of CTC7160 self-tapping screws and hooked steel rods. The CTC7160 screws were the same as the screws used in the first stage bending tests. The steel rods were made of cold-rolled steel. From the tensile tests conducted on 9 steel rods, the yield strength and ultimate tensile strength of steel rods were measured to be 18.9 kN and 20.1 kN, with coefficients of variation of 5.2% and 5.1%, respectively. Full tensile test results on the steel rods can be found in Appendix V.

4.3.4 Testing Methods

The test setup in the second phase bending tests was the same as the first phase bending tests (Fig. 4.4). The mid-span deflections of the floors were measured by string potentiometers and the relative slips between timber and concrete were measured by LVDTs. However, the loading

procedure in the second phase bending tests contained a pre-loading cycle as shown in Fig. 4.14 which was adopted from EN 26891 (1991). The load was applied to 40% of the estimated peak load F_{est} and maintained at this load level for 30 s. The load was then reduced to 10% of the estimated peak load F_{est} and maintained for another 30 s. Thereafter, the load was increased monotonically until the specimen failed. The loading rate was 3 mm/min for all the specimens. The peak load F_{est} for the specimens was estimated to be 150 kN initially but was adjusted to 190 kN and 200 kN for specimens SPR-2 and SPR-3, respectively, after specimen SPR-1 was tested.

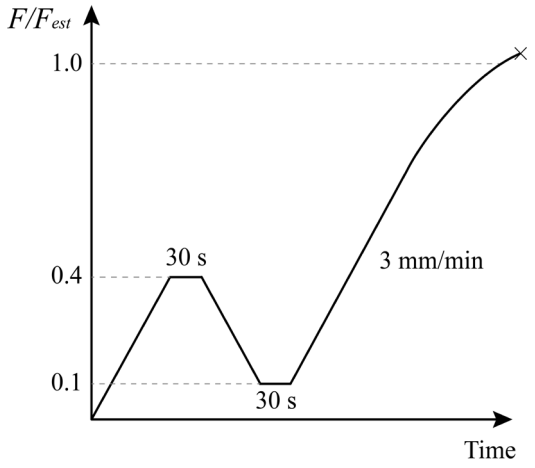

Fig. 4.14 Loading procedure in the second phase bending tests

4.3.5 Test Results

Results from the second phase bending tests, including failure pattern, load-deflection relationship, relative slip between timber and concrete, and effective bending stiffness, are presented and discussed in this section. Besides, the test results were compared with the results from the first phase bending tests. In the first phase bending tests, specimens SPU-1 and SPU-6 had the same geometry properties (effective span, concrete thickness, and locations and sizes of notches) as the three specimens in the second phase bending tests. Except for the reinforcements in the notches, the main differences between the reinforced and unreinforced specimens were the concrete strength class and cross-section sizes of timber due to moisture content change. Although two screws were installed in each notch in specimen SPU-1, due to the small number of screws and short anchorage length in concrete, the specimen can also be considered as unreinforced.

Failure modes

During the bending tests, no obvious damage was observed on the reinforced floor specimens. The final failure of three composite floors with reinforced notches was timber member combined bending and tensile failure at the bottom, as shown in Fig. 4.15(a) and (c), which was different from the concrete notch shear failure in the unreinforced specimens SPU-1 and SPU-6 (Fig. 4.5). In specimen SPR-2, immediately after the timber member bending failure, the concrete at the top was crushed, as shown in Fig. 4.15(b). Nonetheless, irrespective of the failure location, the failure for both reinforced and unreinforced floors was brittle. Around the reinforced notched regions, only fine cracks can be observed in concrete, as shown in Fig. 4.15(d). The end slips between timber and concrete in the reinforced floors were not observable after the test, as shown in Fig. 4.15(e). On the contrary, the crack enlargement, gap opening, and large relative slip were distinct in the unreinforced specimens (Fig. 4.5).

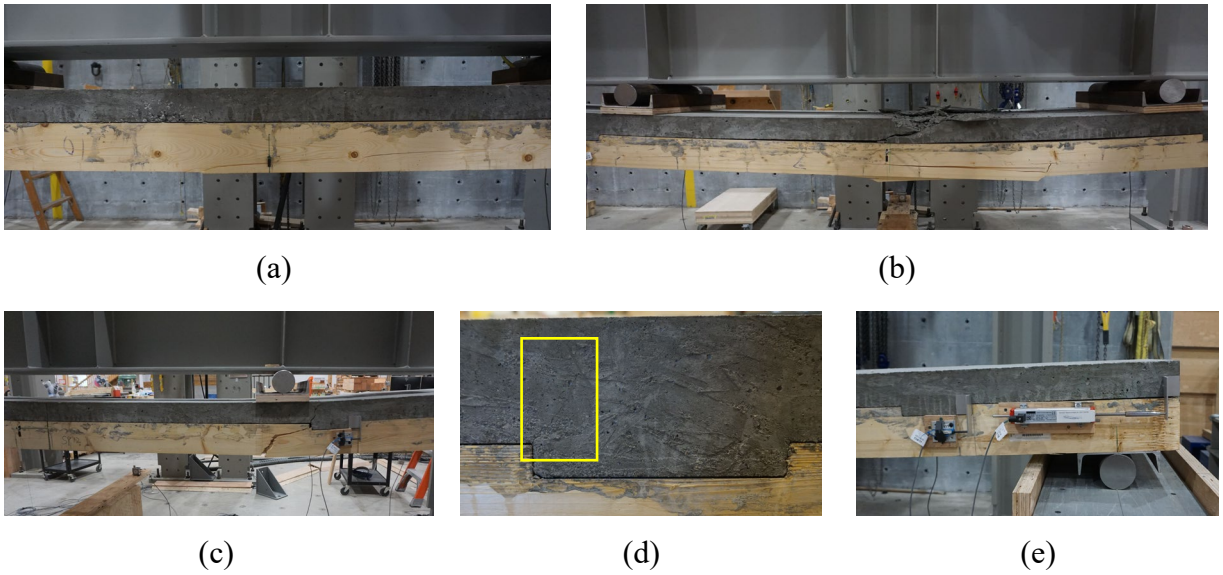

Fig. 4.15 Typical failure modes of reinforced composite floors under bending (a) Bending failure of timber at the bottom of specimen SPR-1; (b) Bending failure of timber at the bottom and concrete crushing at the top of specimen SPR-2; (c) Bending failure of timber at the bottom of specimen SPR-3; (d) Concrete cracking in the notched region in specimen SPR-1; and (e) End slip of specimen SPR-2 after failure.

Load-deflection relationships and relative slips

The relationships between the applied load and mid-span deflection of the specimens with reinforced notches are shown in Fig. 4.16. In Fig. 4.16(a)-(c), the theoretical load-deflection relationships for the full composite and non-composite floors are plotted against the measured data. The bending stiffness of the non-composite and full composite floors are determined according to Eq. 4.2 and Eq. 4.3, respectively. In Fig. 4.16(d), the load-deflection relationships of the specimens with reinforced notches are compared with the load-deflection curves of specimens SPU-1 and SPU-6.

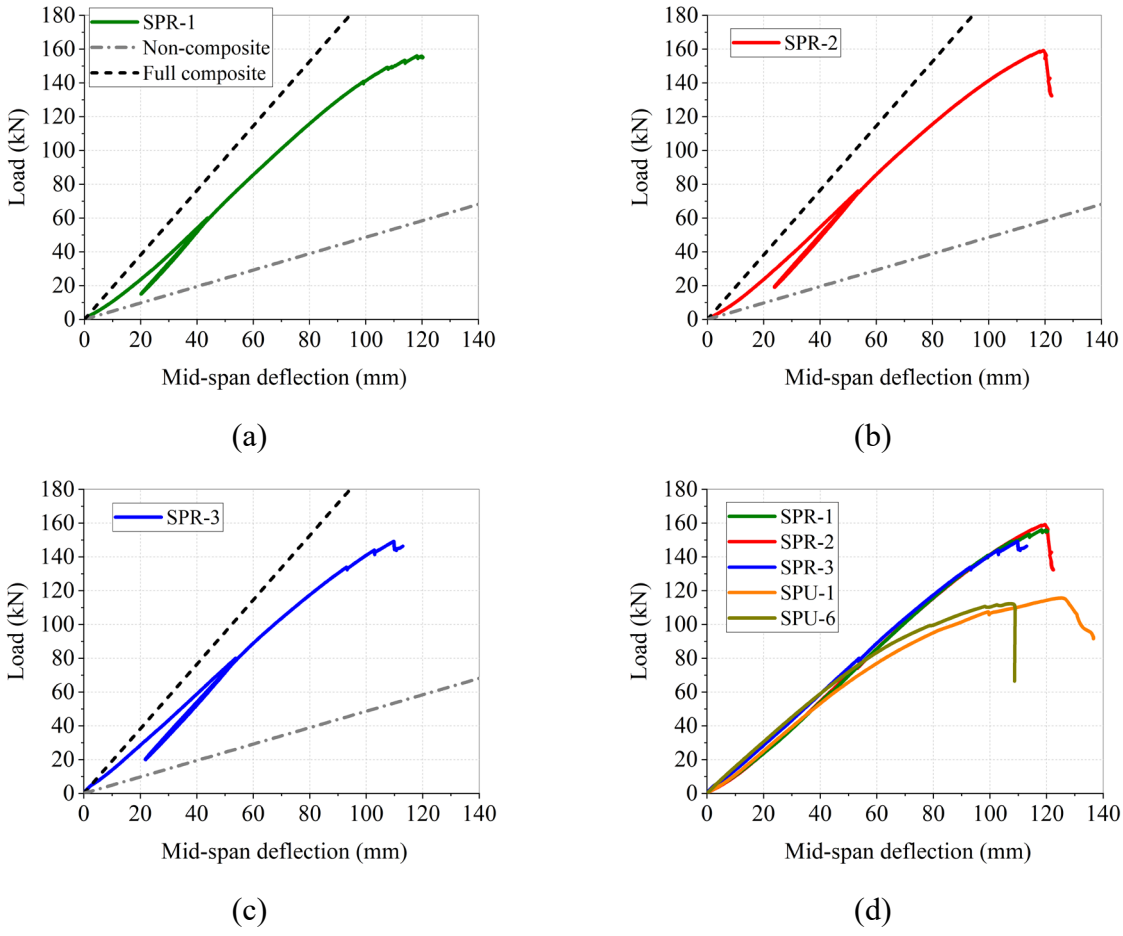

Fig. 4.16 Load-deflection relationships of floor specimens with reinforced notches (a) specimen SPR-1; (b) specimen SPR-2; (c) specimen SPR-3; and (d) comparison between reinforced and unreinforced specimens.

From Fig. 4.16(a)-(c), it can be seen that the composite floors with reinforced notches had high bending stiffness but were not fully composite. The relationships between load and deflection for reinforced specimens were almost linear up to failure. The comparison of the load-deflection curves between specimens in Fig. 4.16(d) shows that the specimens with reinforced notches had almost identical load-deflection relationships with each other. It can also be observed that the slopes of the load-deflection curves at the initial stage for the reinforced and unreinforced specimens were at the same level. However, the reinforced floor specimens exhibited higher ultimate bending stiffness and load-carrying capacity than the unreinforced floor specimens.

The peak load P_{max}, serviceability bending stiffness EI, and ultimate bending stiffness $(EI)_{ult}$ of the reinforced specimens are summarized in Table 4.3. The serviceability bending stiffness EI and ultimate bending stiffness of the floors were determined from Eq. 4.4 and Eq. 4.8, respectively. Once the serviceability bending stiffness EI is determined, the composite efficiencies of the floors can be determined according to Eq. 4.5 and Eq. 4.6.

Table 4.3 Results from bending tests on the composite floors with reinforced notches

Specimen	P_{max} (kN)	EI (kN/mm)	λ_1	λ_2	$(EI)_{ult}$ (kN/mm)	End slip at peak load (mm)
SPR-1	156	5711	70.6%	90.4%	5757	1.6
SPR-2	159	5836	72.9%	91.3%	5730	1.5
SPR-3	149	5773	71.7%	90.9%	5700	0.9

P_{max}: peak load; EI: Serviceability bending stiffness; λ_1: composite efficiency by stiffness; λ_2: composite efficiency by deflection; $(EI)_{ult}$: ultimate bending stiffness.

Compared to specimens SPU-1 and SPU-6, the serviceability bending stiffness EI of the reinforced floors only improved slightly (4% increase on average), indicating that the addition of screws and steel rods in the notches had little contribution on the notched connection stiffness under the serviceability limit state. As a result, the composite efficiencies of the floors only enhanced marginally after the reinforcements were installed. On average, the composite efficiency by stiffness increased from 67.3% to 71.7%, while the composite efficiency by deflection

increased from 89.0% to 90.9%. On the contrary, the ultimate bending stiffness of the reinforced specimens were significantly higher than that of the unreinforced specimens. For unreinforced specimens SPU-1 and SPU-6, the ultimate bending stiffness $(EI)_{ult}$ dropped 14.5% and 10.4%, respectively, from their serviceability bending stiffness EI. The ultimate bending stiffness $(EI)_{ult}$ of the reinforced specimens was at the same level as their serviceability bending stiffness EI and the maximum drop was less than 2%. This could be explained by the small crack opening in concrete at the notched regions due to the reinforcements in the connections, as a result, both the concrete layer bending stiffness and notched connection shear stiffness were less affected by concrete cracking at the ultimate stage.

Due to the high stiffness and high strength of the reinforced notched connections throughout the bending tests, the reinforced floors failed in timber instead of connections. Consequently, the ultimate load-carrying capacities of the reinforced specimens were on average 35.7% higher than the unreinforced specimens. It can be concluded that steel reinforcements in the notches mainly take effect at the ultimate stage of the floors under external loads which help to maintain the floor bending stiffness and maximize the load-carrying capacities. Comparing three reinforced specimens with different levels of reinforcement, no distinct difference can be found in terms of the peak load P_{max}, serviceability bending stiffness EI, and ultimate bending stiffness $(EI)_{ult}$.

The relationships between the applied loads and average end slips of the composite specimens are shown in Fig. 4.17. The average end slip corresponding to the peak load P_{max} for each specimen is listed in Table 4.3, which is the mean value of four slips measured at the floor ends. From Fig. 4.17, it can be observed that the reinforced specimens had significantly lower slips than the unreinforced specimens, especially under high load levels. The three specimens with reinforcements in the notches had similar end slips, however, a small decrease of the end slip can be observed when more reinforcements were used in the notches. The end slip for specimen SPR-3 was almost zero up to 25 kN. However, the increase of the end slips with the applied load indicates the semi-rigidity of the connections in resisting the shear forces. Full results of the measured relative slips of the specimens are shown in Appendix IV.

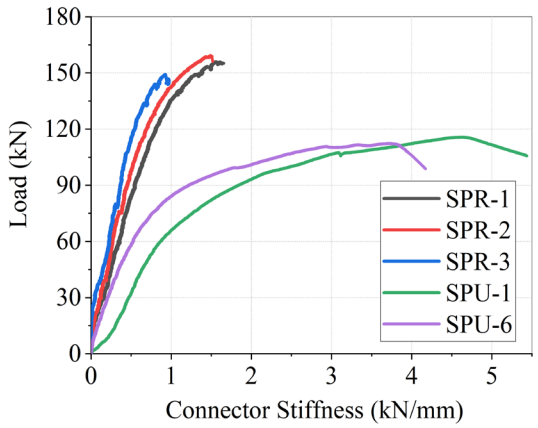

Fig. 4.17 Comparison of the averaged end slip between reinforced and unreinforced floor specimens

4.3.6 Discussion

From the bending tests on the composite floors with reinforced notches, it can be concluded that the additional reinforcements in the notched connections have two major effects on the floor bending performance:

(1) The notched connections and the concrete layer were almost intact before the final failure of the composite floors. The strengths of timber panels were fully employed thus the reinforced floors had higher ultimate load-carrying capacities than the unreinforced floors.

(2) Due to the controlled failure pattern, the behaviours of the floor specimens were more consistent than the unreinforced floors. The bending stiffness, including serviceability and ultimate bending stiffness, and the load-carrying capacity of the reinforced specimens were more reliable and predictable than the unreinforced specimens. This will be discussed again in Chapter 5.

Although being efficient in restricting the crack opening in concrete, the steel reinforcements in the notches can be simplified to reduce the complexity during installation. The steel rods in the horizontal direction can be made continuous longitudinally or transversely, as shown in Fig. 4.18. The horizontal steel rods can also be incorporated with the shrinkage reinforcement in the concrete layer. The number of steel reinforcement can be different in each notch depending on the internal forces in each notch.

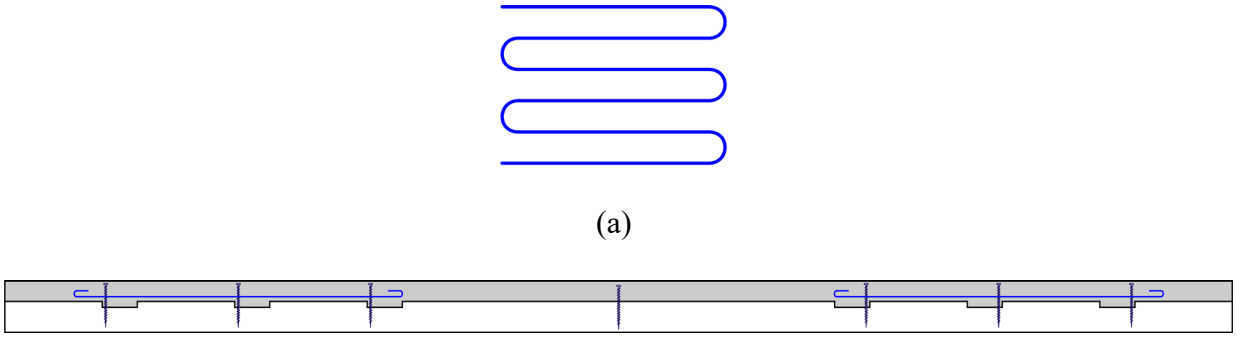

(a)

(b)

Fig. 4.18 Simplification of the steel reinforcement in the composite floors (a) Continuous steel rod in the transverse direction (b) Continuous steel rod in the longitudinal direction

After specimen SPR-1 was tested, the concrete layer was crushed using a hammer to expose the screws and steel rods, as shown in Fig. 4.19. No obvious deformation on the steel reinforcements or withdraw of screws can be observed, which indicates that the steel rods and screws were still at the elastic stage before the floor failed. It can thus be concluded that no more than six rows of reinforcements (in about 100 mm spacing) are needed to effectively prevent the crack enlargement of concrete in the notched regions.

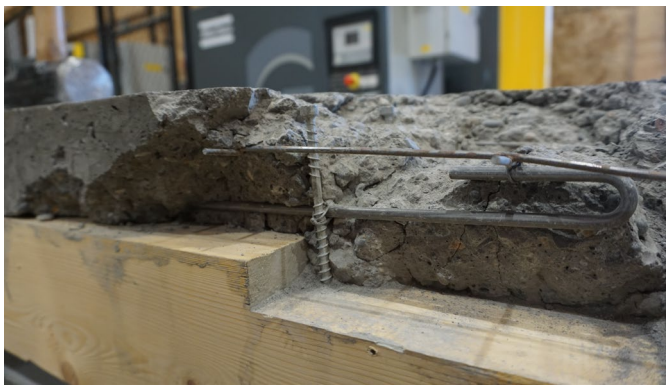

Fig. 4.19 Exposed screw and steel rod in specimen SPR-1 after being tested

4.3.7 Conclusions from Phase-2 Bending tests

In the second phase bending tests, a high-performance mass timber panel-concrete composite floor system with reinforced notched connections was developed and tested. The composite floor system takes advantage of the high stiffness of notched connections and high tensile strength of steel reinforcements, resulting in a floor system with a relatively high composite efficiency, high ultimate bending stiffness, and high load-carrying capacity. Since the notches were reinforced to prevent stiffness degradation and concrete shear failure, the final failure of the floor specimens was the controlled timber bending failure. Compared to the unreinforced floors, the ultimate load-carrying capacities of the reinforced floors were significantly improved and more predictable due to the near linear-elastic behaviour of the materials. The reinforced notches improved the consistency and reliability of the floor bending properties. The similar bending stiffness and peak loads of three floors with different levels of reinforcements suggest a lower level of reinforcement would be sufficient to prevent the notch failure and concrete crack enlargement. Further simplifications can be made to the steel reinforcements to reduce the complexity of the composite floor construction.

4.4 Dynamic Tests

4.4.1 Introduction

The bending tests on the composite floors focused on the short-term static bending performance of the floors. Except for the static performance, MTP-concrete composite floors can also be governed by the dynamic performance under human walking or rotating machinery at the service state. This section discusses the dynamic properties of MTP-concrete composite floors measured from vibration tests conducted before the destructive bending tests. Vibration tests were conducted on the GLT panels and MTP-concrete composite floors before and after concrete casting to measure the natural frequencies, mode shapes, and damping ratios of the floors. In addition, deflection tests and walking tests were conducted on the MTP-concrete composite floors to evaluate the floor dynamic performance. Test results such as floor bending stiffness from the dynamic tests were compared with the bending test results and the differences were discussed.

4.4.2 Testing Methods

Experimental modal tests were conducted on twelve single-span GLT panels before concrete casting. The GLT panels were tested with notches cut on the panels except for specimen SPU-8. Before the first phase bending tests, modal tests, static deflection tests, and walking tests were performed on nine single-span MTP-concrete composite floors after concrete casting and 28-day curing. Modal tests were also conducted on double-span composite floors with two different supporting conditions (additional support added to the mid-span or third span). Before the second phase bending tests, model tests and walking tests were conducted on three single-span MTP-concrete composite floors.

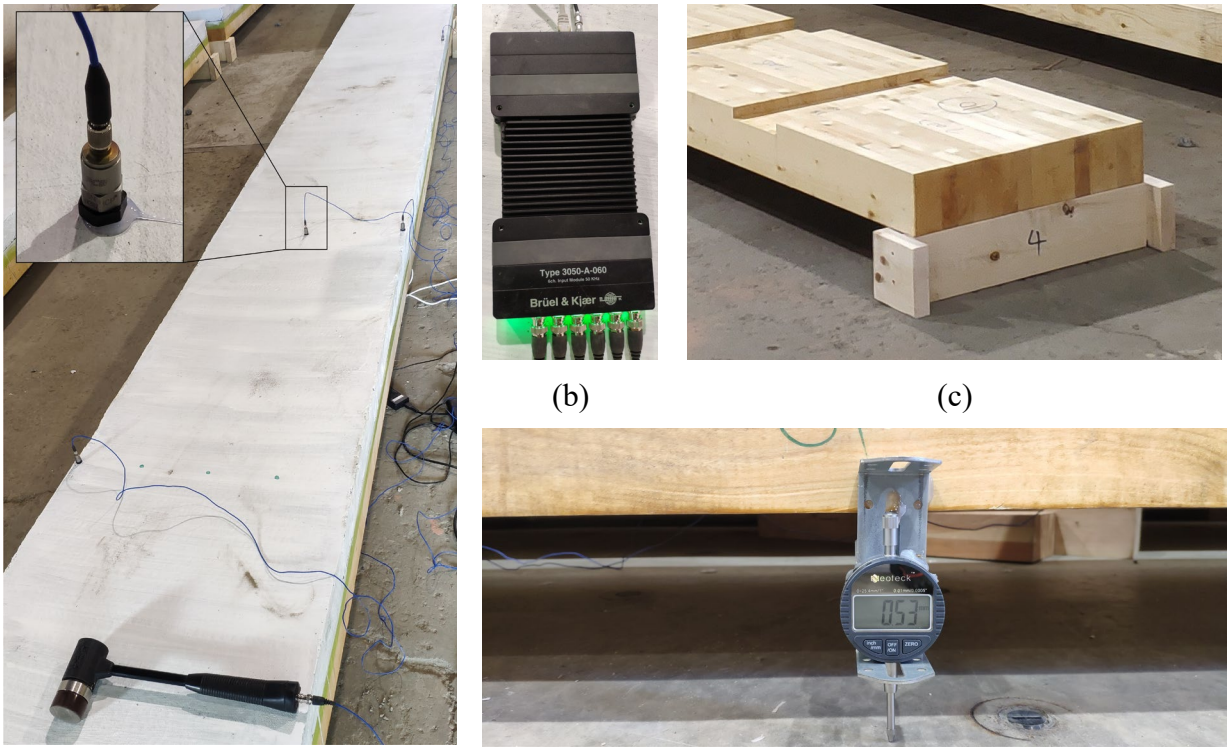

(a) (b) (c) (d)

Fig. 4.20 Vibration tests and deflection tests on composite floor specimens (a) Piezoelectric accelerometers and the impulse hammer; (b) Multi-channel signal conditioner; (c) Support made of dimension lumber; and (d) Dial indicator in the deflection tests.

Experimental modal tests were performed on GLT panels and composite floors with simple support and multiple-support conditions to measure modal parameters such as natural frequencies, mode shapes, and damping ratios. The panels were sitting on the supports made with 38 mm × 140 mm dimension lumber with the narrow edge sitting on the ground, as shown in Fig. 4.20(c). Due to the long span of the floors, the supporting condition of the floors can be considered as simply supported. The roving impact hammer tests were performed using an instrumented impulse hammer (PCB, model 086D05), piezoelectric accelerometers (PCB model 352C04, nominal sensitivity 1.02 mV/(m/s^2), frequency range 0.5–10000 Hz), a multi-channel dynamic analyzer module (Brüel & Kjær, type 3050-A-060), and a PC-based data acquisition system (BK connect®). To accurately measure the first few natural frequencies and mode shapes of single-span floors, a 5 by 5 grid was plotted on each specimen, as shown in Fig. 4.21. Each point was tested three times under the hammer impact and averaged to obtain smooth frequency response functions. Accelerometers were attached at four points to precisely capture the first few mode shapes of interest up to 200 Hz. The testing procedure for the double-span composite floors was similar except additional support was added and five accelerometers were mounted on the floors, as shown in Fig. 4.21.

Walking tests were conducted on six single-span composite floors (specimens SPU-1, SPU-7, SPU-8, SPR-1, SPR-2, and SPR-3) with accelerometers mounted along the floor to record the floor response. The tester weighed about 75 kg walked from one end of the floor to the other and then walked back. For the rest of the specimens, walking tests were performed without accelerometers to subjectively evaluate the floor vibration performance. Before the first phase bending tests, deflection tests were conducted on nine single-span unreinforced composite floors by measuring the mid-span deflections of floors under a point load of 0.774 kN acting at mid-span. The deflections of the floors at mid-span were measured at both sides using dial indicators, as shown in Fig. 4.20(d).

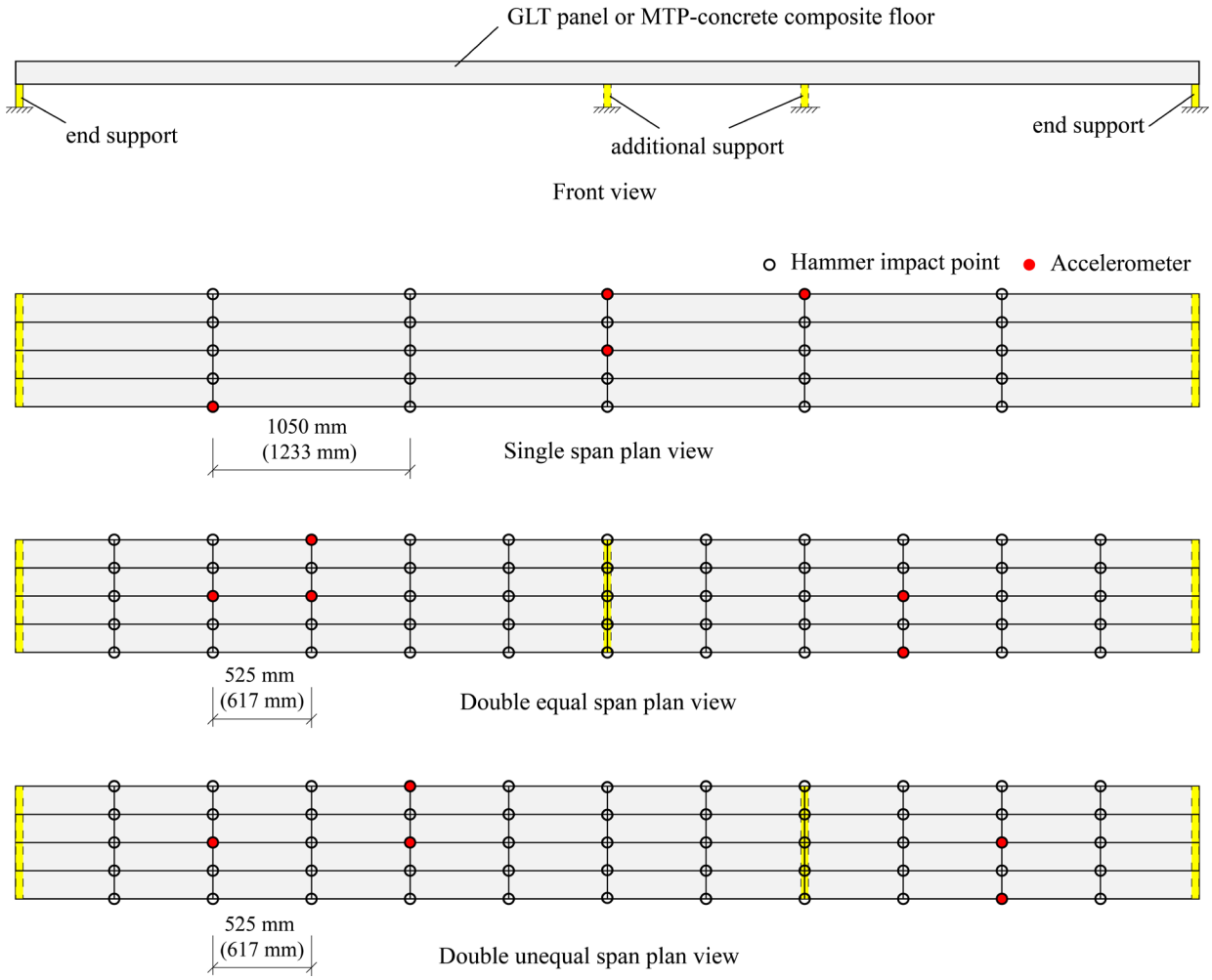

Fig. 4.21 Locations of accelerometers and locations applied with hammer impact force in the roving impact hammer test (numbers in the brackets represent dimensions of specimen SPU-2)

4.4.3 Test Results and Discussion

Frequencies and mode shapes

The modal parameters (natural frequencies, damping ratios, and mode shapes) of GLT panels and MTP-concrete composite floors were extracted from the experimental modal analysis performed in the BK connect® software package. The natural frequencies of the specimens were estimated from the resonant frequencies in the frequency response functions (FRF) that were transformed from the recorded time history acceleration waveforms using Fast Fourier Transformation (FFT). The first four natural frequencies for the single-span GLT and MTP-concrete composite floors are

listed in Table 4.4, where f_{20} represents the first flexural frequency, f_{30} the second flexural frequency, f_{21} the first torsional frequency, and f_{40} the third flexural frequency. The fundamental natural frequencies for the double-span unreinforced MTP-concrete composite floors are also listed in Table 4.4. The corresponding mode shapes for single and double span floors are shown in Fig. 4.22.

Table 4.4 Measured natural frequencies (Hz) of the floor specimens

Specimen	GLT panels				MTP-concrete composite floors					
	single span				single span				double equal span	double unequal span
	f_{20}	f_{30}	f_{21}	f_{40}	f_{20}	f_{30}	f_{21}	f_{40}	fundamental frequency	
SPU-1	6.8	24.4	30.4	54.6	8.5	24.9	31.4	45.0	21.6	16.9
SPU-2	4.9	18.0	26.3	39.7	6.5	21.4	23.9	40.1	18.9	13.6
SPU-3	6.8	24.3	29.8	52.2	8.6	26.8	28.3	46.8	20.1	16.6
SPU-4	6.9	25.6	28.4	54.8	8.5	27.1	31.1	47.7	23.7	16.3
SPU-5	6.9	26.3	28.9	58.0	8.8	27.2	30.6	48.1	22.9	16.6
SPU-6	6.6	23.8	29.8	52.3	8.4	25.0	28.4	42.9	20.1	15.1
SPU-7	6.8	24.4	30.4	54.6	8.1	26.9	29.7	49.3	23.2	15.9
SPU-8	6.9	26.4	32.0	55.1	7.1	17.6	21.1	34.5	18.9	13.4
SPU-9	6.6	24.5	28.0	55.3	8.9	27.7	31.4	50.1	27.9	14.7
SPR-1	6.8	25.5	28.3	57.8	9.0	28.8	41.0	50.0	/	/
SPR-2	6.6	23.4	29.8	50.8	7.5	23.5	35.3	41.0	/	/
SPR-3	6.6	24.3	29.3	53.3	7.3	25.5	38.0	44.3	/	/

Note: f_{20} is the fundamental natural frequency (first flexural frequency); f_{30} is the second flexural frequency; f_{21} is the first torsional frequency; f_{40} is the third flexural frequency.

The frequency response functions (FRF) obtained from FFT for the GLT panel and composite floor of specimen SPU-1 are shown in Fig. 4.23. Each resonant frequency is clearly displayed in the spectrum plots, even though the increase of mass in the composite floor significantly reduced

the maximum amplitude of acceleration compared to the bare GLT panel. From Fig. 4.23, it can be seen that the natural frequencies of the composite floor moved closer to each other compared with the bare GLT panel.

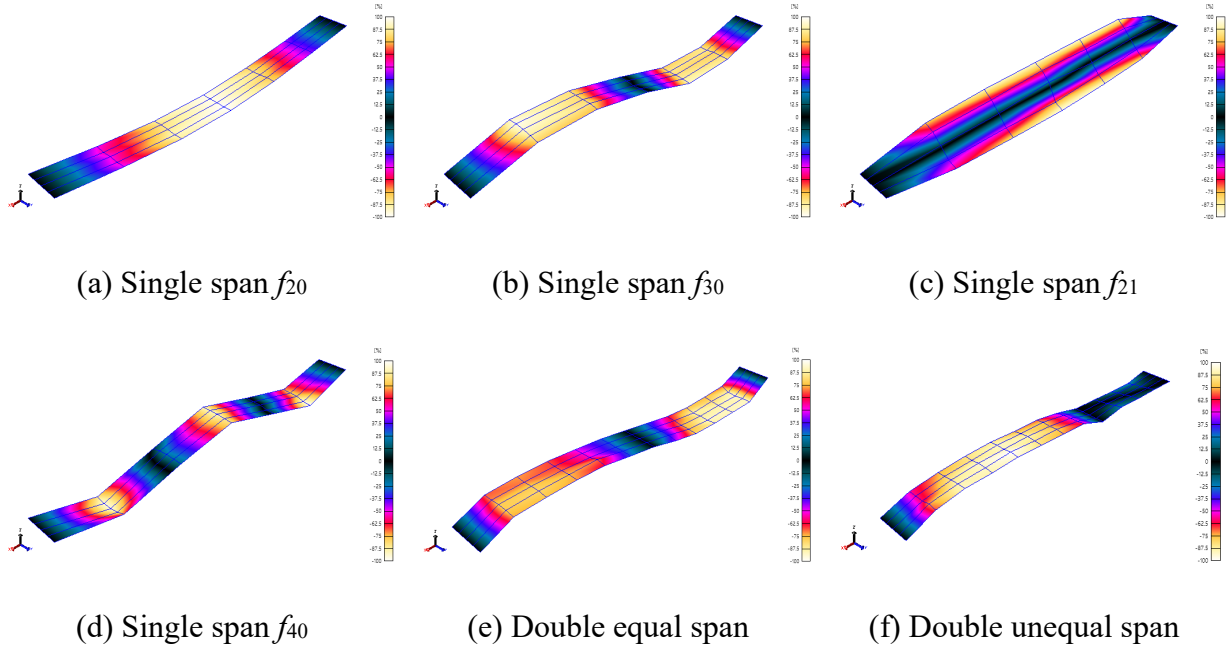

(a) Single span f_{20} (b) Single span f_{30} (c) Single span f_{21}

(d) Single span f_{40} (e) Double equal span (f) Double unequal span

Fig. 4.22 Mode shapes of GLT panels and MTP-concrete composite floors

The natural frequencies of floors are affected by the floor span, total mass, and flexural stiffness. Natural frequency increases with the floor flexural stiffness while decreases with the span and mass. Table 4.4 shows that the fundamental natural frequencies f_{20} of the composite floors are higher than that of GLT panels, indicating that the increase of flexural stiffness of composite floors outweighs the mass increase of floors. The success of the concrete layer in increasing modal frequencies of floors has also been observed by Neve and Spencer-Allen (2015). The governing effect of the flexural stiffness can also be seen from the second flexural frequency f_{30} which was slightly higher in the composite floors than in the GLT panels. However, in higher-order flexural mode, the weight increase offsets the flexural stiffness increase, as most of the composite floors had lower frequencies in the third flexural mode f_{40} than GLT panels. Since the notched connections were designed for single-span floors, the stiffness of these discrete connections was less effective in higher-order flexural mode. Torsional mode frequencies f_{21} for GLT panels and

composite floors were at the same level and the effect of concrete on the torsional mode is unclear and would require further study.

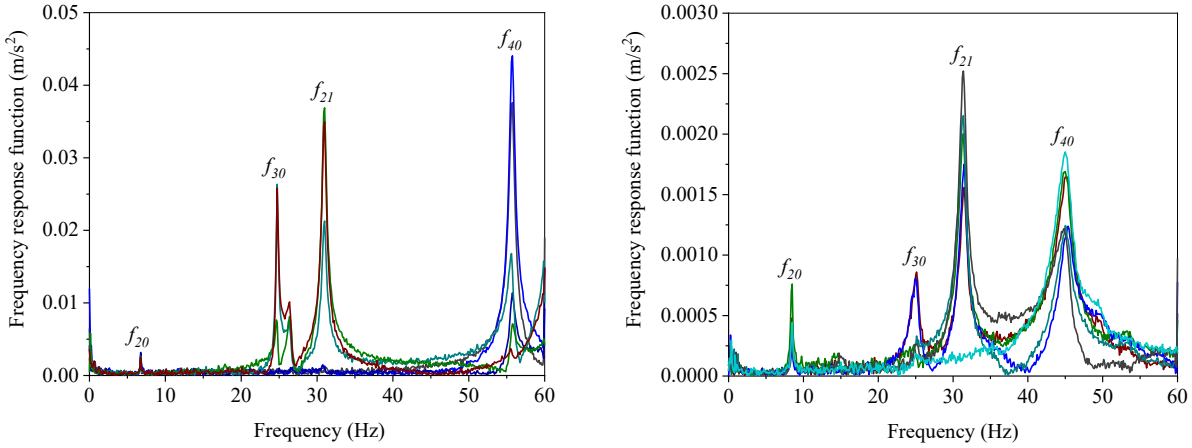

(a) GLT panel (b) MTP-concrete composite floor

Fig. 4.23 Frequency response functions (FRF) of specimen SPU-1 from the roving impact hammer test

Since the fundamental natural frequency is the basic performance parameter governing the vibration performance of floors, the following discussion mainly focuses on the fundamental natural frequency f_{20}. Table 4.4 shows the fundamental natural frequency of MTP-concrete composite floors increased significantly after additional support was added to the single span floors. In the continuous floors, the double equal span floors had higher frequencies than the unequal span floors, as the floor stiffness is governed by the longest span in the continuous floors. To show the effect of span on the floor frequency more clearly, the measured fundamental natural frequencies of unreinforced composite floors with 85 mm concrete thickness in different spans are shown in Fig. 4.24(a). As a typical span in office or residential buildings, most composite floors were measured in 6.3 m. Specimen SPU-2 had a slightly longer span (7.4 m) which resulted in a drop in the fundamental natural frequency. The fundamental natural frequencies for the double equal span floors are shown in Fig. 4.24(a) as the equivalent single-span floors with half of the original span. Fig. 4.24(a) shows a clear decreasing trend of the fundamental natural frequency with the increase of span. The theoretical fundamental natural frequencies of the full- and non-composite

floors are also plotted in Fig. 4.24(a). The fundamental natural frequencies of full- and non-composite floors were predicted from Eq. 4.11 under the assumption of the Euler-Bernoulli beam.

$$f_{20} = \frac{\pi}{2L^2}\sqrt{\frac{EI}{\rho_c A_c + \rho_t A_t}} \tag{4.11}$$

In Eq. 4.11, ρ_c and ρ_t are the densities of concrete and timber, respectively; A_c and A_t are the cross-section areas of concrete and timber, respectively; and L is the floor span. The bending stiffness EI for the non-composite floor and full composite floor were determined from Eq. 4.2 and Eq. 4.3, respectively.

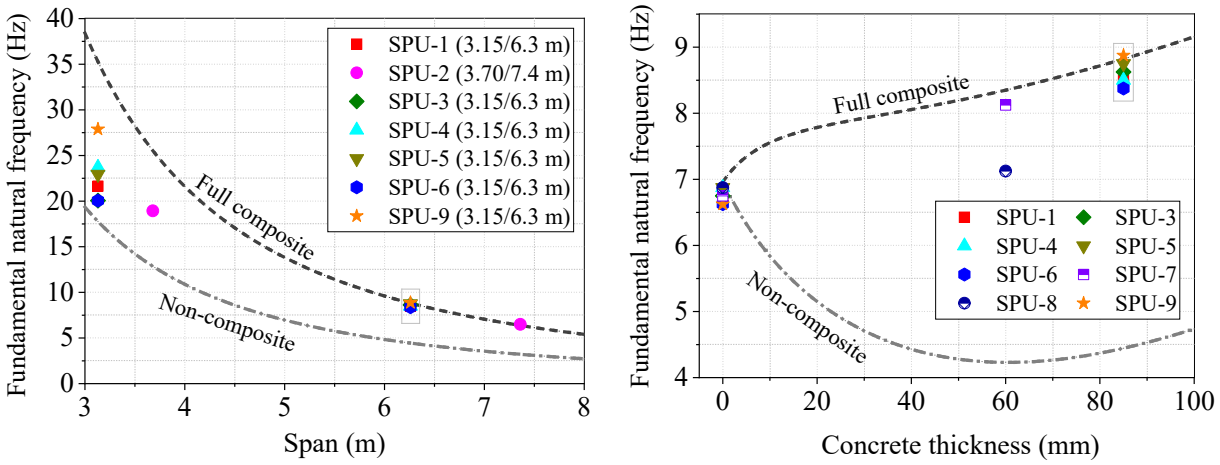

(a) (b)

Fig. 4.24 Measured fundamental natural frequencies of MTP-concrete composite floors and comparison with the theoretical fundamental natural frequencies of the full- and non-composite floors (a) Fundamental natural frequency varying with the floor span (85 mm concrete thickness) (b) Fundamental natural frequency varying with the concrete layer thickness (6.3 m span)

As can be seen from Fig. 4.24(a), the measured fundamental natural frequencies for the original single-span composite floors were close to the full composite frequency (upper limit). However, discrepancies can be observed between the measured frequencies and the predicted upper limit for the double-span floors. The reasons for this are believed to be a combination of:

a) Due to the initial deflections of composite floors under the gravity load, the specimens were not evenly sat on three supports after additional support was added to the mid-span. Thus, the composite floors were more flexible than the theoretical double-span floors.

b) The shear connections were designed for the single-span floors and were not as effective in the double-span floors. As a result, the effective bending stiffness for double-span floors was lower than single-span floors.

c) Shear deformation accounts for a larger portion in shorter span floors. Thus, the theoretical upper limit of the fundamental natural frequency should be lower than the predicted value using the Euler-Bernoulli beam theory.

Except for the floor span, the concrete thickness is another factor contributing to the variation of the fundamental natural frequency of MTP-concrete composite floors. The fundamental natural frequencies for the 6.3 m span GLT and unreinforced MTP-concrete composite floors are plotted in Fig. 4.24(b), together with the theoretical frequencies of full- and non-composite floors. As can be seen from Fig. 4.24(b), the fundamental natural frequency of composite floors generally increases with the concrete thickness. Most specimens had fundamental natural frequencies close to that of the full composite. Specimen SPU-6 had a slightly lower fundamental natural frequency than the rest of the specimens with 85 mm concrete thickness. This may be due to the initial gap between the two layers since the screw fasteners were not installed in the notches in specimen SPU-6. Among the composite floors with a 6.3 m span, specimen SPU-8 had the lowest fundamental natural frequency which was close to the fundamental natural frequencies of GLT panels. Nevertheless, the fundamental natural frequency of specimen SPU-8 was far above the theoretical non-composite frequency. Since specimen SPU-8 had no connection between timber and concrete, the stiffness between the two layers came solely from friction between the two layers.

Except for the span, concrete thickness, and existence of shear connections, other factors such as connection stiffness and the number of connections had little effect on the fundamental natural frequency of the composite floors. Specimens SPU-3 (fewer connections than the reference specimen) and SPU-4 (shallower connections than the reference specimen) had similar fundamental natural frequencies as the reference specimen. Rijal et al. (2015) found that increasing the number of notches had minimal effect on the natural frequencies of timber-concrete composite beams. Numerical studies on a timber-concrete composite floor conducted by Dackermann et al.

(2016) showed that the fundamental natural frequency of the floor was not affected when up to 50% of the shear connectors have been removed.

For three reinforced composite floors, the theoretical fundamental natural frequencies for the full and non-composite floors are 9.0 Hz and 4.5 Hz, respectively. The fundamental natural frequency of specimen SPR-1 was equal to the full composite floor fundamental natural frequency like most of the unreinforced floors with connections. However, specimens SPR-2 and SPR-3 had fundamental natural frequencies (7.5 Hz) that were significantly lower. The lower fundamental natural frequencies in specimens SPR-2 and SPR-3 were the result of the shrinkage crack in the concrete layer, which was not found in specimen SPR-1. After concrete cracking due to shrinkage, the steel mesh in the concrete layer was too weak to maintain the integrity of concrete and the dynamic bending stiffness of the floor was reduced. To mitigate the negative effect of concrete cracking on the dynamic properties of the floor, stronger shrinkage reinforcement should be used in the concrete layer.

Damping

The vibration of floors produces mechanical energy which is dissipated through viscous damping. The damping ratios of the first flexural mode for GLT panels and MTP-concrete composite floors are shown in Table 4.5. The damping ratios were estimated from the frequency response functions (FRFs) using the rational fraction polynomial method. As shown in Table 4.5, the measured damping ratios for the composite floors were higher than those for GLT panels. As a dimensionless measure of damping, the damping ratio is dependent on the actual damping, mass, and stiffness of the floor. Since the composite floors had both higher flexural stiffness and mass than bare GLT panels, the actual damping was even higher in the composite floors due to the additional concrete layer and friction at the timber and concrete interface.

Damping characterizes how quickly transient vibration decays as energy dissipates through friction within and between materials. In the case of the tested GLT and composite floors, damping depends on the nature of materials, the friction at the interface of timber and concrete, and the boundary conditions. Eurocode 5 (CEN 2014) suggests using 1% damping ratio for timber floors. Except for composite specimen SPU-8 which had no connection in the floor, the damping ratios

for all the tested floor specimens were lower than 1%. However, it should be noted that damping is often measured with a great degree of uncertainty. In the actual structural systems, damping depends mostly on the presence of non-structural elements such as ceiling, mechanical equipment, partitions, and furnishings. Higher damping ratios are thus expected in the actual structure systems than the measured damping ratios on bare panels in this study.

Table 4.5 Damping ratios (in percentage) of GLT panels and MTP-concrete composite floors

Specimen	GLT	MTP-concrete composite floor
SPU-1	0.33	0.80
SPU-2	0.32	0.75
SPU-3	0.39	0.70
SPU-4	0.44	0.71
SPU-5	0.45	0.70
SPU-6	0.43	0.77
SPU-7	0.33	0.69
SPU-8	0.48	1.02
SPU-9	0.35	0.66

Vibration serviceability performance

In this section, the measured vibration parameters of the floor specimens including fundamental natural frequencies, deflections under a point load, and accelerations under human walking were compared with the existing vibration design criteria to evaluate the vibration performance of MTP-concrete composite floors.

The average fundamental natural frequencies of the 6.3 m span GLT panels and unreinforced MTP-concrete composite floors (with 85 mm concrete thickness) were 6.8 Hz and 8.6 Hz, respectively. Dolan et al. (1999) proposed that acceptable vibration for wood floors will be obtained if the floor has sufficient stiffness to keep the fundamental natural frequency above 15 Hz, which is higher than the measured fundamental natural frequencies of all the tested single-span GLT panels and composite floors. All the double-equal-span and most double-unequal-span

MTP-concrete composite floors had fundamental natural frequencies higher than 15 Hz. However, the fundamental natural frequency as a sole measure of floor vibration performance is often inadequate and the 15 Hz criterion may be too conservative for MTP-concrete composite floors with heavy concrete topping.

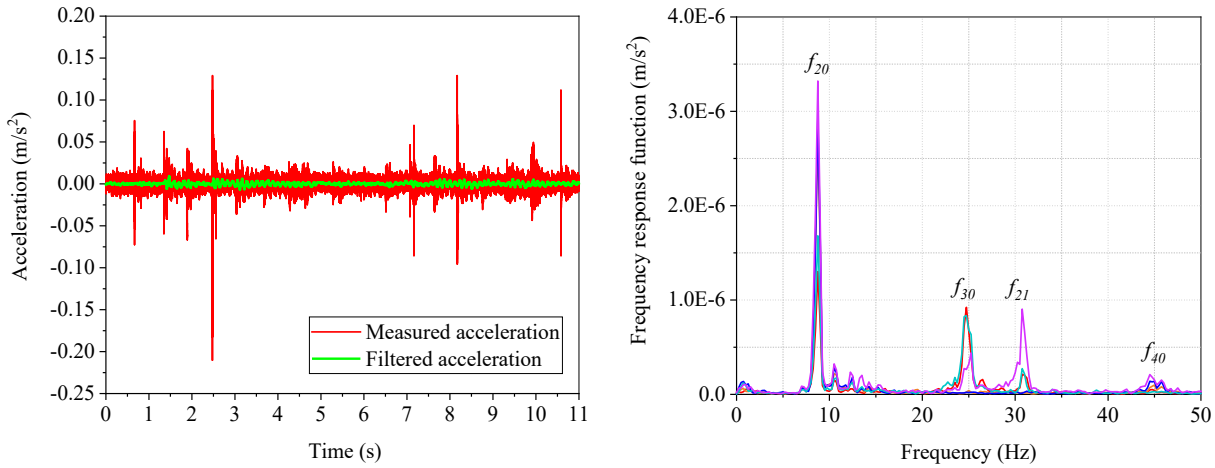

(a) Acceleration at mid-span (b) Frequency response functions

Fig. 4.25 Response of specimen SPU-1 under human walking excitation

Walking tests were performed on specimens SPU-1, SPU-7, SPU-8, SPR-1, SPR-2, and SPR-3 to measure the floor response under human walking activities. Fig. 4.25(a) shows the acceleration waveforms captured by the accelerometer mounted at the centre of specimen SPU-1 which shows the transient response of the floor under human walking excitations. The FRFs obtained from five accelerometers mounted on the floor are shown in Fig. 4.25(b). The natural frequencies of the floor according to the FRF spectrum were slightly different from the roving impact hammer test results due to the additional weight of the participant which was about 75 kg.

The recorded acceleration waveforms from walking tests were weighted according to ISO 2631-2 (2003) to exclude frequency contents to which humans are insensitive (ISO 10137 2007; Murray et al. 2016). Then the 1s root-mean-square (RMS) accelerations are computed according to Eq. 4.12

$$a_{RMS}=\sqrt{\int_{t_0}^{t_0+1}[a(t)]^2dt} \approx \sqrt{\frac{1}{N}\sum_{k=i}^{i+N-1} a_k^2} \quad (4.12)$$

where t_0 represents any starting point during the measurement period and N is the number of discrete acceleration data points in one second. The maximum RMS accelerations during the walking tests for the specimens are shown in Table 4.6 and compared with the RMS acceleration baseline limit provided by ISO 10137 (2007) for human response to continuous sinusoidal accelerations. For a quiet office building, a multiplying factor of 2 can be applied to the baseline curve for continuous and intermittent vibrations. As shown in Table 4.6, the RMS accelerations of MTP-concrete composite floors were lower than the ISO 10137 (2007) baseline limit even before the multiplying factor has been applied.

Table 4.6 Maximum accelerations measured from the walking tests and the tolerance limits (unit: m/s^2)

Specimen	ESPA		Root-mean-square acceleration		
	measured	tolerance limit[a]	measured	ISO baseline[b]	tolerance limit[c]
SPU-1	0.004	0.054	0.0029	0.0054	0.0108
SPU-7	0.006	0.050	0.0042	0.0051	0.0102
SPU-8	0.003	0.049	0.0022	0.0050	0.0100
SPR-1	0.006	0.055	0.0043	0.0056	0.0112
SPR-2	0.003	0.049	0.0023	0.0050	0.0100
SPR-3	0.005	0.049	0.0033	0.0050	0.0100

[a]Tolerance limit for office, residences, and quiet areas according to AISC steel design guide (Murray et al. 2016)

[b]Baseline in ISO 10137 (2007)

[c]After a multiplying factor of 2 (for quiet office) has been applied to the ISO 10137 baseline (ISO 2007)

The peak acceleration limit of floors under human walking is provided by the AISC steel design guide for sinusoidal acceleration (Murray et al. 2016). The measured peak accelerations of floors are not directly comparable to the sinusoidal peak acceleration tolerance limits. Therefore, the equivalent sinusoidal peak acceleration (ESPA) is computed by multiplying the RMS accelerations by $\sqrt{2}$. Table 4.6 shows the determined ESPA values of the floor specimens and the sinusoidal

peak acceleration limits. The ESPA values of MTP-concrete composite floors under human walking were lower than the suggested tolerance limit (Murray et al. 2016).

The deflections of unreinforced MTP-concrete composite floors under a concentrated load acting at mid-span are shown in Table 4.7 where the deflections were linearly normalized to 1 kN load from the applied load of 0.774 kN. Table 4.7 also listed the tolerance limits for the static deflection of floors under 1 kN point load proposed by Onysko et al. (2000), Hamm et al. (2010), and Hu et al. (2016). The performance criterion proposed by Onysko et al. (2000) does not explicitly include dynamic response but it controls vibrational response by adjusting the stiffness of the floor system. The criterion requires that for spans between 5.5 m and 9.9 m, the deflection under 1 kN point load at mid-span be limited to $2.55 \,/\, L^{0.63}$ (mm) with the span L in m. The measured deflections for five out of nine specimens were unable to meet this requirement. For the rest of the specimens, the measured deflections were close to the proposed threshold. Hamm et al. (2010) developed criteria stating that floors with higher demands should have fundamental natural frequencies higher than 8 Hz and deflection lower than 0.5 mm under 2 kN concentrated load, while floors with lower demands should have fundamental natural frequencies higher than 6 Hz and deflection lower than 1 mm under 2 kN concentrated load. The deflections of the measured floor specimens failed to meet the requirements for either higher or lower demands in the criteria of Hamm et al. (2010). The performance criterion proposed by Hu et al. (2016), which is the most liberal one among three deflection limits, requires that the deflection of floors under 1 kN point load be lower than

$$\delta \leq \left(\frac{f_{20}}{6.23}\right)^{2.94} \tag{4.13}$$

From Table 4.7, it can be seen that, except for Specimen SPU-8, the measured deflections of MTP-concrete composite floors were lower than the deflection limit proposed by Hu et al. (2016).

Overall, the comparisons between the test results and existing design criteria to control the vibration of floors yield inconsistent results. The tested MTP-concrete composite floors should have acceptable vibration performance according to the RMS acceleration limit in ISO 10137 (2007), peak acceleration limit in AISC steel design guide (Murray et al. 2016), and the deflection limit proposed by Hu et al. (2016). However, the floor vibration is likely unacceptable according to the required minimal fundamental natural frequency proposed by Dolan et al. (1999) and

deflection limits in the criteria of Hamm et al. (2010). The deflections of most MTP-concrete composite floors were at the level around the deflection limit proposed by Onysko et al. (2000).

Table 4.7 Mid-span deflections of MTP-concrete composite floors under 1 kN concentrated load and comparison with the tolerance limits (mm)

Specimen	Measured deflection	Tolerance limit 1[a]	Tolerance limit 2[b]	Tolerance limit 3[c]
SPU-1	0.76	0.80	0.25 or 0.5	2.49
SPU-2	1.09	0.72	0.5	1.13
SPU-3	0.81	0.80	0.25 or 0.5	2.58
SPU-4	0.76	0.80	0.25 or 0.5	2.49
SPU-5	0.70	0.80	0.25 or 0.5	2.76
SPU-6	0.88	0.80	0.25 or 0.5	2.41
SPU-7	1.06	0.80	0.25 or 0.5	2.16
SPU-8	3.27	0.80	0.5	1.47
SPU-9	0.67	0.80	0.25 or 0.5	2.85

[a]According to Onysko et al. (2000).
[b]According to Hamm et al. (2010) where 0.25 mm is for higher demands floors and 0.5 mm is for lower demands floors.
[c]According to Hu et al. (2016).

From walking tests and subjective evaluation by five participants on all the single-span MTP-concrete composite floors, the vibration of floors was "unacceptable" due to the excessive perceptible vibration. This means that the acceleration criteria in ISO 10137 (2007), AISC steel design guide (Murray et al. 2016), and deflection limits proposed by Onysko et al. (2000) and Hu et al. (2018) might not be stringent enough. The vibration of double-span MTPCC floors under human walking was generally acceptable which validates the frequency limit proposed by Dolan et al. (1999). It should be noted that the tested floor strips were narrow (0.6 m). The actual MTP-concrete composite floors are expected to have lower deflection and acceleration under human walking since the concrete layer is continuous over mass timber panels (Sebastian et al. 2020). The tested floor strips in this study serve as the lower bound when both concrete and timber are discontinuous in the transverse direction. Walking tests on full-scale MTP-concrete composite

floors are required to further verify the existing standards and evaluate the vibration performance of MTP-concrete composite floors.

Floor flexural stiffness

When the span, mass, and boundary conditions of the floor are determined, the floor flexural stiffness becomes the governing factor for the floor serviceability performance under static and dynamic loads. This section compares the floor flexural stiffness determined from vibration and bending tests.

From the vibration tests, the flexural stiffness of composite floors (refer to as "dynamic flexural stiffness $(EI)_d$") can be estimated from the fundamental natural frequency f_{20} by neglecting the shear deformation of floors (i.e. Euler-Bernoulli beam theory) as

$$(EI)_d = (\rho_c A_c + \rho_t A_t)(\frac{2L^2 f_{20}}{\pi})^2 \tag{4.14}$$

Symbols in Eq. 4.14 have been explained in Eq. 4.11. For bare GLT panels, Eq. 4.14 reduces to

$$(EI)_{dt} = \rho_t A_t(\frac{2L^2 f_{20}}{\pi})^2 \tag{4.15}$$

The flexural stiffness for bare GLT panels and MTP-concrete composite floors determined from vibration tests according to Eq. 4.14 and Eq. 4.15 are listed in Table 4.8 and plotted in the histogram in Fig. 4.26 against the floor static bending stiffness. The theoretical flexural stiffness for the non-composite and full composite floors according to Eq. 4.2 and Eq. 4.3 are also plotted in Fig. 4.26. The static bending stiffness of GLT panels was estimated from Young's modulus of timber and cross-section sizes of GLT. As can be seen from Fig. 4.26, irrespective of the testing method, the flexural stiffness for most of the composite floors improved significantly from the bare GLT panels. On average, the flexural stiffness of MTP-concrete composite floors was about 6 times the bare GLT panel flexural stiffness. The estimated static flexural stiffness of GLT panels is slightly higher than the measured dynamic flexural stiffness of GLT panels due to the notches cut on the panels. The dynamic flexural stiffness of composite floors is close to the theoretical full-composite stiffness with the exception of specimens SPU-8, SPR-2, and SPR-3. Specimen SPU-8 relied solely on friction to resist the relative slip between two layers, while specimens SPR-2 and

SPR-3 had shrinkage cracks in the concrete layer. The static bending stiffness of composite floors measured from four-point bending tests was notably lower than the full composite stiffness, as well as the measured dynamic flexural stiffness except for specimens SPR-2 and SPR-3. Student T-tests (paired data and two-tailed distribution) conducted on two groups of MTP-concrete composite floor flexural stiffness showed that, at a significance level of 0.05, a significant difference was detected between the static bending stiffness and dynamic flexural stiffness.

The dynamic flexural stiffness of the composite floors is less affected by the connection stiffness and number of connections than the static bending stiffness. As an example, specimen SPU-4 used shallow notches (13 mm) between timber and concrete thus its static bending stiffness was 20% lower than the reference specimen (25 mm notch depth). This effect cannot be observed from the dynamic flexural stiffness. Specimen SPU-3 used reduced number of notched connections which caused a slight decrease in the static bending stiffness, but not a decrease in dynamic flexural stiffness. An extreme example is specimen SPU-8 which was designed without connection between two layers. The dynamic flexural stiffness of specimen SPU-8 was 3.7 times of its static bending stiffness. The static bending stiffness of MTP-concrete composite floors is less affected by concrete shrinkage cracks than the dynamic flexural stiffness, with examples of the reinforced specimens SPR-1, SPR-2, and SPR-3. This phenomenon can be explained by the fact that the concrete layer was under compression in the static bending tests thus the shrinkage cracks were closed under compression. A counterexample is specimen SPU-9 which shows significantly lower static bending stiffness than its dynamic flexural stiffness. The low static bending stiffness in specimen SPU-9 was due to concrete tensile cracking at the bottom under the negative bending moment.

The phenomenon of different levels of floor flexural stiffness in different tests can be explained by the level of deformation of floors. In the vibration tests, the deformations of floors were very small and the gap opening between timber and concrete can be neglected. The slip resistance between timber and concrete was provided by not only the notches but also the friction and screw fasteners. In the four-point bending tests, however, due to the larger deformation, concrete and timber tended to have different curvatures and a gap was formed between two layers. The shear stiffness between two layers was mainly provided by notched connections which experienced cracking around the notched corners.

Table 4.8 Dynamic flexural stiffness (kNm^2) of GLT panels and MTP-concrete composite floors

Specimen	GLT panels	MTP-concrete composite floors
SPU-1	937	6827
SPU-2	934	7628
SPU-3	937	7029
SPU-4	972	6827
SPU-5	972	7235
SPU-6	902	6628
SPU-7	937	4802
SPU-8	972	3693
SPU-9	902	7443
SPR-1	937	7314
SPR-2	902	5079
SPR-3	902	5079

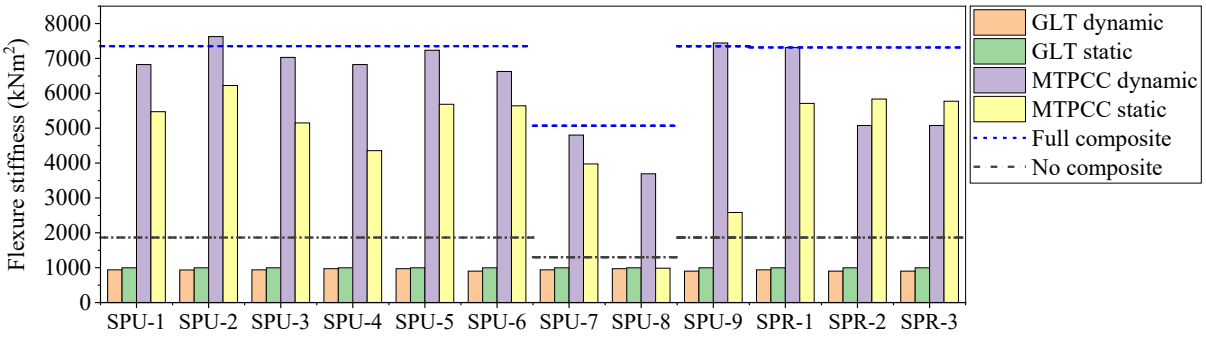

Fig. 4.26 Comparison of the dynamic and static flexural stiffness of GLT panels and MTP-concrete composite floors

4.4.4 Conclusions from Vibration Tests

From the floor vibration tests, the following conclusions can be drawn:

1. The addition of the concrete layer in mass timber panel-concrete composite floors is beneficial to the dynamic properties of the composite floors. Both the flexural stiffness and

fundamental natural frequencies of the floors have been improved after a concrete layer was connected to bare GLT panels.

2. Due to the small deformation and multiple sources of slip resistance of composite floors in the vibration tests, the dynamic flexural stiffness for most of the MTP-concrete composite floors was close to full composite and higher than the static bending stiffness of floors under larger deformation.
3. The dynamic properties of the composite floors were most affected by the concrete thickness, floor span, concrete shrinkage cracks, and existence of connections, while the connection stiffness and number of connections had insignificant effects on the floor dynamic properties.

The vibration tests focused on the built-in dynamic properties of MTP-concrete composite floors with notched connections. Walking tests and subjective evaluation on the composite floors showed that the floor vibration cannot meet occupancy comfort when the narrow floor strips are not transversely connected. The dynamic evaluation on the floor strips cannot fully represent the composite floors in reality and vibration tests on the full-scale MTP-concrete composite floors should be investigated in future studies.

4.5 Conclusions

This chapter discusses the static bending tests and vibration tests on twelve full-size MTP-concrete composite floors. Results from bending and vibration tests serve as important references for the future evolvement of MTP-concrete composite floors with notched connections. The main findings from the tests as well as the design recommendations for MTP-concrete composite floors are summarized below:

1. To achieve enough composite efficiencies in MTP-concrete composite floors with notches, the floors should have enough notched connections and the notches should have enough depth. The proper number and sizes of notches depend on the floor span and timber member thickness. For the tested floor span (6-7 m), 65% composite efficiency (by stiffness) can be achieved when 6 notched connections with 25 mm depth were used.

2. To achieve high ultimate strengths in MTP-concrete composite floors, the notched connections in the floors should be reinforced with steel reinforcements to control the crack enlargement and stiffness degradation of the connections. By reinforcing the notched connections with proper steel reinforcements, the shear failure in the concrete notch can be avoided and the failure pattern and ultimate strength of the floors can be more predictable and reliable.
3. The ductility of the MTP-concrete composite floors under bending can be achieved by timber crushing in the shallow notched connections. To maintain enough composite efficiency and load-carrying capacity in the floor, shallower notches can be installed at locations that have high bending moments and low shear forces, while deeper notches can be installed at locations that have low bending moments and high shear forces.
4. Under the negative bending moments, the concrete layer should be reinforced with longitudinal reinforcements to take tensile forces after concrete cracking. The bending stiffness of the composite floor is much lower under negative bending moments than under positive bending moments because of concrete cracking. However, by reinforcing the concrete layer with proportioned reinforcements, the composite floor can have a ductile failure pattern and high load-carrying capacity.
5. The composite floors with notches and had no concrete shrinkage cracks exhibited dynamic flexural stiffness that were close to the full composite floor bending stiffness. To mitigate the negative effect of concrete shrinkage cracks on the dynamic properties of the composite floors, the concrete layer should be reinforced with enough shrinkage reinforcement to maintain the continuity of the concrete layer at the serviceability state.
6. Without being connected to the timber panels, the concrete layer cannot contribute to the static bending stiffness of the floors and the improvement of the floor fundamental natural frequency was negligible. To fully employ the beneficial effects of the concrete layer on the static and dynamic performance of the composite floors, the concrete layer should be connected to the timber panels with shear connections.

Chapter 5

Discrete Bond Composite Beam Model

5.1 Introduction

Chapter 3 and Chapter 4 discussed the structural performance of notched connections under shear and notch-connected MTP-concrete composite floors under bending, respectively. The structural performance of the composite floor system is strongly dependent on the notched connection design. An analytical method is desired to associate the connection behaviour with the composite floor behaviour and reliably predict the structural performance of composite floors. The composite beam model should be able to consider the discrete and semi-rigid features of notched connections and accurately predict the deflection and internal forces in the composite floors.

This chapter discusses the development and application of a discrete bond composite beam model proposed for the notch-connected timber-concrete composite floors. The model was developed based on a "release and restore" procedure (Byfield 2002), which is similar to the force method in structural analysis. The model was verified by existing composite beam models and a finite element model. The proposed composite beam model was then used to predict the bending stiffness of MTP-concrete composite floors. A parametric study was also carried out to study the composite floor bending stiffness subjected to various geometric factors. In the end, the composite beam model was extended beyond the elastic stage to predict the ultimate load-carrying capacities of MTP-concrete composite floors. The proposed composite beam model is not restricted to timber-concrete composite floors with notched connections but can be used for any two-layer composite floors with discrete connection systems.

5.2 Model Development

5.2.1 Assumptions

The underlying assumptions for this analytical model are:

(1) There is no separation between concrete and timber when the composite floor is under bending. The vertical deflection and curvature of both layers are treated as equal.
(2) Friction between timber and concrete is neglected and all the shear forces are resisted by the notched connections.
(3) Euler-Bernoulli beam theory holds for timber and concrete layers and their shear deformation is thus not considered.
(4) The composite floor is subjected to the positive bending moment thus concrete is under compression and timber is under tension.

This analytical solution contains four steps, namely partition, release, restore, and combine, which will be explained in detail below.

5.2.2 Partitioning

Although the notches can be made in various shapes, only the rectangular notches are considered in this analytical solution for simplicity. The analytical model can be modified if other types of notches are used. A mass timber panel-concrete composite floor connected with rectangular notches is shown in Fig. 5.1(a). Although the notches have a certain length, the shear forces are only transferred at the load-bearing surfaces through the compressive contact between timber and concrete. The discontinuity of shear force transmission causes the discontinuous internal forces along the floor. Thus, the first step of this analytical solution is to partition the composite floor into several individual segments. Two partitioning methods exist for MTP-concrete composite floors with notched connections, as shown in Fig. 5.1(b) and (c). The first partitioning method considers the actual sizes of the notches and the reduction of the timber member cross-section due to notches. Thus, the notched regions are partitioned as individual segments and the notch depth is treated as a gap between the concrete layer and the timber layer. However, since the sizes of notches are usually small compared to the sizes of the timber member, a simplified partitioning method is to only consider the load-bearing surfaces in the notches and neglect the reduction of the timber cross-section in the model derivation. The following derivation of the model is based on the first partitioning method in Fig. 5.1(b) as the model can easily be simplified for the second partitioning method.

It is assumed that the composite floor is divided into n segments and the length for each segment from left to right is denoted as

$$l_1,\ l_2,\ l_3, \dots ,\ l_n$$

Connections are assumed to exist at the supports of the composite floor as well as two sides of the notches, thus $n + 1$ connections exist in the floor. From left to right, the stiffness of connection is denoted as

$$k_1,\ k_2,\ k_3,\ \dots\ ,\ k_{n+1}$$

The free-body diagram for each segment under the external load is shown in Fig. 5.2(a) where the connectors are not included in the partitioned segments. Since friction is neglected, no shear force is transmitted in the interlayer between timber and concrete, so timber and concrete have constant axial forces within each segment. In any cross-section, timber and concrete have internal forces including axial forces, shear forces, and bending moments. If no external force is acting along the beam axis, the resultant axial force of the composite cross-section should be zero, meaning that the axial forces in timber and concrete are equal in magnitude. The equilibrium of moment in any cross-section of segment i is

$$M(x) = M_c(x) + M_t(x) + N_i(\frac{h_c+h_{ti}}{2} + h_{gi}) \tag{5.1}$$

where $M(x)$ is the external moment acting on the composite cross-section; $M_c(x)$ and $M_t(x)$ are the moments acting on concrete and timber, respectively; N_i is the axial force in two components; and h_c, h_{ti}, and h_{gi} are the thickness of concrete, timber, and gap, respectively. The bending moments and axial forces in timber and concrete cannot be determined directly from Eq. 5.1 since the composite system is statically indeterminate. Instead, a "release-and-restore" procedure is adopted to determine the internal forces.

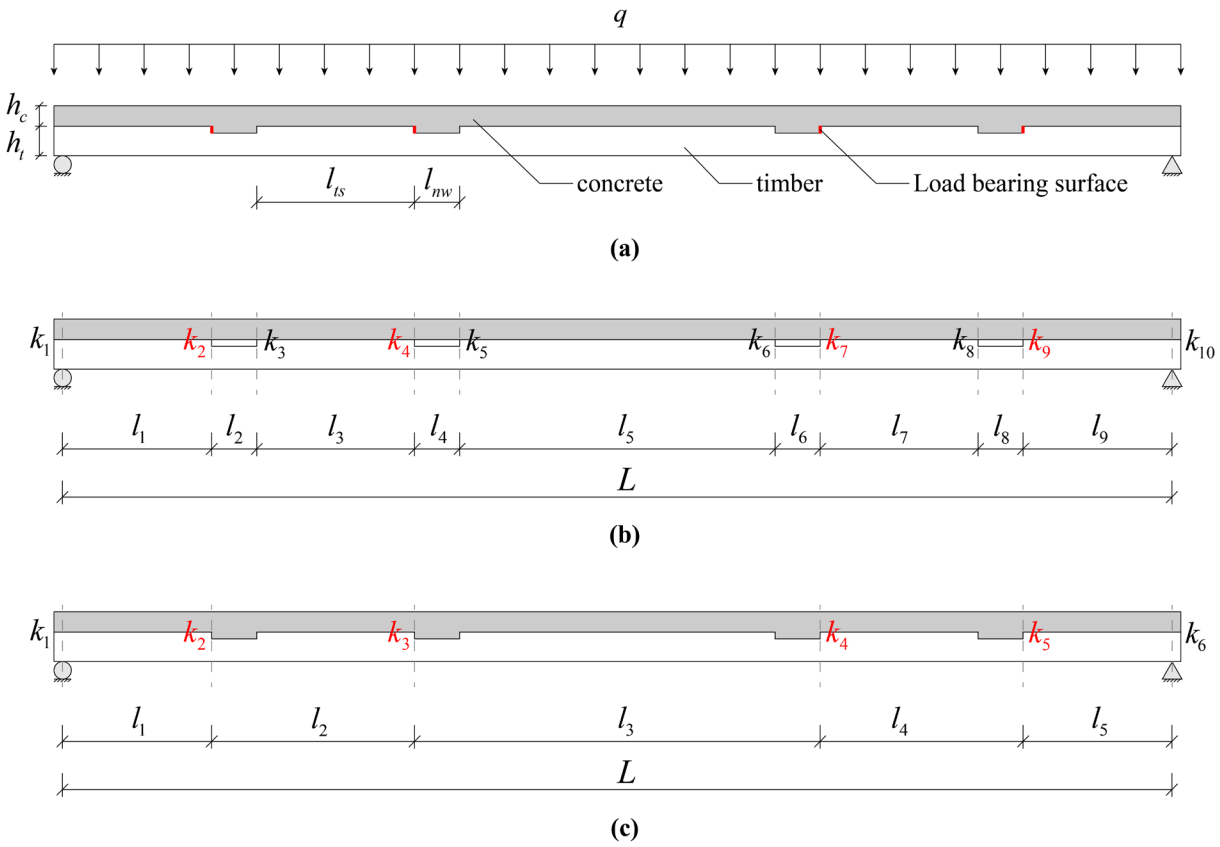

Fig. 5.1 Original MTP-concrete composite floor with notches and two partitioning methods (a) Originally notch connected composite floor; (b) Partitioned composite floor according to the sizes of the notches; and (c) Partitioned composite floor according to the load-bearing surfaces in the notches.

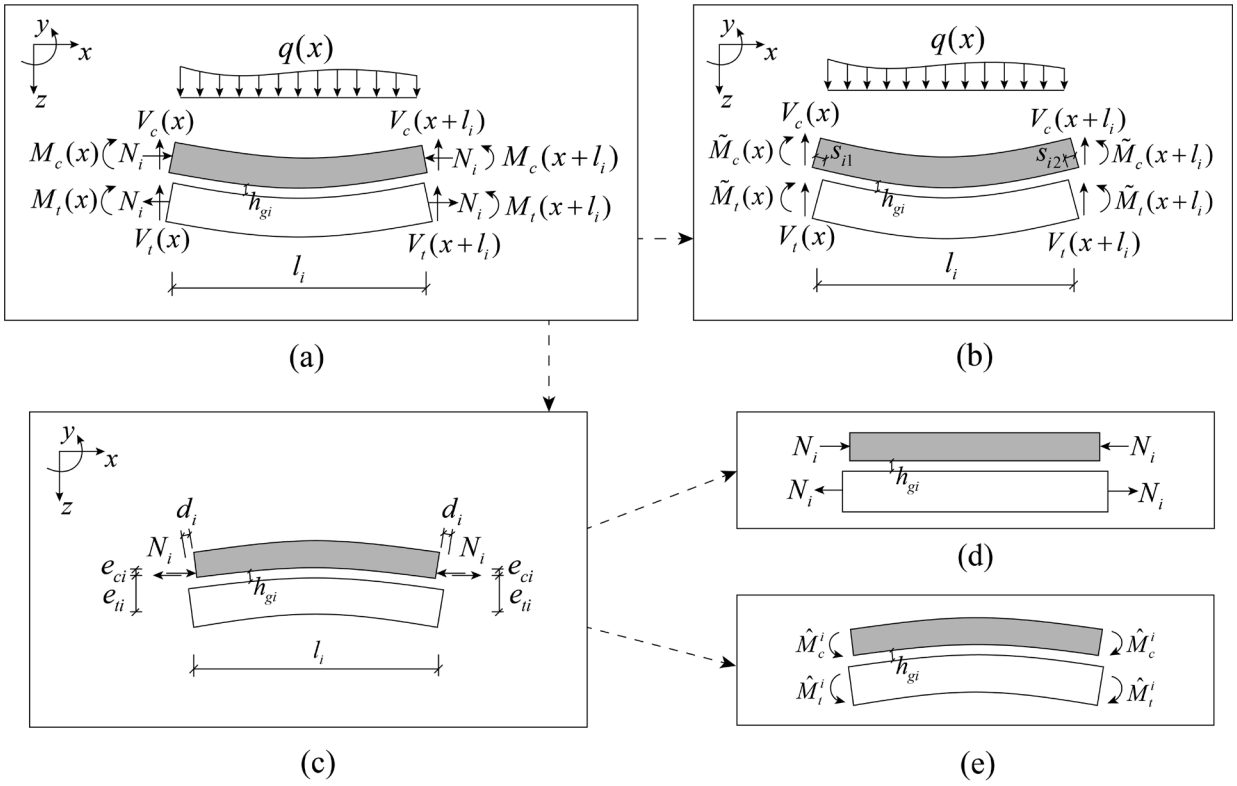

Fig. 5.2 Free body diagram for the partitioned segment in the composite floor (a) Original segment; (b) Released segment; (c) Restored segment; (d) Axial forces acting on the segment; (e) Restored moments acting on the segment.

5.2.3 Released Segment

In this step, the axial forces in each segment are released. Since friction is neglected, the two components can have free slip under the external load, as shown in Fig. 5.2(b). The curvature of timber and concrete at any point along the beam is assumed to be equal. Based on the Euler-Bernoulli beam theory, the curvature $\kappa_1(x)$ of the released segment can be determined as

$$\kappa_1(x) = \frac{\widetilde{M}_c(x)}{E_c I_c} = \frac{\widetilde{M}_t(x)}{E_t I_{ti}} \tag{5.2}$$

where $\widetilde{M}_c(x)$ and $\widetilde{M}_t(x)$ are the moments in concrete and timber in the released segment, and $E_c I_c$ and $E_t I_{ti}$ are the bending stiffness of concrete and timber, respectively. Since the axial forces are released, the external moment in any cross-section is just the summation of bending moments in timber and concrete.

$$M(x) = \widetilde{M}_c(x) + \widetilde{M}_t(x) \tag{5.3}$$

According to Eq. 5.2 and Eq. 5.3, the moments in concrete and timber can be obtained from the external moment as

$$\widetilde{M}_c(x) = \frac{E_c I_c}{E_c I_c + E_t I_{ti}} M(x) \tag{5.4}$$

$$\widetilde{M}_t(x) = \frac{E_t I_{ti}}{E_c I_c + E_t I_{ti}} M(x) \tag{5.5}$$

The shear forces in timber and concrete are the derivatives of their respective moment

$$V_c(x) = \frac{d\widetilde{M}_c(x)}{d(x)} = \frac{E_c I_c}{E_c I_c + E_t I_{ti}} \frac{dM(x)}{dx} = \frac{E_c I_c}{E_c I_c + E_t I_{ti}} V(x) \tag{5.6}$$

$$V_t(x) = \frac{d\widetilde{M}_t(x)}{d(x)} = \frac{E_t I_{ti}}{E_c I_c + E_t I_{ti}} \frac{dM(x)}{dx} = \frac{E_t I_{ti}}{E_c I_c + E_t I_{ti}} V(x) \tag{5.7}$$

where $V(x)$ is the shear force in the composite cross-section. Stresses at the top and bottom of concrete can be expressed as

$$\tilde{\sigma}_c^{top} = -\frac{E_c h_c}{2(E_c I_c + E_t I_{ti})} M(x) \tag{5.8}$$

$$\tilde{\sigma}_c^{btm} = \frac{E_c h_c}{2(E_c I_c + E_t I_{ti})} M(x) \tag{5.9}$$

At this stage, concrete is assumed to be able to resist tensile stresses. In later steps, the tensile stresses at the bottom of concrete will be significantly reduced due to the shear connections with timber. Stresses at the top and bottom of timber are

$$\tilde{\sigma}_t^{top} = -\frac{E_t h_{ti}}{2(E_c I_c + E_t I_{ti})} M(x) \tag{5.10}$$

$$\tilde{\sigma}_t^{btm} = \frac{E_t h_{ti}}{2(E_c I_c + E_t I_{ti})} M(x) \tag{5.11}$$

According to Hooke's law, strains at the bottom of concrete and top of timber are

$$\tilde{\varepsilon}_c^{btm} = \frac{h_c}{2(E_c I_c + E_t I_{ti})} M(x) \tag{5.12}$$

$$\tilde{\varepsilon}_t^{top} = -\frac{h_{ti}}{2(E_c I_c + E_t I_{ti})} M(x) \tag{5.13}$$

The length change at the bottom of concrete and top of timber can be obtained through the integration of strain along the length of segment i.

$$\tilde{\Delta}_c^{btm} = \int_{x_i}^{x_i+l_i} \tilde{\varepsilon}_c^{btm} dx = \frac{l_i \bar{M}_i h_c}{2(E_c I_c + E_t I_{ti})} \tag{5.14}$$

$$\tilde{\Delta}_t^{top} = \int_{x_i}^{x_i+l_i} \tilde{\varepsilon}_t^{top} dx = -\frac{l_i \bar{M}_i h_{ti}}{2(E_c I_c + E_t I_{ti})} \tag{5.15}$$

in which $\bar{M}_i$ is the averaged external moment along segment i and is defined as

$$\bar{M}_i = \frac{1}{l_i} \int_{x_i}^{x_i+l_i} M(x) dx \tag{5.16}$$

and x_i is the distance between the left-hand side of segment i to the left support of the composite floor

$$x_i = \begin{cases} 0 & , \quad i = 1 \\ \sum_{m=1}^{m=i-1} l_m , & 2 \le i \le n \end{cases} \tag{5.17}$$

The difference of length change between the bottom of concrete and top of timber is

$$\lambda_i = \tilde{\Delta}_c^{btm} - \tilde{\Delta}_c^{top} = \frac{(h_c + h_{ti})}{2(E_c I_c + E_t I_{ti})} l_i \bar{M}_i \tag{5.18}$$

As shown in Fig. 5.2(b), the length change between the bottom of concrete and top of timber is the summation of relative slips between timber and concrete at two sides of segment i.

$$s_{i1} + s_{i2} = \lambda_i , i = 1, \ldots, n \tag{5.19}$$

5.2.4. Restored Segment

Due to the constraints provided by the shear connections, timber and concrete are not able to slide freely, and there will be axial forces in timber and concrete caused by the shear forces transmitted by the connections. In this step, the axial forces acting on timber and concrete are considered, as shown in Fig. 5.2(d), where timber is assumed to resist tension and concrete is subjected to compression. The axial forces induce a bending moment in the composite cross-section. The net moment in the composite cross-section, however, should be zero since all the external forces are already considered in the released segment, Fig. 5.2(b). To balance out the bending moment caused

by the axial forces, there should be a group of bending moments acting on timber and concrete in the reverse direction, as shown in Fig. 5.2(e), so that

$$\widehat{M}_c^i + \widehat{M}_t^i = N_i(\frac{h_c+h_{ti}}{2} + h_{gi}) \tag{5.20}$$

The restored moments, $\widehat{M}_c^i$ and $\widehat{M}_t^i$, are the differences between the original moments, $M_c(x)$ and $M_t(x)$, and the released moments, $\widetilde{M}_c(x)$ and $\widetilde{M}_t(x)$, in timber and concrete layers. In each segment, the axial forces are constant, so are the restored moments. Similarly, the curvature in timber and concrete should be equal in the restored segment

$$\kappa_2^i = \frac{\widehat{M}_c^i}{E_c I_c} = \frac{\widehat{M}_t^i}{E_t I_{ti}} \tag{5.21}$$

Combining Eq. 5.20 and Eq. 5.21, the restored moments in concrete and timber can be obtained as

$$\widehat{M}_c^i = \frac{E_c I_c N_i}{E_c I_c + E_t I_{ti}}(\frac{h_c+h_{ti}}{2} + h_{gi}) \tag{5.22}$$

$$\widehat{M}_t^i = \frac{E_t I_{ti} N_i}{E_c I_c + E_t I_{ti}}(\frac{h_c+h_{ti}}{2} + h_{gi}) \tag{5.23}$$

Rearranging Eq. 5.20, it can be found that the axial forces in Fig. 5.2(d) and bending moments in Fig. 5.2(e) can be merged into a group of axial forces acting at the same position that is eccentric to the centre of both layers, as shown in Fig. 5.2(c). The eccentricities of the axial forces to the centre of concrete and centre of timber are

$$e_{ci} = \frac{\widehat{M}_c^i}{N_i} = \frac{E_c I_c}{E_c I_c + E_t I_{ti}}(h_{gi} + \frac{h_c+h_{ti}}{2}) \tag{5.24}$$

$$e_{ti} = \frac{\widehat{M}_t^i}{N_i} = \frac{E_t I_{ti}}{E_c I_c + E_t I_{ti}}(h_{gi} + \frac{h_c+h_{ti}}{2}) \tag{5.25}$$

which are only dependent on the material and cross-section properties of the composite floor. The eccentric axial forces induced a curvature κ_2^i in the segment that is in the opposite direction to the curvature $\kappa_1(x)$ caused by the external load, which indicates the effectiveness of the connections in reducing the deflection of the composite section. Under the eccentric axial forces, the stresses at the top and bottom of concrete are

$$\hat{\sigma}_c^{top} = \frac{N_i e_{ci} h_c}{2I_c} - \frac{N_i}{A_c} \tag{5.26}$$

$$\hat{\sigma}_c^{btm} = -\frac{N_i e_{ci} h_c}{2I_c} - \frac{N_i}{A_c} \tag{5.27}$$

The stresses at the top and bottom of timber are

$$\hat{\sigma}_t^{top} = \frac{N_i e_{ti} h_{ti}}{2I_{ti}} + \frac{N_i}{A_{ti}} \tag{5.28}$$

$$\hat{\sigma}_t^{btm} = -\frac{N_i e_{ti} h_{ti}}{2I_{ti}} + \frac{N_i}{A_{ti}} \tag{5.29}$$

These stresses are constant along each segment due to the constant axial forces. The strains at the bottom of concrete and top of timber are

$$\hat{\varepsilon}_c^{btm} = -\frac{N_i e_{ci} h_c}{2E_c I_c} - \frac{N_i}{E_c A_c} \tag{5.30}$$

$$\hat{\varepsilon}_t^{top} = \frac{N_i e_{ti} h_{ti}}{2E_t I_{ti}} + \frac{N_i}{E_t A_{ti}} \tag{5.31}$$

The length changes at the bottom of concrete and top of timber are

$$\hat{\Delta}_c^{btm} = \hat{\varepsilon}_c^{btm} l_i = -\frac{N_i l_i}{E_c}\left(\frac{e_{ci} h_c}{2I_c} + \frac{1}{A_c}\right) \tag{5.32}$$

$$\hat{\Delta}_t^{top} = \hat{\varepsilon}_t^{top} l_i = \frac{N_i l_i}{E_t}\left(\frac{e_{ti} h_{ti}}{2I_{ti}} + \frac{1}{A_{ti}}\right) \tag{5.33}$$

The difference in length change between the bottom of concrete and top of timber is

$$\hat{\Delta}_t^{top} - \hat{\Delta}_c^{btm} = N_i \theta_i \tag{5.34}$$

where

$$\theta_i = \frac{l_i}{E_t}\left(\frac{e_{ti} h_{ti}}{2I_{ti}} + \frac{1}{A_{ti}}\right) + \frac{l_i}{E_c}\left(\frac{e_{ci} h_c}{2I_c} + \frac{1}{A_c}\right) \tag{5.35}$$

Due to the symmetry of the segment under eccentric axial forces, the relative slips are the same at two sides of the segment, as shown in Fig. 5.2(c).

$$d_i = \frac{1}{2} N_i \theta_i \,,\ i = 1, \ldots, n \tag{5.36}$$

5.2.5 Combining Segments

The internal forces in the segments from the release and restore steps should be combined to form the actual internal forces in the segments. And then, partitioned segments need to be assembled to form the continuous floor by applying the compatibility conditions. As shown in Fig. 5.3, the slips at two sides of each segment should be compatible with the slips of the adjacent segments

$$d_{i-1} - s_{(i-1)2} = s_{i1} - d_i \ , \ \ i = 2, \ldots, n \tag{5.37}$$

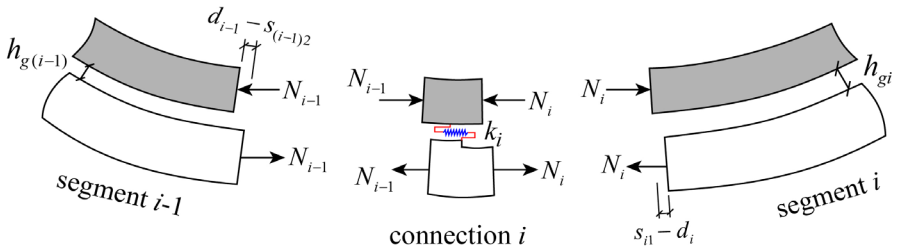

Fig. 5.3 Combining adjacent segments with a connector in between

When combining adjacent segments, the connector in between (notch in this case) has to be considered. If the floor is simply supported, then the relation between the shear force transmitted by the ith connection T_i and the axial forces in the adjacent segments is

$$T_i = \begin{cases} N_i \ , \ i = 1 \\ N_i - N_{i-1} \ , 2 \le i \le n \\ -N_{i-1} \ , \ i = n+1 \end{cases} \tag{5.38}$$

Equation 5.38 shows that the axial force in segment i is the accumulation of shear forces transmitted by all the connections on the left of the segment

$$N_i = \sum_{m=1}^{i} T_m \ , \ \ i = 1, \ldots, n \tag{5.39}$$

Considering the stiffness of the connections, the shear forces transferred by the connections are

$$T_i = \begin{cases} k_i(s_{i1} - d_i) \ , & i = 1, \ldots, n \\ k_i\left(d_{i-1} - s_{(i-1)2}\right) \ , & i = n+1 \end{cases} \tag{5.40}$$

Substituting Eq. 5.40 into Eq. 5.39 yields

$$N_i = \sum_{m=1}^{i} k_m(s_{m1} - d_m)\ ,\ i = 1, \ldots, n \tag{5.41}$$

Eq. 5.38 shows that the shear force transferred by the last connector T_{n+1} and the axial force in the last segment N_n has the relation of

$$T_{n+1} + N_n = 0 \tag{5.42}$$

Substituting Eq. 5.40 and Eq. 5.41 into Eq. 5.42 yields

$$\sum_{i=1}^{n} k_i(s_{i1} - d_i) + k_{n+1}(d_n - s_{n2}) = 0 \tag{5.43}$$

Equation 5.43 has another meaning, which is the summation of all the shear forces transmitted by the connectors is zero.

There are two extreme cases for the connection stiffness in composite floors. The lower bound is when the connection stiffness is zero or no connection is used, in which case timber and concrete can slide freely. The solution for this case can simply be obtained by letting all the connection stiffness equal to zero. The upper bound of the connection stiffness is when the connections are perfect-rigid with infinite stiffness, in which case no slip occurs at the positions of connections. Eq. 5.41 and Eq. 5.43, which become meaningless for this case, can be replaced by Eq. 5.44 and Eq. 5.45.

$$s_{i1} = d_i\ ,\ i = 1, \ldots, n \tag{5.44}$$

$$s_{i2} = d_i\ ,\ i = 1, \ldots, n \tag{5.45}$$

If the composite beam has a fixed end, Eq. 5.39, Eq. 5.41, and Eq. 5.43 for simply supported beams should be adjusted. In fact, the fixed end is corresponding to the case when the connection at the support has infinite stiffness. For example, if a cantilever beam (fixed at the right end) is considered, then Eq. 5.39 and Eq. 5.41 still hold, but Eq. 5.43 becomes void but can be replaced by

$$s_{n2} = d_n \tag{5.46}$$

5.2.6 Governing Equations

The unknown axial forces N_i and relative slips d_i, s_{i1}, and s_{i2} in each segment can be determined by solving a system of linear equations 5.19, 5.36, 5.37, 5.41, and 5.43, which can be presented in a matrix format.

Applying Eq. 5.36, Eq. 5.41 can be rearranged as

$$2d_i = \theta_i \sum_{m=1}^{i} k_m(s_{m1} - d_m),\ i = 1, \ldots, n \tag{5.47}$$

Thus only the relative slips s_{i1}, s_{i2}, and d_i are left to be solved. The unknown slips can be grouped into three vectors as shown below

$$\{S_1\} = [s_{11}, s_{21}, s_{31}, \cdots, s_{n1}]^T \tag{5.48}$$

$$\{S_2\} = [s_{12}, s_{22}, s_{32}, \cdots, s_{n2}]^T \tag{5.49}$$

$$\{D\} = [d_1, d_2, d_3, \cdots, d_n]^T \tag{5.50}$$

Eq. 5.47 can then be expressed in the matrix form as

$$2\boldsymbol{I}\{D\} + \boldsymbol{\Theta}\boldsymbol{K}\{D\} - \boldsymbol{\Theta}\boldsymbol{K}\{S_1\} = 0 \tag{5.51}$$

where $\boldsymbol{I}$ is the $n \times n$ identity matrix

$$\boldsymbol{I} = \begin{bmatrix} 1 & & & & \\ & 1 & & & \\ & & 1 & & \\ & & & \ddots & \\ & & & & 1 \end{bmatrix}_{n \times n} \tag{5.52}$$

and $\boldsymbol{\Theta}$ and $\boldsymbol{K}$ are the parameter matrix and stiffness matrix, respectively.

$$\boldsymbol{\Theta} = \begin{bmatrix} \theta_1 & & & & \\ & \theta_2 & & & \\ & & \theta_3 & & \\ & & & \ddots & \\ & & & & \theta_n \end{bmatrix}_{n \times n} \tag{5.53}$$

$$\boldsymbol{K} = \begin{bmatrix} k_1 & & & & \\ k_1 & k_2 & & & \\ k_1 & k_2 & k_3 & & \\ \vdots & \vdots & \vdots & \ddots & \\ k_1 & k_2 & k_3 & \dots & k_n \end{bmatrix}_{n\times n} \tag{5.54}$$

Eq. 5.19 can be expressed as

$$\{S_1\} + \{S_2\} = \{\Lambda\} \tag{5.55}$$

where

$$\{\Lambda\} = [\lambda_1, \lambda_2, \lambda_3, \cdots, \lambda_n]^T \tag{5.56}$$

Eq. 5.37 and Eq. 5.43 can be combined as

$$\boldsymbol{W}_1\{S_1\} + \boldsymbol{W}_2\{S_2\} - (\boldsymbol{W}_1 + \boldsymbol{W}_2)\{D\} = 0 \tag{5.57}$$

where

$$\boldsymbol{W}_1 = \begin{bmatrix} 0 & 1 & 0 & \cdots & 0 \\ 0 & 0 & 1 & \cdots & 0 \\ 0 & 0 & 0 & \ddots & \vdots \\ \vdots & \vdots & \vdots & \cdots & 1 \\ k_1 & k_2 & k_3 & \cdots & k_n \end{bmatrix}_{n\times n} \tag{5.58}$$

$$\boldsymbol{W}_2 = \begin{bmatrix} 1 & & & & \\ & 1 & & & \\ & & \ddots & & \\ & & & 1 & \\ & & & & -k_{n+1} \end{bmatrix}_{n\times n} \tag{5.59}$$

The unknown slip vectors $\{S_1\}$, $\{S_2\}$, and $\{D\}$ can be determined by solving equations 5.51, 5.55, and 5.57. As long as not all the connection stiffness is zero, slip vector $\{S_1\}$ can be determined as

$$\{S_1\} = [\boldsymbol{W}_2 - \boldsymbol{W}_1 + (\boldsymbol{W}_1 + \boldsymbol{W}_2)(2\boldsymbol{I} + \boldsymbol{\Theta K})^{-1}\boldsymbol{\Theta K}]^{-1}\boldsymbol{W}_2\{\Lambda\} \tag{5.60}$$

Slip vectors $\{S_2\}$ and $\{D\}$ can be determined as

$$\{S_2\} = \{\Lambda\} - \{S_1\} \tag{5.61}$$

$$\{D\} = (2\boldsymbol{I} + \boldsymbol{\Theta K})^{-1}\boldsymbol{\Theta K}\{S_1\} \tag{5.62}$$

The axial force vector can be calculated as

$$\{N\}=2\boldsymbol{\Theta}^{-1}\{D\} \tag{5.63}$$

where

$$\{N\} = \{N_1, N_2, N_3, \ldots, N_n\} \tag{5.64}$$

For rigid connections, equations 5.51 and 5.57 can be replaced by equations 5.65 and 5.66.

$$\{S_1\} = \{D\} \tag{5.65}$$

$$\{S_2\} = \{D\} \tag{5.66}$$

In consideration of equation 5.55, the slip vectors $\{S_1\}$, $\{S_2\}$, and $\{D\}$ for rigid connections can simply be expressed as

$$\{S_1\} = \{S_2\} = \{D\} = \frac{\{\Lambda\}}{2} \tag{5.67}$$

Once the slips are determined, axial forces and bending moments acting on timber and concrete can be derived, and then the distributions of stresses, deflection, and relative slip between two components can be determined. By superimposing the stresses at the release and restore stages, the stresses at the top and bottom of concrete are given by

$$\sigma_{ct}(x) = -\frac{E_c h_c M(x)}{2(E_c I_c + E_t I_{ti})} + \frac{N_i e_{ci} h_c}{2I_c} - \frac{N_i}{A_c} \tag{5.68}$$

$$\sigma_{cb}(x) = \frac{E_c h_c M(x)}{2(E_c I_c + E_t I_{ti})} - \frac{N_i e_{ci} h_c}{2I_c} - \frac{N_i}{A_c} \tag{5.69}$$

The stresses at the top and bottom of timber are expressed as

$$\sigma_{tt}(x) = -\frac{E_t h_{ti} M(x)}{2(E_c I_c + E_t I_{ti})} + \frac{N_i e_{ti} h_{ti}}{2I_{ti}} + \frac{N_i}{A_{ti}} \tag{5.70}$$

$$\sigma_{tb}(x) = \frac{E_t h_{ti} M(x)}{2(E_c I_c + E_t I_{ti})} - \frac{N_i e_{ti} h_{ti}}{2I_{ti}} + \frac{N_i}{A_{ti}} \tag{5.71}$$

The moments acting on concrete and timber are derived as

$$M_c(x) = \frac{E_c I_c}{E_c I_c + E_t I_{ti}} M(x) - N_i e_{ci} \tag{5.72}$$

$$M_t(x) = \frac{E_t I_{ti}}{E_c I_c + E_t I_{ti}} M(x) - N_i e_{ti} \tag{5.73}$$

The strains at the bottom of concrete and top of timber are presented by

$$\varepsilon_c^{btm}(x) = \frac{h_c M(x)}{2(E_c I_c + E_t I_{ti})} - \frac{N_i}{E_c}\left(\frac{1}{A_c} + \frac{e_{ci} h_c}{2I_c}\right) \tag{5.74}$$

$$\varepsilon_t^{top}(x) = -\frac{h_{ti} M(x)}{2(E_c I_c + E_t I_{ti})} + \frac{N_i}{E_t}\left(\frac{1}{A_{ti}} + \frac{e_{ti} h_{ti}}{2I_{ti}}\right) \tag{5.75}$$

Curvature in timber and concrete along the beam axis is stated by

$$\kappa(x) = \frac{M_t(x)}{E_t I_{ti}} = \frac{M_c(x)}{E_c I_c} = \frac{M^{tot}(x)}{E_t I_{ti} + E_c I_c} \tag{5.76}$$

where $M^{tot}(x)$ is the summation of moments in timber and concrete

$$M^{tot}(x) = M(x) - N_i\left(\frac{h_{ti} + h_c}{2} + h_{gi}\right) \tag{5.77}$$

Once the moment in timber or concrete, or their summation is known, the deflection of the beam at any position can be calculated using Mohr integral method.

$$\delta(t) = \int_0^L \frac{\hat{M}(x,t) M^{tot}(x)}{E_t I_{ti} + E_c I_c} dx \tag{5.78}$$

where $\hat{M}(x,t)$ is the moment caused by a unit force acting on the floor at the position of $x = t$. For a simply supported beam, $\hat{M}(x,t)$ can be expressed as

$$\hat{M}(x,t) = \begin{cases} (L-t)x/L\,, 0 \le x \le t \\ (L-x)t/L\,, t < x \le L \end{cases} \tag{5.79}$$

The rotation of the cross-section is the derivative of deflection which can be expressed as

$$r(t) = \int_0^L \frac{\partial \hat{M}(x,t)}{\partial t} \frac{M^{tot}(x)}{E_t I_{ti} + E_c I_c} dx \tag{5.80}$$

Alternatively, the deflection and rotation can be determined by integrating Eq. 5.76, and the unknown constants generated from integration can be determined from the boundary conditions.

From the left support to any cross-section in the floor, the difference in length change between the bottom of concrete and top of timber is

$$\bar{\Delta}(x) = \int_0^x \varepsilon_c^{btm}(x) dx - \int_0^x \varepsilon_t^{top}(x) dx \tag{5.81}$$

Substituting equations 5.74 and 5.75 into Eq. 5.81 yields

$$\bar{\Delta}(x) = \int_0^x \frac{h_c + h_{ti}}{2(E_c I_c + E_t I_{ti})} M(x) dx - \int_0^x \left(\frac{1}{E_c A_c} + \frac{1}{E_t A_{ti}} + \frac{e_{ci} h_c}{2E_c I_c} + \frac{e_{ti} h_{ti}}{2E_t I_{ti}}\right) N(x) dx \tag{5.82}$$

The relative slip between timber and concrete at the left support of the floor is

$$\Delta_0 = s_{11} - d_1 \tag{5.83}$$

The relative slip between timber and concrete at any location along the floor is

$$\Delta(x) = \Delta_0 - \bar{\Delta}(x) \tag{5.84}$$

5.2.7 Summary

Although the above solution is developed for MTP-concrete composite floors with notches, the model can be used to describe any two-layer composite beams or floors with discrete connections. Due to the generality of the solution, the external loads, boundary conditions, and locations of connections in the beam or floor are not restricted. The developed composite beam model can also be applied to situations when a gap was formed between timber and concrete due to a rigid foam insulation layer placed between timber and concrete or a layer of plywood or OSB placed to act as the formwork for concrete. When concrete is cast directly on top of mass timber panels and the notch sizes are small relative to the timber member sizes, the gap between timber and concrete along the floor can be neglected and the composite beam model can be simplified. The verification of the proposed composite beam model is discussed in the following sections.

5.3 Model Verification

In this section, the proposed discrete bond composite beam model is validated and compared with several existing composite beam models as well as a finite element model through two examples. The performance of the composite beams with discrete connection systems within the linear elastic range and the limitations of the commonly used continuous bond beam models are discussed.

5.3.1 Propped Cantilever

In the first example, the discrete bond composite beam model is carried out on a propped composite cantilever, and the calculated results are verified and compared with several existing composite

beam models. The two-layer composite beam connected with equally spaced discrete connections (steel rods with washers) is subjected to a uniformly distributed load. The dimensions, material properties, and connection stiffness of the beam are shown in Fig. 5.4. For comparison purposes, the same geometric characteristics and material properties are assumed as the example in Nguyen et al. (2011a).

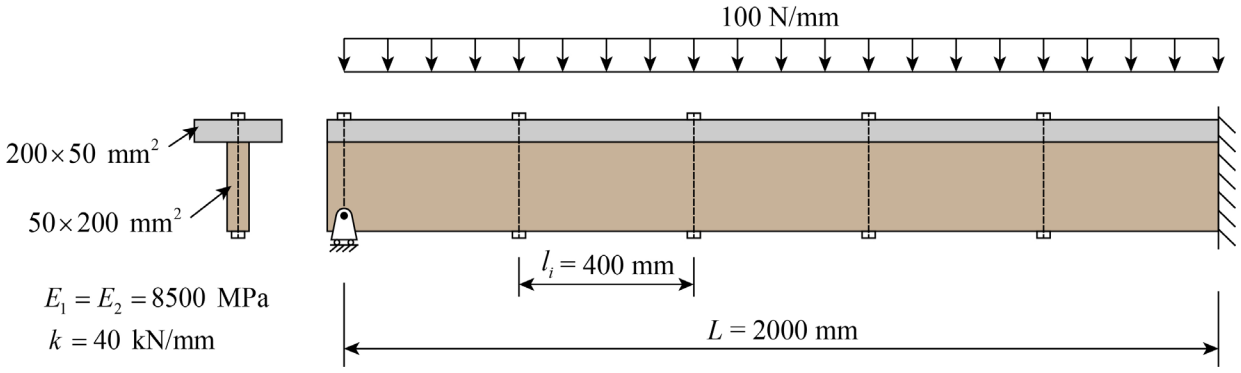

Fig. 5.4 Propped composite cantilever subjected to a uniformly distributed load

Six composite beam models with different assumptions and simplifications are compared in this example. Three discrete bond beam models considered are the proposed method, the numerical framework model proposed by Grosse et al. (2003a), and the hybrid numerical-analytical method proposed by Nguyen et al. (2010). Besides, three continuous bond beam models are considered: the gamma method in Eurocode 5 (2014), the simplified analysis method proposed by Girhammar (2009), as well as the well-known Newmark's composite beam model (1951). The smeared shear stiffness in the continuous bond beam models is calculated by dividing the stiffness of a single connection by the spacing of connections along the beam.

The deflection, rotation, curvature, and relative slip between two layers along the beam are calculated by different models and shown in Fig. 5.5. Fig. 5.5(a) plots the deflection profile along the span. The deflections calculated by three discrete bond beam models are almost the same with negligible differences. The exact solution by Newmark's model (1951) predicts deflection that is very close to those from the discrete bond models (with about 1% difference). The deflection is significantly underestimated by the gamma method. This is partly because the gamma method was

developed for the simple support condition. The effective bending stiffness of the composite beam has been overestimated by the gamma method for the propped-cantilever support condition. The simplified method by Girhammar (2009) considered the effective beam span according to the actual boundary condition ($0.699L$ in this case) in the determination of the effective bending stiffness. An improved estimation can be achieved by this simplified analysis method (with about 4% difference to the discrete bond beam models). Similar results can be found in the rotation prediction shown in Fig. 5.5(b). With the exception of the gamma method, all models predict very close results to each other, with Girhammar's simplified analysis method (2009) slightly deviates from the rest. The primary disagreement between the discrete bond models and Newmark's model (1951) is at the regions around connections where a non-smooth rotation was predicted by the discrete bond beam models. The gamma method, again, gives an underestimation of rotation along the beam.

The prediction of curvature along the span is illustrated in Fig. 5.5(c). Discontinuous distribution of the curvature that jumps between adjacent segments can be captured by the discrete bond beam models, while the continuous bond beam models predict continuously distributed curvature. According to the discrete bond beam models, although the external moment along the beam is continuous, the abrupt change of axial forces at two sides of the connections causes the sudden change of bending moments as well as the curvature in the sub-components. At the left support of the beam, the curvature predicted by the continuous bond beam models is zero due to zero external moment at the support. According to the discrete bond beam models, the connection at the support sustains a certain shear force which induces axial forces and bending moments in timber and concrete, thus a non-zero curvature at the left support is predicted. Among three continuous bond models, Newmark's model (1951) predicts the closest result to the discrete bond models, especially in the region near the fixed end.

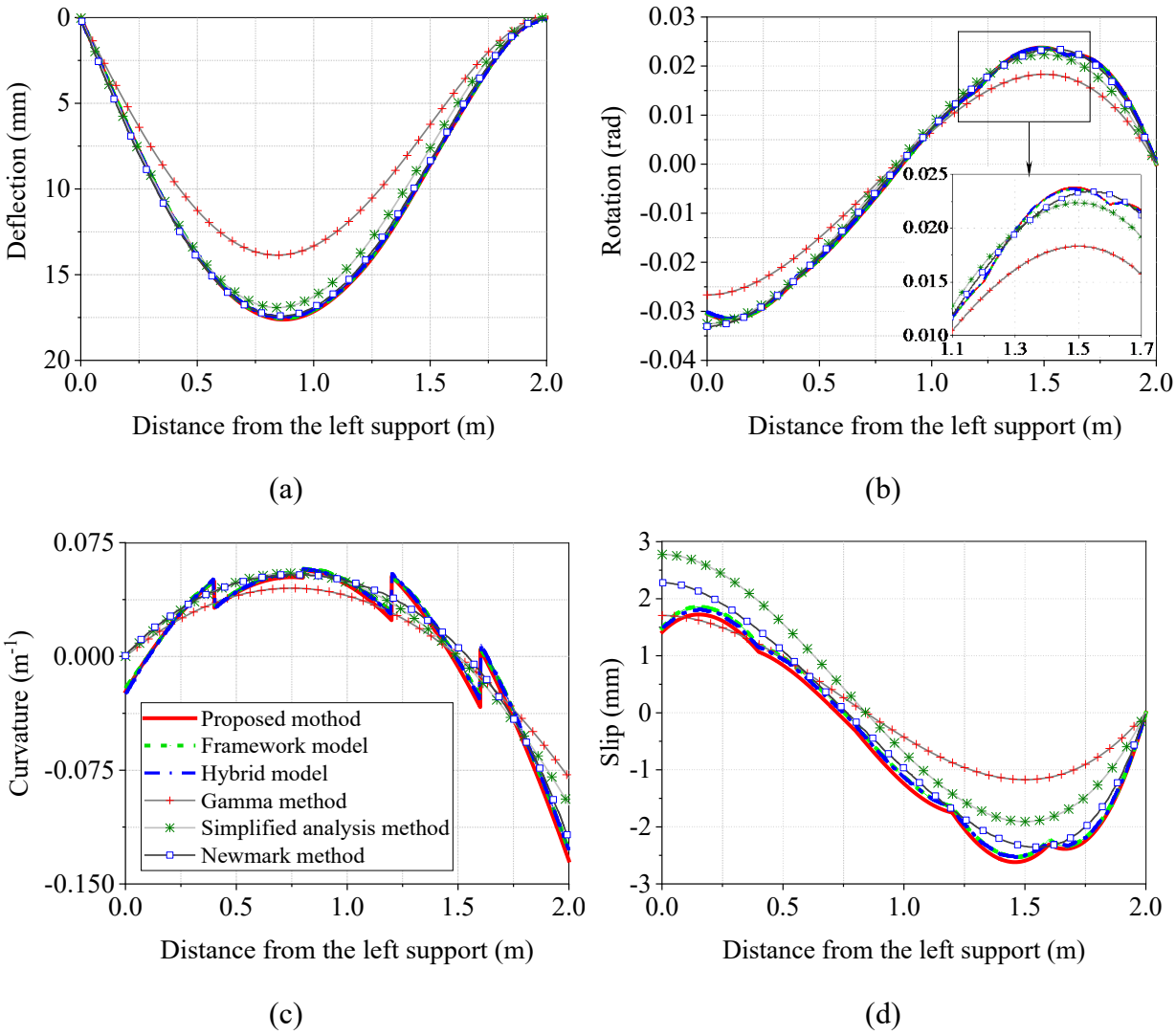

Fig. 5.5 Behaviour of the propped cantilever under the uniformly distributed load predicted by different composite beam models (a) Deflection; (b) Rotation; (c) Curvature; and (d) Relative slip between two layers.

Fig. 5.5(d) compares the relative slip between two layers along the beam axis predicted by different models. Slip from the framework model (Grosse et al. 2003a) is converted from the displacement and rotation of beam elements for modeling timber and concrete. The slip predicted by the continuous bond beam models is continuous and smooth. On the contrary, the slip predicted by the discrete bond beam models is not smooth at the locations of connections. The non-smooth slip indicates the discontinuity of the first derivative of slip which is due to the sudden change of axial

forces between adjacent segments, as can be seen from equation 5.82. From Fig. 5.5(d), it can be seen that the discrete connections reduce relative slip at local areas around the connections.

The three discrete bond beam models compared in this example yield very close results to each other. The proposed method presented in Section 5.2 provides a closed-form solution that is easy to enforce, as the internal actions can simply be obtained by solving no more than a group of linear equations. Among the three continuous bond models, Newmark's model (1951) provides results that are closest to the discrete bond models, especially for deflection and rotation. The gamma method overestimates the beam effective bending stiffness and underestimates the deflection, rotation, and relative slip. The simplified analysis method by Girhammar (2009) is easy to use but the predicted results are found to be not as accurate as the exact solutions. In general, the continuous bond beam models are not able to reflect the discontinuous or non-smooth distribution of rotation, curvature, and slip for discrete connected beams.

5.3.2 Simply Supported Composite Floor Strip

In the second example, a simply supported MTP-concrete composite floor connected with notches is investigated using the proposed beam model and the finite element method. The composite floor has a span of 6 m and is subjected to a uniformly distributed load of 3 N/mm, as shown in Fig. 5.6. The width of the floor strip is 600 mm. The notch length is 150 mm and the timber shear length between notches is 550 mm. Six notched connections are symmetrically arranged about the mid-span. The thicknesses for timber and concrete are 130 mm and 90 mm, respectively. The notch depth is 25 mm and the connection stiffness is assumed to be 600 kN/mm. The complete dimensions and material properties of the floor are illustrated in Fig. 5.6. Based on the proposed composite beam model, the deflection, relative slip, internal forces, and stress distributions in the floor under the applied load are calculated and illustrated in Fig. 5.7. The reduction of the timber cross-section due to notches is not considered in the composite beam model.

For comparison, a two-dimensional finite element model was built for the composite floor in the general-purpose finite element software ABAQUS (2017). Four-node bilinear plan stress quadrilateral (CPS4) elements were used to model timber and concrete. The nominal element size is about 10 mm in most of the areas while a denser mesh with a 5 mm nominal element size is used

in the region of concrete protrusions. A frictionless behaviour between timber and concrete was defined in the tangential direction and a hard contact was defined in the normal directions. In the normal direction, a stiffness scale factor of 5 is used to reduce element penetration and mesh sensitivity issues. Only half of the floor is built in the model due to symmetry. The deflection, relative slip, and stress distributions obtained from the finite element model are shown in Fig. 5.7(a)-(b) and (f)-(i). The deformed shapes of concrete and timber with the distribution of bending stresses are illustrated in Fig. 5.8.

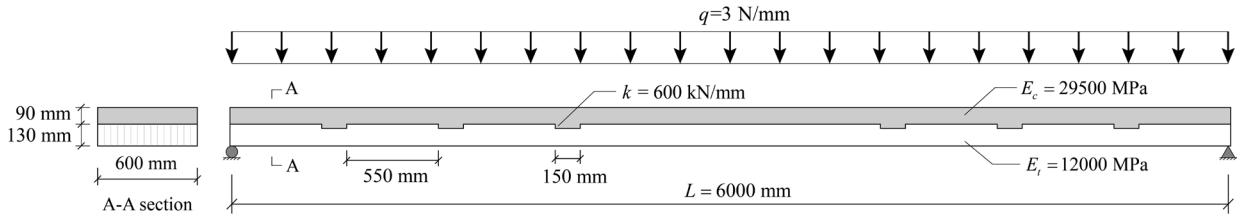

Fig. 5.6 MTP-concrete composite floor connected with notches under a uniformly distributed load

As shown in Fig. 5.7(a), the deflection of the floor is in a parabolic shape with the maximum deflection at the mid-span. With the chosen mesh size and the stiffness scale factor in the finite element model, an excellent agreement of deflection can be achieved between the proposed beam model and the finite element model. Fig. 5.7(b) shows the relative slip between timber and concrete. The impact of discrete connections on restricting the slip is clearly visible from the non-smooth slip distribution. The slip is not uniformly increasing from mid-span to the supports. Instead, it is constrained at the regions around connections and released at regions far away from connections.

The internal forces calculated from the composite beam model are shown in Fig. 5.7(c)-(e). In Fig. 5.7(c), the moment distribution along the beam shows a huge gap between the internal moments in timber and concrete and the external moment in the composite cross-section. Moments in timber and concrete are significantly reduced in the segments strengthened with connections but not in the external ones, where the summation of moments in the sub-components equals the external moment. The shear force distribution along the beam, as shown in Fig. 5.7(d), is not affected by the discrete connections. In fact, the shear force distribution in the discrete connected composite

beams is identical to the shear force distribution in the non-composite beams. The axial force in timber or concrete shows a stepwise increase from supports to the mid-span, Fig. 5.7(e), and the difference of axial forces between adjacent segments represents the shear force resisted by the connection in between. It can be seen that the connections near supports resist higher shear forces than the connections near the mid-span.

In Fig. 5.7(f)-(i), the bending stresses at the top and bottom of timber and concrete show an oscillating pattern, especially for the stresses at the bottom of concrete and top of timber. The bending stresses at the top of concrete and bottom of timber largely increase from supports to the mid-span with the maximum stresses appear at mid-span. On the contrary, the bottom of concrete and top of timber resist both tensile and compressive stresses at different locations, and the maximum stresses do not appear at the mid-span but around the external connections. This is particularly important as it is a common practice that only the bending stress at mid-span is examined.

The stress distributions computed from the proposed method are in good agreement with the finite element model in general. However, due to the sharp corners of the notches, stress singularity can be observed near the connections in the finite element model. In real structures, the stress distribution around the notched connections is more complex than regions far away from connections, and stress concentration around notches can cause cracking of concrete under the service load. The cracking of concrete will be discussed in Section 5.6 as part of the post-elastic behaviour of the composite floors.

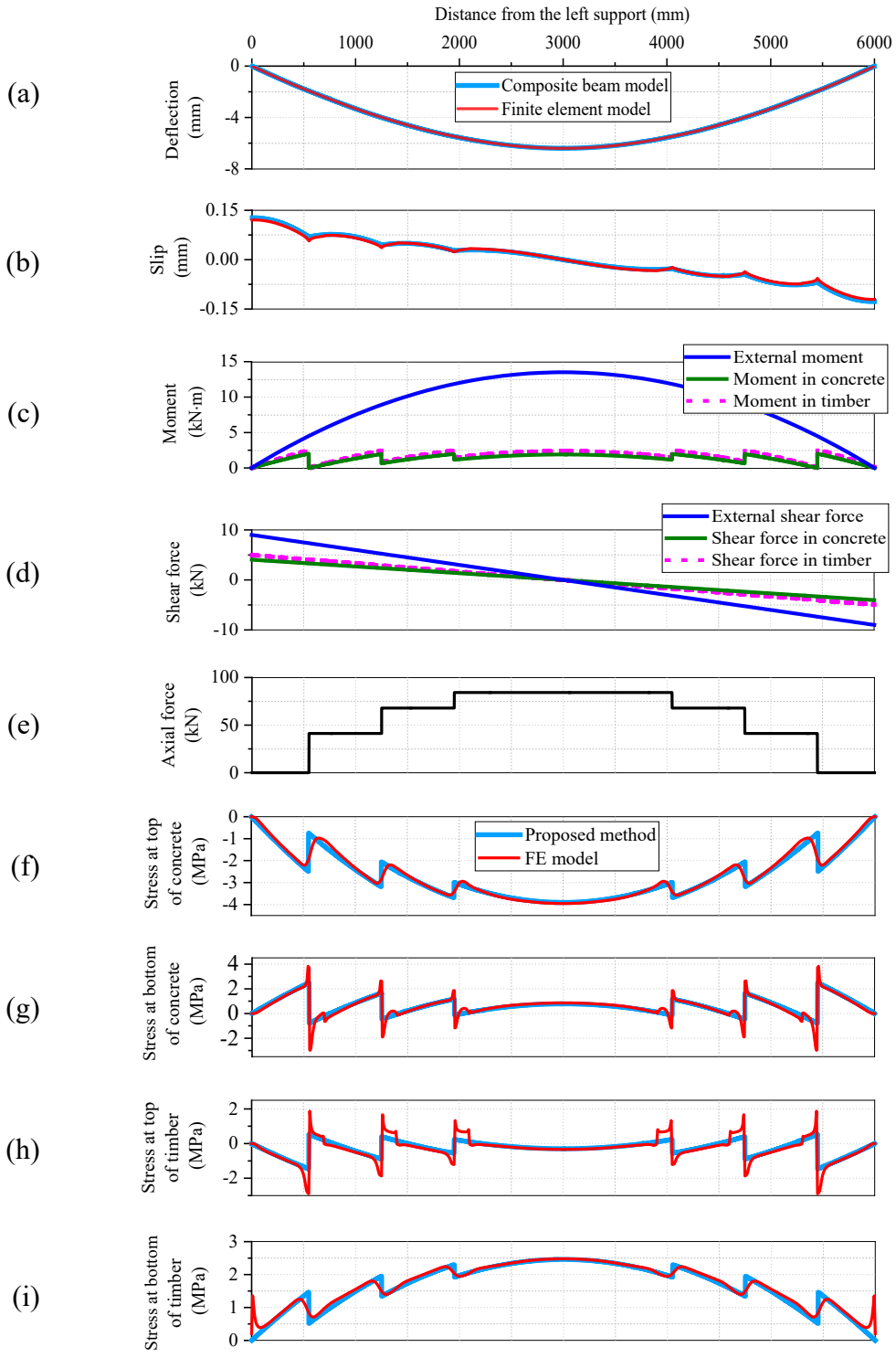

Fig. 5.7 Internal actions in a simply supported notch-connected MTP-concrete composite floor under uniformly distributed load (a) Deflection; (b) Relative slip; (c) Moment; (d) Shear force; (e) Axial force; (f) Stress at the top of concrete; (g) Stress at the bottom of concrete; (h) Stress at the top of timber; (i) Stress at the bottom of timber.

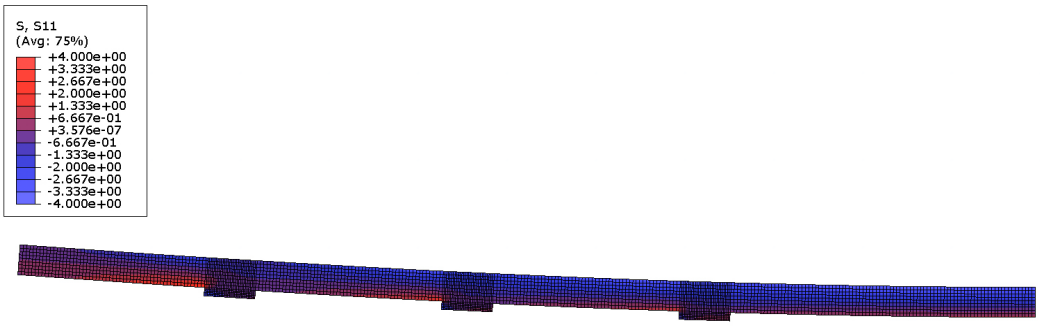

(a)

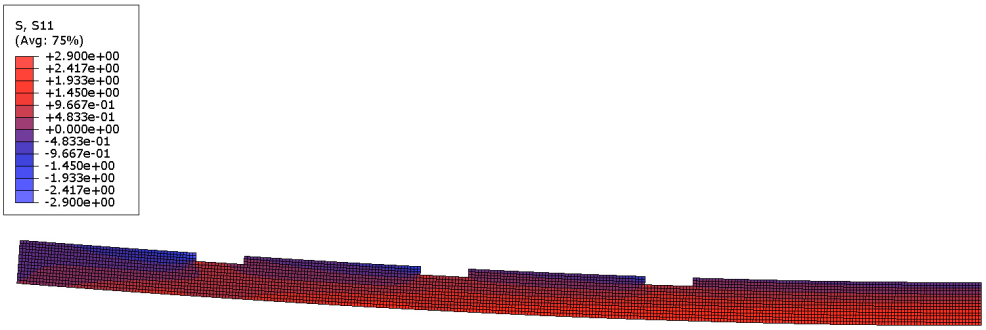

(b)

Fig. 5.8 Deformation and bending stress distribution in concrete and timber in the composite floor from the finite element modeling (the deformation scale factor is 20) (a) Concrete; (b) Timber

In the two external segments of the composite floor, the stresses at the top and bottom of sub-components are equal in magnitude since the sub-components are solely subjected to the bending moment, and the neutral axes of the sub-components are located at the centre of their cross-sections. With the increase of axial force in the sub-components from supports to the mid-span, the stress peaks moved to the top of concrete and bottom of timber as a result of neutral axes moved to the opposite directions. In other words, the discrete connections increase the bending stiffness of the composite beam by pulling the neutral axes in the sub-components closer to each other. This effect can be identified from the bending stress distribution contour in timber and concrete in Fig. 5.8, where concrete is primarily subjected to compression and timber is essentially subjected to tension.

5.3.3 Summary

The proposed composite beam model is verified by comparing the predictions with those obtained from existing composite beam models and a finite element model. The comparison focuses on linear-elastic behaviour only. The internal actions in the MTP-concrete composite floor predicted by the proposed beam model are consistent with the finite element model predictions. The material properties, connection stiffness, and dimensions of the MTP-concrete composite floor in the example were assumed thus the predicted results are not comparable with the test results. The comparison between the model predictions and the test measurements within the linear-elastic range reported in Chapter 4 is discussed in Section 5.4. The developed model is further extended to predict failure of the composite floors in Section 5.6 and the predicted results are verified with the test measurements reported in Chapter 4.

5.4 Composite Floor Bending Stiffness Prediction

From the bending and vibration tests on the MTP-concrete composite floors discussed in Chapter 4, it can be concluded that the design of MTP-concrete composite floors is often governed by the floor serviceability limit states rather than the ultimate limit states. The bending stiffness of MTP-concrete composite floors is a critical factor for the floor deflection and vibration performance. In this section, the proposed composite beam model is used to predict the static bending stiffness of MTP-concrete composite floors and the results are verified by the test measurements.

The derivation of the composite beam model in Section 5.2 provides no explicit expression for the effective bending stiffness of the composite floors. However, when the geometry, loading, and boundary conditions of the floor are symmetric, an equivalent bending stiffness $(EI)_{eqv}$ can be adversely obtained from the mid-span deflection of the floor. The deflection at the mid-span of the floor can be determined as

$$\delta(L/2) = \int_0^L \frac{\hat{M}(x,L/2)M^{tot}(x)}{E_c I_c + E_t I_{ti}} dx = \int_0^L \frac{\hat{M}(x,L/2)M(x)}{(EI)_{eqv}} dx \tag{5.85}$$

where $\hat{M}(x, L/2)$ is the bending moment when a unit force is acting at mid-span. After the deflection at mid-span is solved with the first integration in Eq. 5.85, the equivalent bending stiffness can be expressed with the mid-span deflection. When the composite floor is simply

supported and subjected to a uniformly distributed load q, the equivalent bending stiffness can simply be expressed as

$$(EI)_{eqv} = \frac{5qL^4}{384\delta(L/2)} \tag{5.86}$$

When a concentrated load P is acting at mid-span, the equivalent bending stiffness of the floor is

$$(EI)_{eqv} = \frac{PL^3}{48\delta(L/2)} \tag{5.87}$$

For two concentrated loads $P/2$ acting at two third points, the equivalent bending stiffness is expressed as

$$(EI)_{eqv} = \frac{23PL^3}{1296\delta(L/2)} \tag{5.88}$$

Equation 5.88 is used to estimate the bending stiffness of twelve tested MTP-concrete composite floors discussed in Chapter 4. In addition, the MTP-concrete composite floor specimens tested by Kudla (2017) are also considered. Similar to the bending tests described in Chapter 4, Kudla (2017) tested simply supported MTP-concrete composite floors with different configurations under four-point bending. The timber in the specimens was GLT GL 24h grade according to EN 14080 (2013) and concrete was classification C 30/37 according to EN 1992-1-1 (2004). The thicknesses of concrete and timber in the specimens were both 120 mm. The width of the specimens was 400 mm. The notches in the specimens had a depth of 20 mm and a length of 160 mm. The Young's modulus of timber was 10907 MPa. The rest of the geometry and material properties of the specimens tested by Kudla (2017) are listed in Table 5.1.

The measured and predicted bending stiffness of the MTP-concrete composite floors are summarized in Table 5.2 and plotted in the histogram in Fig. 5.9. The bending stiffness of each tested composite floor was determined from the linear regression to the load-deflection curves in the range of 10-40% of the peak load, which is considered as the service load level (EN 26891, 1991). For the predicted bending stiffness, two partitioning methods were used in the composite beam model to estimate the bending stiffness of MTP-concrete composite floors (Fig. 5.1). As discussed in Section 5.2, the first method considers the actual timber cross-section due to the presence of notches; while the second method neglects the notches and assumes the timber cross-section is constant along the floor. As the inputs of the composite beam model, the stiffness of

notched connections was estimated according to Eq. 3.2. Since the shear modulus of timber was not measured, the ratio of shear modulus to the longitudinal Young's modulus of timber was assumed to be 5%.

Table 5.1 Geometry and material properties of MTP-concrete composite floors tested by Kudla (2017)

Specimen	Replicate	Span (m)	Number of notches	Timber shear length (mm)	Screws in the notch	E_c (MPa)
SP10	3	3.9	2	300	2 SPAX8160 [b]	25900
SP40	2	3.9	2	300	None	25900
SP50	3	3.9	2	300	2 SPAX8160 [b,c]	25900
SP11	3	5.9	6	300-700 [a]	2 SPAX8160 [b]	25267
SP12	3	5.9	6	300-700 [a]	2 SPAX8160 [b,d]	25267
SP41	3	5.9	6	300-700 [a]	None	25267

[a] From supports to the mid-span, the timber shear length increased from 300 mm to 405 mm, and then to 700 mm.

[b] Self-drilling washer head screw SPAX® 8×160 according to National Technical Approval Z-9.1-449 (2012).

[c] Screws were installed in the timber in front of the notch; in addition, timber was reinforced with 6 shorter washer head screws (SPAX® 8×100) that were fully embedded into timber.

[d] Screws were installed in the timber in front of the notch.

As can be seen from Table 5.2 and Fig. 5.9, the method that considers the timber cross-section reduction due to notches yields lower bending stiffness than the method neglecting the notches. However, the difference is small for the specimens especially when the notches are shallow and the number of notches is small. The largest difference resides in specimens SPR-1, SPR-2, and SPR3 where the bending stiffness estimated using the second method is 2% higher than the bending stiffness estimated using the first method. The smallest difference exists in specimens SP10, SP40, and SP50 where the difference is less than 0.5%. Since the notches in the investigated

composite floors were small relative to the dimensions of the timber element, it is acceptable to neglect the reduction of the timber cross-section in the bending stiffness estimation of the composite floors.

The estimated floor bending stiffness by the composite beam model show a good agreement with the test results. The estimated floor bending stiffness is generally higher than the test results except for specimens SPU-2, SP40, and SP50. Besides specimens SPU-4 and SP11, the estimated results are within 10% of the measured results and more than half of the specimens had the estimated bending stiffness within 5% of the measured results. The estimated bending stiffness of specimen SPU-4 using two methods are both more than 20% higher than the measured result. This overestimation is most likely due to the gap opening between timber and concrete during the bending test since the notches in specimen SPU-4 were only 13 mm. The gap opening reduced the bearing area between timber and concrete in the notched regions which caused low connection stiffness and low floor bending stiffness. The gap opening is not considered in the composite beam model and it should be prevented in practice by using deeper notches or additional steel fasteners. Overall, the proposed discrete bond composite beam model can reliably estimate the notch-connected MTP-concrete composite floor bending stiffness with practically acceptable accuracy.

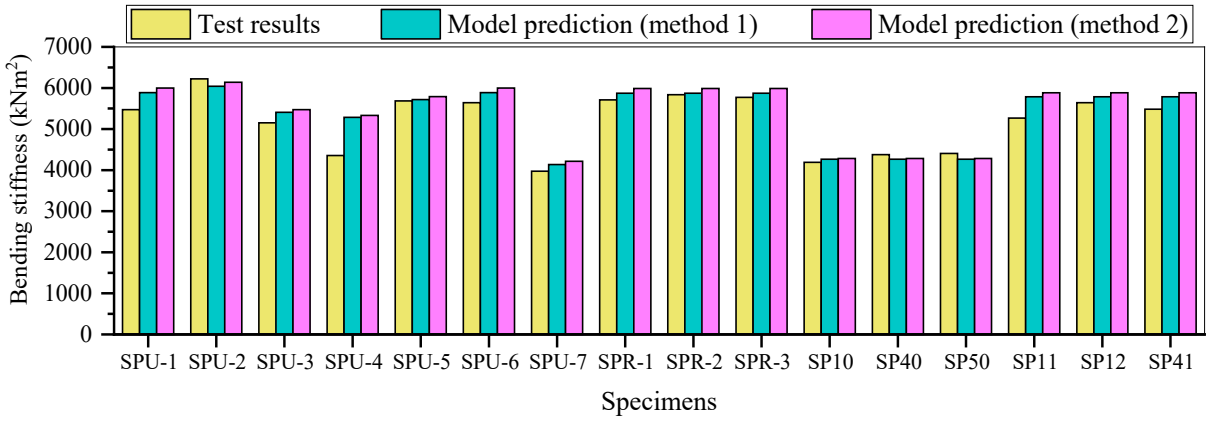

Fig. 5.9 Comparison of the MTP-concrete composite floor bending stiffness between measured and estimated results

Table 5.2 Comparison of the measured and predicted floor bending stiffness (kNm^2)

Specimen		Measured	Predicted (method 1)	Predicted (method 2)
This study	SPU-1	5473	5888 (7.6%) [b]	6000 (9.6%)
	SPU-2	6223	6042 (-2.9%)	6138 (-1.4%)
	SPU-3	5152	5408 (5.0%)	5471 (6.2%)
	SPU-4	4356	5284 (21.3%)	5332 (22.4%)
	SPU-5	5686	5719 (0.6%)	5791 (1.8%)
	SPU-6	5642	5888 (4.4%)	6000 (6.3%)
	SPU-7	3975	4136 (4.1%)	4216 (6.1%)
	SPR-1	5711	5873 (2.8%)	5988 (4.9%)
	SPR-2	5836	5873 (0.6%)	5988 (2.6%)
	SPR-3	5773	5873 (1.7%)	5988 (3.7%)
Kudla (2007)	SP10	4189 [a]	4264 (1.8%)	4283 (2.2%)
	SP40	4377 [a]	4264 (-2.6%)	4283 (-2.1%)
	SP50	4407 [a]	4264 (-3.2%)	4283 (-2.8%)
	SP11	5267 [a]	5787 (9.9%)	5883 (11.7%)
	SP12	5642 [a]	5787 (2.6%)	5883 (4.3%)
	SP41	5482 [a]	5787 (5.6%)	5883 (7.3%)

[a] Average bending stiffness of specimens in the same group.

[b] Numbers in the brackets are the differences between the predicted and measured results.

5.5 Parametric Study on the Floor Bending Stiffness

After being verified, the proposed composite beam model can be used to estimate the bending stiffness of MTP-concrete composite floors with different geometries and to optimize the connection design in the composite floor systems. In this section, parametric studies are carried

out on a 6 m span MTP-concrete composite floor using the proposed composite beam model. The width of the floor is assumed to be 1 metre. The timber and concrete thicknesses are assumed to be 120 mm and 80 mm, respectively. The length of notches is assumed to be 200 mm and the notches are symmetrically arranged about the mid-span. The floor is subjected to a uniformly distributed load. The material properties of timber and concrete are taken from Table 3.6 except that the shear modulus of timber in the longitudinal-transverse plane G_{LT} is taken as 5% of Young's modulus in the longitudinal direction E_t. The connection stiffness of notched connections is determined according to Eq. 3.3.

The studied geometry factors of the composite floor are the number of notched connections, locations of connections, notch depth, as well as the relative thickness of concrete and timber in the composite floor. Since the depth of notches is a factor being investigated, the actual timber cross-section is considered in the composite beam model (partitioning method 1). The bending stiffness $(EI)_{eqv}$ of the composite floors with varying geometry factors are calculated according to Eq. 5.86 and normalized to the composite efficiency factor according to Eq. 4.5. As a reference, the bending stiffness of the bare timber floor that has the same total thickness as the composite floor is also calculated according to Eq. 5.89

$$(EI)_{bt} = \frac{E_t b(h_t+h_c)^3}{12} \tag{5.89}$$

where b is the width of the floor (1 m) and h_t and h_c are the thickness of timber and concrete, respectively. The bending stiffness of the composite floors should be higher than the same thickness bare timber floor to show advantages of the composite floor system.

5.5.1 Number and Locations of Connections

The effects of number and locations of notched connections on the bending stiffness of MTP-concrete composite floors are investigated first. The bending tests on the composite floors show that the floors should have enough connections to achieve high-composite action between two layers. However, an excessive number of notched connections can slow down the manufacturing process and increase the cost, as the notches on timber panels are usually cut by CNC machines before concrete casting. Besides, unnecessary notches cut on timber have little contributions to the

bending stiffness of the composite floor but can reduce the cross-section area and thus the load-carrying capacity of timber. Therefore, an optimal number of connections should be designed in the composite floor to achieve high composite efficiency without increasing the cost or reducing the ultimate strength of the floor. In addition to the number of connections, the floor bending stiffness also depends on the locations of connections due to the discrete feature of the notches. The COST Action report (Dias et al. 2018b) suggests that the length of notches should not be shorter than 150 mm and the timber shear length should not be shorter than eight times of the notch depth. These requirements stipulate the minimal spacing for notches. However, there is no guideline about the optimum locations or spacing of notches.

The composite efficiency of the investigated floor changes with the number and locations of notched connections are illustrated in Fig. 5.10. The depth of notches is assumed to be 25 mm. As can be seen from Fig. 5.10, when the number of connections increases from two to eight, the maximum composite efficiency of the floor increases from less than 0.5 to almost 0.8. A significant increase in the composite efficiency can be observed when the number of connections increases from two to four. However, with the further increase of the number of connections, the increasing rate becomes smaller. There is no distinct advantage to use eight or more notched connections in the studied floor as the increase of the composite efficiency from six to eight connections is practically negligible. The equivalent bending stiffness of the composite floor with two notched connections is lower than the same thickness bare timber floor bending stiffness. To achieve equivalent floor bending stiffness higher than the bare timber floor bending stiffness, at least four connections should be used.

It can also be observed from Fig. 5.10 that the composite efficiency of the floors also depends on the locations of the connections. The effect of the connection location is especially notable when fewer connections are used. Since the notch length is not changing (200 mm), the locations of notches depend solely on the timber shear lengths in front of notches. In each floor, the timber shear lengths are assumed to be identical and simultaneously change for all the notches. When two, four, six, and eight connections are used, the optimal timber shear lengths are about 700 mm, 500 mm, 350 mm, and 250 mm, respectively. With a limited number of connections in the floor, choosing the optimal connection spacing or location is considered an effective measure to achieve the maximum composite efficiency of the floor without increasing the cost.

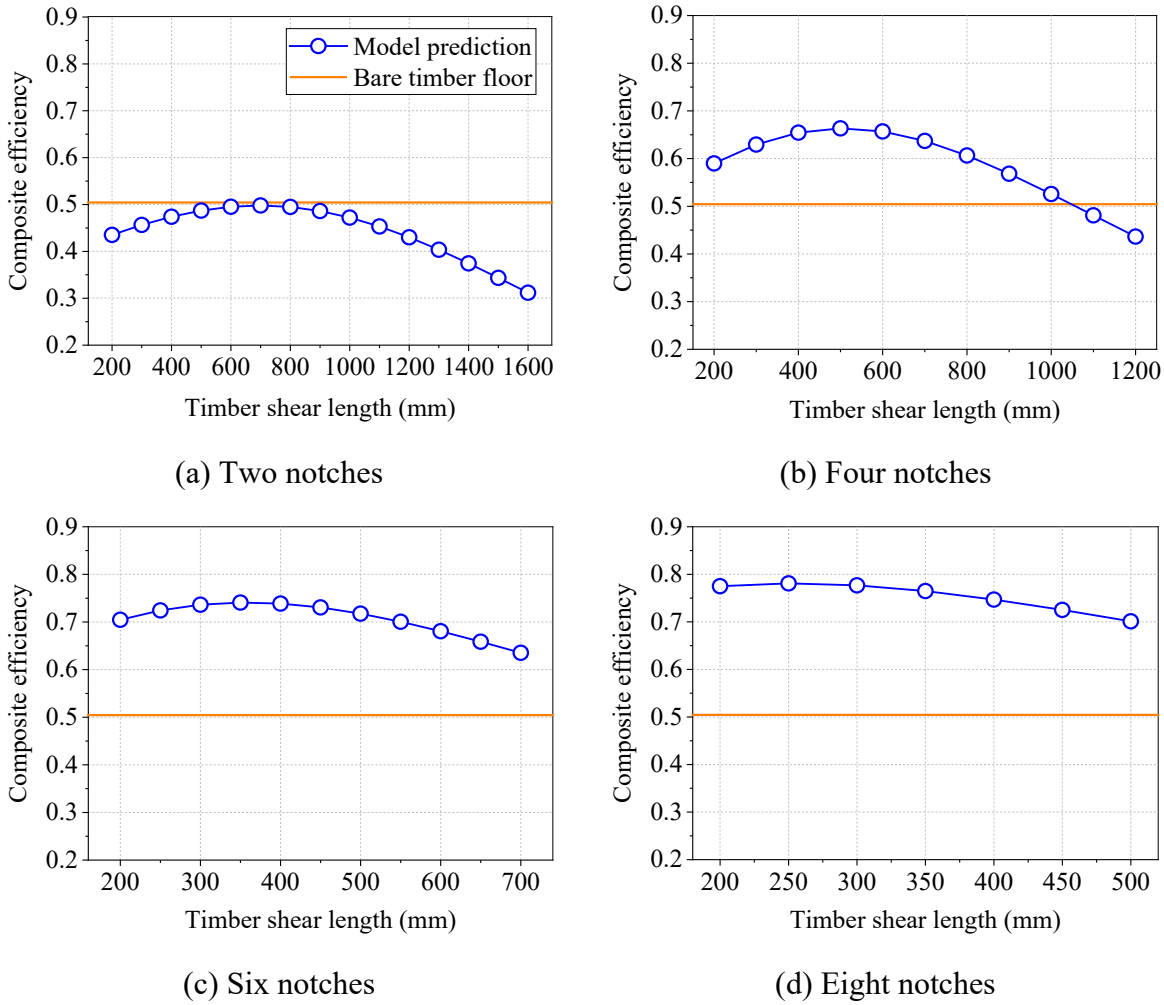

Fig. 5.10 Composite efficiency of MTP-concrete composite floors affected by the number and locations of notched connections

5.5.2 Notch Depth

The depth of notches is another important factor in determining the overall structural performance of the composite floors. The COST Action report (Dias et al. 2018b) suggests that the notch depth in building applications should be in the range of 20 to 30 mm. According to Eq. 3.2, deeper notches can provide higher stiffness than shallower notches due to the larger bearing areas. However, deeper notches remove a larger portion of the timber cross-section and reduce the bending stiffness and load-carrying capacity of the timber components. When the notch depth increases in the composite floor, the increase of the connection stiffness and decrease of the timber cross-section create a paradox that brings uncertainties to the overall structural performance of the

floor. It is hard to balance the opposite effects of the notch depth in the design. Thus, a parametric study is employed to provide some insights.

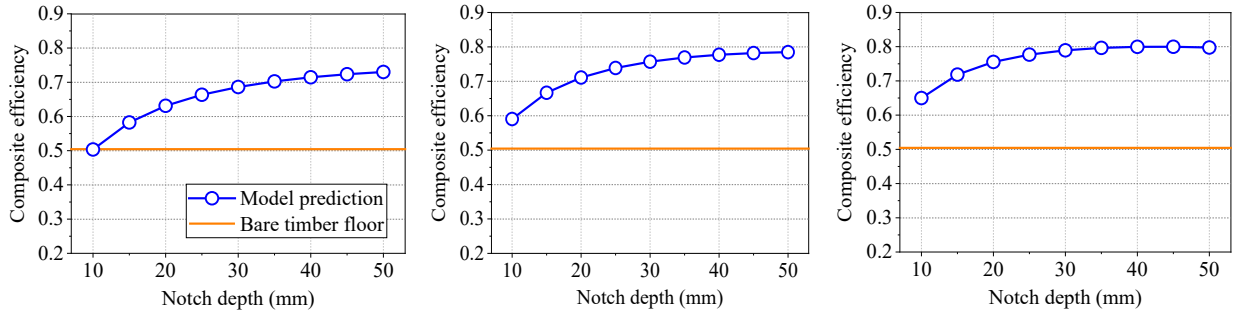

(a) Four notches (b) Six notches (c) Eight notches

Fig. 5.11 Composite efficiency of MTP-concrete composite floors affected by the notch depth

Fig. 5.11 shows the effect of the notch depth on the composite efficiency of the investigated composite floor when four, six, and eight connections are used. The timber shear lengths are 500 mm, 400 mm, and 300 mm, respectively, when four, six, and eight connections are used. As can be seen from Fig. 5.11, the composite efficiency of the floor rapidly increases with the notch depth when the notch depth is small, indicating that the connection stiffness dominates the floor bending stiffness when the notch depth is small. However, with the further increase of the notch depth, the additional contribution from deeper notches to the floor bending stiffness becomes smaller. Fig. 5.11 shows that the optimal notch depth depends on the number of notches used in the floor. In the investigated range of the notch depth (10-50 mm), a slowly increasing trend can still be observed for the floor with four connections when the notches reached 50 mm depth. The bending stiffness of the floor with six notches barely increases after the notches reached 45 mm. The bending stiffness of the floor with eight connections stopped increasing when the notch depth reached about 40 mm. From a practical standpoint of view, the notch depth of 40 mm, 35 mm, and 30 mm can provide high enough composite efficiencies when four, six, and eight notches are used. As will be discussed in Section 5.6, deeper notches are not recommended since they contribute little to the further improvement of the floor bending stiffness but can significantly reduce the load-carrying capacities of the floors.

5.5.3 Relative Thickness of Concrete and Timber

In the above discussion, the thicknesses of concrete and timber are not changing in the floors with different connection designs. However, the thickness of the composite layers especially the concrete layer can have a major impact on the static and dynamic performance of the composite floors. The relative thickness of concrete to timber is an early decision made in the floor design. For a given timber member, irrespective of the connection stiffness, the composite floor bending stiffness increases with the thickness of concrete overlaid on the timber member. However, it is often desirable to minimize the total thickness of the floor system to reduce the height of the building, increase the clear height of each story, and reduce the weight of the floor. This section sets out to discuss the relative thickness of concrete to timber when the total thickness of the floor system is determined.

Fig. 5.12 shows the bending stiffness of the composite floor varying with the thickness of the concrete layer in the floor. The total thickness of the composite floor is kept at 200 mm while the concrete thickness varies in the range of 50 mm to 100 mm, which corresponds to 25% to 50% of the total floor thickness. In Fig. 5.12, the theoretically full composite (upper bound), non-composite (lower bound), and the same thickness timber floor bending stiffness are also plotted according to equations 4.3, 4.2, and 5.89, respectively. The bending stiffness of the composite floors are divided by the bending stiffness of the bare timber floor to normalize the results. Four MTP-concrete composite floors with different connection designs are considered. The labels of floors in Fig. 5.12 are composed of the number of notches, depth of notches, and the timber shear length. For example, 6-20-400 refers to the floor with six notched connections, 20 mm notch depth, and 400 mm timber shear length.

As can be seen from Fig. 5.12, with enough number of notched connections (no less than four) and notch depth (no less than 15 mm), the bending stiffness of the floor is higher than the bare timber floor of the same total thickness. However, except for the full composite floor for which the floor bending stiffness slowly increases with the concrete thickness, the rest of the floor bending stiffness decreases with the concrete thickness first and then increases again. The floors with higher composite actions (more connections and deeper notches) are less affected by the relative thickness of concrete and timber than the floors with lower composite actions (fewer connections and shallower notches).

The portion of concrete in the composite floors not only affects the static performance such as the bending stiffness of the floor, but also the total mass and thus the dynamic and acoustic performance of the floor. A certain thickness of concrete can reduce the acceleration of bare timber floors under human walking or rotating machinery. However, a higher relative thickness of concrete does not create an improved floor bending stiffness, and the natural frequency of the floor is expected to decrease due to the increased mass. For the composite floor studied in this section, a large concrete thickness should be avoided to reduce the total weight without sacrificing the bending stiffness of the floor.

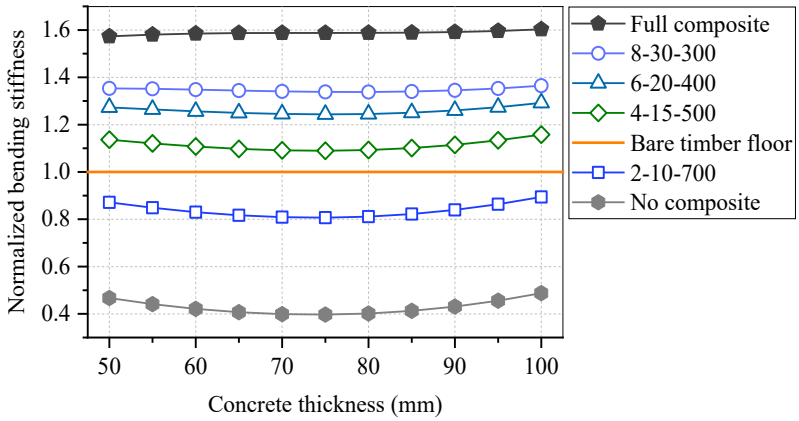

Fig. 5.12 MTP-concrete composite floor bending stiffness varying with the thickness of concrete

5.6 Composite Floor Ultimate Strength Prediction

5.6.1 Introduction

The above discussion focused on the serviceability performance of MTP-concrete composite floors where the materials are linear elastic and the crack of concrete is not considered. Although the concrete cracking may appear at the serviceability limit state, it usually has a negligible effect on the bending stiffness of MTP-concrete composite floors. However, if the ultimate strengths of the composite floors are being considered, the damages on the materials and the nonlinearity of connections under shear have to be taken into account. This section discusses the ultimate strength prediction of MTP-concrete composite floors. To do this, the proposed composite beam model is

extended beyond the elastic stage and a methodology is developed to accommodate all the possible failure modes of MTP-concrete composite floors under bending. The predicted load-carrying capacities and failure patterns of floors are verified by the test results.

5.6.2 Methodology

Under the external load, the damages or failures that could happen in MTP-concrete composite floors are shown in Fig. 5.13. After the initial elastic stage, the cracks appear at the bottom of concrete (**a** in Fig. 5.13) due to the tensile stresses in concrete exceeded the concrete tensile strength. For common unreinforced notched connections, the cracking of concrete causes the connection stiffness degradation and redistribution of internal forces in the floor. With the further increase of the external load, the composite floor could fail in the timber layer, concrete layer, or in the connections. The timber layer could fail due to shear (**e** in Fig. 5.13) or combined bending and tension (**d** in Fig. 5.13). The concrete layer could fail due to shear (**c** in Fig. 5.13) or combined bending and compression (**b** in Fig. 5.13). The failure of the notched connections could be compression or shear failure in timber or concrete (**f-i** in Fig. 5.13). Depending on the geometry and material properties of timber and concrete, the notched connections can fail in either of these failure modes. However, except for the compression failure of timber in front of the notch, the rest of the failure modes are brittle. If one of the connections fails in a brittle manner, the deflection of the floor will suddenly increase due to the sudden decrease in the bending stiffness, and the interlayer shear forces will redistribute to other connections. The suddenly increased shear forces in other connections usually cause the immediate failure of other connections and thus the failure of the entire floor system. If the timber compressive failure is triggered in the notched connections, the connections are considered to be yielded without unloading. The composite floor will not lose the load-carrying capacity immediately until more connections are yielded and then a brittle failure pattern is triggered in the timber or concrete layer.

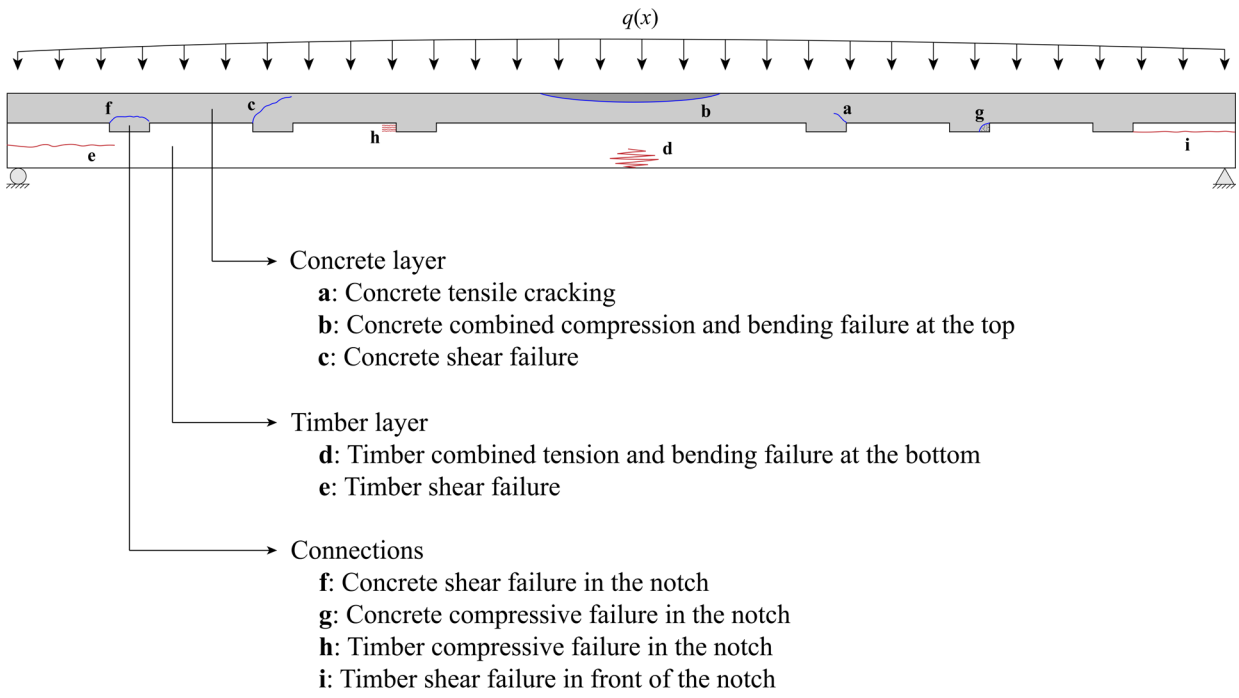

Fig. 5.13 Possible failure patterns and damages of MTP-concrete composite floors with notches under bending

The procedure to determine the ultimate strength and failure pattern of MTP-concrete composite floors under bending is shown in the flowcharts in Fig. 5.14. The most ideal failure pattern for the composite floors is the connections progressive yielding before a brittle failure pattern is triggered. The following sections describe the failure mechanism and design equations in each stage. The design procedure for the composite floors with reinforced notched connections is slightly different as the concrete cracking can be safely disregarded. This will be discussed in detail in Section 5.6.6.

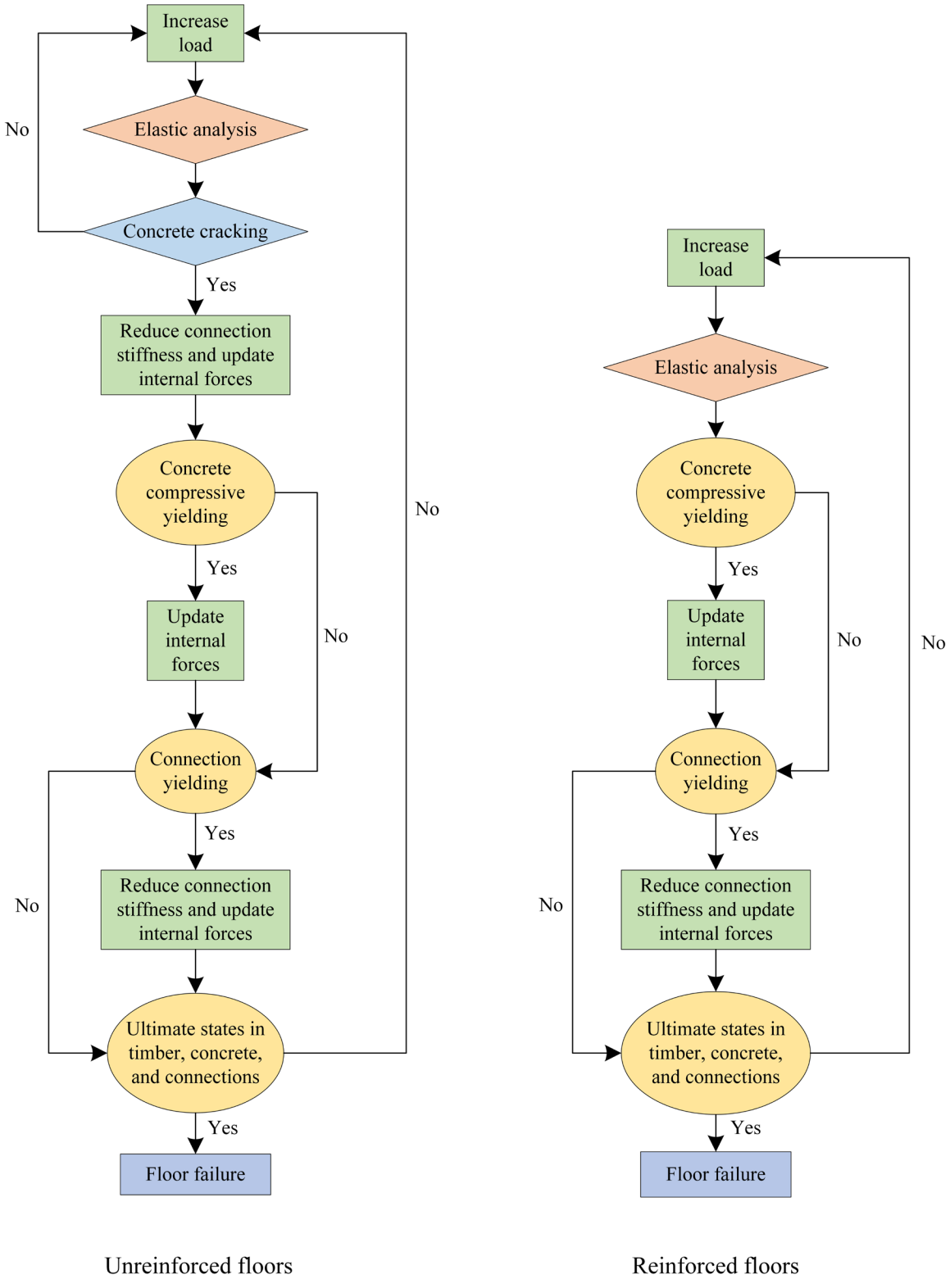

Fig. 5.14 Flowcharts to determine the strength and failure pattern of MTP-concrete composite floors with unreinforced and reinforced notched connections

5.6.3 Concrete Failure

Under the positive bending moment, the concrete layer at the top of MTP-concrete composite floors is subjected to combined compression and bending, which results in a large portion of the compression zone at the top and a small portion of tension zone at the bottom. Before the final failure, the concrete layer can experience severe damages under the external load. Concrete is assumed to be linear elastic under tension until the tensile strength f_{ct} is reached, as shown in Fig. 5.15. At the elastic stage, the stresses in concrete linearly vary with the strains according to Hooke's law. When the tensile stress at the bottom of concrete reaches the tensile strength f_{ct}, cracks develop in concrete and a new state of equilibrium is achieved under external loads. Concrete under compression is assumed to be bilinear. When the compressive stress at the top of concrete reaches the compressive strength f_c', concrete yields under compression. The ultimate compressive state is when the strain at the top of concrete reaches the ultimate compressive strain ε_{cu}. The concrete layer can also fail due to brittle shear. The mechanisms of concrete under tension, compression, and shear are discussed below.

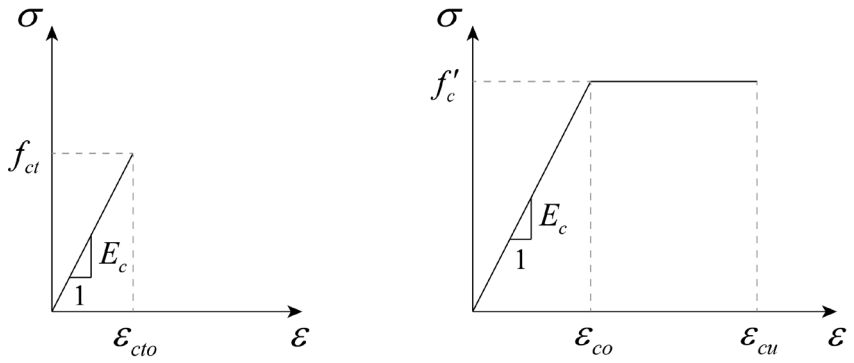

Fig. 5.15 Simplified stress-strain relationships of concrete under tension and compression

Concrete cracking

Similar to most mechanical connectors in MTP-concrete composite floors, the notched connections are not fully rigid and can only provide partial composite action to the composite floors. As a result, a small portion of concrete at the bottom is under tension. Fig. 5.16(a) shows

the tension zone of the concrete layer in the MTP-concrete composite floor shown in Fig. 5.6 under the uniformly distributed load. Due to the discrete connections, the neutral axis in the concrete layer is not constant. The stress distributions at the top and bottom of concrete are shown in Fig. 5.7(f) and (g). The maximum tensile stress in each segment is compared with the tensile strength of concrete f_{ct}, which can be estimated from its compressive strength f_c' (CSA A23.3-19) as

$$f_{ct} = 0.6\lambda\sqrt{f_c'} \tag{5.90}$$

where λ is the factor to account for the concrete density. For normal density concrete (2150 to 2400 kg/m^3), λ is taken as 1. If the tensile strength is not reached, concrete is still at the elastic state. If the tensile strength is reached, concrete is cracked below the neutral axis. Thereafter concrete is only able to resist compressive stresses above the neutral axis. The cracked height of concrete in each segment is simplified as constant and is taken as the highest height of the neutral axis in the segment, as shown in Fig. 5.16(b).

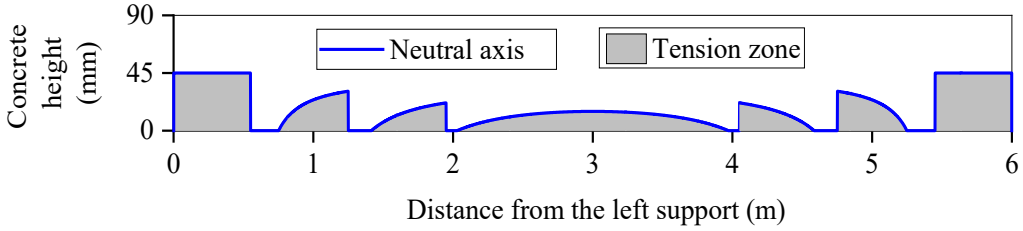

(a) Neutral axis of concrete at the elastic state

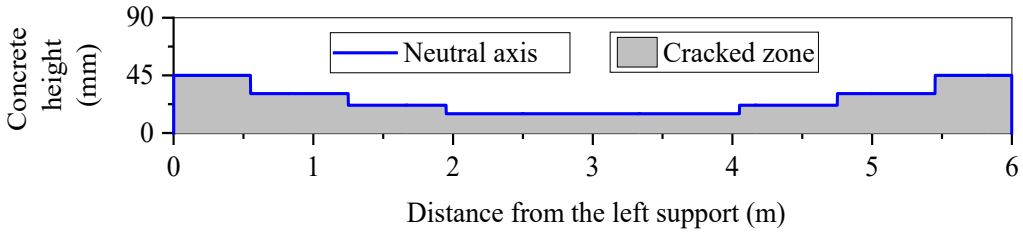

(b) Cracked zone in concrete after tensile strength is reached in each segment

Fig. 5.16 Tension zone and cracked zone in the concrete layer of the composite floor

To consider the effect of concrete cracking on the internal forces in the composite floor, an external force N_{cb} is applied to the tensile zone of concrete to eliminate the tensile stresses in concrete, as shown in Fig. 5.17. The magnitude of the force N_{cb} is

$$N_{cb} = \frac{1}{2} b h_{ct} \sigma_{cb} \tag{5.91}$$

where b is the floor width, σ_{cb} is the tensile stress at the bottom of concrete calculated according to Eq. 5.69, and h_{ct} is the cracked height of concrete which can be determined from the compressive stress σ_{ct} at the top and tensile stress σ_{cb} at the bottom of concrete as

$$h_{ct} = \frac{\sigma_{cb} h_c}{\sigma_{cb} + \sigma_{ct}} \tag{5.92}$$

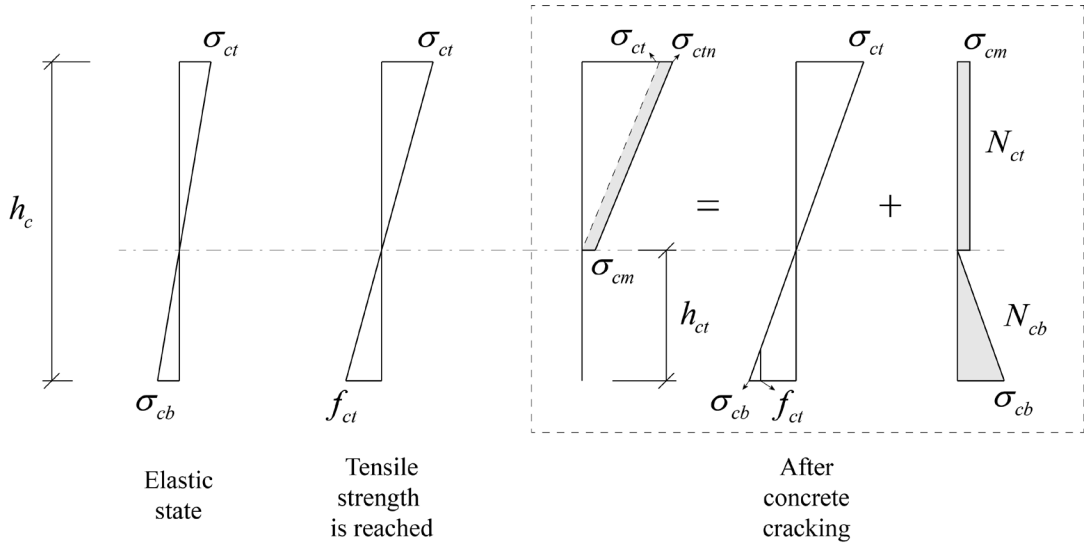

Fig. 5.17 Stress distribution in the concrete cross-section before and after concrete cracking

However, the added external force N_{cb} on concrete reduces the bending moment in concrete. To avoid the reduction of bending moment in concrete, another force N_{ct} has to act on the compression zone of concrete with a magnitude of

$$N_{ct} = \frac{N_{cb}(h_c/2 - h_{ct}/3)}{h_{ct}/2} \tag{5.93}$$

The axial force N_{ct} increases the compressive stresses in concrete but does not change the curvature of concrete. The updated compressive stress at the top of concrete is

$$\sigma_{ctn} = \sigma_{ct} + \frac{N_{ct}}{b(h_c - h_{ct})} \tag{5.94}$$

The updated compressive stress at the bottom of the concrete compression zone is

$$\sigma_{cm} = \frac{N_{ct}}{b(h_c - h_{ct})} \tag{5.95}$$

Since the resultant axial force in the composite cross-section should be zero, an additional tensile force is generated in the timber cross-section with a magnitude of

$$N_{in} = N_{cb} + N_{ct} \tag{5.96}$$

The concrete cracks are concentrated around the load-bearing surfaces of notched connections. After concrete cracking, the connections experience stiffness degradation with the crack enlargement. For the notched connections, the connection stiffness after concrete cracking can be conservatively taken as the ultimate stiffness of notched connections and calculated according to Eq. 5.97

$$k_{ult} = \varphi_{kc} k \tag{5.97}$$

where φ_{kc} is the ratio of the ultimate connection stiffness to the initial connection stiffness. According to the connection shear test results described in Chapter 3, when the timber shear length to the notch depth has large ratios (≥ 14), φ_{kc} can be approximately taken as 0.7. A more accurate φ_{kc} factor should be examined in the future.

To summarize, the cracking of concrete raises the internal axial forces in timber and concrete and reduces the bending stiffness of the composite floor due to the reduced connection stiffness. The bending moments in timber and concrete experienced no sudden change thus the displacement of the floor is continuous before and after concrete cracking, and the displacement and curvature of timber and concrete layers are the same (no gap opening).

Concrete compressive yielding and crushing

After the compressive stress at the top of concrete reaches the compressive strength f_c', concrete starts to show nonlinear behaviour. The concrete layer does not fail immediately after the compressive strength f_c' is reached but enters a compressive yielding stage until a larger portion of concrete has reached the compressive strength f_c' and the concrete top has reached the ultimate compressive strain ε_{cu}, as shown in Fig. 5.18. The ultimate compressive strain ε_{cu} of concrete is assumed to be 0.0035 (CSA A23.3-19). Since the compressive stress of concrete cannot exceed its compressive strength f_c', if the compressive stress in concrete determined according to Eq. 5.94 exceeds the compressive strength f_c', the stress has to be reduced to the compressive strength f_c'. The yield height of concrete can thus be determined as

$$h_{cy} = \frac{\sigma_{ctn} - f_c'}{\sigma_{ctn} - \sigma_{cm}} (h_c - h_{ct}) \tag{5.98}$$

Because of concrete yielding, the axial forces in timber and concrete are both reduced. The reduced axial force in concrete and timber is

$$N_{de} = \frac{1}{2} (\sigma_{ctn} - f_c') h_{cy} b \tag{5.99}$$

The updated axial force in timber after concrete cracking and yielding is

$$N_{tn} = N_t + N_{in} - N_{de} \tag{5.100}$$

Concrete yielding also causes the decrease of bending moment in concrete and increase of bending moment in timber. The updated bending moment in timber after concrete yielding is

$$M_{tn} = M_t + N_{de} (h_c + \frac{h_t}{2} - \frac{h_{cy}}{3}) \tag{5.101}$$

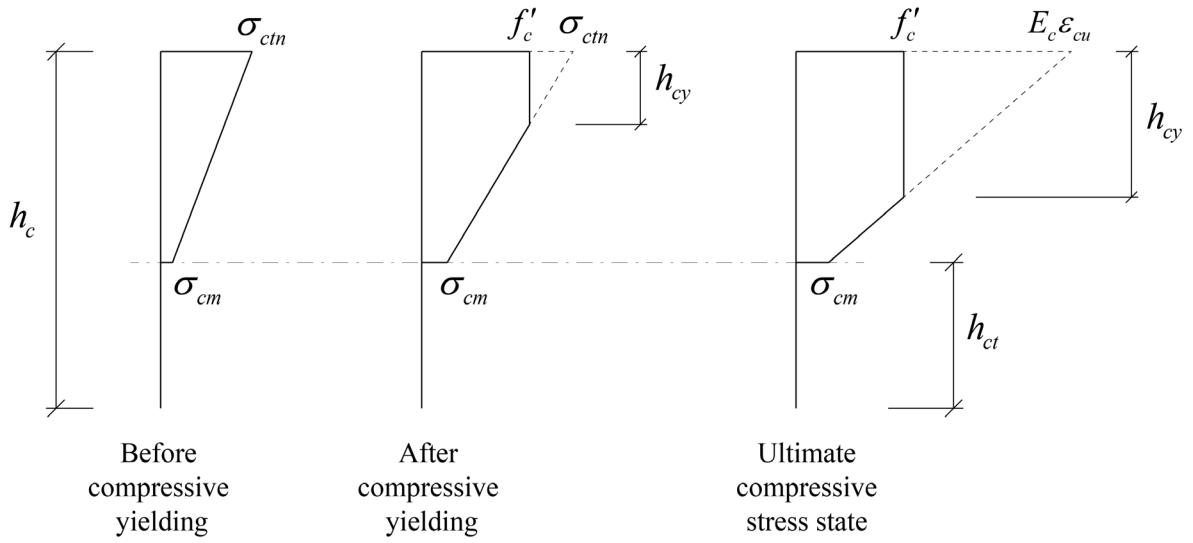

Fig. 5.18 Stress distribution in the concrete cross-section after concrete yields under compression

Concrete shear failure

The shear behaviour of the concrete layer in MTP-concrete composite floors is similar to the one-way concrete slabs. Although rarely governs, the shear capacity of concrete should be checked along with the tensile and compressive strengths of concrete. Due to the thin and wide shape of the concrete layer, transverse reinforcement such as stirrups are not installed in the concrete layer. Therefore the shear forces are resisted by concrete itself. According to Canadian concrete design standard A23.3-19, the shear resistance of the concrete slab can be calculated as

$$V_{cr} = \lambda\beta\sqrt{f_c'}bd_v \tag{5.102}$$

In Eq. 5.102, factor β accounts for the shear resistance of cracked concrete and can be taken as 0.21 as long as the concrete thickness is not greater than 350 mm. Factor d_v is the effective shear depth and is taken as $0.72h_c$.

5.6.4 Timber Failure

The timber layer is subjected to combined tension and bending when MTP-concrete composite floors are under positive bending moments. As shown in Fig. 5.13, the final failure of timber could

be combined tension and bending failure or shear failure. Similar to the material properties of concrete, timber is assumed to be linear elastic until tensile failure or compressive yielding, as shown in Fig. 5.19. Due to the eccentric bending, the compressive stresses at the top of timber are lower than the tensile stresses at the bottom of timber. Thus timber can be assumed to be linear elastic before final failure. Since the notched connections reduce the cross-section area of timber, the internal forces in timber should be checked not only at locations that have the highest bending moment, axial force, or shear force, but also at locations that have reduced cross-section areas.

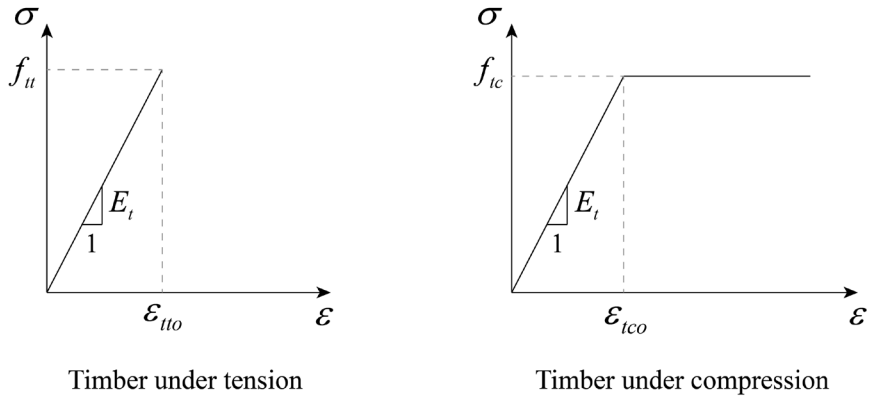

Fig. 5.19 Stress-strain relationships of timber under tension and compression

Timber Combined Tension and Bending Failure

The bending moment M_{tn} and tensile force N_{tn} in timber at any location along the floor should satisfy the following interaction equation

$$\frac{N_{tn}}{T_{tr}} + \frac{M_{tn}}{M_{tr}} \leq 1 \tag{5.103}$$

The axial force N_{tn} and bending moment M_{tn} in timber are determined from Eq. 5.100 and Eq. 5.101, respectively. The bending moment resistance M_{tr} of timber can be calculated as

$$M_{tr} = f_{tb} S_t \tag{5.104}$$

where f_{tb} is the bending strength of timber and S_t is the timber section modulus. The tensile load resistance T_{tr} of timber can be calculated as

$$T_{tr} = f_{tt} A_t \tag{5.105}$$

where f_{tt} is the tensile strength of timber parallel to grain and A_t is the cross-section area of timber. From Eq. 5.104 and Eq. 5.105, it can be seen that the moment resistance M_{tr} and tensile load resistance T_{tr} of timber are both lower in the notched regions than other regions due to the reduced cross-section area.

Timber Shear Failure

In MTP-concrete composite floors, the timber layer is rarely governed by the shear resistance since MTP-concrete composite floors are usually long-span systems. However, the shear resistance of timber should be examined along with its bending resistance, especially at the notched regions. The shear stress distribution in the timber cross-section is parabolic. The maximum shear force V_t in timber should not exceed the timber shear resistance V_{tr}

$$V_t \leq V_{tr} = \frac{2}{3} f_{ts} A_t \tag{5.106}$$

In Eq. 5.106, f_{ts} is the shear strength of timber parallel to the grain. The applied shear force V_t at any location of timber is determined from Eq. 5.7.

5.6.5 Connection Failure or Yielding

Besides the failure of timber and concrete layers, the MTP-concrete composite floors could also fail in the connections. Depending on the failure mode of the notched connection, the failure of the connection can cause the sudden failure of the entire floor system or just the reduction of floor bending stiffness. Four notched connection failure modes are considered: timber shear failure in front of the notch, timber compression failure at the load-transfer area, concrete compression failure at the load-transfer area, and concrete notch shear failure, as shown in Fig. 5.13. Although these failures happen in either timber or concrete, they are considered as connection failures since the ultimate strengths of the materials are compared with the shear forces resisted by the connections. Except for timber compression failure in front of the notch which involves crushing of wood fibers, the rest of the failure modes are brittle and can cause the failure of the entire floor

system. The load-carrying capacity of notched connections has been discussed in Section 3.5 and is briefly repeated here. It should be noted that the empirical factors in the following equations are derived from limited experimental studies on the notched connections. The validity of these empirical factors needs to be further examined.

The connection strength due to timber compressive yielding in front of the notch is

$$P_{tc} = \varphi_{tc} f_{tc} b d_{nc} \tag{5.107}$$

where f_{tc} is the compressive strength of timber in the longitudinal direction, d_{nc} is the depth of the notch, and φ_{tc} is the correction factor for timber compressive strength which is estimated to be 0.84 from connection shear tests.

Similarly, the connection strength due to concrete compressive failure in the notch is

$$P_{cc} = f_c' b d_{nc} \tag{5.108}$$

Equation 5.108 does not contain any empirical factor although the compressive stress in concrete is not uniformly distributed initially (Fig. 3.15(b)). However, since concrete has a low tensile strength, the compressive stress is expected to be uniform after the concrete cracking at the notched corner. In MTP-concrete composite floors, the compressive strength of concrete is usually higher than that of timber, thus the compressive failure of concrete rarely governs.

The connection strength due to the timber shear-off failure in front of the notch is

$$P_{ts} = \varphi_{ts} f_{ts} b l_{ts} \tag{5.109}$$

where f_{ts} is the longitudinal shear strength of timber, l_{ts} is the shear length of timber, and φ_{ts} is the correction factor due to the non-uniform distribution of shear stresses (Fig. 3.15(e)). From the push-out tests on notched connections, the correction factor φ_{ts} can be empirically assumed to be 0.4 (Fig. 3.16).

Finally, the connection strength due to concrete shear failure in the notch can be expressed as

$$P_{cs} = \varphi_{cs} \sqrt{f_c'} b l_{nw} \tag{5.110}$$

where l_{nw} is the notch length and φ_{cs} is the empirical factor for the concrete shear strength. The shear failure of concrete can be difficult to predict due to the complex failure mechanism.

According to the floor bending test results, φ_{cs} can be inversely estimated to be 0.38 which is significantly lower than the recommended value of 0.99 by AASHTO standard (2003) on concrete shear keys in segmental bridges. The low shear strength of concrete notches in MTP-concrete composite floors is likely caused by the boundary conditions of notches. In the push-out tests on notched connections, the uplifting of concrete was restricted by the normal stresses. However, the normal stresses did not exist in MTP-concrete composite floors. Before the shear failure of notched connections in MTP-concrete composite floors, the rotation of the concrete notch due to crack enlargement could be observed. More research is required to validate the empirical factor φ_{cs}.

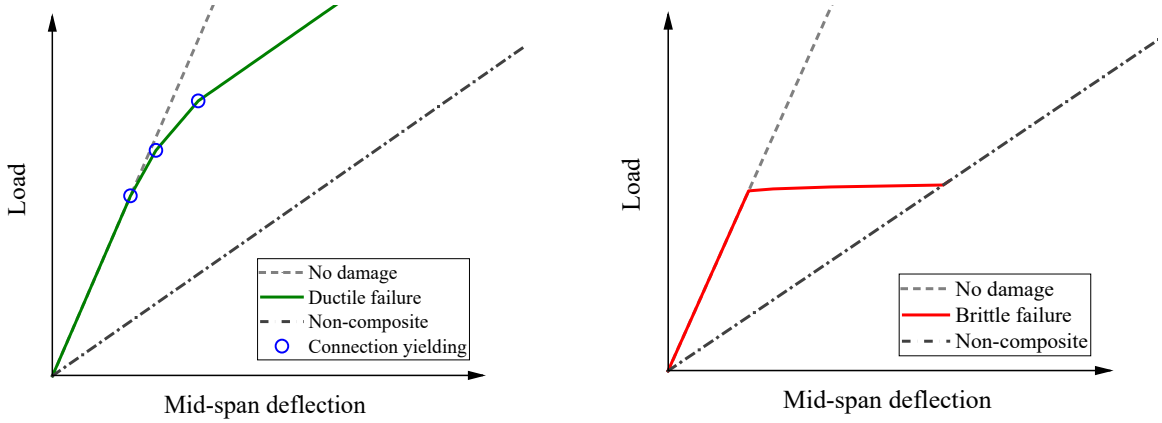

(a) Connection progressive yielding (b) Connection brittle failure

Fig. 5.20 Load-deflection relationships of composite floors when the connections fail in ductile and brittle patterns

The shear forces in the connections are calculated under each load level according to Eq. 5.38 and compared with the connection strength. Fig. 5.20 illustrates the load-deflection relationships of the composite floors when the connections fail in two different patterns. If the timber compressive strength is reached first in the connections, the shear forces in the connections do not unload but the connections do not take higher shear forces henceforth. If there are other connections in the floor, the increased external force is taken by the other connections until they also yield. The overall bending stiffness of the floor is decreased gradually with the consecutive yielding of the connections. If all the connections are yielded, the bending stiffness of the floor reduces to the

non-composite floor, as shown in Fig. 5.20(a). The ultimate failure of the floor will be eventually triggered if timber or concrete reaches its ultimate bending strength. If one of the connections fails in a brittle manner, the shear force in the connection is suddenly unloaded which causes a sudden increase in the floor deflection and the composite floor is deemed as failed, as shown in Fig. 5.20(b).

5.6.6 Composite Floor with Reinforced Notches

The above discussion considered the cracking of concrete, the connection stiffness degradation after concrete cracking, and the failure of connections in concrete. However, if the notched connections are reinforced with sufficient steel reinforcements to take tensile forces after concrete cracking and constrain the crack enlargement, the notched connections experience almost no stiffness degradation, and the shear failure of concrete in the notch is also prevented. Thus, for MTP-concrete composite floors with reinforced notches, the concrete cracking, connection stiffness degradation, and shear failure of the concrete notch can be safely disregarded. As a result, the MTP-concrete composite floors with reinforced notches have higher ultimate bending stiffness and load-carrying capacity than the floors with unreinforced notches, and the undesired failure patterns are effectively avoided. The design procedure for MTP-concrete composite floors with reinforced notches is shown in Fig. 5.14. To use this simplified design procedure, the reinforced notches should satisfy the following requirements:

(1) The reinforcements are installed around the load-bearing area in the notch where crack could develop;
(2) The steel reinforcements are properly anchored in concrete and timber to effectively take tensile forces after concrete cracking.
(3) Sufficient reinforcements are installed in the notch to restrict the crack enlargement of concrete.

The sufficient level of reinforcement in the notched connections should be determined through test investigation or numerical modeling.

5.6.7 Verification

The above-mentioned procedure is validated from the bending test results on seven MTP-concrete composite floors with unreinforced notched connections and three MTP-concrete composite floors with reinforced notched connections. The floor geometry and material properties of timber and concrete are described in Chapter 4. The initial connection stiffness of the notched connections can be estimated from Eq. 3.3. The GLT panels in the floor specimens were made of No. 2 or better grade SPF dimension lumbers. The tensile strength of timber parallel to grain f_{tt} was estimated from the bending strength as $f_{tb}/1.86$ according to the tensile tests and bending tests on SFP lumber (Grade No 2 or better) conducted by Niederwestberg et al. (2018). The compressive strength of timber parallel to grain f_{tc} was assumed to be equal as the tensile strength f_{tt}. The shear strength of timber is taken as $f_{tb}/7.6$, which is the relation between the shear strength and bending strength of Lodgepole Pine and Subalpine Fir (Wood Handbook 2010).

Under each load level, the internal forces in the MTP-concrete composite floors are checked at several critical locations. Fig. 5.21 shows an example of an MTP-concrete composite floor with six identical notched connections. To check for cracking and compressive yielding of concrete in the MTP-concrete composite floor, the tensile stresses at the bottom of concrete and compressive stresses at the top of concrete are checked at sections A, B, C, and E where the local stress peaks appear in each segment. The bending resistance of timber is checked at sections C, D, and E. Sections C and E have the highest bending moment and axial force, respectively; while section D has the narrowest cross-section area. Similarly, the shear forces in timber and concrete are checked at locations that have the highest shear force and locations with the narrowest cross-section. To examine the connection yielding or failure, the interlayer shear forces are checked in all the notched connections.

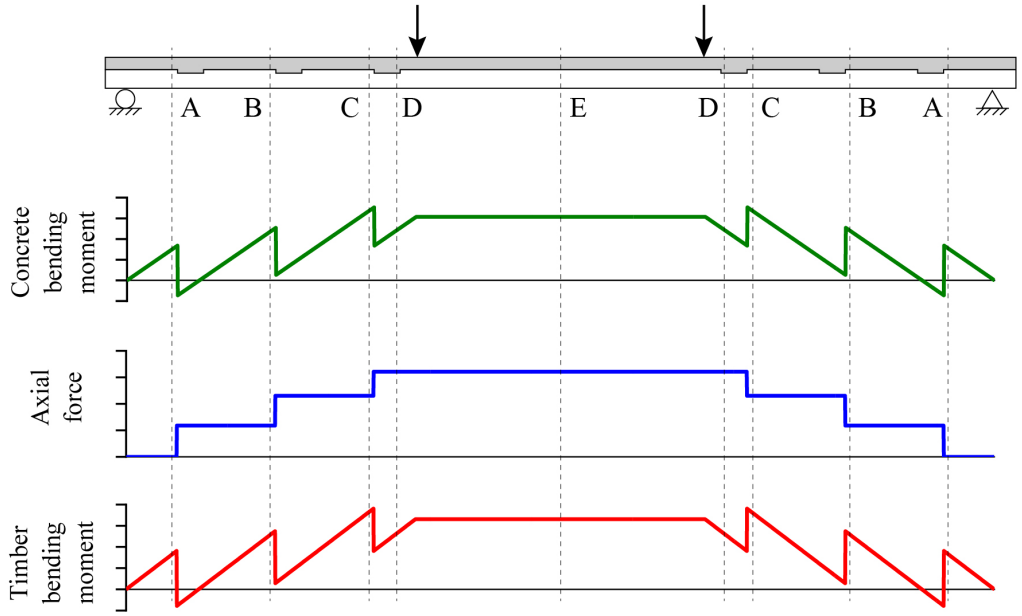

Fig. 5.21 Critical locations and internal forces in the composite floor under four-point bending

The comparisons between the measured and predicted load-deflection relationships for the floor specimens are shown in Fig. 5.22. Since the timber layer is assumed to be linear elastic until failure (except for the local areas around the connections), the mid-span deflection of the floor is determined from Eq. 5.111.

$$\delta(L/2) = \int_0^L \frac{\hat{M}(x,L/2)M_t(x)}{E_t I_t} dx \tag{5.111}$$

The external load increased incrementally and the internal forces in the floor under each load level are updated according to the flowchart in Fig. 5.14. The predicted ultimate strengths and failure modes of the composite floors are compared with the measured results as shown in Table 5.3. As can be seen from Fig. 5.22 and Table 5.3, the model can accurately predict the failure pattern for most of the specimens and the predicted ultimate strengths of the floors are generally in good agreement with the measured results. The predicted ultimate strengths of the floor specimens are within 10% of the measured strengths except for specimens SPU-2, SPU-3, and SPU-5.

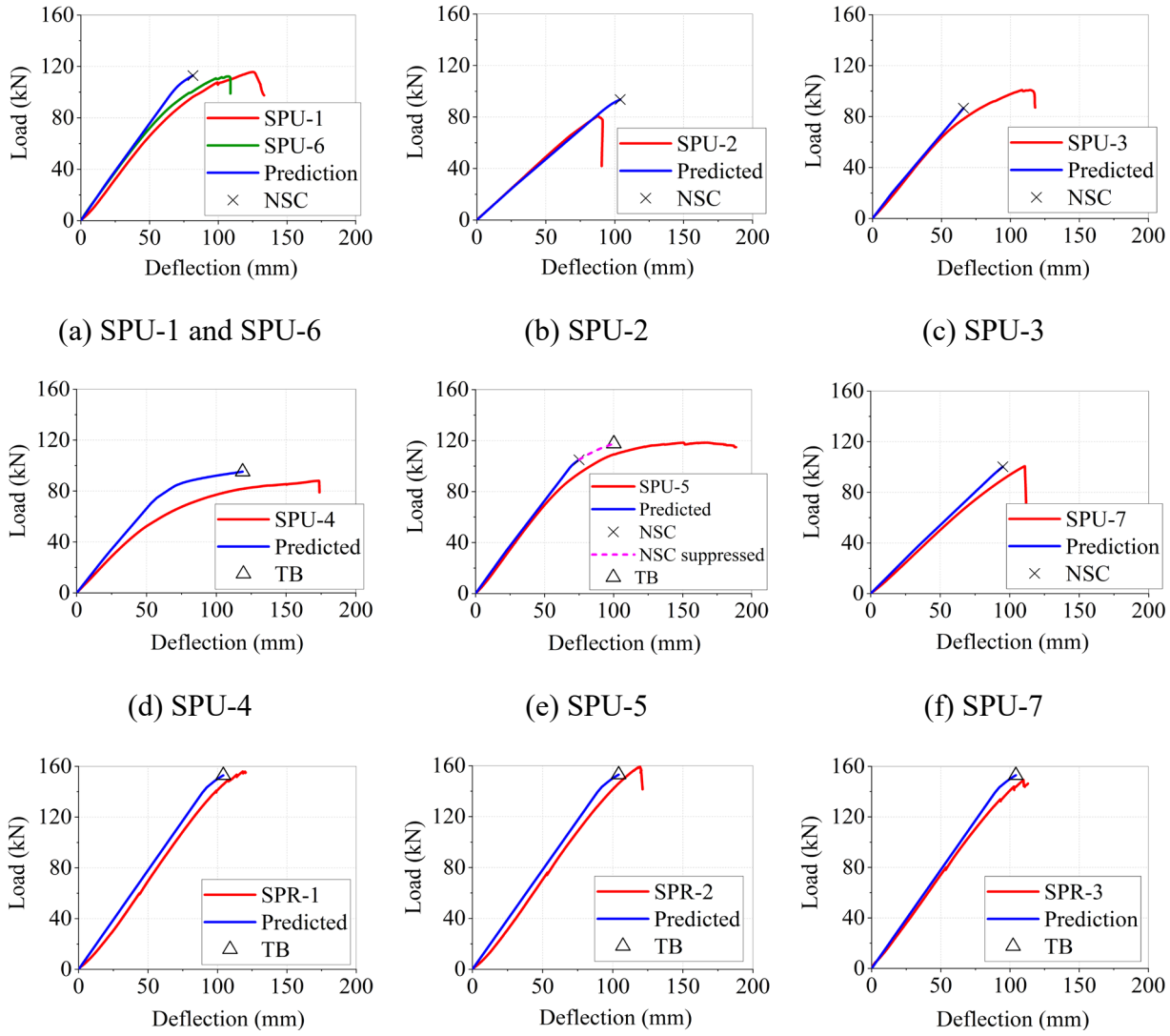

Fig. 5.22 Measured and predicted load-deflection relationships of MTP-concrete composite floors under bending (NSC: concrete notch shear failure; TB: timber member bending failure)

The ultimate strengths for specimens SPU-2, SPU-3, and SPU-5 are overestimated 15.8%, underestimated 14.2%, and underestimated 11.4% by the model, respectively. Specimens SPU-2 and SPU-3 both failed due to concrete notch shear failure. The discrepancy between the predicted and measured strengths is the result of the large variation of the concrete notch shear capacity. As discussed in Eq. 5.110, the predicted shear capacity of concrete notches exhibits great uncertainty due to the lack of enough test data. The underestimation of the ultimate strength of specimen SPU-

5 by the model was also due to the underestimation of the concrete notch shear capacity. If the concrete shear failure in the notch is suppressed, the predicted failure mode of specimen SPU-5 by the model will be the timber member bending failure observed in the test and the predicted load-carrying capacity of the specimen will be 117.6 kN which is only 0.7% lower than the measured strength.

Table 5.3 Measured and predicted load-carrying capacities and failure patterns of the floor specimens

Specimen	Load-carrying capacity (kN)		Failure mode	
	Measured	Predicted	Observed	Predicted
SPU-1	115.6	112.9 (-2.3%)	Concrete notch shear failure	
SPU-2	80.8	93.6 (15.8%)	Concrete notch shear failure	
SPU-3	100.9	86.6 (-14.2%)	Concrete notch shear failure	
SPU-4	88.1	95.2 (8.1%)	Timber member bending failure	
SPU-5	118.4	104.9 (-11.4%)	Timber member bending failure	Concrete notch shear failure
SPU-6	112.2	112.9 (0.6%)	Concrete notch shear failure	
SPU-7	100.6	100.2 (-0.4%)	Concrete notch shear failure	
SPR-1	156.0	152.9 (-2.0%)	Timber member bending failure	
SPR-2	159.2	152.9 (-4.0%)	Timber member bending failure	
SPR-3	149.2	152.9 (2.5%)	Timber member bending failure	

Note: Numbers in the brackets are the differences between the predicted and measured results.

For specimens SPU-1, SPU-4, SPU-5, and SPU-6, the actual displacements of the specimens at the ultimate state are larger than the predicted displacements. The connections likely experienced

a larger degradation after concrete cracking and the gap opening between timber and concrete was not negligible at the final stage during the test. The predicted load-deflection curves for the specimens with reinforced notches are in high agreement with the measured curves. The reinforced floor specimens showed high consistency in terms of the ultimate strength as the floor performance was not impacted by concrete cracking and concrete notch shear failure. As a result, the composite beam model is also more reliable in predicting the ultimate strengths of floors with reinforced notches.

5.6.8 Summary

This section discusses the ultimate strength prediction to the MTP-concrete composite floors with notches under a positive bending moment. The proposed composite beam model is extended beyond the elastic stage to consider the concrete cracking, connection stiffness reduction, connection yielding, and concrete compressive yielding. The internal forces in the floors are updated according to the damages on the materials. The final failure of the composite floors could be the bending or shear failure of timber or concrete layers, or compressive or shear failure of the notched connections. The composite beam model can accurately predict the failure pattern of the composite floors and the estimated peak loads can generally match the measured results. The ultimate load for the timber bending failure can be more accurately predicted by the composite beam model than the concrete shear failure in the notches. It is recommended to reinforce the notched connections with steel reinforcements to prevent the concrete shear failure in the notches. For the unreinforced notches, a large safety factor should be used when estimating the shear force resistance of concrete notches.

5.7 Conclusions

This chapter introduces a discrete bond composite beam model to estimate the internal forces in MTP-concrete composite floors with notches. A release and restore procedure is used to solve the internal forces in the composite floors. The predictive capability of the composite beam model is verified by comparing its predictions with those from several other composite beam models and a finite element model through two examples. Compared with the continuous bond composite beam

models, the proposed beam model can capture the non-continuous distribution of internal forces and local stress peaks in the composite floors with discrete connections. Compared to the numerical methods to model the discrete-connected composite beams, the proposed beam model provides closed-form solutions for engineers and designers to calculate the internal forces in the composite floors.

The validated composite beam model is used to predict the bending stiffness of MTP-concrete composite floors and a good correlation was achieved between the estimated and measured results. Parametric studies were then carried out to study the effects of the notched connection design and relative thickness of concrete and timber on the bending stiffness of the composite floors. It was found that the notched connections, including number, sizes, and locations, as well as the relative thickness of concrete to timber in the composite floors, can be optimized to achieve high floor bending stiffness without reducing the load-carrying capacity or increasing the self-weight of the floor.

Finally, the discrete bond composite beam model is extended beyond the elastic stage to consider the damages and nonlinear behaviours of the materials. To predict the ultimate load-carrying capacities of the composite floors, the ultimate stress states of timber, concrete, and connections are defined. The composite beam model can accurately predict the failure patterns and peak loads for most of the composite floor specimens. However, it is recommended to reinforce the notched connections to avoid notched connection shear failure in concrete and enhance the reliability of the floor load-carrying capacity.

Chapter 6

Conclusions

This thesis focuses on the structural performance of notched connections under shear and notch-connected mass timber panel-concrete composite floors under bending. The structural performance of the composite system was investigated with experimental, numerical, and analytical methods. The ultimate research goal of the thesis is to optimize the notched connection design and improve the structural efficiency of timber-concrete composite floors.

Experimental and numerical investigations were conducted on the notched segments first. The connections with different configurations exhibited different stiffness and strength and failed in different patterns. The following conclusions can be drawn from the research on the notched connections:

- The push-out tests showed that the notch depth mainly affects the connection stiffness and failure pattern, while the timber shear length mainly affects the connection strength and failure pattern. Deeper notches tend to fail in a brittle manner while shallower notches tend to fail in a ductile manner. A limited number of self-tapping screws in the notch had a negligible effect on the connection stiffness and strength. The orientation of timber is crucial to the connection stiffness and strength.
- Finite element modeling on the notched connections showed that the connection stiffness is most impacted by the material properties of timber and the notch depth. An empirical formula was proposed to estimate the notched connection stiffness which is used as the input in the composite beam model to predict the composite floor bending stiffness. Empirical equations were also proposed to estimate the connection strength and were verified by the test results.

Based on the studies on the notched connections, full-size mass timber panel-concrete composite floors were constructed and tested under static bending and vibration. The main conclusions from the tests on the composite floors are

- The bending stiffness, strength, and failure pattern of the composite floors with unreinforced notched connections under static bending are affected by the number and geometry of notched connections and the concrete layer thickness. The composite floors with shallow notches had low bending stiffness but ductile failure pattern, while the composite floors with deep notches had high bending stiffness but brittle failure pattern. After the notches were reinforced with orthogonal steel ties, the brittle failure of concrete was prevented in the notches, and higher load-carrying capacities were achieved in the floors.
- The vibration tests on the mass timber panel-concrete composite floors showed that the addition of the concrete layer improved the fundamental natural frequencies and damping ratios of the floors. Different notched connection designs had minor effects on the vibration properties of the composite floors. The composite action in the floors was close to full composite in the dynamic tests.

To determine the internal forces in the composite floors, a discrete bond composite beam model was proposed which considers the discrete and semi-rigid features of notched connections. The composite beam model is validated by other analytical composite beam models and numerical composite beam models. Parametric studies were carried out to study the structural performance of the composite floors affected by the connection designs and concrete layer thickness, from which the following conclusions can be drawn:

- With the increase of the notch depth and the number of notched connections, the composite efficiencies of the floors increase first and then decrease. The optimal number and depth of notched connections depend on the floor span and the timber member thickness. In a certain range, the relative thickness of concrete to timber in the composite floors has no significant effect on the composite floor bending stiffness.

Thereafter, the composite beam model is extended to the post-elastic stage to describe the concrete cracking, concrete yielding, connection yielding, and failures of concrete, timber, and connections. The bending stiffness, ultimate strengths, and failure patterns of the composite floors predicted by the discrete bond beam mode were verified by the test results.

The main contributions of this thesis are summarized below:

(1) Based on the experimental studies and numerical modeling on the notched connections, empirical formulas are proposed to estimate the notched connection stiffness and load-carrying capacity. The empirical formula to predict the notched connection stiffness has been proved to be both simple and accurate.
(2) The test investigations on the notched connections and mass timber panel-concrete composite floors gained insights into the static and dynamic properties of the composite systems, identified key factors that impact the structural performance of the composite system, and added additional data to the current state of the art.
(3) The proposed discrete bond composite beam model provides an analytical solution to determine internal forces and deflections of composite floors connected with discrete connections. Combined with the empirical formulas of the connection stiffness and strength, the composite beam model can be used to predict the bending stiffness, load-carrying capacity, and failure pattern of mass timber panel-concrete composite floors with notches.
(4) The proposed orthogonal reinforcements tested in the notched connections have been proven to be effective in restricting the crack enlargement and shear failure of the concrete notch. The installation of the orthogonal reinforcements effectively prevents the undesired failure patterns of the structure and the floor performance becomes more reliable.

In conclusion, the notched connections present a simple and efficient solution to connect mass timber panels to concrete in the composite floors. The research work in this thesis showed that, with the proper design of notched connections and the relative thickness of timber and concrete, mass timber panel-concrete composite floors can be structurally efficient and predictable, and less susceptible to large deflection and vibration.

Chapter 7

Outlook

The research work in this thesis demonstrates promising outcomes in terms of the structural performance of mass timber panel-concrete composite floors with notches. However, the structural performance of the composite system has not been thoroughly investigated in the thesis and future research needs are stated in this chapter.

In the push-out tests on the notched connections, the sizes of the connections were restricted due to the test setup. The vertical restriction on the specimens that prevented the uplifting of concrete had a positive effect on the connection stiffness. Finally, the measured connection stiffness was affected by the slip measurement method. Thus, the measured connection stiffness from the push-out tests could overestimate or underestimate the connection stiffness. Furthermore, only the timber shear failure and timber compressive failure were observed in the connection shear tests while concrete failure was not observed. Future research on notched connections can be investigated through the bending tests on short-span composite beams where the connection behaviour is close to the actual connection behaviour in the composite floors.

In the composite floor bending tests, most of the unreinforced floor specimens failed due to concrete shear failure in the notches. The shear failure of concrete in the notched connections is brittle and difficult to predict. Although an empirical equation was proposed to estimate the concrete shear strength, the prediction can be highly unreliable. Thus, the shear failure of concrete in the notch should be avoided. A reinforcing solution that used orthogonal steel ties in the notches was tested and proven to be effective in preventing concrete shear failure. However, the number of reinforcements installed in the notches likely exceeded the requirements and the minimal number of reinforcements should be determined through future testing.

In the bending tests, only one floor specimen was tested under the negative bending moment. The specimen showed good ductility since the concrete layer was reinforced with proportioned longitudinal reinforcement. However, the specimen had lower bending stiffness due to the cracking of concrete. As a result, the bending stiffness in a multi-span continuous floor is not

constant. Research is needed to develop design guidelines for the continuous timber-concrete composite floors.

In the connection tests and floor bending tests, concrete was cast directly on top of mass timber panels. Due to the nature of the notched connections, it is not ideal to put an insulation layer between timber and concrete. A waterproof paint was used on timber to avoid the water exchange between timber and concrete but has been proven to be inadequate. A more efficient water barrier should be evaluated in future studies. Additionally, the possible acoustic issues of the composite floors need to be addressed in the future.

Due to the narrow width of the composite floor specimens, the dynamic performance of the composite floors was unsatisfactory to the participants. Further vibration tests and subjective evaluations on the full-size mass timber panel-concrete composite floors are required. The beneficial effects of concrete on the dynamic performance of the floor when the concrete layer is sitting on the timber panels without connections was inconclusive from the limited tests and further investigations are needed.

In the proposed composite beam model, the shear deformations of timber and concrete layers were not considered. Thus, the composite beam model is best used to describe long-span composite floors but can underestimate the deflection for short-span composite floors. The friction between timber and concrete was ignored in the model. Future research can include friction in the model to better estimate the structural behaviour of the composite floors.

Except for the above-mentioned research needs, future studies should also be conducted to address the long-term performance, fire-resistance rating, two-way load-carrying capacity, as well as the diaphragm behaviour of mass timber panel-concrete composite floors.

Bibliography

ABAQUS/CAE. 2017. ABAQUS/CAE User's Manual, Version 6.17. Providence: Dassault Systèmes Simulia.

Aira, J.R., Arriaga, F., Íñiguez-González, G., Guaita, M. 2015a. Failure modes in halved and tabled tenoned timber scarf joint by tension test. Construction and Building Materials 96: 360–367.

Aira, J.R., Descamps, T., Parys, L.V., Léoskool, L. 2015b. Study of stress distribution and stress concentration factor in notched wood pieces with cohesive surfaces. European Journal of Wood and Wood Products 73: 325–334.

American Association of State Highway and Transportation Officials (AASHTO). 2003. Guide Specifications for Design and Construction of Segmental Concrete Bridges (2nd edition). Washington, DC, USA.

ASTM International. 2014. ASTM C469/C469M-14 Standard Test Method for Static Modulus of Elasticity and Poisson's Ratio of Concrete in Compression. West Conshohocken, PA, USA.

ASTM International. 2014. ASTM D143-14 Standard Test Methods for Small Clear Specimens of Timber. West Conshohocken, PA, USA.

ASTM International. 2015. Standard Test Methods of Static Tests of Lumber in Structural Sizes. ASTM D198–15. West Conshohocken, PA, USA.

ASTM International. 2018. ASTM C39/C39M-18 Standard Test Method for Compressive Strength of Cylindrical Concrete Specimens. West Conshohocken, PA, USA.

ASTM International. 2020. ASTM C39/C39M-20 Standard Test Method for Compressive Strength of Cylindrical Concrete Specimens. West Conshohocken, PA, USA.

Auclair, S.C., Sorelli, L., Salenikovich, A. 2016. A new composite connector for timber-concrete composite structures. Construction and Building Materials 112: 84–92.

Auclair, S.C., Hu, L., and Ramzi, R. 2018. Design method for vibration control of timber-concrete composite floor. FPInnovations, Pointe-Claire, QC, Canada.

Auclair, S.C. 2020. Design guide for Timber-Concrete composite floors in Canada. Special Publication SP-540E, FPInnovations, Pointe-Claire, QC, Canada.

Boccadoro, L., Frangi, A. 2014. Experimental analysis of the structural behavior of timber-concrete composite slabs made of beech-laminated veneer lumber. Journal of Performance of Constructed Facilities 28(6): A4014006.

Boccadoro, L. 2016. Timber-concrete composite slabs made of beech laminated veneer lumber with notched connection (Doctoral Thesis). ETH Zurich, Switzerland.

Boccadoro. L., Zweidler, S., Steiger, R., Frangi, A. 2017a. Bending tests on timber-concrete composite members made of beech laminated veneer lumber with notched connection. Engineering Structures 132: 14-28.

Boccadoro, L., Steiger, R., Zweidler, S., Frangi, A. 2017b. Analysis of shear transfer and gap opening in timber–concrete composite members with notched connections. Materials and Structures 50: 231.

Brunner, M., Romer, M., Schnüriger, M. 2007. Timber-concrete-composite with an adhesive connector (wet on wet process). Materials and Structures 40: 119–126.

Byfield M.P. 2002. Analysis of composite beams with widely spaced shear connectors. The Structural Engineer 80(13):31-33.

Ceccotti, A. 2002. Composite concrete-timber structures. Progress in Structural Engineering and Materials 4:264-275.

CEN. 1991. Timber structures-Joints made with mechanical fasteners-General principles for the determination of strength and deformation characteristics. EN 26891. Brussels, Belgium.

CEN. 2004. EN 1992-1-1: Design of concrete structures – Part 1-1: General rules and rules for buildings. Brussels, Belgium.

CEN. 2013. EN 14080: Timber structures – Glued laminated timber and glued solid timber – Requirements. Brussels, Belgium.

CEN. 2014. Eurocode 5: Design of timber structures—Part 1-1: General—Common rules and rules for buildings. EN 1995-1-1:2004+A2:2014. Brussels, Belgium.

Clark, L.G. 1953. Deflection of laminated beams. Transactions of the American Society of Civil Engineers 119(1): 721-736.

Clouston, P., Schreyer, A. 2008. Design and Use of Wood–Concrete Composites. Practice Periodical on Structural Design and Construction 13(4): 167-174.

CSA Group. 2019a. Design of concrete structures. A23.3-19. Toronto, Ontario, Canada.

CSA Group. 2019b. Engineering design in wood. O86-19. Toronto, Ontario, Canada.

Dackermann, U., Li, J., Rijal, R., Crews, K. 2016. A dynamic-based method for the assessment of connection systems of timber composite structures. Construction and Building Materials 102: 999-1008.

Deam, B.L., Fragiacomo, M., Buchanan, A.H. 2008. Connections for composite concrete slab and LVL flooring systems, Materials and Structures 41: 495-507.

Derikvand, M., Fink, G. 2021. Deconstructable connector for TCC floors using self-tapping screws. Journal of Building Engineering 42: 102495.

Dias, A.M.P.G. 2005. Mechanical behaviour of timber-concrete joints. Thesis, Technische Universiteit Delft, Netherlands.

Dias, A.M.P.G, Cruz, H.M.P., Lopes, S.M.R., van de Kuilen, J.W. 2000. Stiffness of dowel-type fasteners in timber–concrete joints. Proceedings of the Institution of Civil Engineers: Structures and Buildings 163(4): 257-266.

Dias, A.M.P.G., Jorge, L.F.C. 2011. The effect of ductile connectors on the behaviour of timber-concrete composite beams, Engineering Structures 33(11): 3033–3042.

Dias, A.M.P.G., Kuhlmann, U., Kudla, K., Mönch, S., Dias, A.M.A. 2018a. Performance of dowel-type fasteners and notches for hybrid timber structures, Engineering Structures 171: 40–46.

Dias, A., Schänzlin, J., Dietsch, P. 2018b. Design of timber-concrete composite structures: A state-of-the-art report by COST Action FP1402 / WG 4, Shaker Verlag Aachen.

Dias, A., Skinner, J., Crews, K., Tannert, T. 2016. Timber-concrete-composites increasing the use of timber in construction. European Journal of Wood and Wood Products 74: 443-451.

DIBt (Deutsches Institut für Bautechnik). 2012. Zulassung Z-9.1-449: SPAX Schrauben als Holzverbindungsmittel. Berlin, Germany.

DIN EN 1995-1-1. 2013. National Annex - Nationally determined parameters - Eurocode 5: Design of timber structures - Part 1-1: General - Common rules and rules for buildings. Deutsches Institut für Normung, Berlin, Germany. [in German]

Döhrer, A., Lehmann, S., Rautenstrauch, K. 2006. The natural adhesive bond between board stacks and mineral surface layers. In: 9th World Conference on Timber Engineering (WCTE), Portland, Oregon, USA.

Dolan, J.D., Murray, T.M., Johnson, J.R., Runte, D., Shue, B.C. 1999. Preventing annoying wood floor vibrations. ASCE Journal of Structural Engineering 125 (1): 19-24.

ETA. 2019. ETA-19/0244: Rotho Blaas CTC screw Self-tapping screws for use in wood-concrete slab kits, European Technical Assessment, Copenhagen, Denmark.

Fernandez-Cabo, J.L., Diez-Barra, R., Fernandez-Lavandera, J., Avila-Jalvo, J.M. 2013. Timber composite beams with a discrete connection system. Proceedings of the Institution of Civil Engineers: Structures and Buildings 166(2): 57-72.

Focacci, F., Foraboschi, P., Stefano, M.D. 2015. Composite beam generally connected: Analytical model. Composite Structures 133: 1237-1248.

Forest Products Laboratory. 2010. Wood Handbook: Wood as an engineering material. Madison, Wisconsin, USA.

FPInnovatios. 2019. CLT handbook (Canadian edition), Special Publication SP-532E, Pointe-Claire, QC, Canada.

Fragiacomo, M., Gutkowski, R.M., Balogh, J., Fast, R.S. 2007. Long-term behavior of wood-concrete composite floor/deck systems with shear key connection detail. Journal of Structural Engineering 133(9): 1307-1315.

Frangi, A., Fontana, M. 2003. Elasto-plastic model for timber-concrete composite beams with ductile connection. Structural Engineering International 13(1): 47-57.

Ghafar, N.H.A., Deam, B., Fragiacomo, M., Buchanan, A. 2008. Vibration performance of LVL-concrete composite floor systems. In Proc. 10th World Conf. on Timber Engineering (WCTE), Miyazaki, Japan.

Girhammar, U.A. 2009. A simplified analysis method for composite beams with interlayer slip. International Journal of Mechanical Sciences 51(7): 515-530.

Girhammar, U.A., Pan, D.H. 2007. Exact static analysis of partially composite beams and beam-columns. International Journal of Mechanical Sciences 49(2): 239-255.

Gong, M. 2019. Lumber-Based Mass Timber Products in Construction. Timber Buildings and Sustainability. IntechOpen.

Grosse, M., Hartnack, R., Lehmann, S., Rautenstrauch, K. 2003a. Modellierung von diskontinuierlich verbundenen Holz-Beton-Verbundkonstruktionen - Teil 1: Kurzzeittragverhalten. Bautechnik 80(8):534-541. [in German]

Grosse, M., Hartnack, R., Rautenstrauch, K. 2003b. Modellierung von diskontinuierlich verbundenen Holz-Beton-Verbunddecken - Teil 2: Langzeittragverhalten. Bautechnik 80(10):693-701. [in German]

Gutkowski, R.M., Brown, K., Shigidi, A., Natterer, J. 2004. Investigation of notched composite wood–concrete connections. Journal of Structural Engineering 130(10): 1553-1561.

Gutkowski, R., Brown, K., Shigidi, A., Natterer, J. 2008. Laboratory tests of composite wood–concrete beams. Construction and Building Materials 22: 1059-1066.

Hamm, P., Richter, A., Winter, S. 2010. Floor vibrations – new results. In Proc. 11th World Conference on Timber Engineering (WCTE), Trento, Italy.

Harte, A.M. 2017. Mass timber-the emergence of a modern construction material. Journal of Structural Integrity and Maintenance 2(3): 121-132.

Hehl, S., Tannert, T., Meena, R., Vallee, T. 2014. Experimental and numerical investigations of groove connections for a novel timber-concrete-composite system. Journal of Performance of Constructed Facilities 28(6): A4014010.

Higgins, C., Barbosa, A.R., Blank, C. 2017. Structural Tests of Concrete Composite-Cross-Laminated Timber Floors. Report No. 17-01. Oregon State University, Corvallis, OR, USA.

Holz-Verbund-Systeme. 2014. Load Bearing Constructions using Wood-Concrete-Composite Technique with glued-in HBV® - Shear Connectors. Technical Dossier HBV – systems, Haibach, Germany.

Hu, L., Cuerrier-Audair, S., Chui, Y. H., Ramzi, R., Gagnon, S., Mohammad, M., Ni, C., and Popovski, M. 2016. Design method for controlling vibrations of wood-concrete composite floor systems. In Proc. 14th World Conference on Timber Engineering (WCTE), Vienna, Austria.

ISO (International Organization for Standardization). 2003. Mechanical vibration and shock-Evaluation of human exposure to whole-body vibration-Part 2: vibration in buildings (1 Hz to 80 Hz). ISO 2631-2, Geneva, Switzerland.

ISO (International Organization for Standardization). 2007. Bases for design of structures – Serviceability of buildings and walkways against vibrations. ISO 10137, Geneva, Switzerland.

Jiang, Y., Crocetti, R. 2019. CLT-concrete composite floors with notched shear connectors. Construction and Building Materials 195: 127-139.

Jiang, Y., Hu, X., Hong, W., Zhang, J., He, F. 2020. Experimental study on notched connectors for Glulam-lightweight concrete composite beams. BioResources 15(2): 2171-2180.

Khelil, A., Kiniagi, C., Boissière, R. 2019. Development of new wood-concrete connectors. 2019 IOP Conference Series: Materials Science and Engineering 652: 012034.

Kudla, K. 2017. Kerven als Verbindungsmittel für Holz-Beton-Verbundstraßenbrücken. Thesis, University of Stuttgart, Germany. [in German]

Kudla, K., Mönch, S., Kuhlmann, U., Volk, D., Götz, T. 2016. Investigations on the slip modulus of a notched connection in timber-concrete composite floors. World conference on timber engineering, Austria.

Kuhlmann, U., Aldi, P. 2010, Ermüdungsfestigkeit von Holz-Beton-Verbundträgern im Straßenbrückenbau. Technical report, University of Stuttgart, Germany. [in German]

Kuhlmann, U., Mönch, S. 2018. Design Parameters of Notched Connections for TCC Structures as Part of Eurocode 5. In: International Network on Timber Engineering Research, Tallinn, Estonia.

Leborgne, M.R., Gutkowski, R.M. 2010. Effects of various admixtures and shear keys in wood – concrete composite beams, Construction and Building Materials 24: 1730–1738.

Liang, S., Gu, H., Bergman, R., Kelley, S. 2020. Comparative life-cycle assessment of a mass timber building and concrete alternative. Wood and Fiber Science 52(2): 217-229.

Linden, M.V.D. 1999. Timber-concrete composite beams. HERON 44(3): 215-239.

Linden, M.V.D. 1999. Timber-concrete composite floor systems. Thesis, Technische Universiteit Delft, Netherlands.

Loebus, S., Dietsch, P., Winter, S. 2017. Two-way spanning CLT-concrete composite slab. International network on timber engineering research (INTER), Kyoto, Japan.

Lukaszewska, E., Johnsson, H., Fragiacomo, M. 2008. Performance of connections for prefabricated timber–concrete composite floors. Materials and Structures 41: 1533-1550.

Mai, K.Q., Park, A., Nguyen, K.T., Lee, K. 2018. Full-scale static and dynamic experiments of hybrid CLT–concrete composite floor. Construction and Building Materials 170: 55–65.

Marchi, L., Pozza, L. 2021. Timber-concrete composite connections using GFRP notches fastened with self-tapping screws: Conceiving, numerical modelling and testing. Construction and Building Materials 294: 123579.

Marchi, L., Scotta, R., Pozza, L. 2017. Experimental and theoretical evaluation of TCC connections with inclined self-tapping screws. Materials and Structures 20: 180.

Martins, C., Santos, P., Almeida, P., Godinho, L., Dias, A. 2015. Acoustic performance of timber and timber-concrete floors. Construction and Building Materials 101: 684-691.

McLain, R. 2018. Acoustics and Mass Timber: Room-to-Room Noise Control. WoodWorks, Washington, DC, USA.

Michelfelder, B.C. 2006. Trag- und Verformungsverhalten von Kerven bei Brettstapel-Beton-Verbunddecken. Thesis, University of Stuttgart, Germany. [in German]

Mirdad, M.A.H., Chui, Y.H. 2019. Load-slip performance of mass timber panel-concrete (MTPC) composite connection with self-tapping screws and insulation layer. Construction and Building Materials 213: 696-708.

Monteiro, S.R.S., Dias, A.M.P.G., Negrão, J.H.J.O. 2013. Assessment of timber-concrete connections made with glued notches: Test set-up and numerical modeling, Experimental Techniques 37(2): 50-65.

Möhler, K. 1956. Uber das Tragverhalten von Biegeträgern und Druckstäben mit zusammengestezten Querschnitten und nachgiebigen Verbindungsmitteln. Technical University of Karlsruhe, Karlsruhe, Germany. [in German]

Mönch, S., Kuhlmann, U. 2018. Investigations on the effects of geometry in timber-concrete composite push-out tests with notched connections. In Proc., 15th World Conference on Timber Engineering (WCTE), Seoul, South Korea.

Murray, T.M., Allen, D.E., Ungar, E.E., Davis, D.B. 2016. Design guide 11: Vibrations of steel-framed structural systems due to human activity (Second edition), American institute of steel construction (AISC), Chicago, USA.

Müller, K., Frangi, A. 2018. 4-point bending tests of timber-concrete composite slabs with micro-notches. In: 15th World Conference on Timber Engineering (WCTE), Seoul, Republic of Korea.

Negrão, J.H.J.D.O., Oliveira, C.A.L.D., Oliveira, F.M.M.D., Cachim, P.B. 2010a. Glued composite timber-concrete beams. I: Interlayer connection specimen tests. Journal of Structural Engineering 136(10): 1236-45.

Negrão, J.H.J.D.O., Oliveira, F.M.M.D., Oliveira, C.A.L.D., Cachim, P.B. 2010b. Glued composite timber-concrete beams. II: analysis and tests of beam specimens. Journal of Structural Engineering 136(10): 1246-54.

Neve, O., Spencer-Allen, L. 2015. Shaking up dance floor design with timber-concrete composites. Proceedings of Institution of Civil Engineers: Construction Materials 168(CM4): 204-212.

Newmark, N.M., Siess, C.P., Viest, I.M. 1951. Tests and analysis of composite beams with incomplete interaction. Proceedings of the Society for Experimental Stress Analysis 9(1): 75-92.

Nguyen, Q.H., Hjiaj, M., Aribert, J.M. 2010. A space-exact beam element for time-dependent analysis of composite members with discrete shear connection. Journal of Constructional Steel Research 66(11): 1330-8.

Nguyen, Q.H., Hjiaj, M., Guezouli, S. 2011a. Exact finite element model for shear-deformable two-layer beams with discrete shear connection. Finite Elements in Analysis and Design 47(7): 718-27.

Nguyen, Q.H., Martinelli, E., Hjiaj, M. 2011b. Derivation of the exact stiffness matrix for a two-layer Timoshenko beam element with partial interaction. Engineering Structures 33(2): 298-307.

Niederwestberg, J., Zhou, J., Chui, Y.H. 2018. Mechanical properties of innovation, multi-layer composite laminated panels. Buildings 8: 142.

NRC (National Research Council Canada). 2015. National Building Code of Canada. NBCC, Ottawa, Ontario, Canada.

Onysko, D.M., Hu, L.J., Jones, E.D., Lenardo, B.D. 2000. Serviceability Design of Residential Wood Framed Floors in Canada. In Proc. 6th World Conference on Timber Engineering (WCTE), Whistler, BC, Canada.

Ouch, V., Heng, P., Nguyen, Q.H., Somja, H., Soquet, T. 2021. A notched connection for CLT-concrete composite slabs resisting to uplift without metallic connectors: experimental investigation. Fib Symposium: Concrete Structures, New Trends for Eco-Efficiency and Performance, Lisbon, Portugal. hal-03254979.

Oven, V.A., Burgess, I.W., Plank, R.J., Wali, A.A.A. 1997. An analytical model for the analysis of composite beams with partial interaction. Computers & Structures 62(3): 493-504.

Pan, B., Qian, K., Xie, H., Asundi, A. 2009. Two-dimentional digital image correlation for in-plane displacement and strain measurement: a review. Measurement Science and Technology 20: 062001.

Rantakokko, T., Salokangas, L. 2000. Design of the Vihantasalmi Bridge, Finland. Structural Engineering International 10(3): 150-152.

Rijal, R., Samali, B., Shrestha, R., Crews, K. 2015. Experimental and analytical study on dynamic performance of timber-concrete composite beams. Construction and Building Materials 75: 46-53.

Schönborn, F., Flach, M., Feix, J. 2011. Bemessungsregeln und Ausführungshinweise für Schubkerven im Holz-Beton-Verbundbau. Beton-und Stahlbetonbau 106(6): 385-393. [in German]

Schnell, J., Kohlmeyer, C., Mikdad, F. 2016. Untersuchung von Schubnocken aus hochfestem Beton zur Schubverbindung in Holzverbundträgern. Fraunhofer IRB Verlag, Stuttgart, Germany. [in German]

Schnabl, S., Saje, M., Turk, G., Planinc, I. 2007. Analytical solution of two-layer beam taking into account interlayer slip and shear deformation. Journal of Structural Engineering 133(6): 886-894.

Sebastian, W.M. 2019. Switch from connection ductility to reinforcement ductility with curvature reversal in timber-concrete composites. Construction and Building Materials 229: 116886.

Sebastian, W., Webb, S., Nagree, H.S. 2020. Orthogonal distribution and dynamic amplification characteristics of partially prefabricated timber-concrete composites. Engineering Structures 219: 110693.

Shamass, R., Zhou, X., Alfano, G. 2015. Finite-Element Analysis of Shear-Off Failure of Keyed Dry Joints in Precast Concrete Segmental Bridges. Journal of Bridge Engineering 20(6): 04014084.

Shephard, A.B., Fischer, E.C., Barbosa, A.R., Sinha, A. 2021. Fundamental Behavior of Timber Concrete-Composite Floors in Fire. Journal of Structural Engineering 147(2): 04020340.

Smith, I., Landis, E., Gong, M. Fracture and fatigue in wood. John Wiley & Sons. 2003.

Steinberg, E., Selle, R., Faust, T. 2003. Connectors for timber–lightweight concrete composite structures. Journal of structural engineering 129(11): 1538-1545.

Tannert, T., Gerber, A., Vallee, T. 2020. Hybrid adhesively bonded timber-concrete-composite floors. International Journal of Adhesion and Adhesives 97:102490.

Tao, H., Yang, H., Liu, W., Wang, C., Shi, B., Ling, X. 2021. Experimental and Nonlinear Analytical Studies on Prefabricated Timber–Concrete Composite Structures with Crossed Inclined Coach Screw Connections. Journal of Structural Engineering 147(5): 04021043.

Thai, M.V., Ménard, S., Elachachi, S.M., Galimard, P. 2020. Performance of notched connectors for CLT-concrete composite floors. Buildings 10(7): 122.

Tommola, J., Jutila, A. 2001. Analysis of wood-concrete composite girder with discrete shear connectors. In: IABSE Symposium on Innovative Wooden Structures and Bridges, Lahti, Finland.

Wymelenberg, K., Northcutt, D., Fretz, M., Stenson, J., Marks, E. 2019. Acoustic Lab Testing (ASTM E492-2016, ASTM E90-2016) of CLT and MPP Wall and Floor Assemblies for Multi-Family Residential Application. University of Oregon, Portland, Oregon, USA.

Yeoh, D. 2010. Behaviour and design of timber-concrete composite floor system. Thesis, University of Canterbury, New Zealand.

Yeoh, D., Fragiacomo, M., Deam, B. 2011a. Experimental behaviour of LVL – concrete composite floor beams at strength limit state. Engineering Structures 33(9): 2697–2707.

Yeoh, D., Fragiacomo, M., Franceschi, M.D., Boon, K.H. 2011b. State of the art on timber-concrete composite structures: Literature review. Journal of Structural Engineering 137(10): 1085–1095.

Yeoh, D., Fragiacomo, M., Franceschi, M.D., Buchanan, A.H. 2011c. Experimental tests of notched and plate connectors for LVL-concrete composite beams. Journal of Structural Engineering 137(2): 261-269.

Zhang, C., Gauvreau, P. 2015. Timber-concrete composite systems with ductile connections. Journal of Structural Engineering 141(7): 04014179.

Zhang, L., Chui, Y.H., Tomlinson, D. 2020. Experimental investigation on the shear properties of notched connections in mass timber panel-concrete composite floors. Construction and Building Materials 234: 117375.

Zhang, L., Zhang, S., Chui, Y.H. 2021. Analytical evaluation to the timber-concrete composite beam connected with notched connections. Engineering Structures 227: 111466.

Appendix I

Load-Slip Curves from Connection Shear Tests

The load-slip curves from push-out tests on ten types of notched connections are shown here. Each type of specimen had six repetitions. Two load-slip curves were measured from each sample with linear variable differential transformers (LVDTs) installed on the two sides of the sample. In specimens L-25-150, L-25-250, and L-25-350, two samples from each type where measured with digital image correlation (DIC), thus only one load-slip curve was obtained from LVDT. In each type of specimen, the first sample was loaded monotonically. Based on the peak load of the first sample, a preloading cycle was applied to the rest of the specimens. The samples measured with DIC were also loaded monotonically. The averaged load-slip curves for each type of specimen are shown in Fig. 3.6.

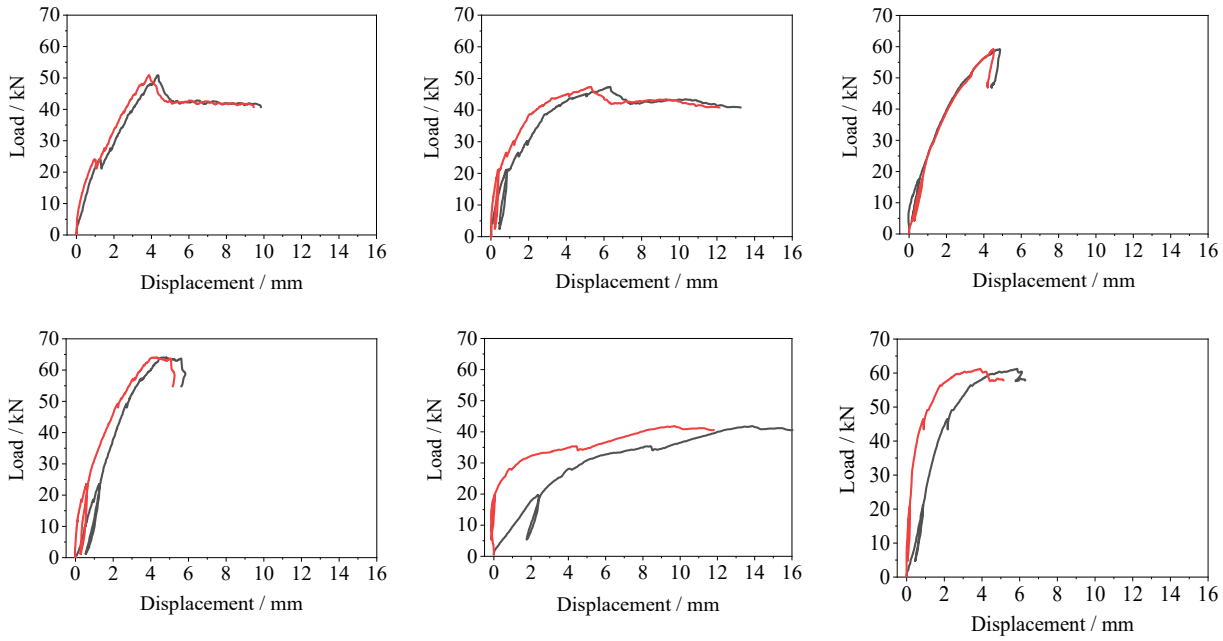

Fig. A1.1 Load-slip curves of connection specimen T-25-180

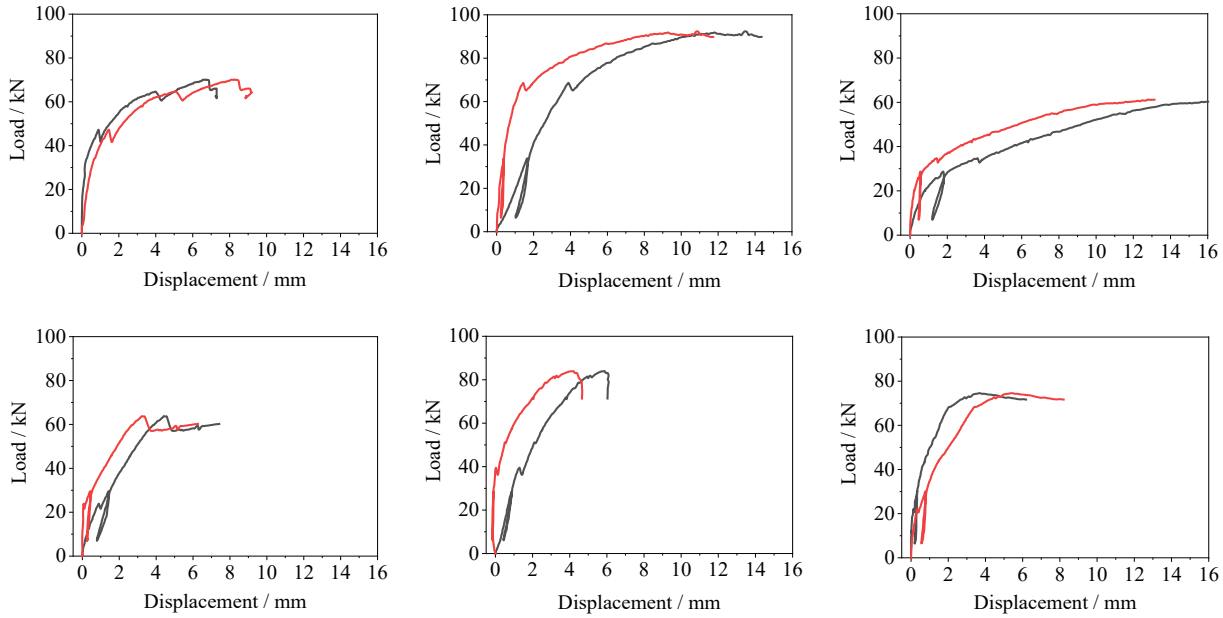

Fig. A1.2 Load-slip curves of connection specimen T-25-180-N

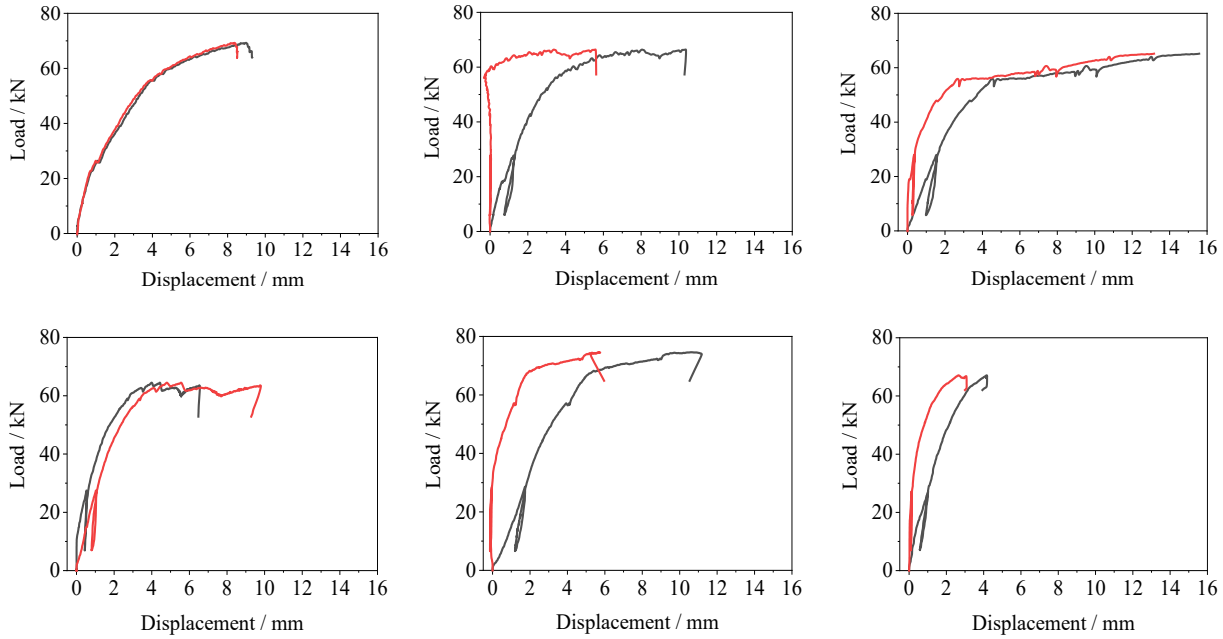

Fig. A1.3 Load-slip curves of connection specimen T-25-180-T

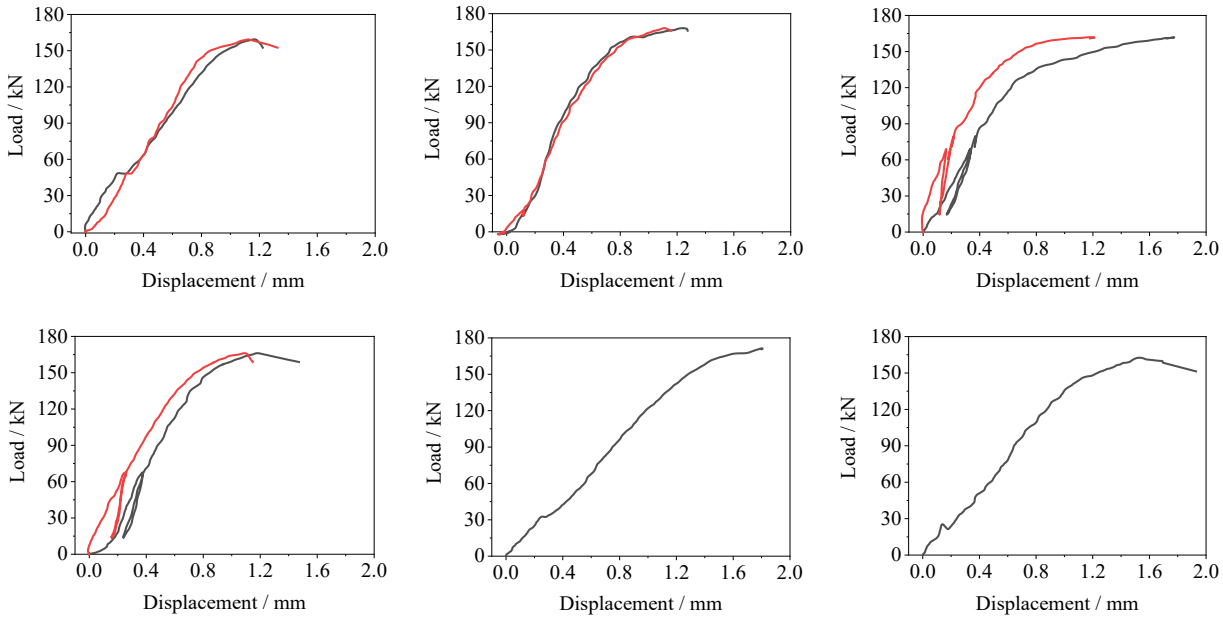

Fig. A1.4 Load-slip curves of connection specimen L-25-250

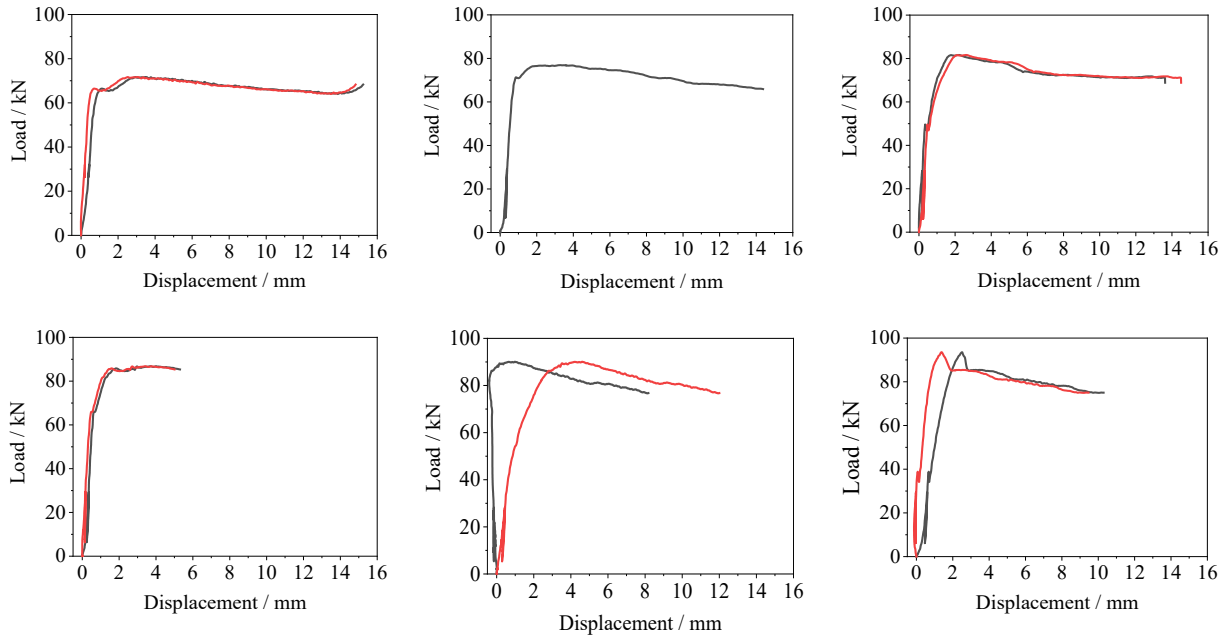

Fig. A1.5 Load-slip curves of connection specimen L-10-250

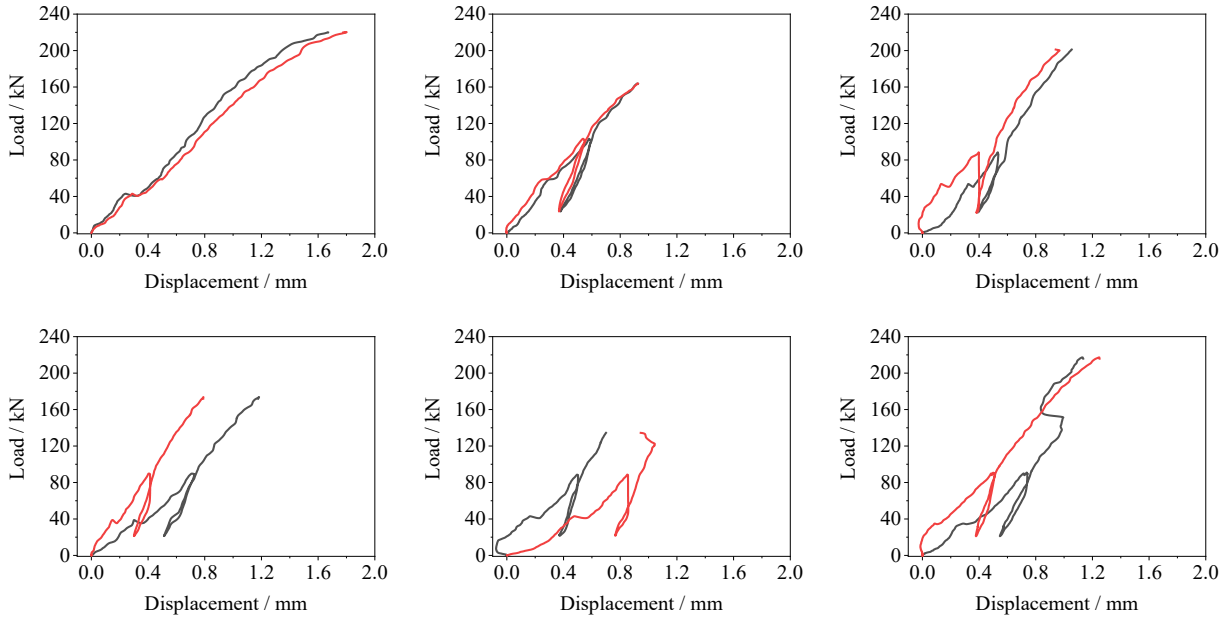

Fig. A1.6 Load-slip curves of connection specimen L-40-250

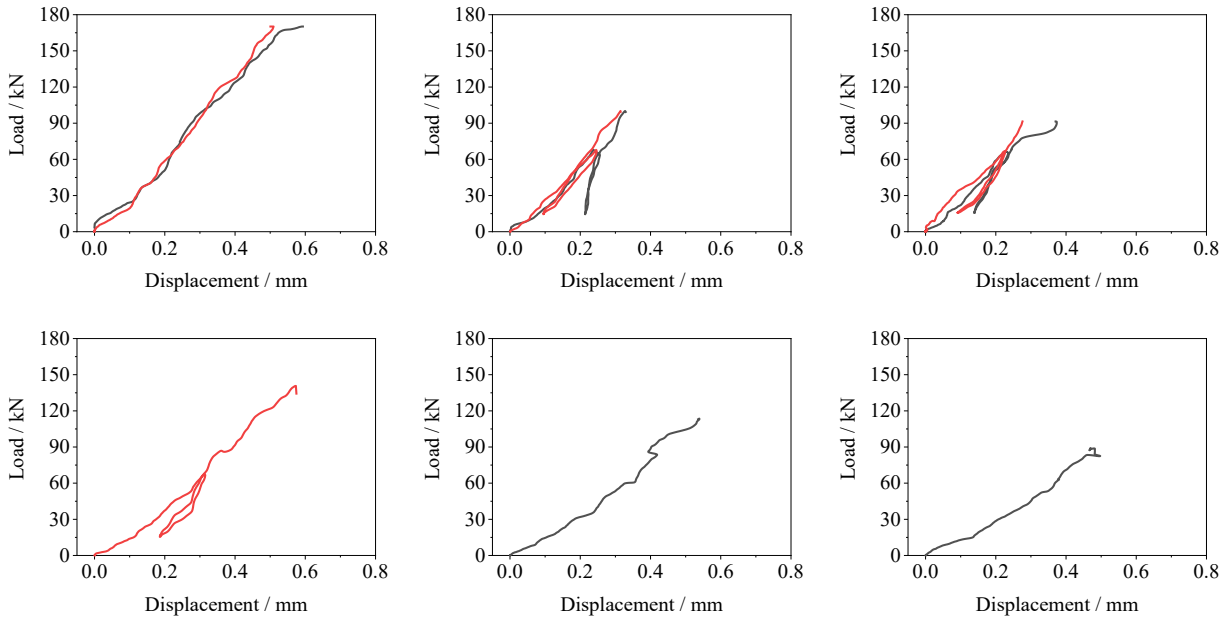

Fig. A1.7 Load-slip curves of connection specimen L-25-150

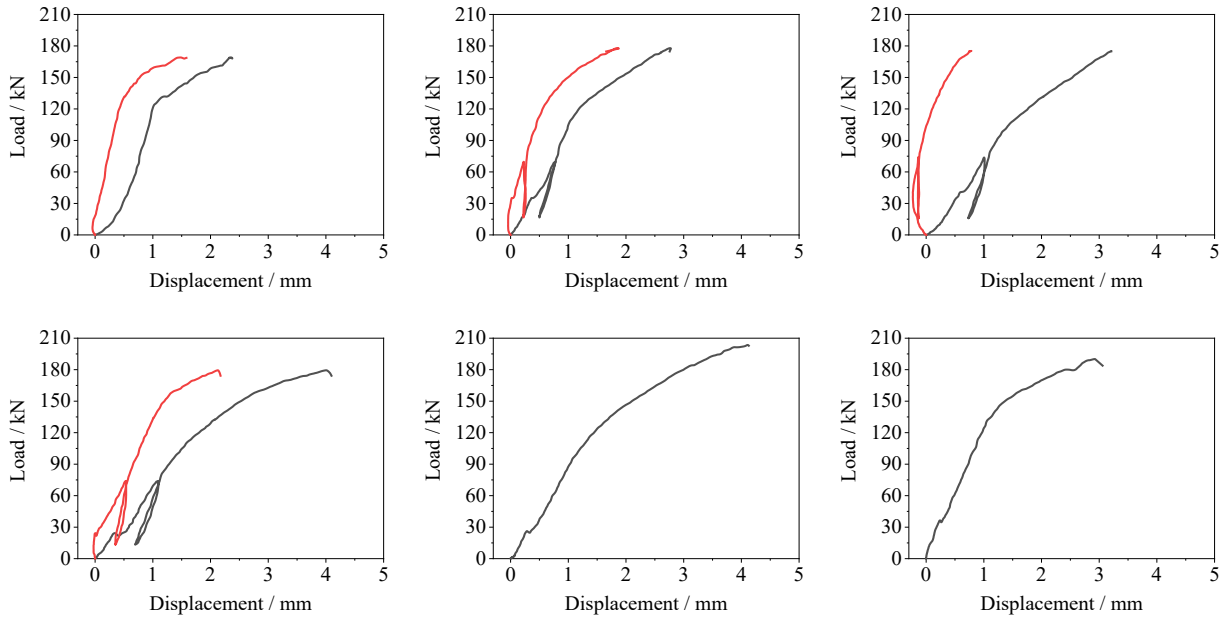

Fig. A1.8 Load-slip curves of connection specimen L-25-350

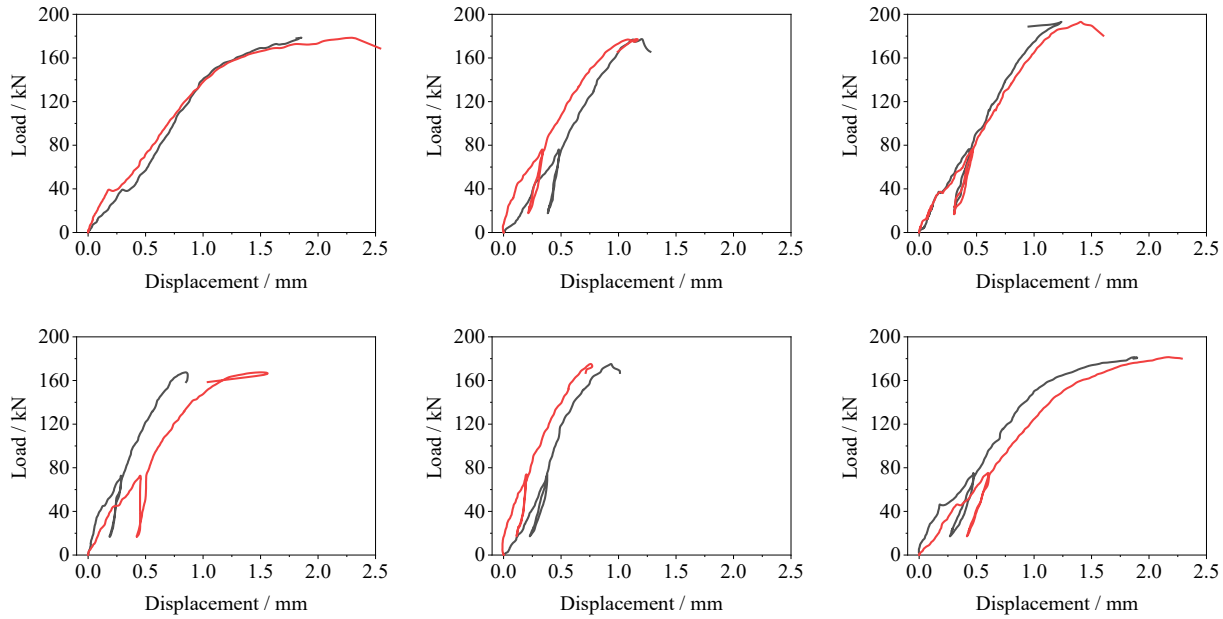

Fig. A1.9 Load-slip curves of connection specimen L-25-250-N

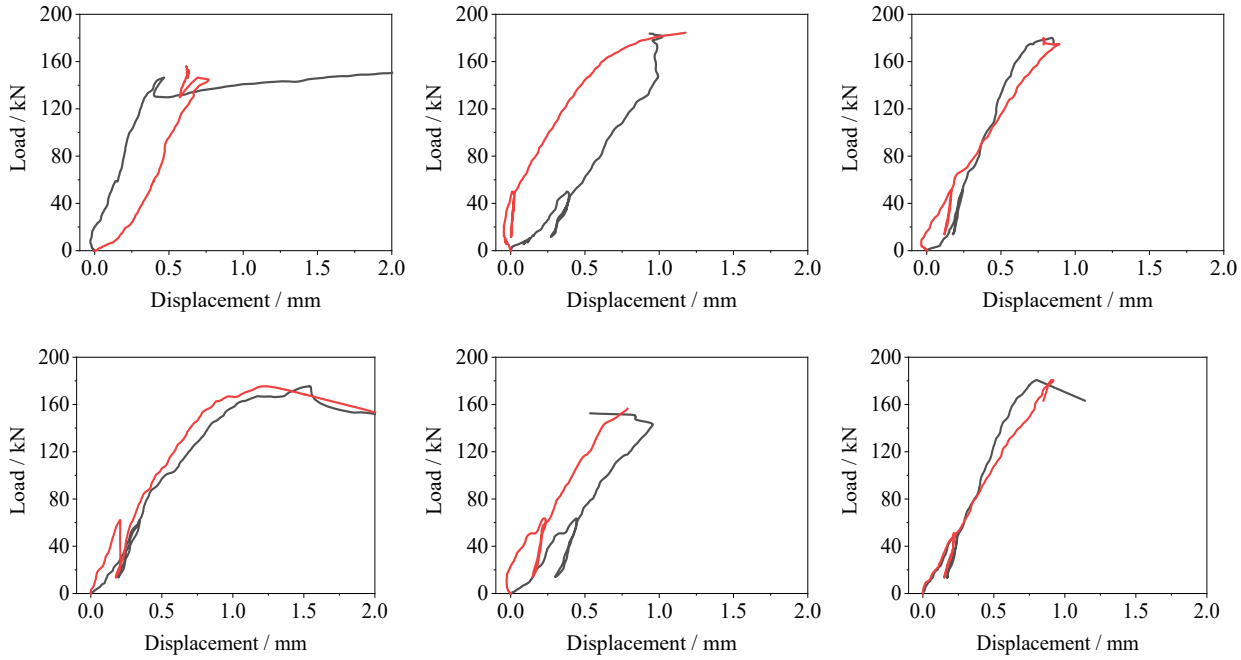

Fig. A1.10 Load-slip curves of connection specimen L-25-250-T

Appendix II

Compression and Shear Tests on Timber

After the push-out tests on the notched connections, compression tests and shear tests were conducted on small clear wood samples that were cut from the untested wood of the same batch according to ASTM D143-14, as shown in Fig. A2.1. The numbers of small clear wood samples for compression tests in the longitudinal direction, transverse direction, and shear tests in longitudinal direction were 22, 21, and 49 respectively. The cross-section dimensions for the compression specimens were 40 mm × 40 mm while the heights were 160 mm and 80 mm for the longitudinal and transverse specimens, respectively. The dimensions of the shear specimens are shown in Fig. A2.2. The compressive strengths of timber in the longitudinal and transverse directions and shear strength in the longitudinal direction were measured from the tests. Besides, the moduli of elasticity (E_t and E_{TT}) and Poisson's ratio (υ_{LT}) of timber were measured using Digital Image Correlation (DIC) method from the compression tests by capturing a sequence of images in every 2s during the tests using two CCD (charge-coupled device) cameras (Vic-3D, Correlated Solutions). The measured properties of timber are listed in Table 3.2. The stress-strain relationships of compression specimens derived from DIC images are shown in Fig. A2.3 for longitudinal and transverse specimens. The Young's modulus of timber was determined from the linear regression to the slopes of stress-strain relationships in the range of 10-40% of the peak loads.

The Poisson's ratio of timber in the longitudinal direction was determined from the longitudinal compression specimens by measuring the vertical compressive strain and horizontal strain in the middle of the specimen. The Poisson's ratio of timber was determined from Eq. A2.1

$$\upsilon_{LT} = -\frac{\epsilon_h}{\epsilon_v} \tag{A2.1}$$

where ϵ_v and ϵ_h are the strains in the vertical and horizontal directions, respectively. The relationships between vertical and horizontal strains in the longitudinal compression specimens are shown in Fig. A2.4.

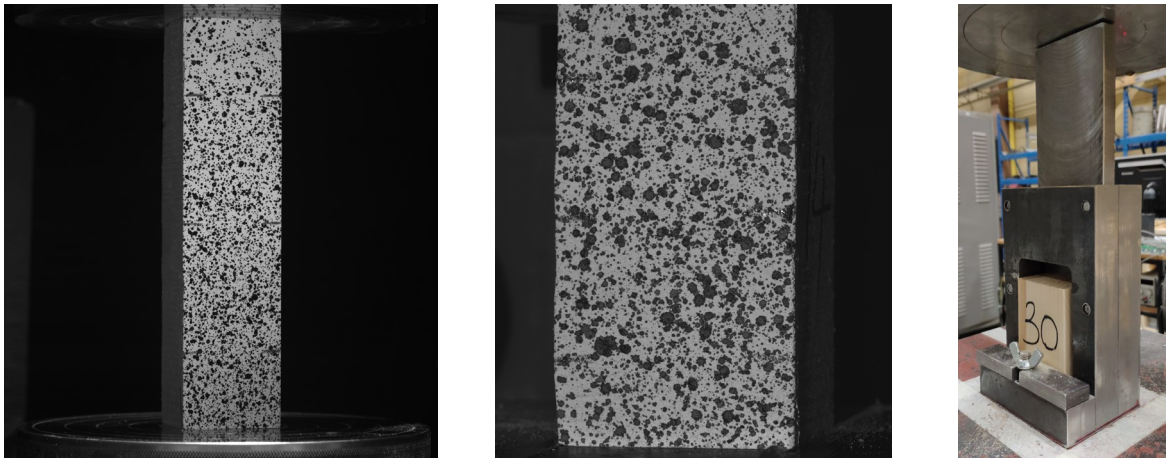

(a) (b) (c)

Fig. A2.1 Material tests on small clear timber samples (a) Compression test parallel to grain; (b) Compression test perpendicular to grain; and (c) Shear test parallel to grain

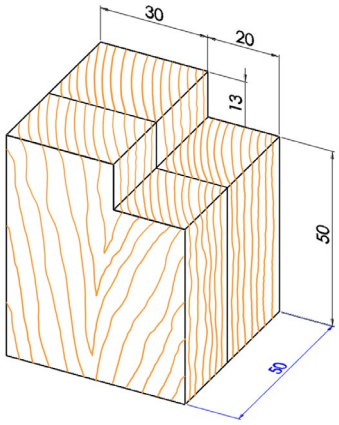

Fig. A2.2 Dimensions of timber shear specimens (unit: mm)

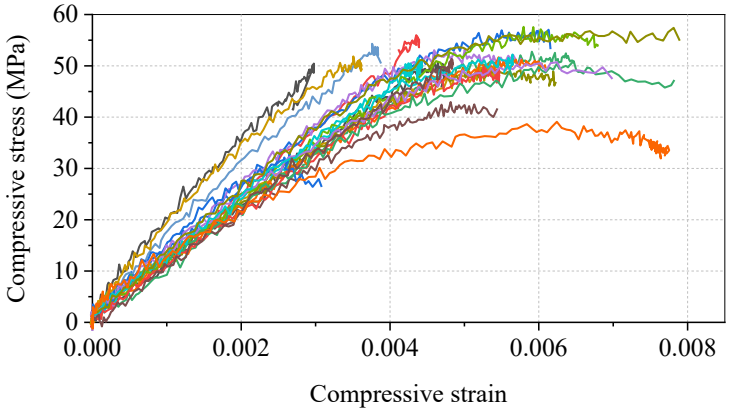

(a) Longitudinal specimens

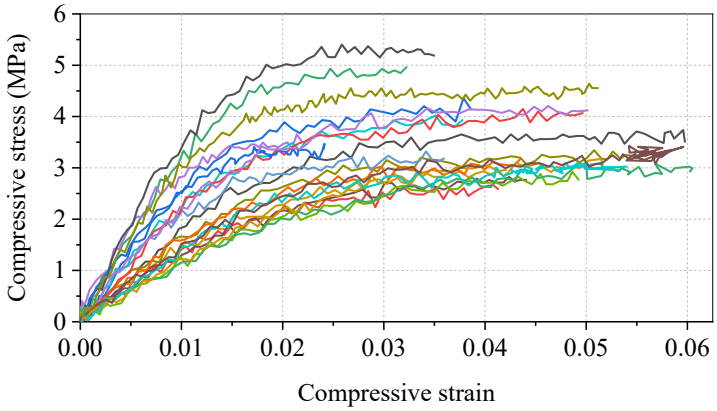

(b) Transverse specimens

Fig. A2.3 Stress-strain relationships of timber compression specimens

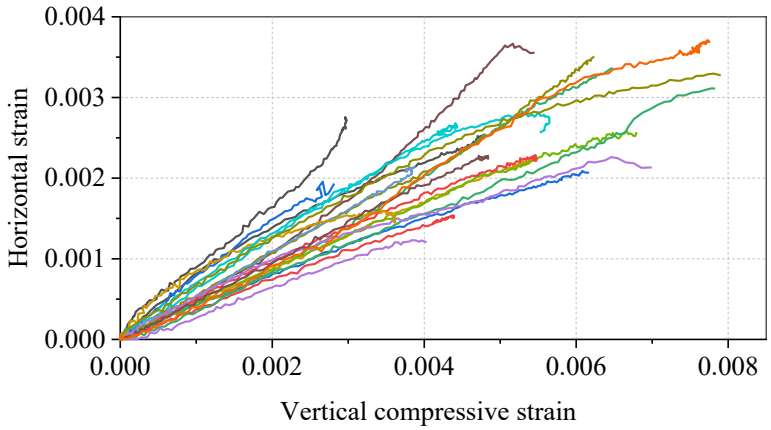

Fig. A2.4 Relationships between vertical and horizontal strains in the longitudinal timber compression specimens

Appendix III

Bending Tests on Timber Beams

After the phase 1 bending tests on the MTP-concrete composite floors, bending tests were conducted on the timber beams to measure the modulus of elasticity (MOE) and modulus of rupture (MOR) of timber. The timber beams were cut from one GLT panel that came from the batch. Nine timber beams with a length of 2.1 m, a width of 190 mm, and a height of 100 mm were made. The effective span of the timber beams was 1.9 m. As shown in Fig. A3.1, the bending tests conducted were three-point bending and the loading rate was 2 mm/min. The mid-span deflections of the beams were measured with strain potentiometers. The typical failure patterns of the timber beams under bending are shown in Fig. A3.2. The measured MOE and MOR of timber were 9061 MPa and 45.9 MPa, with coefficients of variation of 5.3% and 6.7%, respectively. The load-deflection relationships of timber beams under bending are shown in Fig. A3.3.

The modulus of elasticity (MOE) of timber was determined from Eq. A3.1

$$E = \frac{1}{48}\frac{L^3}{I}\frac{P}{v} \tag{A3.1}$$

where L is the beam span, I is the second moment of area of the beam, and P/v is the slope of the load-deflection curve in the range of 10-40% of the peak load.

Fig. A3.1 Three-point bending test on a timber beam

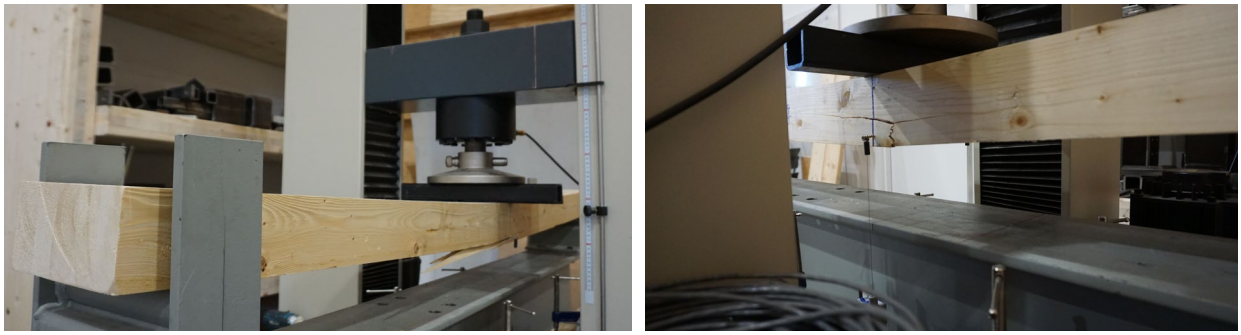

Fig. A3.2 Typical failure modes of timber beams under bending

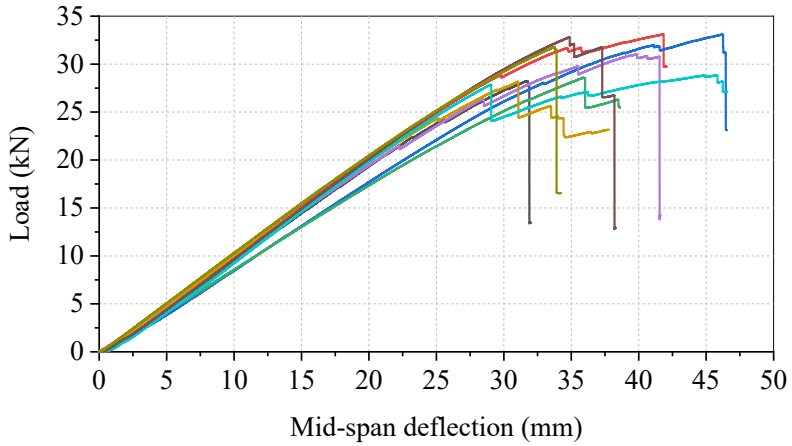

Fig. A3.3 Load-deflection relationships of timber beams under bending

Appendix IV

Load-Slip Curves of Composite Floors from Bending Tests

In the bending tests on twelve MTP-concrete composite floors, the relative slips between timber and concrete at the interface were measured at each notched connection and the floor ends, as shown in Fig. A4.1. The load-slip relationships for each composite floor specimen are shown in Fig. A4.2 to Fig. A4.13. The load-deflection curves were plotted separately at four different regions in the composite floors: front-left, front-right, back-left, and back-right. Specimen SPU-3 contained four notched connections thus only three slips were measured at each region. Specimen SPU-8 had no connections and the relative slips were measured at the floor ends and third points of the floor span. The relative slip data were not available at the notched connections measured with digital image correlation (DIC). In specimens SPU-1 and SPU5, the relative slips between timber and concrete were significantly higher on the right side (pin support) than the left side (roller support). For the rest of the specimens, the relative slips were similar on the two sides. The averaged end slips of each specimen are listed in Table 4.2 and Table 4.3.

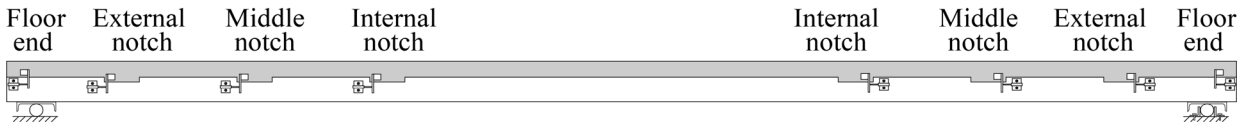

Fig. A4.1 Locations of linear variable differential transformers (LVDTs) on the composite floors

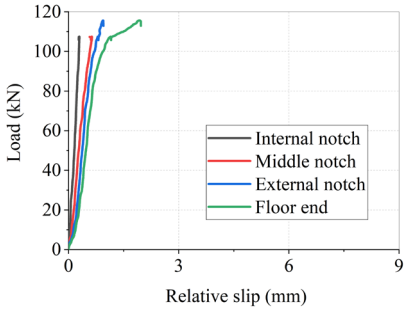

(a) Front-left

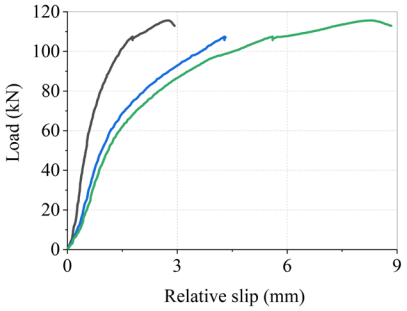

(b) Front-right

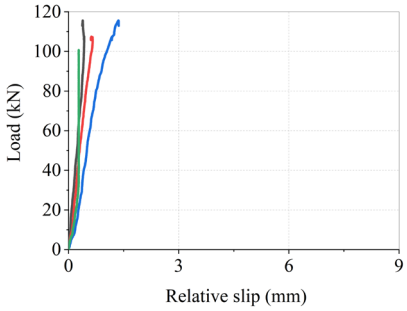

(c) Back-left

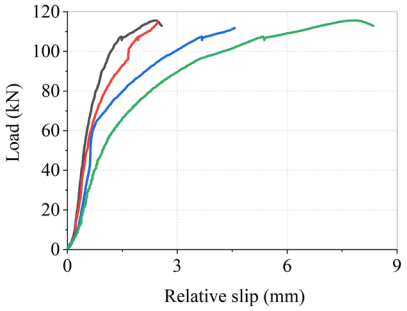

(d) Back-right

Fig. A4.2 Load-slip curves of floor specimen SPU-1

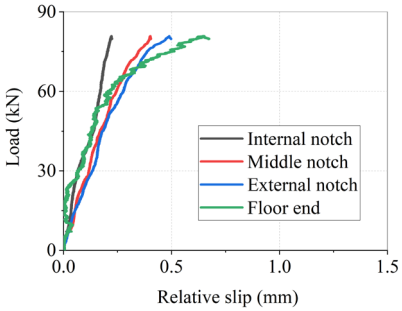

(a) Front-left

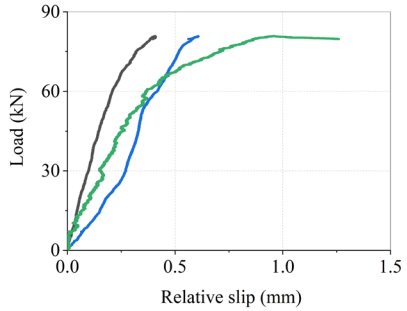

(b) Front-right

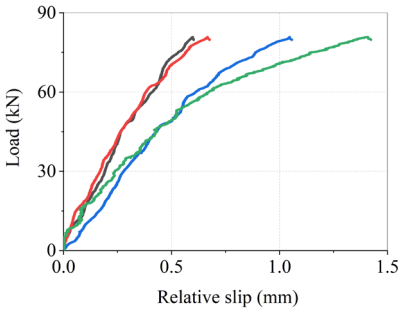

(c) Back-left

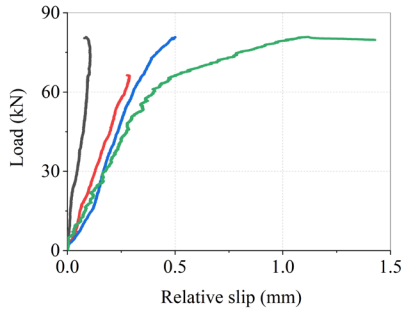

(d) Back-right

Fig. A4.3 Load-slip curves of floor specimen SPU-2

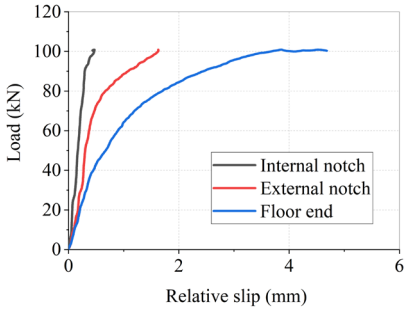

(a) Front-left

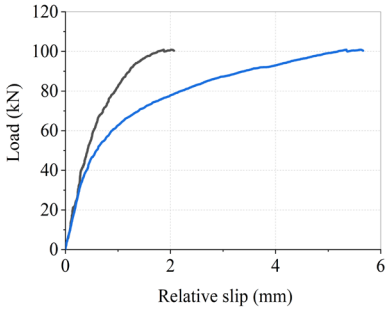

(b) Front-right

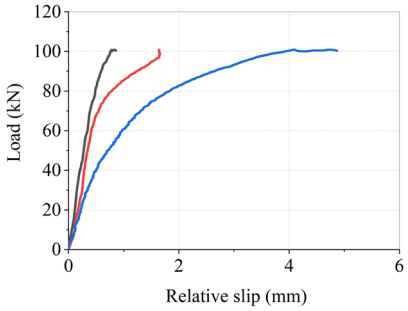

(c) Back-left

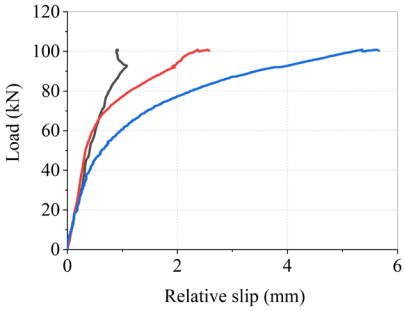

(d) Back-right

Fig. A4.4 Load-slip curves of floor specimen SPU-3

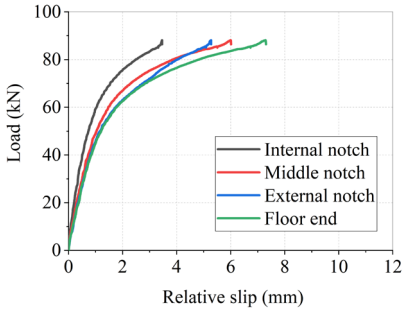

(a) Front-left

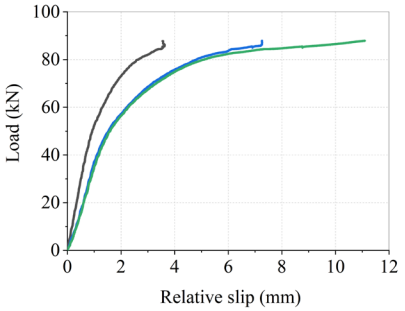

(b) Front-right

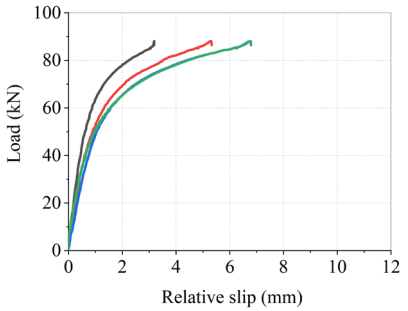

(c) Back-left

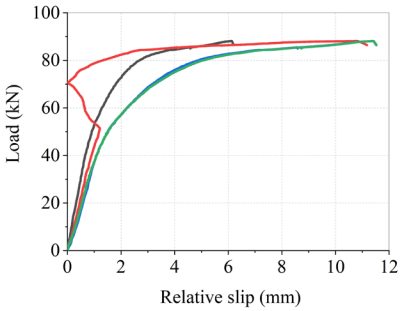

(d) Back-right

Fig. A4.5 Load-slip curves of floor specimen SPU-4

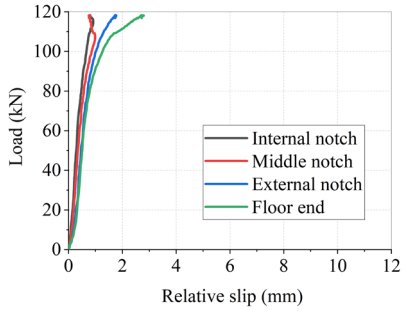

(a) Front-left

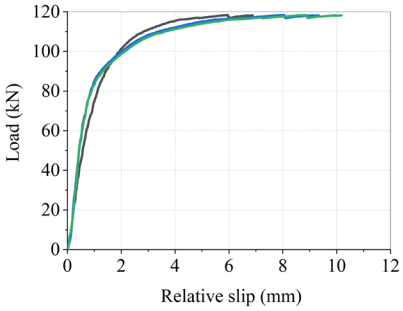

(b) Front-right

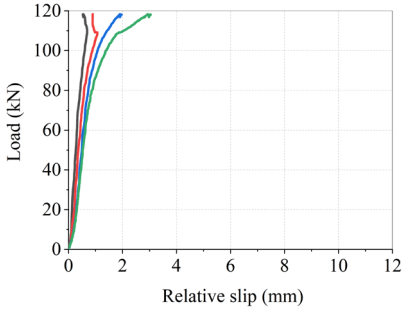

(c) Back-left

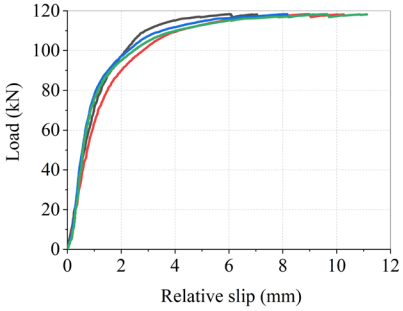

(d) Back-right

Fig. A4.6 Load-slip curves of floor specimen SPU-5

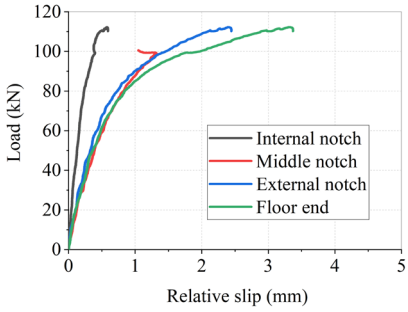

(a) Front-left

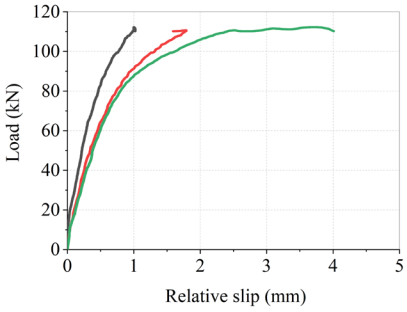

(b) Front-right

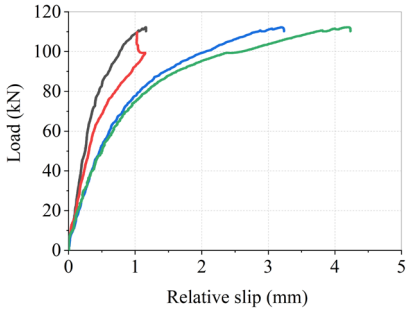

(c) Back-left

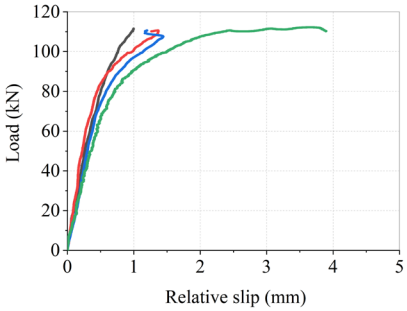

(d) Back-right

Fig. A4.7 Load-slip curves of floor specimen SPU-6

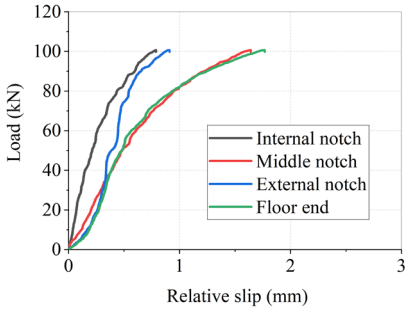

(a) Front-left

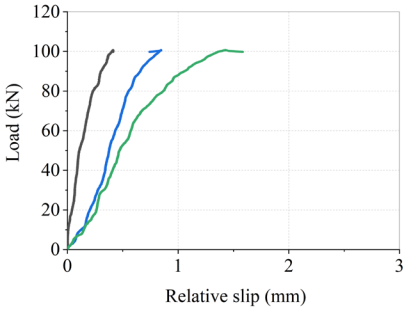

(b) Front-right

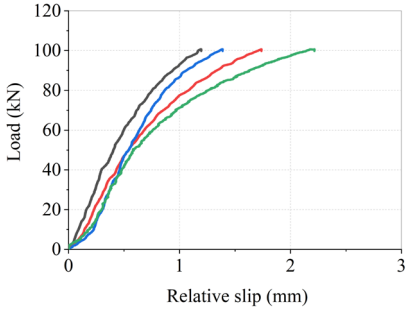

(c) Back-left

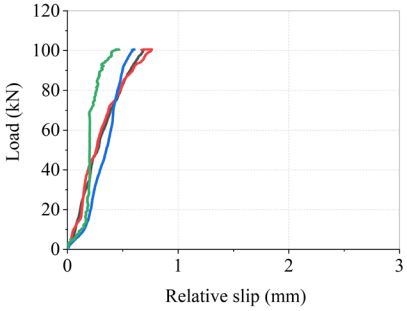

(d) Back-right

Fig. A4.8 Load-slip curves of floor specimen SPU-7

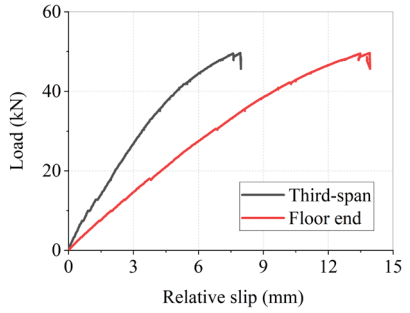

(a) Front-left

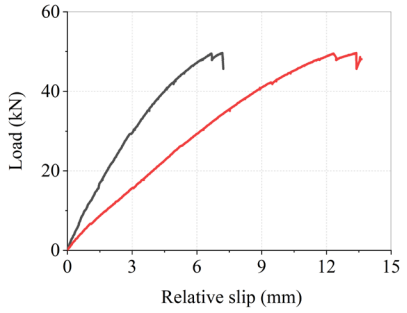

(b) Front-right

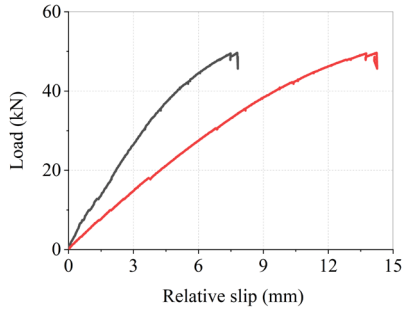

(c) Back-left

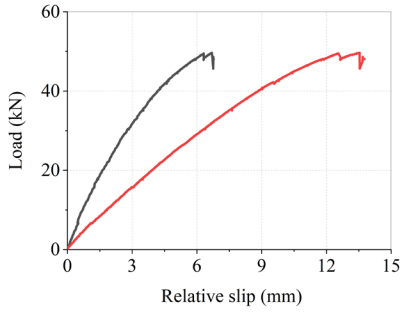

(d) Back-right

Fig. A4.9 Load-slip curves of floor specimen SPU-8

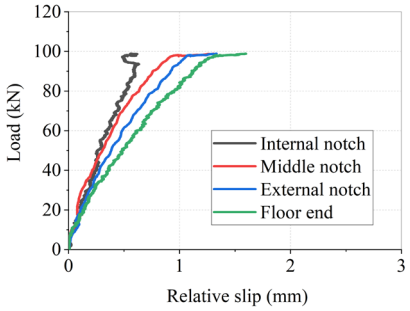

(a) Front-left

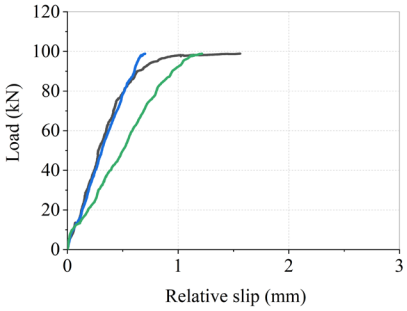

(b) Front-right

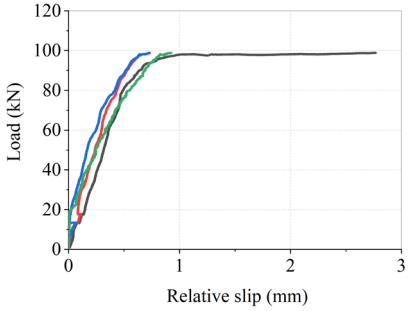

(c) Back-left

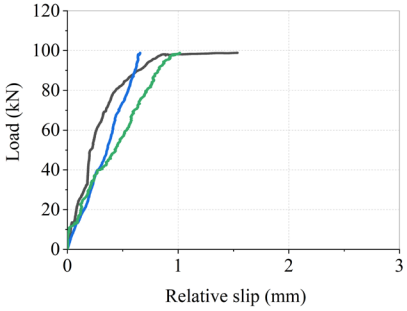

(d) Back-right

Fig. A4.10 Load-slip curves of floor specimen SPU-9

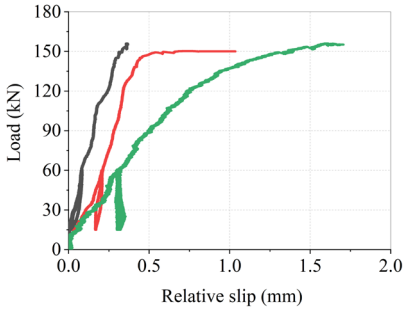

(a) Front-left

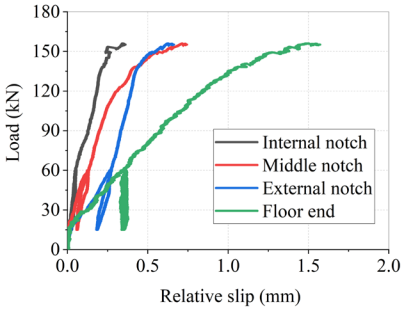

(b) Front-right

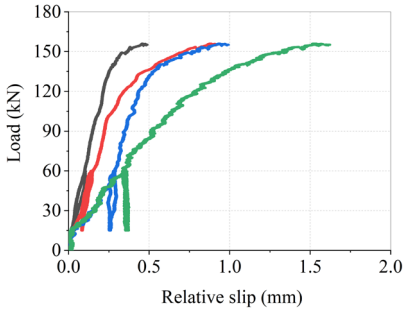

(c) Back-left

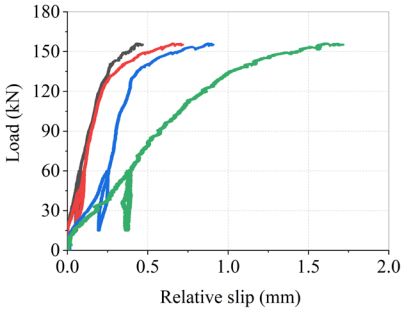

(d) Back-right

Fig. A4.11 Load-slip curves of floor specimen SPR-1

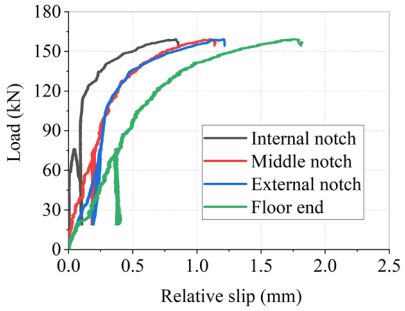

(a) Front-left

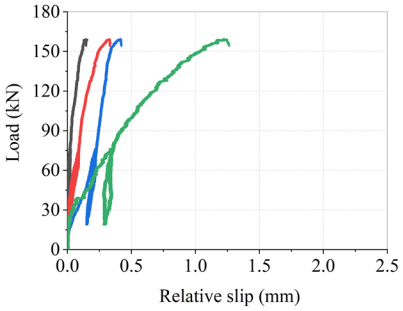

(b) Front-right

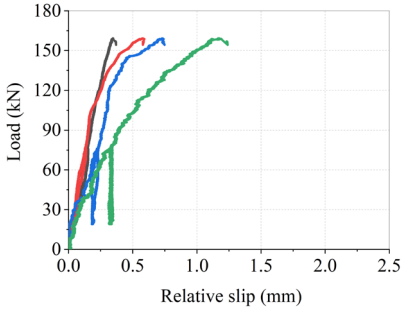

(c) Back-left

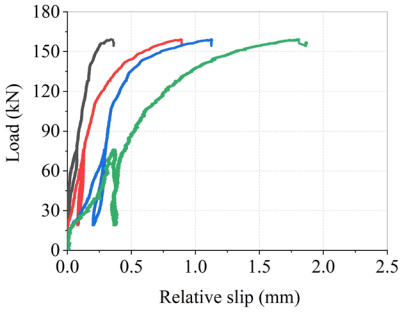

(d) Back-right

Fig. A4.12 Load-slip curves of floor specimen SPR-2

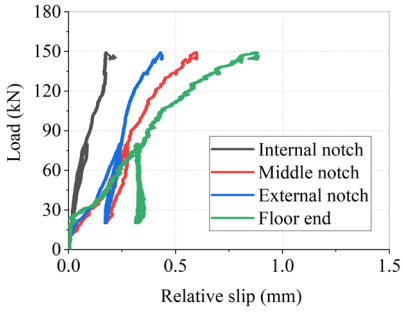

(a) Front-left

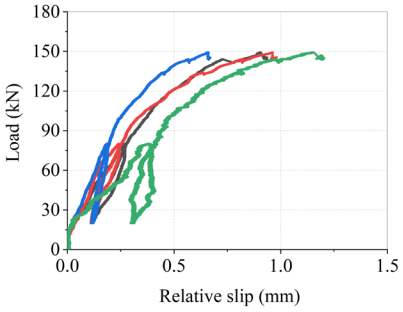

(b) Front-right

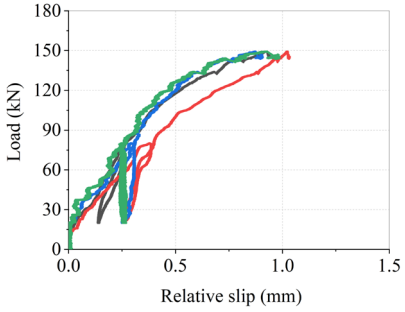

(c) Back-left

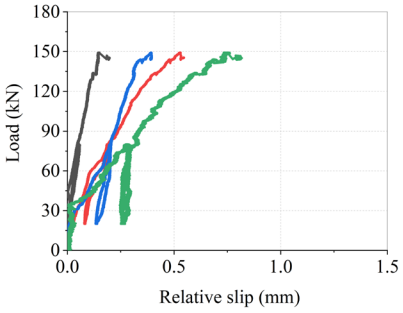

(d) Back-right

Fig. A4.13 Load-slip curves of floor specimen SPR-3

Appendix V

Tensile Tests on Screws and Steel Rods

After phase two bending tests on the composite floors, tensile tests were conducted on the untested steel reinforcements in the notched connections, as shown in Fig A5.1. The reinforcements installed in the notches were composed of CTC7160 self-tapping screws and hooked steel rods. The CTC7160 screws were the timber-to-concrete fastener with specific CE certification according to ETA 19/0244 (2019). The screws were made of galvanized carbon steel. The nominal diameter of screws was 7 mm and the shank diameter was 5 mm. The steel rods were made of cold-rolled steel. The diameter of the steel rods was 6 mm.

Tensile tests were conducted on 13 screws and 9 steel rods. The loading rate was 1 mm/min. The relationships between the applied load and the loading head movement are shown in Fig. A5.2. Under the tensile load, the screws failed in a brittle manner while the steel rods failed in a ductile way. The measured average tensile strength of screws was 23.4 kN with a coefficient of variation of 8.9%. The average yield strength and ultimate tensile strength of steel rods were measured to be 18.9 kN and 20.1 kN, with coefficients of variation of 5.2% and 5.1%, respectively.

(a) (b)

Fig. A5.1 Tensile tests on (a) Self-tapping screws and (b) Steel rods

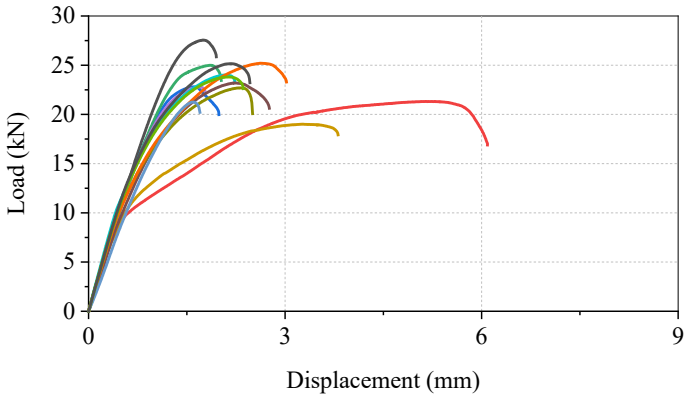

(a)

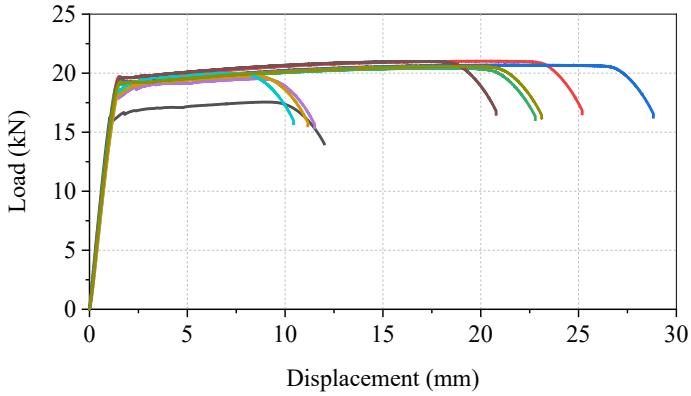

(b)

Fig. A5.2 Relationships between the applied tensile force and loading head movement for (a) Self-tapping screws and (b) Steel rods